

**THE TECTONIC AND MAGNETIC EVOLUTION OF THE CENTRAL SEGMENT
OF THE ARCHEAN LA GRANDE GREENSTONE BELT, CENTRAL QUÉBEC**

BY

THOMAS SKULSKI

**A thesis submitted to the Faculty of Graduate Studies and
Research in partial fulfillment of the requirements for the
degree of Master of Science**

**Department of Geological Sciences
McGill University, Montréal, Québec, Canada**

© Thomas Skulski, 1985

Abstract

The record of an Archean continental rift is preserved in the folded and faulted supracrustal succession in the central part of the La Grande greenstone belt. The base of the succession is obscured by syntectonic tonalite intrusions. Volcanoclastics and sediments deposited in shallow water are overlain by large volumes of submarine basalts and minor basaltic andesites that were extruded on submarine lava plains. Coarse, westerly-derived, clastic sediments were deposited on a submarine fan overlying the volcanics, while banded iron formation was formed in the deeper parts of the basin. Late-stage basaltic andesites and related volcanoclastics and sediments were emplaced in shallow water, during a period when the basin was locally emergent. The presence of metasedimentary and granitic xenoliths in the volcanic rocks, and the granitic provenance of the basin-filling sediments, indicate that the supracrustal pile was formed on continental crust. The basaltic rocks are tholeiitic, with flat REE profiles (10x chondrite), and low Mg#, and are believed to have evolved by fractional crystallization of komatiitic parents in large, shallow, subcrustal magma chambers. The late-stage basaltic andesites and andesites have high Mg, Ni, Cr and Zr and low Ti, V and Y contents, as well as high LREE abundances (100x chondrite) and it is proposed here that they have formed by fractional crystallization of a komatiitic parent combined with assimilation of a tonalitic crustal contaminant. The La Grande

greenstone belt is considered to have been a westwardly propagating continental rift in which the initial subsidence recorded by the supracrustal succession was the result of lithospheric thinning.

SOMMAIRE

Les vestiges d'un rift continental d'âge Archéen sont préservés dans la séquence plissée et faillée de roches volcanosédimentaires dans la partie centrale de la bande de roches vertes de la Grande. La base de cette succession est masquée par la mise en place d'intrusions syntectoniques de composition tonalitique. Une séquence de sédiments clastiques et de volcanoclastiques, déposée en milieu marin peu profond, est recouverte d'un important empilement de basaltes, en grande partie, et d'andésites basaltiques, épanchés sur de grandes plaines sous-marines. Alors que des sédiments clastiques grossiers, dont la source est localisée à l'ouest, s'accumulaient sur l'empilement volcanique pour former un cône de déjection sous-marin, des formations de fer se formaient dans les parties plus profondes du bassin. Des andésites basaltiques tardives, ainsi que les sédiments et volcanoclastiques associés, furent déposés en eau peu profonde lors d'une période d'émergence locale du bassin. La présence de xénolithes d'origine métasédimentaire et granitique dans les dépôts volcaniques, ainsi que l'origine granitique des sédiments qui comblent le bassin, suggèrent que la succession volcanosédimentaire fut accumulée sur une croûte continentale. Les roches basaltiques tholéïtiques, montrent des patrons de REE plats (10 x chondrite) et des rapports $Mg/Mg+Fe(t)$ peu élevés, suggérant qu'ils dérivent de liquides parentaux de composition komatiitiques par un processus de cristallisation fractionnée ayant pris place dans de vastes chambres magmatiques situées à

de faibles profondeurs. Les andésites et andésites basaltiques tardives montrent des valeurs élevées en Mg, Ni, Cr, Zr et HREE (100 x chondrite) et de basses valeurs en Ti, V, et Y et semblent être le produit d'un processus combiné de cristallisation fractionnée à partir d'un liquide parental komatiitique et de l'assimilation d'un contaminant de composition tonalitique. La bande de roches vertes de La Grande est finalement interprétée comme représentant un rift continental se propageant vers l'ouest, pour lequel la subsidence initiale, dont la séquence volcano-sédimentaire est le témoin, fut le résultat d'un amincissement de la lithosphère.

Acknowledgements

Andrew Hynes initiated this project and I have had the great pleasure of having had his full support, attention and guidance throughout the course of this work. I am grateful to Don Francis for providing constructive criticism on many aspects of this work. I have greatly benefited in having had the privilege to work closely with Karen Stamatelopoulou-Seymour, Benoit Rivard and Mian Liu. I will always have fond memories of the adventures in northern Quebec I shared during the summer of 1983 with my assistant Leonard Valensky and our colleagues Benoit Rivard, James Brennan, Sharon Baillie, Mian Liu, Karen Stamatelopoulou-Seymour and Francine Robert. I have greatly enjoyed discussing aspects of my work as well as topics more diverse in a smoke-filled seedy Portugese bar on St. Lawrence street in the early hours of Tuesday mornings with Jim Clark, Bob Linnen, Bob Wares (whenever his wife would let him go out!) Serge Nadeau (the only igneous petrologist in the bunch) and George Cutter (whenever we could tear him away from some obscure journal on statistical mechanics or the like). I would like to thank Benoit Rivard, Christine Payette and Anne Charland for helping me with French translations. A special thanks is extended to all my colleagues at McGill who have made my stay there a stimulating experience including Greg Eiché, John Gartner, André Lalonde and Karin Olson. I am grateful to Tariq Ahmedali for his active interest and advice in the geochemical work and to Richard Yates for his advice and services as departmental draftsman and photographer. I am thankful to John

Ludden and the staff at the GINNA lab for their interest in my work and for providing me with the use of their INAA facilities. This research has been supported by NSERC, FCAC and EMR grants to Andrew Hynes and Don Francis and support from the Carl Rheinhardt Fund to Thomas Skulski. The field work was aided by SDBJ and SEBJ and I am grateful to the individuals in these organizations for their help. Finally I would like to thank my family and France Peloquin for all of their help in my studies and I dedicate this thesis to them.

Table of Contents

Chapter	page
1	Introduction and Statement of the Problem.....1
1.1	Introduction.....1
1.2	Statement of Problem.....6
2	Regional Setting and Geology of the LG-3 area.....8
2.1	Regional Setting of the La Grande Greenstone Belt..8
2.2	Access, Physiography and Previous Work in the LG-3 Area.....13
2.3	Geological Setting of the LG-3 Segment and the Lac Coutaceau Dykes.....15
2.3.1	Local Setting and General Stratigraphy.....15
2.3.2	Structural History.....17
2.3.3	Metamorphism and Secondary Alteration.....31
3	Field Relations and Petrography.....35
3.1.1	Unit 1 Volcanoclastics and Metasediments, Field Relationships.....35
3.1.2	Petrography of the Lower Volcanoclastics and Metasediments.....37
3.2.1	Unit 2 First-Cycle Volcanics, Field Relationships..38
3.2.2	Petrography of the First-Cycle Volcanics.....43
3.3.1	Unit 3 Metasediments, Field Relationships.....47
3.3.1.1	Siltstone-Sandstone Facies.....48
3.3.1.2	Conglomerate Facies.....51
3.3.1.3	Banded Iron Formation Facies.....53
3.3.2	Petrography of the Metasediments.....53
3.3.3	Paleocurrents.....58
3.4.1	Unit 4 Second-Cycle Volcanics, Field Relationships.61
3.4.2	Petrography of the Second-Cycle Volcanics.....63
3.5.1	Intrusive Rocks, Field Relationships.....65
3.5.2	Petrography of the Intrusive Rocks.....68
4	Facies Associations, Paleoenvironment, Paleogeography and Provenance.....74
4.1.1	Lower Volcanoclastics and Metasediments.....74
4.1.2	Provenance of the Lower Volcanoclastics and Metasediments.....75
4.2	First-Cycle Volcanics.....75
4.3.1	Metasediments, Facies Association.....78
4.3.2	Provenance of the Metasediments.....87
4.4	Second-Cycle Volcanics.....90
4.5	Summary.....90
5	Geochemistry of the Volcanic and Synvolcanic Intrusive Rocks.....94
5.1	Introduction.....94
5.2	The First-Cycle Volcanics.....94
5.3	Second-Cycle Volcanics and the Lac Coutaceau Dykes.....114

Table of Contents (continued)

chapter		page
6	Petrogenesis of the Volcanic and Synvolcanic Intrusives.....	132
6.1	Introduction.....	132
6.2.1	Petrogenesis of the First-Cycle Volcanics.....	132
6.2.2	The First-Cycle Volcanics and Mafic Magmatism in the La Grande Greenstone Belt.....	141
6.3.1	Petrogenesis of the Second-Cycle Volcanics and the Lac Coutaceau Dykes.....	156
7	The Tectonic Evolution of the La Grande Greenstone Belt.....	167
7.1	Archean Tectonics.....	167
7.2	The Tectonic Setting of the La Grande Greenstone Belt.....	169
7.3	A Model of Passive Rifting in the La Grande Greenstone Belt.....	172
8	Conclusions.....	181
8.1	Summary and Conclusions.....	181
8.2	Recommendations for Future Work.....	183
	References.....	185
	Appendix A: Analytical Methods, Sampling Criteria and Preparation.....	A1
	Appendix B Whole Rock Chemistry, Sample Location and Modal Composition of Granitic Intrusives.....	B1
	First-Cycle Volcanics.....	B1
	Second-Cycle Volcanics.....	B6
	Lac Coutaceau Dykes.....	B7
	Modal Composition of Granitic Intrusives.....	B9
	Sample Location Map.....	B10
	Petrography of analysed samples.....	B11
	Appendix C Plates.....	C1
	Appendix D Geological Map of the LG-3 Area.....	pocket

List of Figures**Page**

- Figure 1 Location map and geology of the La Grande greenstone belt (after Avramtchev, 1982).....9
- Figure 2 Poles to bedding (So), intersection lineation (L1, So \wedge S1) and minor folds (F1) in unit 3 Metasediments.20
- Figure 3 Poles to S1 in the First-Cycle Volcanics (a) south and (b) north of the Chain Lakes Fault.....23
- Figure 4 L2 intersection lineations (S2 \wedge S1, contoured) and F2 minor fold axes (crosses) measured in units 1-3....26
- Figure 5 F2 minor folds measured in the Metasediments north of the Chain Lakes fault.....28
- Figure 6 Poles to S2 fracture cleavage in units 1 and 2 south of the Chain Lakes fault.....29
- Figure 7 D2 structural model showing the relationship between the Chain Lakes fault and the S2 fabric.....30
- Figure 8 Classification of arenites in the Metasediments north of the Chain Lakes fault.....56
- Figure 9 Measured stratigraphic section in the Metasediments south of the chain Lakes fault. The location of the section is shown in Fig. 11.....60
- Figure 10 Measured stratigraphic section in the Metasediments exposed north of the Chain Lakes fault.....82
- Figure 11 Facies map of the unit 3 Metasediments.....83
- Figure 12 Paleogeographic and depositional model for the Archean supracrustal succession in the central part of the La Grande belt.....93
- Figure 13 (a) Zr/Y and (b) Mg/Mg+Fe (Mg#) versus Zr (ppm) for the First-Cycle Volcanics.....97
- Figure 14 (a) Si, (b) Ti, (c) Al, (d) Fe, (e) Mg, (f) Ca, (g) Na and (h) K (all in cations%) versus Zr (ppm).....100
- Figure 15 (a) Mg versus Fe, (b) Ti versus Mg and (c) Al versus Si (all in cation%) for the First-Cycle Volcanics..104
- Figure 16 (a) Ni, (b) Sr, (c) P, (d) Cr, (e) V, (f) Y and (g) Sc versus Zr (all in ppm) for the First-Cycle Volcanics.....107
- Figure 17 Chondrite normalized REE in the First-Cycle

List of Figures (continued)	page
Volcanics.....	109
Figure 18 (a) $(La/Sm)_n$ and (b) $(La/Yb)_n$ versus $(La)_n$ in the First-Cycle Volcanics and Lac Goyer komatiites.....	111
Figure 19 (a) Si, (b) Ti, (c) Al, (d) Fe, (e) Mg, (f) Ca, (g) Na and (h) K (all in cation%) versus Zr (in ppm) for the Second-Cycle Volcanics and Lac Coutaceau dykes.....	116
Figure 20 (a) Mg versus Fe, (b) Ti versus Mg and (c) Al versus Si (all in cation%) for the Second-Cycle Volcanics and Lac Coutaceau dykes.....	120
Figure 21 (a) Ca, (b) Al and (c) Si versus Mg (all in cation%) for the Second-Cycle Volcanics and Lac Coutaceau dykes.....	122
Figure 22 (a) Y, (b) Cr, (c) Ni and (d) Sc versus Zr (all in ppm) for the Second-Cycle Volcanics and Lac Coutaceau dykes.....	125
Figure 23 Chondrite normalized REE in the Second-Cycle Volcanics and Lac Coutaceau dykes.....	127
Figure 24 (a) Zr/Y versus Zr (all in ppm), (b) $(La/Yb)_n$ versus $(La)_n$ and (c) $(La/Sm)_n$ versus $(La)_n$ for the Second-Cycle Volcanics and Lac Coutaceau dykes.....	129
Figure 25 Results of Rayleigh fractional crystallization model calculations for Fe-enrichment in the basalts of the First-Cycle Volcanics.....	140
Figure 26 (a) clinopyroxene and (b) plagioclase projections in the isomolar haplobasaltic quaternary system plagioclase, olivine, silica and clinopyroxene for the First-Cycle Volcanics.....	143
Figure 27 (a) Mg versus Fe, (b) Ti versus Mg and (c) Si versus Mg (all in cation%) for lavas of the First-Cycle Volcanics and lavas and intrusives from other parts of the La Grande greenstone belt.....	147
Figure 28 (a) Ca versus Mg, (b) Al versus Mg and (c) Al versus Si (all in cation%) for lavas of the First-Cycle Volcanics and lavas and intrusives from other parts of the La Grande greenstone belt.....	149
Figure 29 (a) Ti/Zr and (b) Zr/Y versus Zr (ppm) for lavas of the First-Cycle Volcanics and from other parts of the La Grande greenstone belt.....	151
Figure 30 Results of the assimilation fractional crystallization calculation, komatiite + rhyolite = OPX	

List of Figures (continued)

page

+ CPX + PLAG + Andesite (Second-Cycle lava).....164

**Figure 31 The results of instantaneous lithospheric
thinning calculations.....176**

List of Tables

Page

Table 1 Lithostratigraphic Units of the La Grande Greenstone Belt (after Fouque et. al., 1979).....10

Table 2 Modal Composition of Selected Arenites in the Metasediments.....55

Table 3 Comparison of Analyses, First-Cycle Volcanics.113

Table 4 Comparison of Analyses, Second-Cycle Volcanics.131

Table 5 Fractional Crystallization Calculation, Fe-Enrichment in the First-Cycle Volcanics High-Mg Basalt = Fe-Rich Basalt + PLAG + OLIV + CPX.....135

Table 6a (Model 1) Rayleigh Fractional Crystallization Calculation (Trace Elements) Fe-Enrichment in the First-Cycle Volcanics High-Mg Basalt = Fe-Rich Basalt + PLAG + OLIV + CPX.....137

Table 6b (Model 2) Rayleigh Fractional Crystallization Calculation (Trace Elements) Fe-Enrichment in the First-Cycle Volcanics High-Mg-Basalt + Fe-Rich Basalt + PLAG + OLIV + CPX.....138

Table 7 Assimilation Fractional Crystallization Model Using a Least-Squares Mixing Calculation for the Second-Cycle Volcanics Komatiite + Rhyolite (Contaminant) = Andesite + OPX + CPX + PLAG.....160

Table 8 Assimilation Fractional Crystallization Calculation using the DePaulo Equation Komatiite + Rhyolite (Contaminant) + Andesite + OPX + CPX + PLAG.....162

Table 9 Parameters Used in the Calculations.....178

List of Plates *

page

Plate 1 Deformed (D1) conglomerates in the Metasediments north of the Chain Lakes Fault.....C2

Plate 2 Folded (F1) siltstones in the Lower Volcanoclastics and Metasediments.....C2

Plate 3 Minor faults (D2) in the Lower Volcanoclastics and Metasediments.....C2

Plate 4 F2 folds in the Lower Volcanoclastics and Metasediments.....C2

Plate 5 F2 box folds in the Second-Cycle Volcanics.....C2

Plate 6 Mafic crystal tuff in the Lower Volcanoclastics.....C2

Plate 7 Bomb-sags in the Lower Volcanoclastics and Metasediments.....C2

Plate 8 Banded iron formation in the Lower Volcanoclastics and Metasediments.....C2

Plate 9 Conglomerates in the Lower Volcanoclastics and Metasediments.....C4

Plate 10 Pillowed basalts in the First-Cycle Volcanics..C4

Plate 11 Plagioclase megacrysts and glomerocrysts in pillow basalts from the First-Cycle Volcanics.....C4

Plate 12 GMP gabbro sills in the First-Cycle Volcanics..C4

Plate 13 Metasedimentary xenoliths in a gabbro sill in the First-Cycle Volcanics.....C4

Plate 14 Xenoliths in gabbro sills from the Lac Guyer area.....C4

Plate 15 Normally graded siltstone-sandstone facies rocks in the Metasediments.....C4

Plate 16 Rhythmically bedded siltstones and sandstones in the Metasediments.....C4

Plate 17 Siltstone-Sandstone and Conglomerate facies rocks in the Metasediments.....C6

Plate 18 Parallel laminated and trough-type crosbedding

* All plates are in Appendix C

List of Plates (continued)	page
in the Metasediments.....	C6
Plate 19 Large-scale trough crossbeds in the Metasediments.....	C6
Plate 20 Tonalite boulders in conglomerates in the Metasediments.....	C6
Plate 21 Channeling of conglomerates into underlying sandstones, Metasediments.....	C6
Plate 22 BIF clasts in an orthoconglomerate in the Metasediments.....	C6
Plate 23 Debris flow sub-facies conglomerates in the Metasediments.....	C6
Plate 24 Shale/siltstone rip-up clasts in the Metasediments.....	C6
Plate 25 Banded iron formation facies of the Metasediments.....	C8
Plate 26 Xenoliths in gabbro sills in the Second-Cycle Volcanics.....	C8
Plate 27 Sandstone dykes in the Second-Cycle Volcanics.....	C8
Plate 28 Epiclastic sandstones in the Second-Cycle Volcanics.....	C8
Plate 29 Intrusive contact of a syntectonic pluton.....	C8
Plate 30 Lac Coutaceau dyke intrusive into a tonalite pluton.....	C8
Plate 31 Lac Coutaceau dyke with basaltic xenolith.....	C8
Plate 32 Photomicrograph of the chilled margin of a pillowed basalt, First-Cycle Volcanics.....	C10
Plate 33 Photomicrograph of plagioclase phenocrysts in the chilled margin of a pillow basalt in the First-Cycle Volcanics.....	C10
Plate 34 Pyroxene phenocrysts in the chill margin of pillow basalts in the First-Cycle Volcanics.....	C12
Plate 35 Photomicrograph of a basaltic andesite in the First-Cycle Volcanics.....	C12
Plate 36 Photomicrograph of a diabasic gabbro from the First-cycle Volcanics.....	C14

List of Plates (continued)

page

Plate 37 Photomicrograph of a subarkose in the Metasediments.....C14

Plate 38 Photomicrograph of a norite in the Second-Cycle Volcanics.....C16

Plate 39 Photomicrograph of a norite in the Second-Cycle Volcanics.....C16

Chapter 1 Introduction and Statement of the Problem

1.1 Introduction

The record of Archean tectonic and magmatic activity is preserved in part in granite-greenstone terranes. These terranes consist predominantly of granitoid plutons and tonalitic gneisses that contain infolds of supracrustals known as greenstone belts. Although the oldest known greenstone belts are 3.4-3.8 Gyr. (eg. Isua, Greenland, Moorbath, 1975; Sebakwian Group, Zimbabwe, Wilson et al., 1978; Barberton, South Africa, Barton et al., 1981) most appear to have formed in the period 2.6-2.7 Gyr. (eg. Superior Province, Canada, Goodwin et al., 1972). Granite-greenstone terranes dominate the Archean provinces of North America, southern Africa and western Australia.

Greenstone belts are commonly intruded by, or in faulted contact with, younger granitoid plutons. Some greenstone belts, however, unconformably overlie older basement rocks (eg. Pongola Supergroup, South Africa, Mathews, 1967; Upper Greenstones, Zimbabwe, Bickle et al., 1975; Yellowknife Supergroup, Canada, Frith et al., 1977).

Archean greenstone belts are commonly preserved as synformal 'keels' with linear or cusped structural trends and large length-to-width ratios. Their metamorphic grade is typically greenschist but may attain amphibolite facies near

contacts with plutons (Jolly, 1980). The overall structure of many greenstone belts appears to have been controlled by vertical tectonic processes associated with the emplacement of syntectonic granitoid plutons (Condie, 1980). Some greenstone belts, however, have undergone early phases of deformation that are dominated by horizontal tectonic processes including thrust faulting, recumbent folding and the emplacement of nappe structures (e.g. Barberton Mountain Land, Ramsay, 1965; Pilbara, Western Australia, Bickle et al., 1980; Williams et al., 1979).

The oldest volcanic rocks in greenstone belts are commonly interpreted to have been erupted in submarine environments, whereas extrusive rocks at higher levels in many successions have field characteristics suggestive of subaerial emplacement. The lower stratigraphic successions preserved in greenstone belts are dominated by tholeiitic basalts and komatiites such as those found in the Abitibi belt of Canada (Dimroth et al., 1982). Tholeiitic basalts are commonly intercalated with, or replaced by, volcanic rocks of calc-alkaline affinity at higher levels within the supracrustal pile (Jolly, 1975, 1980; Thurston et al., 1983). The ratio of komatiitic to calc-alkaline volcanic rocks generally decreases up section. Volcanic rocks of alkaline affinity are relatively rare in Archean successions and are generally found at the highest levels of the supracrustal pile, unconformably overlying tholeiites and calc-alkaline volcanic rocks (e.g. Bijou Point, Ontario, Smith et al., 1974; Oxford Lake, Manitoba, Brooks et al., 1982).

Sedimentary rocks are found throughout greenstone successions. However, the largest accumulations are generally in the upper levels. They are predominantly clastic rocks such as immature lithic arenites, arkoses, siltstones and conglomerates. Mature clastic sedimentary rocks, such as orthoquartzites, are comparatively rare in Archean greenstone belts. Chemical sediments found in greenstone belts include, in decreasing order of abundance: banded iron formation, dolomites, and evaporites. Formation of many greenstone belts was followed by the development of sedimentary basins (e.g. the Timiskaming Group, Abitibi belt, Canada, Dimroth et al., 1982; and other examples referenced in Bickle et al., 1982).

A variety of depositional environments has been documented in Archean greenstone successions. These include fluvial (braided stream and alluvial fan) (Sioux Lookout, Canada, Turner et al., 1973), and submarine fan complexes, (Pilbara, Western Australia, Eriksson, 1981). In the Pilbara of Western Australia, Eriksson (op. cit.) has demonstrated an abrupt transition from terrigenous (braided alluvial) to marine (submarine fan) sediments without any shallow marine facies, thus suggesting a narrow continental shelf. Similar transitional terrigenous-to-marine successions have been described in a number of other greenstone belts (e.g. Mahitou Lookout, Canada, Walker et al., 1971; Sioux Lookout, Turner et al., 1973; Barberton Mountain Land, Eriksson, 1980). In the Barberton Mountain Land an initial steep-rift margin (abrupt terrigenous-to-marine facies

transition) was succeeded by the development of a shelf-rise margin with a well developed continental shelf upon which extensive deltaic, barrier beach and tidal flat sediments accumulated (Eriksson, 1978, 1980).

Many models have been proposed to explain the origin and evolution of Archean greenstone belts. Classical models of Archean crustal evolution, including density inversion models, (MacGregor, 1951) and mantle convection models (Fyfe, 1974, Williams, 1977) and models which treat greenstone belts as Archean analogues of modern oceanic crust (Glikson, 1971, 1972; Glikson et al., 1976; and Goodwin et al., 1970), have been reviewed elsewhere (e.g. Windley, 1977; Condie, 1981).

Continental-rift tectonic settings have been proposed for a number of greenstone belts which have sedimentary contacts with underlying sialic basement, as well as those belts which are believed, based on the provenance of their sediments, to have formed close to, if not directly on continental crust (e.g. Barberton, Eriksson, 1980). Some of the earliest rift models, which do not address the actual mechanism of rifting, include those of Anhaessler (1971), and Windley (1973). Hunter (1974) and Condie and Hunter (1976) have proposed that continental rifting in the Archean may have been initiated by upwelling mantle plumes. Mantle plume models are appealing in that they provide a mechanism to initiate rifting, as well as a means of generating komatiites by multistage melting (Arndt, 1977). These

models require that subsidence occurs as a result of isostatic compensation due to the erosion of the continental crust associated with an early phase of domal uplift.

A passive model of continental rifting has been formulated by McKenzie (1978) to explain the evolution of sedimentary basins formed in continental settings. This model entails two stages of subsidence. The initial subsidence is in response to immediate isostatic adjustments associated with thinning of the continental crust. The second stage of subsidence, termed thermal subsidence (Royden et al., 1980), is a result of isostatic compensation associated with density increases that occur with conductive cooling and thickening of the lithosphere. McKenzie et al. (1980), Bickle et al. (1982) and Misbet (1984a, 1984b) have suggested that this model could explain the evolution of Archean volcano-sedimentary basins that are unconformably overlain by sediment-dominated basins (such as the Belingwe greenstone belt, Zimbabwe; Witwaterstrand and Transvaal, South Africa). The early-formed volcanic-dominated successions would have formed during periods of initial subsidence when the heat flow was high, whereas overlying sedimentary basins may have formed during the period of thermal subsidence (Bickle et al., 1982).

Some workers have appealed to a marginal-basin model for Archean granite-greenstone terranes (Tarney et al., 1977, Windley, 1977). Tarney et al. (op. cit.) have suggested that the Cretaceous Rocas Verdes complex of southwestern Chile, a

fossil marginal basin, has an overall tectonic setting and a record of magmatism that closely parallels that found in granite-greenstone terranes.

Some Archean greenstone belts have features comparable with modern island arcs (Langford et al., 1976). Dimroth et al. (1982, 1983a, 1983b) have suggested on the basis of structure, igneous petrochemistry, paleoenvironment and paleogeography that the Abitibi belt may be an Archean analogue of a modern arc-forearc complex. The Internal northern and External southern Zones are believed to represent the main arc complex and the forearc terrane respectively. The External Zone is believed, on the basis of isostatic arguments, to have been emplaced on oceanic crust, whereas the Internal Zone may have been formed on either thinned continental or oceanic lithosphere (Dimroth et al., 1984). The Internal Zone is believed to have been subsequently underplated by shallow level calc-alkaline plutons (Dimroth et al., *ibid.*)

Choice between these models must be based on all the available geological and geophysical data for a given greenstone belt. Given the complexities of individual greenstone belts and the large time span involved between various granite-greenstone forming episodes, it is unlikely that one model applies to all belts.

1.2 Statement of the Problem

This thesis addresses a number of aspects of Archean crustal evolution in the La Grande greenstone belt of central Quebec. A transect in the central portion of this belt provides the main data base for an interpretation of the tectonic setting and magmatic evolution of the volcano-sedimentary succession and plutonic rocks. The first part of this thesis deals with the overall setting of the belt, stratigraphic relationships of the central segment, petrography and field relationships of the various lithologies, and the structural and metamorphic history. A paleoenvironmental and paleogeographic reconstruction of the central segment is then presented. The second part of this thesis concerns the geochemistry of the volcanic rocks and synvolcanic intrusives and the nature of the physical and chemical processes that controlled their evolution. Finally, a preliminary tectonic model of the pre-deformational evolution of the belt is proposed, and a number of tests of this model are suggested for future investigations.

Chapter 2 Regional Setting and Geology of the LG-3 Area

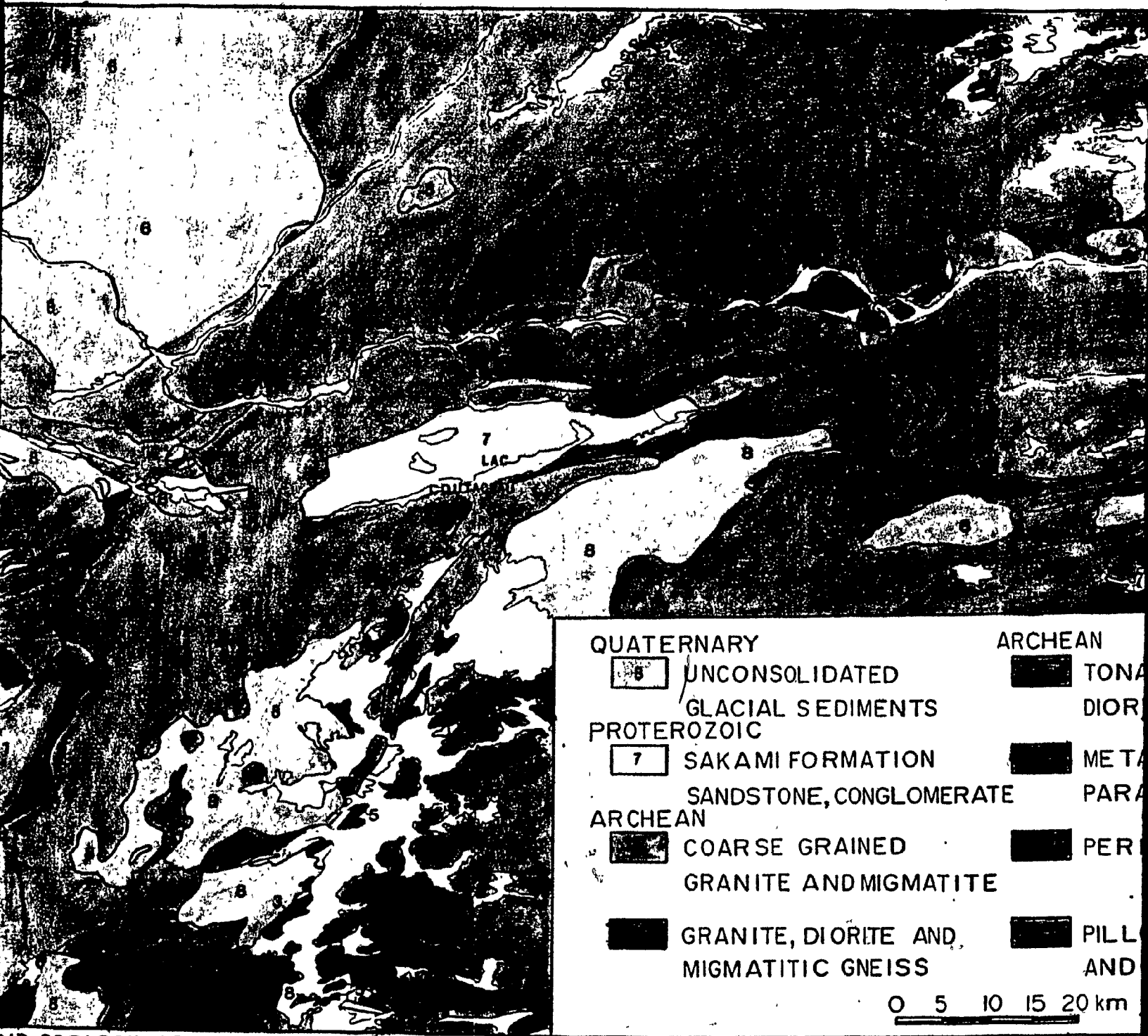
2.1 Regional Setting of the La Grande Greenstone Belt

The Archean La Grande greenstone belt consists of a series of NE to ENE to E trending synforms of volcano-sedimentary rocks that extend eastward from James Bay some 450 km toward central Québec (Fig. 1). Radiometric ages (K/Ar) determined on biotite and muscovite separates of volcano-sedimentary rocks from the GrandeBaleine River area (Fig. 1) give a mean age of 2500 ± 125 Ma for two samples (Lowdon, 1960; Eade, 1966). Eade has suggested that this age determination and those determined on granitoid intrusives and gneisses (Eade op. cit., units 1-6) indicate that the last phase of metamorphism to reset the K/Ar isotopic system was at approximately 2500 Ma (Kenoran orogeny). Regional mapping of the La Grande greenstone belt includes the work of Eade et al. (1957) and Eade (1966) (at a scale of 1:500,000); Fouque et al. (1979) (1:250,000); Sharma (1977) (1:100,000); Avramtchev (1983) (1:250,000); and Ciesielski (1984) (1:250,000).

Fouque et al. (1979) divided the rocks of the La Grande area into eleven lithostratigraphic units (Table 1). They divided the lowermost unit, which comprises the greenstone succession, into two cycles. The first-cycle is comprised of mafic volcanic rocks, including massive and pillowed basalts, and intercalated mafic tuffs, and may contain banded iron formation near its top. The second-cycle, which they tentatively



FIGURE 1 LOCATION MAP AND GEOLOGY OF THE LA GRANDE GREENSTONE



GEOLOGY OF THE LA GRANDE GREENSTONE BELT (AFTER AVRAMTCHEV, 1982)



QUATERNARY

8 UNCONSOLIDATED
GLACIAL SEDIMENTS

PROTEROZOIC

7 SAKAMI FORMATION
SANDSTONE, CONGLOMERATE

ARCHEAN

8 COARSE GRAINED
GRANITE AND MIGMATITE

8 GRANITE, DIORITE AND
MIGMATITIC GNEISS

ARCHEAN

8 TONALITE, GRANODIORITE
DIORITE AND GRANITE

8 METASEDIMENTS, BIOTITE
PARAGNEISS, MIGMATITE

8 PERIDOTITE AND GABBRO

8 PILLOW BASALT, SEDIMENTS,
AND VOLCANOCLASTICS

0 5 10 15 20 km

GREENSTONE BELT (AFTER AVRAMTCHEV, 1982)

Table 1 Lithostratigraphic Units of the La Grande Greenstone Belt (after Fouque et. al., 1979)

Proterozoic.....n....Diabasic-textured gabbro

Early Helikien.S....Sakami Formation

SERIE LAGUICHE AND ASSOCIATED GRANITIZATION

Early Aphebian
or Archean..... γ 3...Post Tectonic Granite

..... γ 2...Leucocratic Granite and Pegmatite

..... μ 2...Migmatites and Granitic Migmatite

..... ϵ 2...Amphibole-Biotite Paragneiss

-----DISCORDANCE-----

SERIE DES VIEUX GNEISS

Archean..... μMigmatitic Gneiss and Migmatite

Undifferentiated

..... γ 1...Foliated Granodiorite-Diorite (Anatectic ?)

..... μ 1...Migmatites-Gneiss, Orthogneiss (Granitic,
Granodioritic)

.....VS...Basic and Acidic Volcanic and Volcano-
Sedimentary Units. Biotite-Amphibole Schists
Amphibole Gneiss, Andesite-basalt, Quartzite
, Arkose, Conglomerate

-----DISCORDANCE (?)-----

FIRST-CYCLE

.....RV...Silts, Tuff, Pillow Lava, Intermediate-
Felsic Flows, Conglomerate

-----DISCORDANCE (?)-----

SECOND-CYCLE

.....RV...Iron Formation, Mafic Tuff-Mafic Lava,
Ultramafic Lava

suggested may be discordant with the first, is comprised of polymict paraconglomerates overlain by finer-grained sedimentary rocks and mafic, intermediate and rare felsic volcanic and volcanoclastic rocks.

Stamatelopoulou-Seymour (ms. in prep., 1985) has erected a detailed stratigraphy of the Archean volcano-sedimentary succession in the vicinity of Lac Guyer (Fig. 1). The lower units in this area consist of a succession of clastic sedimentary rocks overlain by rhyodacites and felsic volcanoclastic rocks. This lower unit is overlain by a thick succession of massive and pillowed basalts which are in turn overlain by a sequence of pillowed peridotitic, pyroxenitic and basaltic komatiites. The third and uppermost unit in the Lac Guyer area is a sequence of pillowed and massive basalts.

Liu (1985) has established a stratigraphy in the supracrustal succession southeast of Lac Guyer (Fig. 1). In this area, mafic volcanoclastic rocks are overlain by pillowed and massive basalts with thin lenses of mafic volcanoclastics intercalated amongst the lower flows. The basalts are overlain by pillowed and massive komatiites and in turn by an upper succession of basalts.

Komatiitic rocks are restricted to the eastern part of the La Grande greenstone belt (Avramtchev, 1983; Liu, 1985). These rocks appear to exist at both the base and near the top of the successions in the vicinity of Lac Guyer.

At least three sets of folds are evident in the Archean supracrustal sequence (Grenon et al., 1977; Fouque et al., 1979; Stamatiopoulou-Seymour, 1982). The first set is rarely preserved and is characterized by microscopic, isoclinal intrafolial folds that are penecontemporaneous with amphibolite-facies regional metamorphism. The second set is characterized by mesoscopic isoclinal folds that are moderately plunging toward the N and S, and are accompanied by a pronounced ENE striking, steeply north-dipping, axial-planar schistosity. The third set is most evident in well foliated lithologies, and is characterized by kink-banding associated with intrafolial shearing and shearing transverse to the foliation.

Two major phases of brittle deformation have been recognized in the La Grande greenstone belt (Fouque et al., 1979): The Serie Laguiche is separated from the Vieux Gneiss (Table 1) by a well-defined lineament which trends N 70° and is evident in satellite imagery (ERTS) (Fouque et al., op cit.; Schumacher et al., 1978). This lineament is believed to represent a sinistral shear zone which defines the margins of the various Sakami sedimentary basins. Fouque et al. (op. cit.) have suggested that the Proterozoic Sakami basins were formed as pull-apart structures. A second phase of brittle deformation resulted in transverse conjugate faults that trend N 20-40° and N 140-160°. These late-stage faults postdate the emplacement of a Proterozoic diabasic gabbro swarm.

A number of workers have investigated the petrology and petrogenesis of the volcanic and intrusive rocks in the La Grande Greenstone Belt. Stamatelopoulou-Seymour (1982, 1983, ms. in prep., 1985) has studied the petrogenetic history of the basalt-komatite and rhyodacite-granodiorite association in the Lac Guyer area. Liu (1985) has investigated the petrogenetic history of basaltic and komatiitic rocks as well as the progressive migmatization of biotite gneisses in the area southeast of Lac Guyer. Rivard et al. (1984, 1985) have studied the petrogenesis of basalts, gabbros, and peridotites in the western part of the La Grande greenstone belt and compared these with the available data from other parts of the La Grande belt. Skulski et al. (1984) have investigated the stratigraphy and petrogenesis of basalts in the central part of the La Grande greenstone belt. Regional models of the tectonic and magmatic evolution of the La Grande greenstone belt have been presented by Liu (1985) and Skulski et al. (1985).

2.2 Access, Physiography and Previous Work in the LG-3 Area

The present study is based on detailed mapping (1:10,000 scale, summer 1983) and sampling of a 45 square km area in the central portion of the La Grande greenstone belt in the vicinity of the LG-3 hydropower station (latitude 53° 39' - 53° 42' N, longitude 76° 05' - 76° 57' W, (Fig. 1). This study also treats a number of samples provided by A. Hynes, that were collected some 25 km to the WSW of the study area along the shores of the LG-2

reservoir (Fig. 1). The LG-3 area is located approximately 450 km north of Matagami, Quebec, and is located within the territorial limits of La Société de Développement de la Baie James (Hydro Québec). Access is by road from Matagami or by plane to the LG-3 airport.

The topography of the LG-3 area is characteristic of a heavily glaciated terrane, as evidenced in the multitude of lakes and swamps (Sharma, 1977). The topography is subdued in areas of predominantly volcanoclastic and sedimentary rocks, such as in the northern and central portions of the map area (Appendix D). In those regions dominated by plutonic and volcanic rocks, (as in the central and western parts of the map area) the topography is rugged and abrupt elevation changes on the order of 165 m can occur. Surface exposure is approximately 30 % in this area. However, recent construction activity has also created excellent roadcuts.

In addition to the regional mapping of the La Grande belt, part of the the LG-3 area has been mapped by Ekstrom (1960) at a scale of 1:57,000. In the early seventies the area was mapped at a scale of 1:50,000 (LaRose, 1975) for the purpose of delimiting uranium mineralization at the base of the Proterozoic Sakami Formation. Drillhole data and geology of the TA-26A and B dam sites on the shores of the LG-3 reservoir (Appendix D) are reported in a 1:2,400 scale map prepared by Tremblay (1982) for the Société d'Énergie de la Baie James. The geology of the LG-3

area has also been discussed in a regional study by Ciesielski (1984). Aeromagnetic maps of the LG-3 area include a 1:31,680 scale map included in a mineral assessment report by Eckstrom (1960), as well as 1:50,000 maps by the Department of Energy, Mines and Resources, Canada and the Department of Natural Resources, Quebec (now known as Ministère de l'Énergie et des Ressources).

2.3 Geological Setting of the LG-3 Segment and the Lac Coutaceau Dykes

2.3.1 Local Setting And General Stratigraphy

The central segment of the La Grande greenstone belt is predominantly ENE trending. However, in the vicinity of LG-3 the belt is arcuate about a composite pluton which intrudes the southern periphery of the greenstone succession (Fig. 1). Toward the SE the greenstone belt pinches out on the eastern limb of a large NNE plunging synform (Eckstrom, 1960; Eade, 1966; LaRose, 1975). The Lac Guyer segment of the La Grande belt appears to lie directly on strike with the eastern limb of this structure (Fig. 1).

In the LG-3 area the volcano-sedimentary succession represents the lowermost stratigraphic unit of Fouques et al. (1979), (unit R.V. Table 1). It may be subdivided into four stratigraphic units. These are, in stratigraphic order: unit 1, Lower Volcanoclastics and Metasediments; unit 2, First-Cycle

Volcanics; unit 3, Metasediments; and unit 4, Second-Cycle Volcanics. The maximum thickness of the exposed strata is approximately 4.6 km. This estimate ignores the possible effect of folding, which is invariably present in the well-stratified units. The base of the supracrustal succession is obscured by younger granitoid intrusives.

There are five suites of syntectonic intrusives in the LG-3 area: the Southern Composite pluton, Middle Tonalite pluton, Northern Tonalite, Northern Porphyritic Tonalite-Granodiorite, and porphyritic tonalite and trondjemite dykes and plugs (Appendix D). The concordance of structural fabrics between various plutons and the supracrustal succession they intrude indicates that these rocks are synchronous with the first phase of deformation.

Nine samples of fine grained diorite (Lac Coutaceau dykes) were collected by A. Hynes along the shores of the LG-2 reservoir WSW of the LG-3 area. These rocks occur as dykes that have mutual crosscutting relationships with local granodiorites that intrude the Archean supracrustal succession (Hynes, personal communication). Based on their similar modal compositions the granodiorites in the Lac Coutaceau area are assumed to be of similar age to the Northern Porphyritic Tonalite and Granodiorite in the LG-3 area.

The youngest intrusive bodies in the LG-3 area are

relatively fresh, diabasic-textured gabbro dykes of probable Proterozoic age. These dykes crosscut all structural fabrics and lithological units. The largest of these dykes strikes approximately ENE and can be traced from the extreme SW corner to the eastern limits of the map area on the shores of the LG-3 reservoir (Appendix D).

The youngest lithological unit in the area is the Proterozoic Sakami Formation. It consists of shallow-dipping to horizontal quartz arenites and conglomerate beds that unconformably overlie the Archean supracrustals in the east-central part of the map area, on the shores of the LG-3 reservoir (Appendix D). Reviews of the stratigraphic and sedimentological characteristics of this formation can be found in Eade (1966) and Fouque et al. (1979).

2.3.2 Structural History

The Archean supracrustal succession in the central part of the La Grande belt has been affected by two phases of deformation. The first phase of deformation (D1) accounts for the synclinal form of the greenstone belt and is contemporaneous with the first phase of metamorphism (M1). The second phase of deformation is characterized by strike slip faulting that has displaced earlier first-order D1 folds and appears to be associated with minor folding (F2) and a low-grade retrograde metamorphism (M2). There is no evidence of early intrafolial folds as suggested by Fouque et al. (1979), and Grenon et al.

(1977), and thus, the D1 and D2 events documented here probably correspond to the D2 and D3 events of these previous workers.

F1 folds are isoclinal folds of bedding surfaces (S0) and have a penetrative axial planar fabric (S1). The absence of any significant pre D1 event is suggested by the polarity in S0 surfaces as determined throughout the map area on the basis of pillow facing in volcanic rocks^{and} normal grading in the Lower Volcanoclastics and Metasediments, volcanoclastics of the First-Cycle Volcanics, and sandstones in the Metasediments and Second-Cycle Volcanics. F1 folds are observed on both a megascopic (wavelengths up to 4 km) and mesoscopic scale (wavelengths up to 5 m). The supracrustal succession has been folded into a large, first-order syncline (informally referred to as the Chain Lakes syncline) which is E-trending and NNE-plunging (ca. 50°, Appendix D). Both limbs dip approximately 70° N (Fig. 2a, b, Appendix D). The hinge zone of the Chain Lakes syncline is defined on the basis of a partial closure in the Metasediments and Second-cycle Volcanics in the western part of the map area (Appendix D), and in conglomerates in the Metasediments in the central part of the map area (Fig. 11). Conglomerates in the Metasediments in the hinge zone are highly deformed (Plate 1), and in the central part of the map area are overlain by siltstones in which the bedding has been transposed into the S1 cleavage.

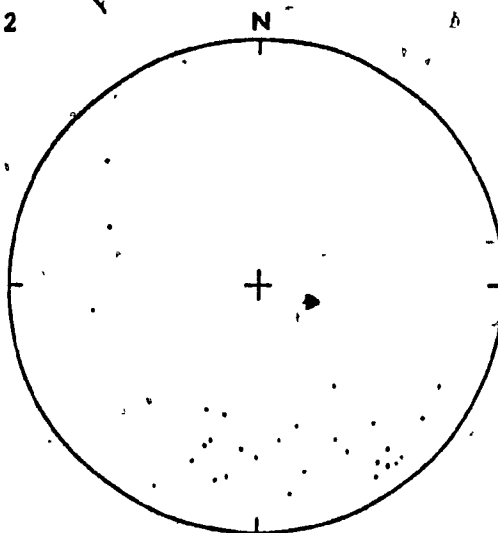
Smaller F1 macroscopic folds (wavelengths up to 150 m) are

Figure 2 Poles to bedding (S_0), intersection lineation (L_1 , $S_0 \wedge S_1$) and minor F_1 folds in Unit 3 Metasediments*. (a) S_0 north of the Chain Lakes Fault, (b) S_0 South of the Chain Lakes Fault and (c) L_1 in the Metasediments north of the Chain Lakes fault (dot) and south (small circle). Minor F_1 fold (cross) was measured north of the Chain Lakes fault.

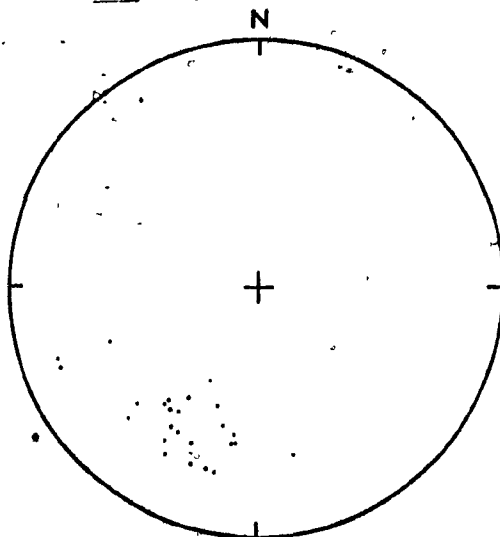
*Figures 2-6 (inclusively) are equal area, lower hemisphere projections.

Figure 2

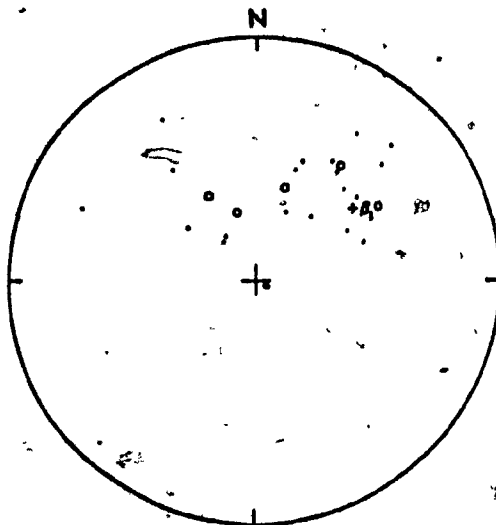
(a)



(b)



(c)

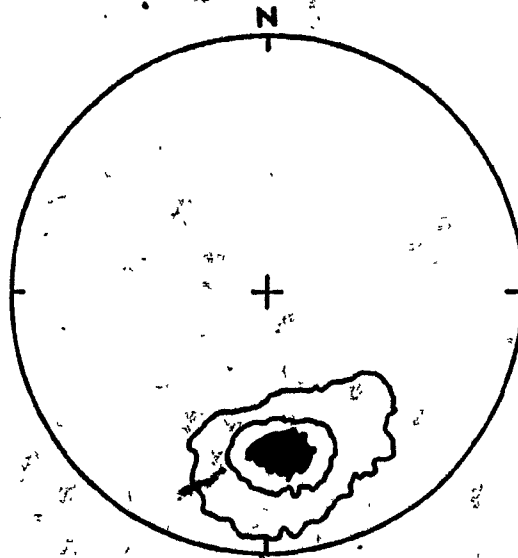


restricted to the stratified sedimentary rocks in the Metasediments and Lower Volcanoclastics and Metasediments (Appendix D). Macroscopic folds are not found in the First-Cycle Volcanics, as evidenced by the straight continuous nature of a glomeroporphyritic marker in the northern limb of the Chain Lakes syncline (Appendix D). Minor F1 mesoscopic folds are found in stratified sedimentary and volcanoclastic rocks in all four units (Plate 2). Mesoscopic folds are typically tight to isoclinal and have moderate plunges (ca. 50°, Fig. 2c).

S1 is a schistosity in amphibolites and epidote amphibolites. The S1 fabric is manifested by the parallel alignment of actinolite, chlorite, plagioclase and quartz in low grade rocks and the parallel alignment of hornblende, plagioclase, biotite and quartz in higher grade rocks. The S1 fabric is preferentially developed in sedimentary and volcanoclastic rocks in general, whereas massive volcanic and plutonic rocks have a less well developed schistosity. The S1 fabric is parallel to the contact between the Southern Composite Pluton and the supracrustal succession and is locally west-striking and north dipping (approximately 70°, Fig. 3a). Toward the east of the map area (Fig. 1), the supracrustal succession becomes arcuate about the Southern Composite Pluton and the S1 fabric becomes progressively more N-striking in this area from W to E. (Eckstrom, 1960). The concordance of bedding in the supracrustal succession, the contact with, and the S1 fabric in the Southern Composite Pluton reflects the synchronous nature of the emplacement of this pluton and the deformation of the

**Figure 3 Poles to S1 in the First-Cycle Volcanics, (a) south
and (b) north of the Chain Lakes fault.**

Figure 3



contours at

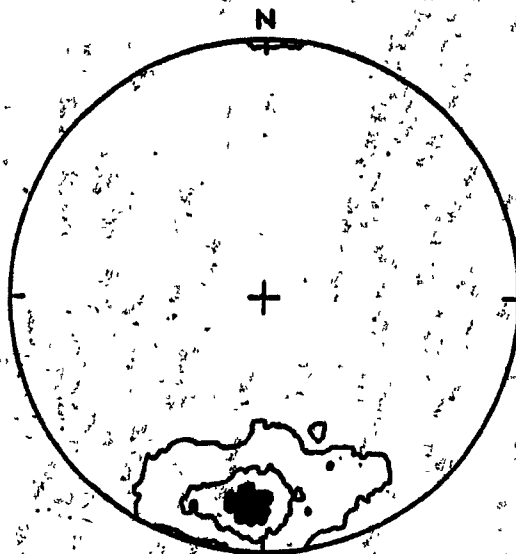
2

12

22% / 1% area

n = 146

3a



contours at

2

12

22% / 1% area

n = 150

3b

greenstone belt.

The second phase of deformation is characterized by strike slip faulting and minor cross-folding. A large, sinistral strike slip fault (informally named the Chain Lakes fault) has displaced the southern limb of the Chain Lakes syncline eastward relative to the northern limb. The fault trace is not exposed. The surface expression of this fault is a marked linear topographic depression that is filled by glacial sediments and a chain of E-W striking lakes in the central part of the map area (Appendix D).

The Chain Lakes fault juxtaposes Lower Volcanoclastics and Metasediments of the southern limb of the Chain Lakes syncline against Metasediments and Second-Cycle Volcanics of the northern limb (Appendix D). A large concentration of minor cross-folds (including kink- and box-type folds in the north, and moderately open, steeply plunging folds in the south) which are NNW trending and associated with a NNW vertical fracture cleavage, occurs in the vicinity of the fault (Appendix D).

The sinistral displacement on the Chain Lakes fault is evidenced by the reappearance of the closure between the Lower Volcanoclastics and Metasediments and the First-Cycle Volcanics in the N, in the S central part of the map area (Appendix D). Furthermore, the Metasediments in the east are not directly correlated on both sides of the fault, whereas the western exposures of this unit in the north can be correlated to the

Metasediments in the south. Evidence for strike slip faulting can be found in other parts of the map area (Plate 3) and it has been reported from other parts of the La Grande belt (Fouque et al., 1979, Grenon et al., 1977).

Minor F2 folds in the southern limb of the Chain Lakes syncline are relatively open, with hinge lines that trend typically N, and plunge toward the NNW at about 50° (Fig. 4). Both symmetric and asymmetric folds occur. They are found predominantly in the Lower Volcanoclastics and Metasediments, where they re-fold earlier S0 and S1 surfaces (Plate 4).

In the northern fault block, kink folds are concentrated in the argillaceous sedimentary rocks of the Second-Cycle Volcanics adjacent to the fault in particular, and in other argillaceous units throughout the map area. The folds adjacent to the fault are predominantly sinistral (viewed down plunge) and are associated with box folds (Plate 5). The hinge lines of the box folds are NNW trending, and the folds plunge variously to the NNW and NNE (ca. 50°). Accurate measurements in this area are not possible as a result of the erratic behaviour of the compass due to the local presence of banded iron formation (BIF). Many of the open folds in the Second-Cycle Volcanics adjacent to the Chain Lakes fault have faulted limbs and are associated with zones of intense brecciation that may be associated with the second phase of deformation. Minor F2 folds in the Lower Volcanoclastics and Metasediments, First-Cycle volcanics, and

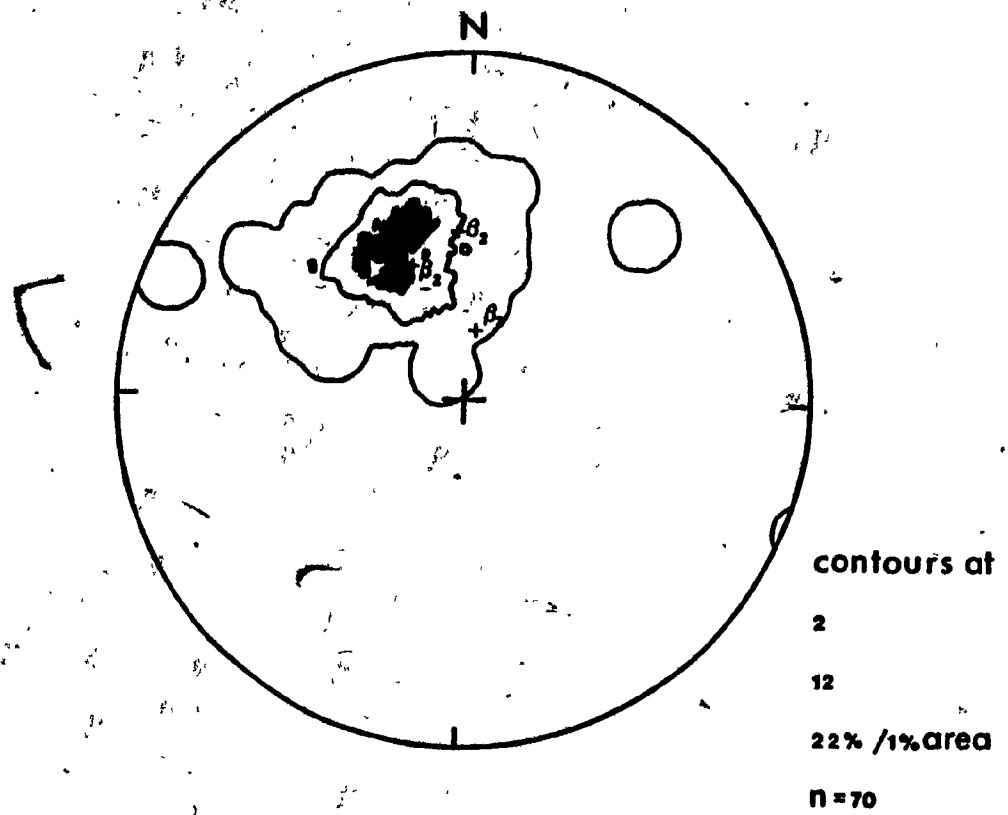


Figure 4 L2 intersection lineations (S2AS1, contoured) and F2 minor fold axes (crosses) measured in units 1-3

Metasediments north of the fault, are predominantly north plunging, but vary in trend (Fig. 5). This variation in trend may be due to the development of a conjugate fold set, or reflect their proximity to the fault, or alternatively, it may be due to the fact that all of these late stage folds cannot be ascribed to a single phase of deformation. Choosing between these alternatives is not possible given the limited data available.

Megascopic F2 folds in the argillaceous sedimentary rocks of the Second-Cycle Volcanics in the central part of the map area are open, asymmetric (sinistral asymmetry) and have hinge lines that trend NNW, and plunge toward the NNE (ca. 55°). These folds have wavelengths of about 5 m and refold earlier S0 and S1 surfaces.

A closely spaced (1-3 cm) fracture cleavage (S2) is developed in the Lower Volcanoclastics and Metasediments in the southern limb of the Chain Lakes syncline. S2 is NNW striking and is almost vertical (Fig. 6). This fabric is believed to be parallel to the axial plane of F2 folds in the southern fault block. It is oriented at approximately 70° to the proposed fault trace and may reflect the development of F2 folding in response to NE-SW compression that ultimately resulted in strike-slip faulting (Fig. 7). This fabric was not observed in the northern fault block.

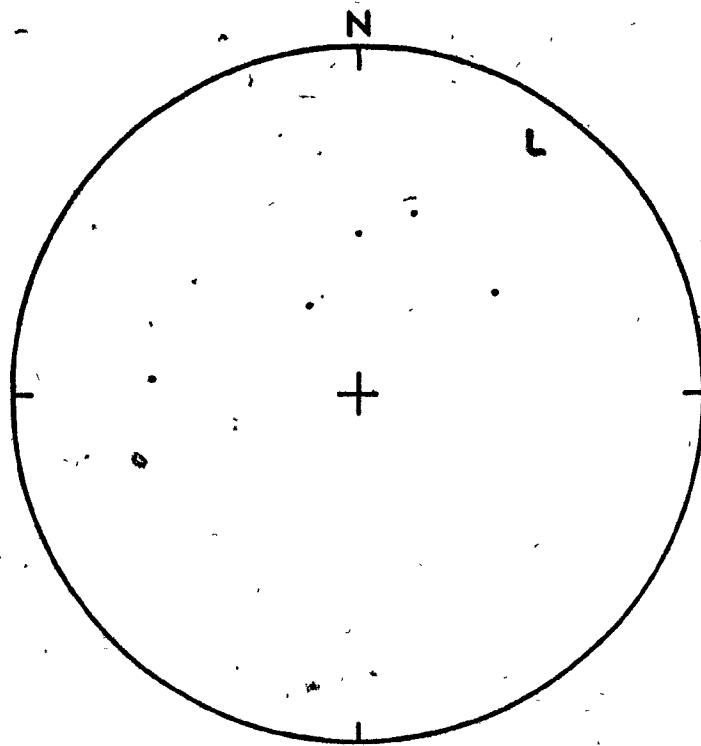
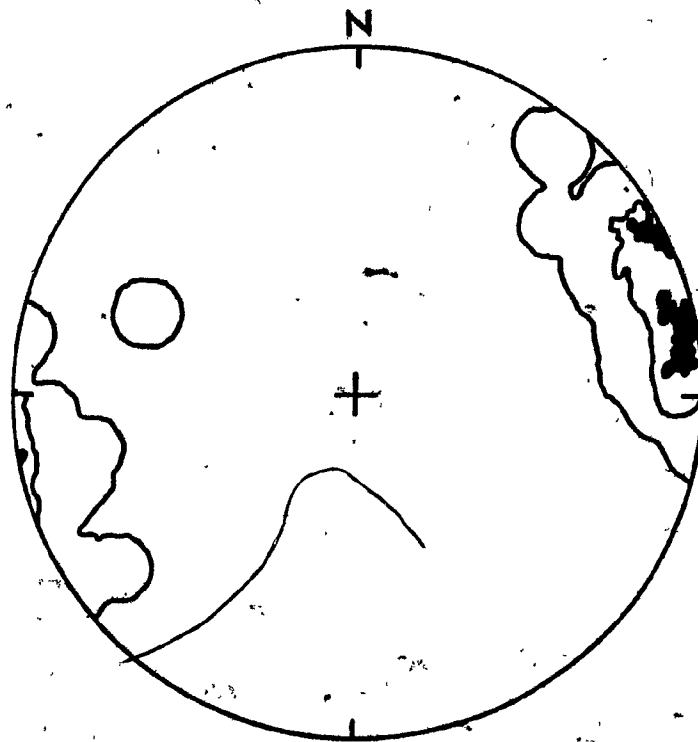


Figure 5 F2 minor folds measured in the Metasediments north of the Chain Lakes fault



contours at
2
12
22% / 1% area
n = 72

Figure 6 +Poles to S2 fracture cleavage in units 1
and 2 south of the Chain Lakes fault

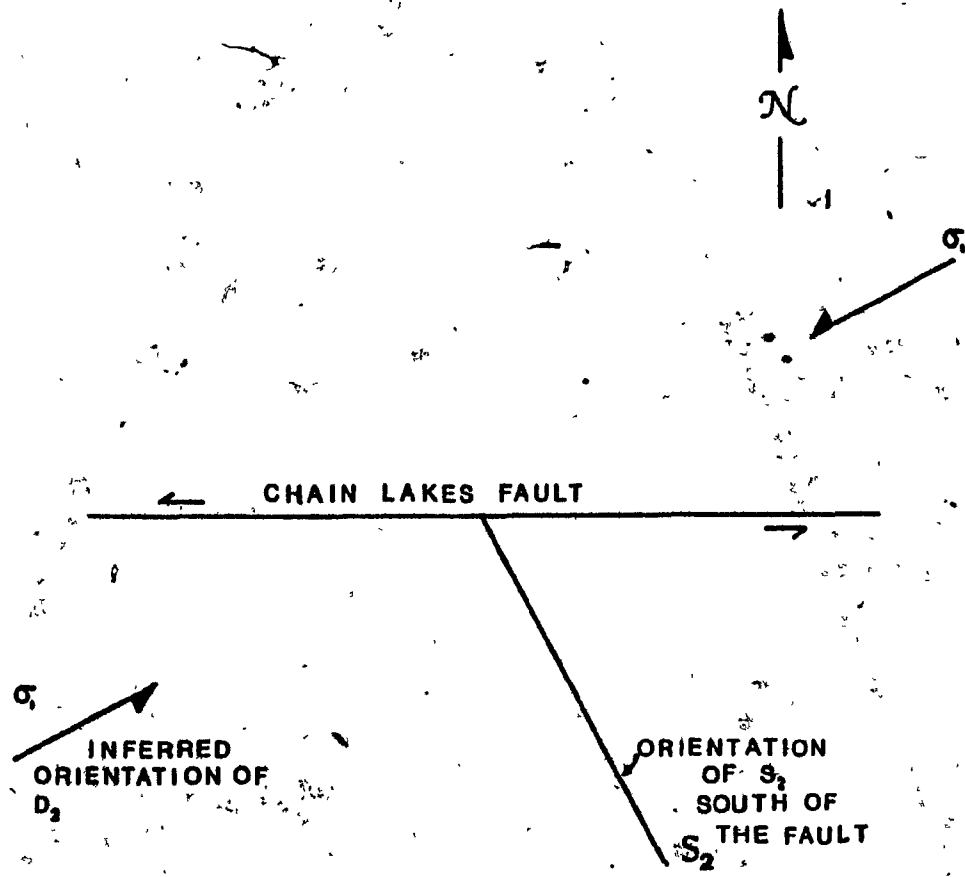


Figure 7 D2 structural model showing the relationship between the Chain Lakes fault and the S_2 fabric

2.3.3 Metamorphism and Secondary Alteration

Two metamorphic events have affected the supracrustal and intrusive rocks in the LG-3 area. The earlier prograde event M1 attains mid-amphibolite facies in the southern fault block and upper greenschist to epidote amphibolite facies in the north. This metamorphic event is broadly contemporaneous with the first phase of deformation and the intrusion of syntectonic plutons, since S1 is defined by the parallel alignment of minerals in the typomorphic assemblage and the metamorphic grade in the supracrustal succession increases toward the contacts with syntectonic plutons.

In the southern limb of the Chain Lakes syncline the metamorphic mineral assemblage in volcanoclastic rocks changes from hornblende-plagioclase-biotite-epidote-quartz to garnet (almandine)-hornblende-plagioclase-biotite-quartz toward the Southern Composite Pluton, although almandine garnet occurs in the BIF in the Metasediments, quite far from the Southern Composite Tonalite pluton, and adjacent to amphibolites that do not contain garnet. The presence of garnet in the BIF is no doubt due to the unusual composition (in particular the Fe content) of these rocks.

In the northern limb of the Chain Lakes syncline the metamorphic grade and degree of recrystallization is lower than in the south. Similarly, in the northern limb the distribution of rocks containing an S1 schistosity is sporadic, and

consequently many of the volcanic and sedimentary rocks preserve evidence of primary textures. The metamorphic grade in the metabasalts of unit 2 varies continuously from middle greenschist facies (actinolite-chlorite-albite-epidote-quartz-sphene) through epidote amphibolite facies (hornblende-epidote-albite-quartz-sphene) to lower amphibolite facies (hornblende-oligoclase-quartz-sphene) adjacent to the syntectonic tonalitic plutons in the central and northern parts of the map area. Sedimentary rocks of unit 3 and volcanoclastic rocks of unit 4 in the central part of the map area in the northern limb of the Chain Lakes syncline have been recrystallized to mid-greenschist facies and are composed of muscovite, chlorite, quartz, albite, and actinolite (in the volcanoclastic units).

Evidence of a retrograde metamorphism, M2, is not widespread in the Lower Volcanoclastics and Metasediments and First-Cycle Volcanics in the southern limb of the Chain Lakes syncline. Retrograde metamorphism occurs in the Southern Composite pluton as chloritization of biotite. S2 in the southern limb is a fracture cleavage that, at least in the case of a single sample examined under the microscope, is not associated with any evident recrystallization. In the northern limb of the Chain Lakes syncline, on the other hand, retrograde metamorphism is evident in many of the rocks. This retrograde metamorphism is characterized by actinolite rims around hornblendes and the appearance of chlorite. These retrograde assemblages occur in amphibolites adjacent to tonalitic plutons,

and are very locally developed in the axial planes of F2 folds, indicating that M2 is synchronous with D2.

The effects of secondary alteration, as well as the late stage metamorphic segregation of monomineralic veins that crosscut M1 fabrics, can be found in all parts of the supracrustal succession. This secondary alteration and veining is only widespread in one part of the southern limb of the Chain Lakes syncline.

The typical alteration products in basalts in the First-Cycle Volcanics are thin quartz veins, calcite veins, epidote veins, and chlorite veins and rare hematite veins. Most of these veins appear to crosscut S1 fabrics, and are thus believed to postdate regional metamorphism. Secondary alteration in the southern limb of the Chain Lakes syncline is rare, apart from the presence of quartz veins, and the replacement of plagioclase by fine grained epidote, calcite, sericite, and clay minerals. Similarly, the sedimentary rocks of unit 3 in the north typically contain secondary carbonates (ankerite and calcite), chlorite and quartz as replacement patches between detrital grains, and as thin veinlets.

On the shores of the LG-3 reservoir (close to the TA-26B dam, Appendix D), in the south, a zone of pervasive alteration has affected the basaltic rocks of the First-Cycle Volcanics. This alteration is of the vein type, and is characterized by the presence of quartz-tourmaline (schorl), and tourmaline-calcite

veins. These veins host pyrite and chalcopyrite mineralization. The veins attain a thickness of approximately 30 cm, and are only closely spaced in a limited number of exposures. These veins crosscut all fabrics and are thus related to a post-tectonic metasomatic event. The lack of crosscutting relationships between these late veins and M2 fabrics precludes an interpretation of the relationship between these two events.

The fine-grained dioritic Lac Coutaceau dykes have been completely recrystallized to a typomorphic assemblage of hornblende-epidote-biotite-oligoclase-quartz +/- diopside. This assemblage may be correlative to the M1 event in the LG-3 area although some of these dykes crosscut previously deformed (D1 ?) supracrustals. Some samples record a retrograde upper greenschist assemblage of actinolite, chlorite, albite and quartz that may be equivalent to the M2 event in the LG-3 area.

Chapter 3 Field Relations and Petrography

In this chapter the field and petrographic relationships of the supracrustal succession and the younger syntectonic plutons are summarized. Particular attention is focussed on features of the supracrustal succession that have a direct bearing on the paleoenvironment and paleogeography of this area (Chapter 4).

3.1.1 Unit 1 Lower Volcanoclastics and Metasediments,

Field Relationships

On the northern limb of the Chain Lakes syncline, the Lower Volcanoclastics and Metasediments are approximately 750 m thick. They consist of interbedded mafic to intermediate volcanoclastic rocks at the base and fine-grained, immature clastic sedimentary rocks, banded iron formation (BIF) and polymict orthoconglomerates near the top. There are numerous thin (0.5-2 m) gabbroic sills. On the southern limb of the Chain Lakes syncline the Lower Volcanoclastics and Metasediments consist of well-bedded, and normally graded mafic volcanoclastic rocks, and fine-grained clastic sedimentary rocks in apparently random sequence, cut by thin (0.25-0.75 m) porphyritic diorite dykes. They are directly overlain by First-Cycle Volcanics in the northern limb of the Chain Lakes syncline, whereas a lateral transition between the two units occurs in the south.

In the northern limb of the Chain Lakes syncline, the volcanoclastic rocks are well-bedded mafic to intermediate fine-

grained tuffs and tuffites, with minor amounts of well-bedded mafic crystal tuff (Plate 6), lenses of well-bedded lapillistone (Plate 3), and some mafic bombs that form bedding-sags (Plate 7). Many of the volcanoclastic rocks are probably strictly epiclastic and occur as well-bedded and graded epiclastic siltstones and sandstones. These epiclastic rocks are interbedded with immature, finely bedded and graded, lutites and arenites and BIF near the top of the unit (Plate 8).

The fine-grained lutites are commonly colour banded and very finely laminated. The arenites are predominantly fine grained subarkoses. A polymict orthoconglomerate occurs as a lensoid deposit interbedded within finer-grained clastic sedimentary rocks (Plate 9). It is well-sorted, and consists of both mafic volcanic (locally derived?) and felsic plutonic cobble-sized clasts (28 cm). The clasts are commonly oblate and may have been flattened tectonically.

The gabbroic sills in the north are generally less than 1 m thick. Some of the sills contain granitoid xenoliths. The sills are medium-grained and have diabasic textures in places. Similar sills are present in the southern limb of the Chain Lakes syncline.

Volcanoclastic rocks of unit 1 in the southern limb of the Chain Lakes syncline consist almost entirely of fine- (1-2 cm) to medium-bedded (2-5 cm) mafic epiclastic siltstones and

sandstones. Despite mid-amphibolite facies metamorphism, original graded bedding is reflected in size gradation in individual hornblende porphyroblasts. There are some interbedded fine-grained clastic sediments that have been recrystallized to quartz, muscovite, plagioclase and hornblende.

3.1.2 Petrography of the Lower Volcanoclastics and Metasediments

In the northern limb of the Chain Lakes syncline, mafic and intermediate tuffs are generally recrystallized to schists, typically consisting of aligned actinolite or hornblende (60%, percentages are visual estimates unless otherwise stated), with smaller amounts of plagioclase (20%), quartz (5%), epidote (10%), traces of secondary chlorite and minor opaque phases. The pervasive schistosity in many of these rocks precludes recognition of microscopic primary textures.

Lapillistones typically consist of felsic lapilli (up to 30%) that have been recrystallized to very fine-grained saussurite with patches of coarser-grained quartz, calcite, muscovite and epidote. These lapilli occur in a groundmass composed of hornblende (30%), quartz (10%) and very fine-grained epidote, plagioclase and calcite (30%).

Epiclastic siltstones consist of fine-grained epidote (20%), hornblende (40%) and quartz (10%) with rare felsic volcanic clasts (<5%) recrystallized to saussurite and coarser epidote and sericite. The subarkoses are completely

recrystallized and are composed of plagioclase (40%), quartz (30%), muscovite (20%), epidote (5%) and traces of biotite (<5%).

Mafic epiclastic sandstones in the southern limb of the Chain Lakes syncline typically consist of idioblastic hornblende (55%) clear, unaltered biotite (5%), quartz (10%), plagioclase (20%), epidote (5%) and traces of an opaque phase(s) (<5%). Immature clastic sediments in the south contain polygonal quartz (55%), large (2 mm), subangular, altered plagioclase (20%), epidote (5%) and traces of an opaque phase(s) (<5%). Porphyritic diorite dykes and sills in the southern limb are composed of phenocrysts of plagioclase (unzoned) (30%), in a groundmass of plagioclase (60%), quartz (15%), hornblende (20%) and traces of an opaque phase(s) (<5%).

3.2.1 Unit 2 First-Cycle Volcanics, Field Relationships

In the northern limb of the Chain Lakes syncline, the First-Cycle Volcanics consist of approximately 3.1 km of submarine, massive and pillowed basalts with associated gabbroic sills, minor hyaloclastite, and small lenses of banded iron formation (BIF). Two distinctive stratigraphic horizons of laterally persistent, glomeroporphyritic and plagioclase porphyritic basalts and gabbroic sills occur within the succession. A thin unit of massive and pillowed basaltic andesite and andesite occurs in discontinuous lenses near the

top. The upper parts of this unit contain minor amounts of fine-grained mafic hyaloclastite, and small lenses of BIF.

In the southern limb of the Chain lakes syncline, pillowed and massive basalts also predominate. Basaltic andesites, BIF and hyaloclastites were not found in this area. Glomeroporphyritic and megacrystic plagioclase gabbro sills occur as small lensoid intrusions at two levels (Appendix D). The degree of original textural preservation is limited in these rocks due to the higher metamorphic grade (mid-amphibolite).

Pillowed flows in the First-Cycle Volcanics occur as 'mattress' and 'ball' forms (Plate 10). They are transitional along strike into massive, laterally continuous basalt flows generally a couple of meters thick. It is commonly difficult to distinguish massive basalt flows, that may have coarse-grained interiors, from massive gabbroic sills (c.f. Dimroth et al., 1982). Massive flows could be positively identified only where they were seen to have well developed chilled margins, lateral gradation into pillows or fine grain size. Brecciated facies appear to be absent in the massive flows and occur very rarely in the pillowed basaltic flows as interstitial fill between individual pillows.

Pillowed basalts are typically fine-grained and aphyric on chilled margins, and have slightly coarser-grained interiors in large pillows. Individual pillows commonly have sharp, dark-colored, fine-grained chilled margins (Plate 11). The pillowed

basalts are not vesicular. Some pillowed flows contain large phenocrysts (up to 2 cm) of plagioclase (in places glomeroporphyritic, Plate 11).

Basaltic andesite and andesite occur primarily as massive flows, although some pillowed facies were also found. These rocks are very light green on the fresh surface. For the most part they are fine-grained to aphyric, but in some cases small (<3 mm) phenocrysts of plagioclase can be found. The flows of basaltic andesite appear to have limited (ca. 50 m) lateral extent, and are commonly 2-3 m thick (Appendix D).

There are many subvolcanic sills in the First-Cycle Volcanics. The largest of these occurs near the base of the unit, and can be traced through discontinuous lenses for approximately 3 km (Appendix D). Although secondary recrystallization has replaced all primary mineralogy, relict textures suggest that this intrusion was a medium-grained, diabasic-textured, gabbro.

Thinner sills occur as discontinuous lensoid or tabular sheets with distinct chilled margins. Their interior portions may be crudely zoned, with fine-grained margins and coarse-grained interiors, and commonly have subophitic textures with amphibole pseudomorphs after clinopyroxene, enclosing plagioclase laths. The groundmass is composed of finer-grained, subhedral plagioclase laths and post-clinopyroxene

pseudomorphs. The presence of abundant euhedral, size-graded clinopyroxene in an a groundmass composed of anhedral, fine-grained phases, indicates that these rocks are orthocumulates.

Sills with glomeroporphyritic and megacrystic plagioclase (GMP) occur in two distinctive horizons within the first-cycle volcanics. These sills are spatially associated with pillowed basalts with similar textures. GMP sills are also found in other parts of the La Grande belt (Stamatelopoulo-Seymour, 1983). They have been termed sills in the present study, although, true intrusive textures were not observed in the field. Since similar textures are found in pillowed basalts, albeit finer grained, they may well be flows (c.f. Dimroth et al., 1982).

Glomeroporphyritic and megacrystic (up to 7 cm) plagioclase occurs in some texturally zoned sills (coarse-grained interiors, finer grained margins) in the northern limb of the Chain Lakes syncline (Plate 12). The outlines of the megacrysts and glomeroporphyritic clusters are typically sharp and individual crystals are commonly euhedral (Plate 12). Some sills, however, contain plagioclase megacrysts with rounded and corroded outlines.

In one location in the east central part of the map area, GMP gabbro sills overlie a medium-grained gabbro sill that contains large rounded xenoliths of mid-amphibolite facies metasediment. The xenoliths are up to 30 cm long (Plate 13). Xenoliths can be traced over only a short distance in the sill

(60 m). Similar crustal xenoliths are associated with GMP sills in the Lac Guyer area (Plate 14) (Liu, 1985). There is no evidence of reaction textures between the xenoliths and the host gabbro.

Mafic volcanoclastics occur mainly in the upper part of the First-Cycle Volcanics in the northern limb of the Chain Lakes syncline. They are lenticular over some 100 m and are up to 5 m wide. The deposits typically consist of medium bedded, normally graded, fine-lapilli-sized mafic fragments, overlain by coarsely laminated, graded tuff. Mafic agglomerate occurs less commonly in beds up to 2 m thick, of limited lateral extent. Individual blocks are of basaltic composition and are typically subangular and up to 27 cm long. The blocks are matrix-supported, and the matrix is a fine- to medium-grained mafic tuff. Microscopic primary textures are not preserved in any of these volcanoclastic rocks due to secondary recrystallization. It is not, therefore, possible to determine whether these rocks may have been reworked by water or density currents.

BIF occurs as lensoid deposits up to 5 m thick and of limited lateral extent (<75 m). The BIF occur intercalated with pillowed and massive basalts in the upper parts of the First-Cycle Volcanics in the northern limb of the Chain Lakes syncline. BIF typically consists of coarsely laminated magnetite-hematite and fine-grained quartz (after chert?). The laminae are typically slightly wavy and laterally continuous and

consist of alternating quartz and magnetite-hematite.

3.2.2 Petrography of the First-Cycle Volcanics

The chilled margins of least-deformed pillow basalts preserve delicate skeletal textures and microphenocrysts (10%). Skeletal crystals of plagioclase, which are completely replaced by saussurite, have swallow-tail terminations (Plate 32). Similar textures have been found in other Archean volcanic rocks (Gelinas et al. 1974; Pearce, 1974) and are common in glassy basaltic rocks such as mid-ocean-ridge basalts (MORB) (Bryan, 1972). The groundmass consists of plumose-textured actinolite and chlorite (Plate 32) that are interpreted to be replacement products after glass.

The finer-grained margins of the least deformed pillowed flows contain microphenocrysts of lath-shaped plagioclase (5%) which are completely replaced by saussurite and patchy quartz (Plate 33). Quartz, calcite and chlorite pseudomorph equant phenocrysts (<5%) that may have been pyroxene (Plate 34). Fine-grained sphene pseudomorphs small (<1 mm) cruciform opaque minerals (10%), that may have been titanomagnetite in the groundmass. Most pillowed basalts contain thin (<1 mm) veins of calcite, quartz or rarely epidote.

GMP pillowed basalts have a groundmass similar to that of the aphyric basalts. Plagioclase megacrysts in these rocks are generally completely replaced by saussurite, quartz, and

calcite. The megacrysts and glomeroporphyritic clusters have sharp boundaries with the groundmass. The maximum size of the megacrysts and glomeroporphyritic clusters is approximately 1 cm, and they may comprise up to 5% of the rock.

Many of the basalts that were analyzed do not retain any primary microscopic textures and are composed of hornblende, very fine-grained plagioclase, epidote, quartz and sphene (after titanomagnetite?). Lower-grade assemblages contain actinolite and chlorite in place of hornblende. Pillowed basalts in the southern limb of the Chain Lakes syncline are generally in the lower amphibolite facies and consist of hornblende, plagioclase, quartz and epidote. In places they attain mid-amphibolite facies, with hornblende, garnet, plagioclase, and quartz.

The basaltic andesites in the upper parts of the First-Cycle Volcanics have abundant microphenocrysts (10%), and microlites of lath-shaped plagioclase (60%) (Plate 35). Fine-grained sphene replaces small opaque grains (5%) that are interstitial to individual microlites in the groundmass. The groundmass (25%) of the pillowed varieties consists of fine-grained chlorite, epidote, actinolite and traces of calcite.

Equigranular gabbros in both the northern and southern fault blocks exhibit considerable modal variation which, with increasing differentiation, is characterized by an increase in modal plagioclase, magnetite, quartz and granophyre, and a

corresponding decrease in clinopyroxene (completely pseudomorphed by hornblende). A medium-grained gabbro from the northern fault block is typical of the least-differentiated gabbros. This rock consists of large (4 mm), subhedral, subophitic clinopyroxene (now hornblende 54%) enclosing small (<2 mm), euhedral plagioclase laths (completely saussuritized 40%). The interstices between clinopyroxenes are composed of small (<2 mm) subhedral or cruciform magnetite, small (<1 mm) interstitial, anhedral, quartz (1%) and traces of thin apatite needles (<1 mm). The order of crystallization in this rock is inferred to be: clinopyroxene and plagioclase (cotectic), magnetite, and finally quartz and apatite.

An equigranular, medium-grained gabbro from the southern fault block has a modal composition typical of the most differentiated gabbroic end member (Plate 36). Post-clinopyroxene pseudomorphs (25%) in this rock are euhedral to slightly rounded, small (1 mm), equant to slightly elongate on (100), and are completely pseudomorphed by hornblende. Subhedral, large (3 mm) plagioclase laths (56%, almost completely saussuritized), partly enclose post-clinopyroxene pseudomorphs. The interstices of this rock are composed of small (<1 mm) granophyric intergrowths and anhedral quartz (6%), subhedral and cruciform magnetite (11%), and small needle-shaped apatite (1%). Secondary minerals include calcite which preferentially replaces hornblende pseudomorphs of clinopyroxene, and biotite which occurs as small (<1 mm) flakes around magnetite. The order of crystallization in this rock is

inferred to be: clinopyroxene and plagioclase (cotectic), magnetite, quartz and apatite.

Gabbroic orthocumulate sills in the First-Cycle Volcanics typically contain up to 60% cumulus clinopyroxene (pseudomorphed by hornblende), and 40% fine-grained (<2 mm) intercumulate plagioclase, quartz and magnetite. The post-clinopyroxene pseudomorphs are subhedral, and vary in size and mode from the fine-grained margins, (30-40% post-clinopyroxene pseudomorphs, 1-2 mm in diameter) to the interior (60% post-clinopyroxene pseudomorphs, 3 mm). The clinopyroxenes have an ophitic texture and enclose small (1 mm) euhedral, completely saussuritized plagioclase laths. Plagioclase enclosed in clinopyroxene and in the groundmass comprises 30% of the rock. The intercumulus material consists of small (1 mm) subhedral plagioclase, small (1 mm) anhedral quartz and minor granophyre (4%), small subhedral titanomagnetite (replaced in part by sphene) (5%), apatite needles (<1%), and secondary epidote and chlorite (5%). The order of crystallization in this rock is inferred to be: early clinopyroxene and plagioclase (cotectic), followed by postcumulus crystallization of plagioclase (clinopyroxene overgrowths on earlier cumulus material?), magnetite, quartz and apatite.

GMP bearing sills consist of up to 80% euhedral megacrysts of plagioclase up to 7 cm in diameter. The megacrysts have sharp contacts with the host groundmass. The plagioclase is commonly

replaced by saussurite, and chlorite, calcite, epidote, and quartz. The groundmass is typically medium grained. Primary textures in the groundmass where preserved, are identical to those in the least differentiated equigranular gabbros.

The xenoliths found in gabbroic sills are medium- to coarse-grained rocks with a pronounced schistosity. They are composed of porphyroblastic garnet (the brown-red color suggests that this may be grossular-rich), sieve-textured staurolite, clinozoisite, muscovite, tremolite, biotite, chlorite (after biotite and garnet), sphene, quartz and traces of plagioclase. Minor opaque phases in this rock have fine-grained sphene replacement rims. The aluminous nature of this assemblage suggests that the protolith of this rock may have been a sediment. The typomorphic assemblage appears to be garnet, muscovite, staurolite and biotite. The clinozoisite, chlorite, tremolite and sphene are probably retrograde.

3.3.1 Unit 3 Metasediments, Field Relationships

Clastic sediments conformably overlie the First-Cycle Volcanics in the northern limb of The Chain Lakes syncline. The sedimentary unit is lens-shaped and attains a maximum thickness of approximately 500 m in the least deformed segment north of the TA-26A dam site (Appendix D). In the southern limb of the Chain Lakes syncline a correlative sedimentary unit is intercalated with the First-Cycle Volcanics. It is also lens-shaped and attains a maximum thickness of 247 m along the

southern shores of the LG-3 reservoir (Appendix D).

The sedimentary rocks of unit 3 consist of lens-shaped deposits of conglomerate within laterally continuous accumulations of interbedded siltstone and sandstone. Banded iron formation (BIF) occurs as large, lens-shaped bodies at the top of the succession in the northern fault block and as clasts within a conglomerate at the base of the succession in the southern fault block. The sedimentary rocks may be assigned to three distinct facies: the siltstone-sandstone facies, the conglomerate facies, and the banded iron formation facies. These facies are described in turn, and an interpretation of the facies association is presented in Chapter 4.

3.3.1.1 Siltstone-Sandstone Facies

The siltstone-sandstone facies contains slates, siltstones, sandstones and minor pebbly conglomerate. The siltstones occur in finely bedded, to well laminated deposits that show normal grading in places, and grade up to, and are interbedded with, laminated slates (all of these rocks have been metamorphosed and will be referred to by their protolith names in this paper). The siltstones are also interbedded with and grade up from sandstones, including immature arkoses and subarkoses, and immature lithic arenite. In the northern limb of the Chain Lakes syncline the siltstones are generally dark colored (typically dark grey to brown) on the fresh surface, and have medium grey-

brown weathered surfaces. The shales are generally dark grey to green on both weathered and fresh surfaces. The immature subarkoses, arkoses and lithic arenites are tan to brown on fresh surfaces and white to pale brown on weathered surfaces. The graywackes are dark grey-green on fresh surfaces and dark grey to brown on weathered surfaces.

The siltstone-sandstone facies is characterized by sets of normally graded coarse clastics (ranging in size from siltstone to fine pebbly conglomerate) with sharp, planar basal contacts, that grade up to finer clastics (including shales, siltstones and fine grained sandstones, Plate 15, 16). The finer clastics are generally finely bedded in coarse end members to well laminated (planar to wavy) in the shales. Primary structures in the finer units are not observed everywhere, probably as a result of preferential weathering and deformation of these divisions. Cross stratification was rarely observed in the finer siltstones and sandstones in the northern limb of the Chain Lakes syncline. However, in one outcrop in the northern fault block, fine-grained graywackes grade normally into laminated siltstones, ripple-drift laminated fine siltstones and finally, fine-wavy laminated shales. The contact between the sandy base of an overlying pebbly conglomerate and the underlying shale is characterized by ball-and-pillow-structure in the sands and flames in the shales. Planar cross stratification, with sets up to 10 cm thick in immature subarkoses, occurs in the section measured in the northern fault block. As a result of the common lack of a third dimension in outcrops, primary sedimentary

structures could not be described from the undersides of beds.

In the southern limb of the Chain Lakes syncline, the siltstone-sandstone facies is characterized by lighter-colored rocks due to the recrystallization of clay minerals associated with the higher metamorphic grade. The shales and siltstones are medium- to dark-grey on both the fresh and weathered surfaces, whereas the sandstones are generally medium-grey on fresh surfaces and light-grey to white on weathered surfaces.

The siltstone-sandstone facies in the southern limb of the Chain Lakes syncline is characterized by successions of coarse to fine clastics with a variety of primary structures. The coarser sandstones of this facies are generally gradational to underlying conglomerates, and are typically characterized by massive and graded sandstone or massive, graded and parallel-laminated sequences of sandstone (Plate 17). Trough-type crossbedded fine sandstones or siltstones occur in thick successions of siltstone-sandstone facies (Plate 18). Trough-type crossbedded sandstones (individual sets up to 3 cm thick) are generally interbedded with coarsely laminated and graded sandstones in alternating successions. Planar and low angle, trough cross-stratified sandstones, with sets up to 10 cm thick, occur interbedded with massive sandstones (Plate 19). Finer clastics are characterized by thinly-bedded siltstones that grade up into laminated shales.

3.3.1.2 Conglomerate Facies

The conglomerate facies in the northern limb of the Chain Lakes syncline is characterized by tabular to lens-shaped deposits of predominantly matrix-supported conglomerates with subrounded, oblate to spheroidal clasts up to 85 cm in diameter. The clasts are mainly tonalitic (Table 2, Plate 20), but a small proportion are intraformational (arenite, siltstone and BIF). Coarse volcanic clasts are very rare. The matrix is generally greater than 15% by volume, and is predominantly in the mudstone to siltstone size range with lesser quantities of sandy matrix. The matrix is either dark grey to green, or brown to green in the mud- and silt-rich varieties and lighter-toned in the sand-rich varieties. Individual beds of paraconglomerate range in thickness from 1 to 10 m. These conglomerates are generally massive, ungraded and disorganized, and have structureless matrices. A few exposures have coarse-tail grading (Fig. 10). The bases of individual conglomerate units are scoured and sharp where observed, and may also be channelled into underlying siltstone-sandstone facies units (Plate 21).

Thin orthoconglomerates are found in parts of the northern limb of the Chain Lakes syncline and are generally characterized by small pebble- to cobble-sized clasts. The clasts are generally of granitoid composition, however, clasts of BIF, clastic sediments and mafic volcanic rocks are found in the western part of the map area (Plate 22). These rocks have coarse sand-sized matrices that are identical to the immature lithic

arenites of the siltstone-sandstone facies. Orthoconglomerates grade up into sandstones and siltstones within individual beds.

In the southern limb of the Chain Lakes syncline the conglomerate facies may be subdivided into two sub-facies. A debris flow sub-facies is characterized by a chaotic distribution of clasts and a gradation from a lower clast-supported conglomerate to an upper matrix-supported conglomerate. The lower clast-supported conglomerates are coarse grained, and contain abundant, angular, BIF clasts (maximum clast-size up to 109 cm) and minor angular to subangular clasts of amphibolite in a matrix of sand-sized comminuted material, mineralogically equivalent to the clasts (Plate 23). The lower clast-supported conglomerate grades up into a matrix-supported conglomerate with some granitic clasts and rare clasts of banded iron formation. The clasts in these conglomerates are considerably finer grained than their underlying counterparts.

The second subfacies of conglomerate is characterized by thin beds (up to 2 m) of clast-supported cobble- to boulder-sized clasts in a sand-sized and subarkosic matrix. The conglomerates have sharp erosive bases, and grade up into thinner, massive divisions of sandstone (Plate 17). The clasts are predominantly tonalitic, subrounded, and oblate to spheroidal. The conglomerates are either massive or crudely normally graded. Some conglomerates consist of shale and siltstone rip-up clasts at the base of depositional units and

grade up into massive sandstone (Plate 24). No clast imbrication was observed.

3.3.1.3 Banded Iron Formation Facies

In the southern limb of the Chain Lakes syncline the only evidence for BIF is in the debris flow conglomerates at the base of the succession. In the northern limb of the Chain Lakes syncline, the BIF facies consists of coarse- to finely-laminated magnetite and quartz that is dark grey on the weathered surface, and grey to black on the fresh surface. The individual units of BIF occur as tabular to lensoid bodies up to 50 m thick. Individual units of BIF can be traced for at least 1 km along strike. The laminations within the BIF are planar to wavy and show some evidence of syndepositional faulting. Individual laminae are discontinuous and wispy, and swell and thin along strike (Plate 25). Rare, thin, discontinuous beds rich in chlorite occur within the BIF. Pyrite-quartz and hematite (specularite) veins crosscut this unit. Disseminated pyrite cubes are common.

3.3.2 Petrography of the Metasediments

Primary sedimentary textures on a microscopic scale are best preserved in the sandstones in the northern fault block. In the southern limb of the Chain Lakes syncline the higher metamorphic grade has resulted in the complete recrystallization of these rocks, and primary microscopic textures are very poorly

preserved. Seven samples of sandstone from the northern fault block were selected for detailed petrographic examination (Table 2). These samples are classified on the Q-F-R ternary diagram (Folk, 1968, see Fig. 8). The compositions vary from immature subarkose to immature arkose and lithic arenite (Fig. 8). 'Immature' is used here to indicate that almost all these rocks contain >10% recrystallized clay minerals.

Immature subarkoses and arkoses have similar grain morphologies, sorting and size-range in the samples examined (Table 2). The matrix is composed of comminuted rock debris, silt-sized quartz and feldspar, and fine-grained sericite and chlorite (the alteration products of unstable detrital fragments). Secondary minerals include quartz, calcite, ankerite and hematite and are generally concentrated in the matrix. Secondary mineral grains crosscut both detrital grain boundaries and matrix minerals. Metamorphism and deformation of these rocks has resulted in the incipient recrystallization of some of the coarser detrital grains, and complete recrystallization of the matrices. A foliation is commonly preserved and is characterized in the least deformed rocks by a parallelism of micaceous minerals and, with increasing degrees of deformation, by the parallelism of detrital fragments.

Detrital quartz grains in all the sandstones are angular to subangular. Detrital feldspars are subangular to subrounded and are albite-oligoclase generally with some sericitization or

Table 2 Modal Composition of Selected Arenites in the Metasediments

SAMPLE NO	ROCK NAME	COMPONENTS (%)								
		1	2	3	4	5	6	7	8	9
TS-X-83										
195A	IMMATURE SUBARKOSE	5.3	15.8	2.9	41.0	16.9	0.1	2.1	0.3	15.3
37A	IMMATURE LITHIC ARENITE	4.0	7.3	1.2	26.3	12.8	0.3	10.9		37.2
685	IMMATURE ARKOSE	1.2	9.9	2.2	22.3	9.7	1.0	9.5	0.4	43.4
44	IMMATURE ARKOSE	0.4	13.6	0.8	17.5	13.9		35.2		18.3
321	TONALITE CLAST	18.9				79.0	2.0			
688	IMMATURE SUBARKOSE	0.2	13.0	3.2	47.4	8.2	0.3	6.3		21.3
326	ARKOSE	0.1	13.7	1.7	26.3	17.6	2.1	29.5		9.0
320	IMMATURE ARKOSE	0.1	16.5	0.5	37.3	18.3	0.6	3.0		18.3

COMPONENTS

- 1 straight extinction quartz
- 2 undulose extinction quartz
- 3 polycrystalline quartz
- 4 coarse silt
- 5 plagioclase
- 6 k-feldspar
- 7 lithic (plutonic)
- 8 lithic (volcanic)
- 9 clay and authigenic constituents

Modal compositions were determined by point counting. A minimum of 1500 points was counted per section.

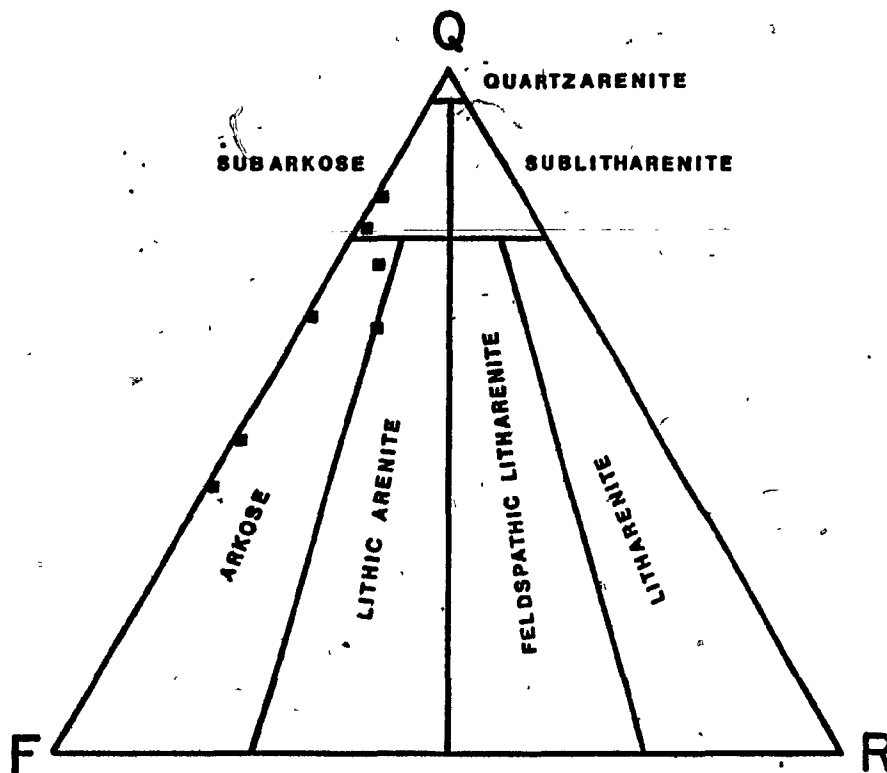


Figure 8 Classification of arenites in the Metasediments north of the Chain Lakes fault (Q is the total amount of quartz, F is the total feldspar and quartzofeldspathic lithic fragments and R is rock fragments)

saussuritization (Plate 37). Subangular grains of slightly sericitized microcline were found in some of the samples (Table 2). Coarse-grained, subangular quartzofeldspathic (plagioclase) lithic grains comprise an important component of the coarse-grained immature arkoses (Plate 37). Individual plutonic lithic fragments are coarse-grained and equigranular, and in a few cases contain some small euhedral crystals of zircon. Lithic sedimentary grains were found only in one sample of arkose, and consist of coarse-grained, subrounded, quartz-rich siltstone.

Immature lithic arenites comprise a small proportion of the sandstones in the northern limb of the Chain Lakes syncline. The lithic fragments in these rocks are, in decreasing order of abundance: tonalite, basalt and siltstone. Monomineralic grains of plagioclase and quartz are also found. Lithic detritus is generally subangular to subrounded, whereas the quartz and plagioclase grains are predominantly subangular. The matrix of these rocks is chlorite-rich and comprises greater than 15% of the rocks. The coarse detritus in these rocks is generally matrix-supported. Secondary quartz, and calcite crosscut all fabrics in these rocks.

Fine, pebbly, clast-supported conglomerates in the northern limb of the Chain Lakes syncline consist of abundant lithic clasts, tonalite (35%), felsic volcanic (<1%), mafic volcanic (<1%) and siltstone (5%). The plutonic and volcanic rock fragments are usually subangular to subrounded, whereas the sedimentary clasts are subrounded. The matrix of these rocks

consists of subangular quartz (20%) and plagioclase (10%), in a finer-grained matrix of silt (20%) and recrystallized chlorite-rich clay minerals (20%). Sand-sized detrital fragments in these rocks are matrix-supported. Tonalitic clasts are equigranular and consist of plagioclase, quartz and hornblende. The felsic volcanic rock fragments are porphyritic and consist of plagioclase and quartz phenocrysts in a groundmass with a trachytic texture. Secondary calcite, chlorite and epidote crosscut the S1 schistosity in these rocks.

3.3.3 Paleocurrents

Twenty-one paleocurrent measurements were made in the section in the southern limb of the Chain Lakes syncline (Fig. 9). These measurements were made on low amplitude (< 3 cm sets) trough- and ripple-laminated sandstones throughout the section (Fig. 9). The crossbedding data have been corrected for folding and tilting by using local bedding and minor folding data. The foreset planes were first untilted and then unfolded. It is not possible to choose uniquely between unfolding or untilting first, and thus the solution presented here is not unique. However, the difference between the vector mean (azimuth) of the paleocurrent data corrected first for tilting and then folding and vice versa is less than one degree. Measurements were taken in exposures in which bedding-parallel strain can be assumed to be minimal; and the orientation of the foreset data when corrected for folding and tilting are assumed to represent the primary

Figure 9 Measured stratigraphic section in the Metasediments south of the Chain Lakes fault. The location of the section is shown in Fig. 11. The section was measured through the entire unit 3 exposures along the southern shores of the LG-3 reservoir. This section is not orthogonal, but is measured diagonally across strike for some 470 m.

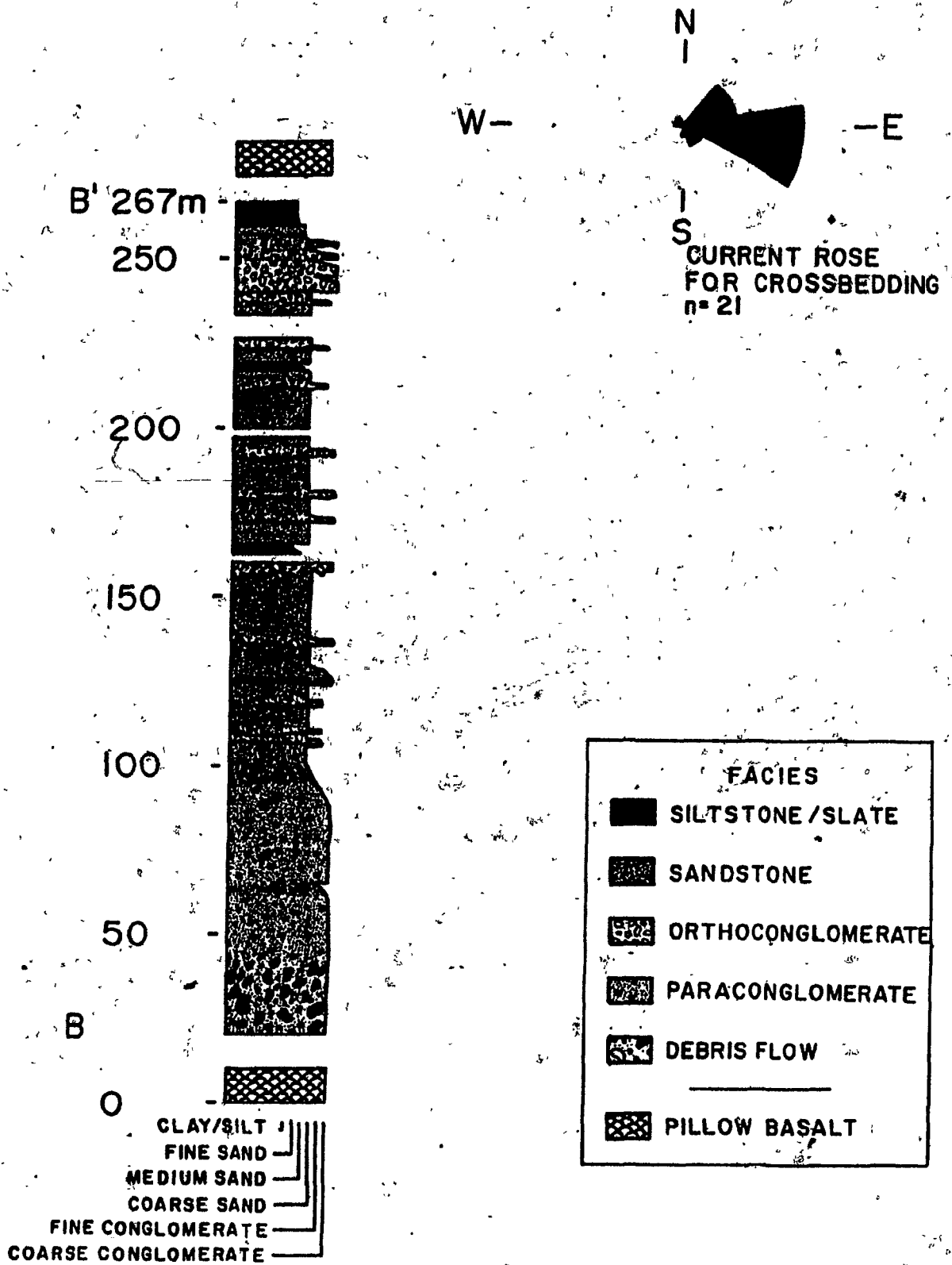


Figure 9

depositional surface.

The vector mean of the corrected data (corresponding to the direction of the vector sum of the data, where each data point is assigned a unit length of 1) is 68° (for data corrected for folding first and then tilting the vector mean is 67.5°). The magnitude of this vector mean (the magnitude of the vector sum of n measurements is constrained to lie between 0 and n) is 19.9, and thus indicates that the 21 data points are unimodally distributed (c.f. Pincus, 1956, see also Fig. 9). On the basis of this data set it would appear that the predominant sediment transport direction was eastward, parallel to the present tectonic strike of the La Grande belt.

3.4.1 Unit 4 Second-Cycle Volcanics, Field Relationships

The Second-Cycle Volcanics are the youngest Archean stratigraphic unit in the LG-3 area. They are comprised of argillaceous sedimentary rocks, minor BIF, intermediate epiclastic rocks, massive basaltic andesites and andesites, and some small gabbroic plugs. They are restricted to the northern limb of the Chain Lakes syncline. The Second-Cycle Volcanics conformably overlie the coarse clastic sediments of unit 3 in the western part of the map area, and BIF in the central and eastern parts of the map area (Appendix D). The aggregate thickness of the Second-Cycle Volcanics is difficult to estimate due to F2 folding and lack of continuous exposure. However, in the least deformed exposures in the western part of the map area

a maximum of 150 m of section is exposed.

The general stratigraphy of the Second-Cycle Volcanics consists of lower green-black argillites overlain by intermediate epiclastic sedimentary rocks. In the western part of the map area the epiclastic rocks are relatively thin and are intercalated with BIF and green-black argillite. They are intruded by a thin (<1 m) gabbroic sill that contains granitic xenoliths up to 10 cm across (Plate 26). In the central part of the map area, green-black argillites appear to be thinner than in the west and are overlain by intermediate epiclastic sedimentary rocks. Two flows of massive basaltic andesite and andesite (each ca. 3 m thick) are intercalated with the epiclastic rocks. The eastern exposures of the Second-Cycle Volcanics are dominated by epiclastic rocks and directly overlie BIF of unit 3. Two small intrusives are found in this area. A noritic plug intrudes the sedimentary rocks and is in turn intruded by a small plug of tonalite.

The grey-green argillites (Plate 27) are massive or coarsely laminated. There is very little interbedded siltstone. In the western part of the map area, thin (ca. 3 cm wide) Neptunian sandstone dykes crosscut the argillites (Plate 34). They can be traced from the base to the top of a cliff-side section through unit 4, for at least 15 m. The sandstones are rusty brown and subarkosic. Since rocks of this composition are not found elsewhere in the Second-Cycle Volcanics, it seems

likely that they were derived from the underlying Metasediments.

The epiclastic rocks found in the Second-Cycle Volcanics consist of sandstones and pebbly conglomerates. The conglomerates are found only in the exposures in the central part of the map area. The epiclastic sandstones are distinctly grey- and green-banded (Plate 28) and consist of thin beds of sand-sized plagioclase, quartz and volcanic grains. They are generally normally graded. The conglomerates consist of pebble-sized, angular, intermediate volcanic clasts in a matrix of epiclastic sandstone. They are clast-supported and are generally massive or normally graded. The conglomerates and sandstones are interbedded, and sandstones normally grade up from underlying conglomerates.

The massive basaltic andesites found in the central part of the map area have brecciated flow tops. The massive flows have fine-grained exteriors and medium-grained interiors. These rocks are typically crosscut by abundant thin quartz veins and are considerably recrystallized in places. The most recrystallized exposures consist of coarse-grained hornblende and plagioclase crosscut by thin veins of quartz and chlorite.

3.4.2 Petrography of the Second-Cycle Volcanics

Massive basaltic andesites of unit 4 are composed of hornblende, actinolite, albite, chlorite, epidote, quartz, calcite, and sphene. The amphiboles in some of these rocks have

blue-green pleochroic hornblende cores and pale green actinolite rims. These volcanic rocks are completely recrystallized and preserve no primary textures.

The epiclastic sandstones consist of plagioclase, quartz, and highly altered grains of plagioclase and chlorite. Almost all the plagioclase has been replaced by saussurite. The matrix consists of chlorite, sericite and actinolite. These rocks have a very pronounced schistosity that obliterates most primary textures.

The noritic plug in the eastern part of the map area is a medium-grained rock that consists of plagioclase (45%), orthopyroxene (pseudomorphed by magnetite and chlorite 30%), hornblende (5%), biotite (5%), quartz and granophyre (5%), magnetite (5-10%), apatite (tr) and chlorite (tr). It has a subophitic texture, in which euhedral plagioclase laths partially enclose rectangular idiomorphic chlorite pseudomorphs after orthopyroxene with small crystals of magnetite on their margins (Plate 38). Hornblende occurs as small euhedral crystals and as reaction rims around post-orthopyroxene pseudomorphs. Biotite occurs as both fine anhedral grains throughout the rock as an alteration product, and as large subhedral crystals interstitial to plagioclase (Plate 38). These larger, subhedral crystals may be primary, since they have straight, well-defined crystal boundaries. Biotite also occurs in reaction rims around hornblende. Interstitial granophyre

occurs between plagioclase laths. Magnetite occurs as subhedral interstitial crystals and as small cruciform composite crystals. It commonly contains exsolution lamellae of ilmenite. The order of crystallization of this rock is inferred to be: orthopyroxene and plagioclase (cotectic), magnetite, hornblende, biotite, and granophyre.

3.5.1 Intrusive Rocks, Field Relationships

The intrusive rocks in the LG-3 area have been tentatively ordered chronologically based on the degree of development of a metamorphic fabric (S1) and on crosscutting relationships where available. The Southern Composite pluton and Northern Tonalite are considered ~~'syntectonic'~~ 'syntectonic', whereas, the less foliated Middle Tonalite pluton, Northern Porphyritic Tonalite-Granodiorite and porphyritic tonalite and trondhjemitic dykes are considered 'late syntectonic'. In this section the field relationships and petrography of these rocks, as well as the Lac Coutaceau dykes, are described.

The syntectonic Southern Composite pluton is a semi-circular mesozonal intrusion approximately 9 km in diameter. It has four distinct zones. In the SW part of the map area (Appendix D), the periphery of the intrusion is characterized by a quartz-plagioclase pegmatite that intrudes the adjacent greenstone (unit 1) along the principal (S1) schistosity. Towards the east, in the south central and south eastern part of the map area, the peripheral phase is a very fine-grained

tonalite. In the interior, the pluton is a medium- to coarse-grained, well foliated, quartz-rich tonalite that is porphyritic in places. Fouque et al. (1979) have mapped the core and largest volume of the pluton (outside the region studied here) as leucocratic granodiorite and migmatite. This pluton has a wide (ca. 1 km) lower- to mid-amphibolite facies metamorphic aureole (see 2.3.3).

The Northern Syntectonic Tonalite pluton is a porphyritic, well-foliated, mesozonal intrusive approximately 12 square km in area. The pluton contains plagioclase, hornblende and biotite phenocrysts in a medium-grained groundmass. It has a thin, diffuse epidote-amphibolite-facies metamorphic aureole in surrounding volcanoclastics and metasediments.

The Middle Tonalite pluton is a late syntectonic, mesozonal intrusive. It has an irregular shape and is locally discordant to the regional tectonic strike, reflecting its relatively late stage emplacement. The pluton has a surface area of 25 square km (Appendix D). The supracrustal country rocks face toward the pluton in the north, thus indicating that the pluton intruded previously deformed rocks. The Middle Tonalite contains seriate and porphyritic phases. The porphyritic tonalite is composed of plagioclase, hornblende and biotite phenocrysts in a groundmass of quartz and plagioclase. Its margins preserve a discontinuous foliation parallel to the regional E-W structural trend and contain numerous xenoliths of amphibolite (basalt). Its

metamorphic aureole is thin and poorly developed, and attains epidote-amphibolite facies in metabasites (unit 2) adjacent to the pluton.

The late syntectonic Northern Porphyritic Tonalite-Granodiorite on the northern margin of the greenstone belt is compositionally and texturally similar to the Middle Tonalite and also contains mafic xenoliths (Plate 29). Both foliated and non-foliated plutonic rocks occur in it. The metamorphic aureole associated with this pluton is thin and very diffuse, attaining epidote-amphibolite facies in the adjacent Lower Volcanoclastics and Metasediments.

Small dykes of late syntectonic tonalite-trondhjemite porphyry intrude unit 1 in the north, and are abundant in the First-Cycle Volcanics in the northern limb of the Chain Lakes syncline. The dykes generally trend parallel to the regional fabric, and are themselves weakly to moderately foliated. Many display thin chilled margins and some contain small xenoliths of wallrock. The dykes may represent apophyses of the Middle Tonalite pluton or the Northern Porphyritic Tonalite-Granodiorite, or both.

A small plug of late syntectonic porphyritic tonalite intrudes the Second-Cycle Volcanics on the SE shore of the LG-3 reservoir. The intrusive is approximately 100 square m in area, and consists of small phenocrysts of plagioclase and quartz in a foliated, fine-grained groundmass. There is abundant quartz

veining. The groundmass of the tonalite weathers white, whereas the fresh surface is pinkish-orange. Small plugs of late syntectonic tonalite also occur in the north-central part of the map area where they intrude the first-cycle volcanics (Appendix D). In this case, however, these small intrusives are coarse-grained and equigranular.

The Lac Coutaceau dykes are fine-grained diorites that range from 1-15 m in width. They contain abundant xenoliths of granodiorite and mafic rocks and intrude previously deformed pillowed basalts and basaltic andesites comprising the supracrustal succession. These dykes appear to be contemporaneous with granodioritic magmatism younger than the supracrustal rocks, as evidenced by mutually crosscutting relationships. Dykes that contain xenoliths of granodiorite are crosscut by granodiorite, while elsewhere diorite dykes intrude the granodiorite (Plate 30). Xenoliths in the dykes range in size from a few centimeters to 50 cm in diameter and show no apparent signs of assimilation by the diorite. In those areas in which the diorite dykes intrude basalts, unresorbed angular xenoliths of basalt are found in the dykes (Plate 31).

3.5.2. Petrography of the Intrusive Rocks

Of the four zones recognized in the Southern Composite pluton (3.5.1) three were sampled and described: the quartz plagioclase pegmatite, the fine-grained tonalite, and the

coarse-grained and porphyritic tonalite.

The quartz plagioclase pegmatite (individual crystals >3 cm) is composed of plagioclase and quartz. The plagioclase is subhedral and sodic (ca. An 5). The quartz has undulose extinction and is commonly recrystallized to a polyhedral, polycrystalline assemblage.

The fine-grained tonalites of the Southern Composite pluton are typically composed of plagioclase phenocrysts with recrystallized and granulated borders. (10%) in a foliated groundmass of biotite (10%), quartz (60%), epidote (5%), muscovite (5%) and plagioclase (10%) with traces of zircon and magnetite. These rocks preserve little evidence of a primary texture apart from the saussuritized plagioclase phenocrysts.

The largest volume of the Southern Composite pluton is comprised of a medium-grained, commonly porphyritic, foliated tonalite. The rock consists of plagioclase phenocrysts (15% point counting, Appendix B), in a groundmass of polygonal quartz (60%), biotite (11%), epidote (2.5%) and plagioclase (10%) with traces of magnetite, hornblende and zircon. Sodium cobalt nitrate staining of these rocks (method after Hutchinson, 1974) reveals no potassic feldspar. The plagioclase phenocrysts have recrystallized, granulated borders and have been replaced by saussurite. Many of the plagioclase phenocrysts are zoned. Chlorite occurs as a secondary replacement after biotite.

The Northern Tonalite is a relatively well foliated rock that is typically composed of plagioclase phenocrysts (up to 8 mm, 12%), in a groundmass of hornblende (7%), plagioclase (30%), quartz (35%), biotite (7%), epidote (5%) and secondary chlorite (4%, after biotite) (Appendix B). Sodium cobaltinitrate staining reveals that all of the feldspar in this rock is plagioclase. Some of the plagioclase phenocrysts are zoned and most are replaced by saussurite. The hornblende in these rocks is generally equant and commonly has a secondary (retrograde) actinolite outer rim.

The porphyritic phase of the Middle Tonalite pluton is foliated in places, and is typically composed of plagioclase (28%, point counting), quartz (1%), hornblende (18%) and chloritized biotite phenocrysts in a groundmass (53%) of fine-grained quartz, plagioclase, sericite, chlorite and traces of epidote and zircon. The plagioclase is generally replaced by saussurite and is compositionally zoned. Some of the quartz phenocrysts are embayed by fine-grained groundmass. Hornblende phenocrysts in these rocks are commonly twinned on (100) and show some evidence of zoning. Sodium cobaltinitrate staining of feldspars in these rocks reveals that plagioclase is the only feldspar.

The northern granodiorite (part of the Northern Tonalite-Granodiorite suite) is composed of microcline and plagioclase phenocrysts in a groundmass of quartz, biotite, and secondary

sericite, epidote and chlorite. The one sample examined is highly foliated and has a pseudomylonitic texture (terminology of Spry, 1969). The strong penetrative fabric in this rock is defined by quartz and biotite. The quartz is polycrystalline and has a strong undulose extinction. The late syntectonic tonalites, on the other hand, are unfoliated and contain both porphyritic and equigranular (medium-grained) phases. The porphyritic phases are composed of large (>6 mm) plagioclase phenocrysts (60%) in a groundmass of quartz (20%), hornblende (5%), biotite (9%), microcline (2%), zircon (trace) and secondary epidote (4%) with traces of chlorite. The plagioclase in these rocks is typically replaced by saussurite.

Late syntectonic porphyritic tonalite dykes consist of plagioclase, hornblende and biotite phenocrysts in a groundmass of quartz, albite, zircon, magnetite and apatite with secondary chlorite, sericite and epidote. The modes of selected specimens are shown in Appendix B. Phenocrysts may account for 20-56% of the volume of these rocks. Plagioclase phenocrysts are commonly zoned, with oligoclase cores and albitic rims. The cores are generally altered to saussurite and the rims to sericite. The groundmass in these rocks is commonly foliated, and this foliation wraps around the larger plagioclase phenocrysts. All the primary biotite and most of the hornblende in these rocks has been replaced by chlorite. Sodium cobaltinitrate staining of these rocks reveals that all of the feldspar in these rocks is plagioclase.

Modes of selected late syntectonic trondjemite dykes are shown in Appendix B. These rocks are porphyritic and contain phenocrysts of quartz and plagioclase. The modal abundance of plagioclase phenocrysts ranges from 24-35% and that of quartz from <1%-11%. Chloritized biotite is the only mafic mineral found and is present in trace quantities. The groundmass is commonly foliated and is composed of quartz, plagioclase, and traces of zircon and magnetite. Secondary minerals include sericite, chlorite, and calcite. The plagioclase phenocrysts are zoned in some of the samples examined, and range in composition from oligoclase to albite. Secondary alteration of plagioclase by saussurite and sericite is common. The quartz phenocrysts are commonly anhedral, or in a few cases, subhedral, and show evidence of embayment by groundmass minerals.

Late syntectonic tonalite plugs are found in both the northern and southern fault block and are typically porphyritic rocks composed of plagioclase (46%, point counting), and hornblende (1%) phenocrysts in a groundmass (76%) of quartz, plagioclase, and biotite with trace apatite, zircon, and magnetite. Secondary minerals include chlorite and sericite. Plagioclase phenocrysts are commonly zoned and show core replacement by saussurite. Although these rocks are discordant, there is a weak foliation apparent in them that suggests that they have been deformed and metamorphosed (D1, M1).

The Lac Coutaceau dykes are fine-grained rocks and are

composed of hornblende, epidote, biotite, oligoclase, quartz +/- diopside. Some samples contain retrograde actinolite (overgrowths on hornblende), chlorite, albite and quartz. There does not appear to be any relict primary mineralogy, or pseudomorphs thereof. Some samples contain xenocrystic plagioclase which is compositionally zoned and has a mortar texture on its periphery. Although these rocks have been completely recrystallized, the uniformly fine grain size and lack of phenocrysts suggests that they may represent chilled liquids.

Chapter 4 Facies Associations, Paleoenvironment, Paleogeography and Provenance

In this chapter, the data from Chapter 3 are used as the basis for a model of the environment of extrusion of the volcanic rocks, and the depositional environment of the sedimentary and volcanoclastic rocks. Some of the implications of this model are tested quantitatively in Chapter 7.

4.1.1 Lower Volcanoclastics and Metasediments.

Mafic volcanoclastic rocks are found in a variety of depositional settings, both subaerial, and submarine (Lajoie, 1984). However, the lateral and vertical transitions to submarine basalts in units 1 and 2 in the southern limb of the Chain Lakes syncline require proximity to a marine environment. The abundance of intercalated volcanoclastic and terrigenous sedimentary rocks at the base of the succession indicates that volcanic activity was contemporaneous with sedimentation during the deposition of the Lower Volcanoclastics and Metasediments. Qualitative limits may be assigned to the depth of emplacement of the Lower Volcanoclastics and Metasediments. The fine grain-size of the sedimentary rocks of this unit, as well as the presence of BIF, and the lack of traction structures throughout, suggest that these rocks were emplaced below wave base in a quiet-water environment. On the other hand, the presence of bomb sags in the northern limb of the Chain Lakes syncline requires that at least part of the depositional environment must have

been at relatively shallow depths (c.f. Fisher et al., 1984). Thus, it would appear that the Lower Volcanoclastics and Metasediments were deposited, at least in part, in water depths characteristic of the littoral zone.

4.1.2 Provenance of the Lower Volcanoclastics and Metasediments

The abundance of volcanic epiclastic and immature terrigenous sediments and the presence of granitic clasts in conglomerates in the northern limb of the Chain Lakes syncline indicate that the Lower Volcanoclastics and Metasediments clastic rocks have a mixed provenance. Both intrabasinal (volcanoclastic) and extrabasinal detritus appear to be present. The compositional immaturity of the terrigenous sedimentary rocks probably reflects only limited reworking of these rocks, and deposition in a tectonically active environment. The intercalation of terrigenous and volcanoclastic detritus suggests that the volcanic activity was episodic, and that periods of waning volcanic activity were characterized by the deposition of terrigenous sediment.

4.2 First-Cycle Volcanics

The First-Cycle Volcanics were extruded in a submarine environment as evidenced by the presence of pillowed flows. The pillows and massive flows in these rocks are not vesicular and may thus have been extruded in a deep-water environment (c.f.

Moore, 1965; Jones, 1969; Dimroth et al., 1982; Fisher et al., 1984). This interpretation is further supported by the general scarcity of hyaloclastic rocks (c.f. Basaltic Volcanism Study Project, 1981; Dimroth et al., 1982a; Fisher et al., 1984).

Dimroth et al. (1982a) have suggested that basaltic lavas erupted on subaqueous lava plains are characterized by monotonous sequences of tholeiitic basalts within which important local centers cannot be recognized, have laterally persistent stratigraphic units and random vertical and lateral proximal to distal facies relations. Massive basalts in these environments are believed to be proximal, and to have formed in lava pools overlying fissures. Pillowed flows, on the other hand, are believed to represent a channeled, marginal facies (Dimroth et al., 1978; Ballard et al., 1979; Baragar, 1984). The First-Cycle Volcanics appear to have some of these characteristics. GMP flows and sills can be traced throughout the map area and are found within the mid parts of the stratigraphy elsewhere in the La Grande belt (Liu, 1985) suggesting that they may have large later lateral extent. Gradual transitions from massive to pillowed facies basalts occur randomly both vertically and laterally in the First-Cycle Volcanics. Felsic volcanic centers are absent from the First-Cycle Volcanics.

Sheet flows or submarine lava plains are commonly found at fast-spreading ridges, such as the East Pacific Rise at 21 N (Normark, 1976) and the Galapagos Rift (Lonsdale, 1977) and are

believed to be the characteristic volcanic landforms produced in areas of high effusion rate, and large extrusive volume (Cousineau et al., 1978; Greeley, 1982). The accumulation of sediments is not appreciable in such environments (Basaltic Volcanism Study Project, 1981). The morphological features of the First-Cycle Volcanics are consistent with their having been derived from vents at which there were high effusion rates.

Throughout most of the First-Cycle Volcanics the facies relationships of flows (pillowed and massive) and low vesicularity are maintained. Thus, the rate of volcanic accumulation was probably rarely great enough to permit marked upward shoaling of the sequence. An extensional tectonic regime might reconcile the inferred large effusion rates with the lack of upward shoaling (see also 7.2). The restriction of mafic volcanoclastic rocks to the upper levels of the unit in the northern limb of the Chain Lakes syncline suggests that the volcanic pile grew at a rate greater than that of subsidence there. Consequently, the volcanic pile may have shoaled upward locally in the late stages of the First-Cycle Volcanics deposition. The volcanoclastic rocks at the top of the unit in the north may have accumulated as a result of shallow-water magmatophreatic eruptions (c.f. Fisher et. al., 1984).

The lateral and vertical transition between the Lower Volcanoclastics and Metasediments and the First-Cycle Volcanics is believed to represent a shallow- to deep-water transition.

Thus the eastward lateral transition from unit 1 to unit 2 in the southern limb of the Chain Lakes syncline reflects an eastward increase in basin depth. Similarly, the vertical transition from The Lower Volcanoclastics and Metasediments and the First-Cycle Volcanics in both the northern and southern limbs of the Chain Lakes syncline records a progressive subsidence.

4.3.1 Metasediments, Facies Association

The geometry of the depositional basin for unit 3 is difficult to delineate, given the limited sedimentological data on the La Grande belt and the uncertain position of its margins. This second point is a problem common to many Archean greenstone belts (Walker, 1978), and arises because to delimit the geometry of a basin it is necessary to identify and palinspastically reconstruct a basin-margin facies. Although a relatively shallow water facies (littoral zone of unit 1) exists at the base of the succession at LG-3 it cannot be used to define the margins of the basin unambiguously, since the Lower Volcanoclastics and Metasediments cannot be stratigraphically pinned to a predepositional basement.

The coarse clastic sedimentary rocks of unit 3 are believed to be re-sedimented. This interpretation is based on the stratigraphic context of this unit - these rocks conformably overlie and are intercalated with the upper parts of a sequence of deep submarine volcanic rocks - and also on the fact that

these rocks have an internal facies organization consistent with that observed in modern and ancient resedimented facies associations. In particular, conglomerate-facies rocks have sharp erosive bases with, and grade up into, siltstone-sandstone-facies rocks (Walker, 1984). Furthermore, the siltstone-sandstone-facies rocks have thick, stacked, partial sequences of primary structures that are similar to those of the Bouma model.

In Chapter 3 it was seen that the predominant sediment transport direction for unit 3 was eastward. An east-dipping paleoslope is also consistent with the eastward lateral transition from relatively shallow-water facies of the Lower Volcanoclastics and Metasediments to the deeper-water facies of the First-Cycle Volcanics in the southern limb of the Chain Lakes syncline (see 4.2). This paleoslope may therefore have existed throughout the deposition and emplacement of units 1, 2 and 3. Its presence may explain the BIF-facies relations of the First-Cycle Volcanics and Metasediments.

A number of lines of evidence indicate that BIF-facies rocks represent background basin sedimentation and can be ascribed to a basin-plain facies association:

- 1) BIF-facies rocks occur as sedimentary drape deposits near the top of unit 2 in the northern fault block. Thus BIF clasts in the debris-flow conglomerates at the base of the southern section (Fig. 9) and in conglomerates in the western exposures of the Metasediments in the north may have been derived from BIF accumulations at the top of the First-Cycle Volcanics.

2) Siltstone-sandstone-facies rocks are vertically transitional up section into BIF-facies rocks in the central exposures of the Metasediments in the north.

3) The coarse clastic sedimentary facies of unit 3 are eastwardly (downslope) transitional into BIF-facies rocks, which thicken from west to east.

4) BIF-facies rocks are interbedded with argillites at the base of unit 4.

5) BIF-facies rocks and slates have been interpreted to be a basinal facies (equivalent to modern hemipelagic sediments) in Archean greenstone belts, where they are interfingered with sedimentary rocks of the resedimented facies association (Walker et al., 1971; Dimroth, 1975; Teal et al., 1977; Hyde et al., 1977; Walker, 1978; Eriksson, 1982, 1980).

The BIF-facies rocks are thin (ca. 2 m) in the western part of the map area where they overlie siltstone-sandstone-facies rocks, and thicken to approximately 50 m in the central parts of the map area (northern limb of the Chain Lakes syncline). They dominate the section in the easternmost exposures of unit 3 (ca. 100 m, Fig. 11). Their increase in thickness from west to east is consistent with an eastward increase in basin depth and consequently a general scarcity of clastic facies in the deeper parts of the basin. Furthermore, BIF-facies rocks thicken and thin along strike, thus suggesting that they are sedimentary drape deposits that fill topographic depressions.

The lateral and vertical facies relationships of the clastic sedimentary rocks of the Metasediments provide insight into the processes that controlled the input of clastic sediment into the basin and the temporal and spatial variations of these sedimentary processes.

Figure 10 Measured stratigraphic section in the Metasediments exposed north of the Chain Lakes fault. The exact location is shown in Fig. 11. The section has been subdivided into fining-upward (F-U) and coarsening-upward (C-U) cycles. This section is comprised of a 27m section measured on a cliff side in overturned beds dipping 51° and striking 270° . A ca. 20m break overlying this surface exposure is followed by a 7.7m section measured in a vertical drillhole (T.F.-347, NQ core, 26.3-76.3 feet (8.01-23.25m) provided by the Societe de Development de la Baie James).

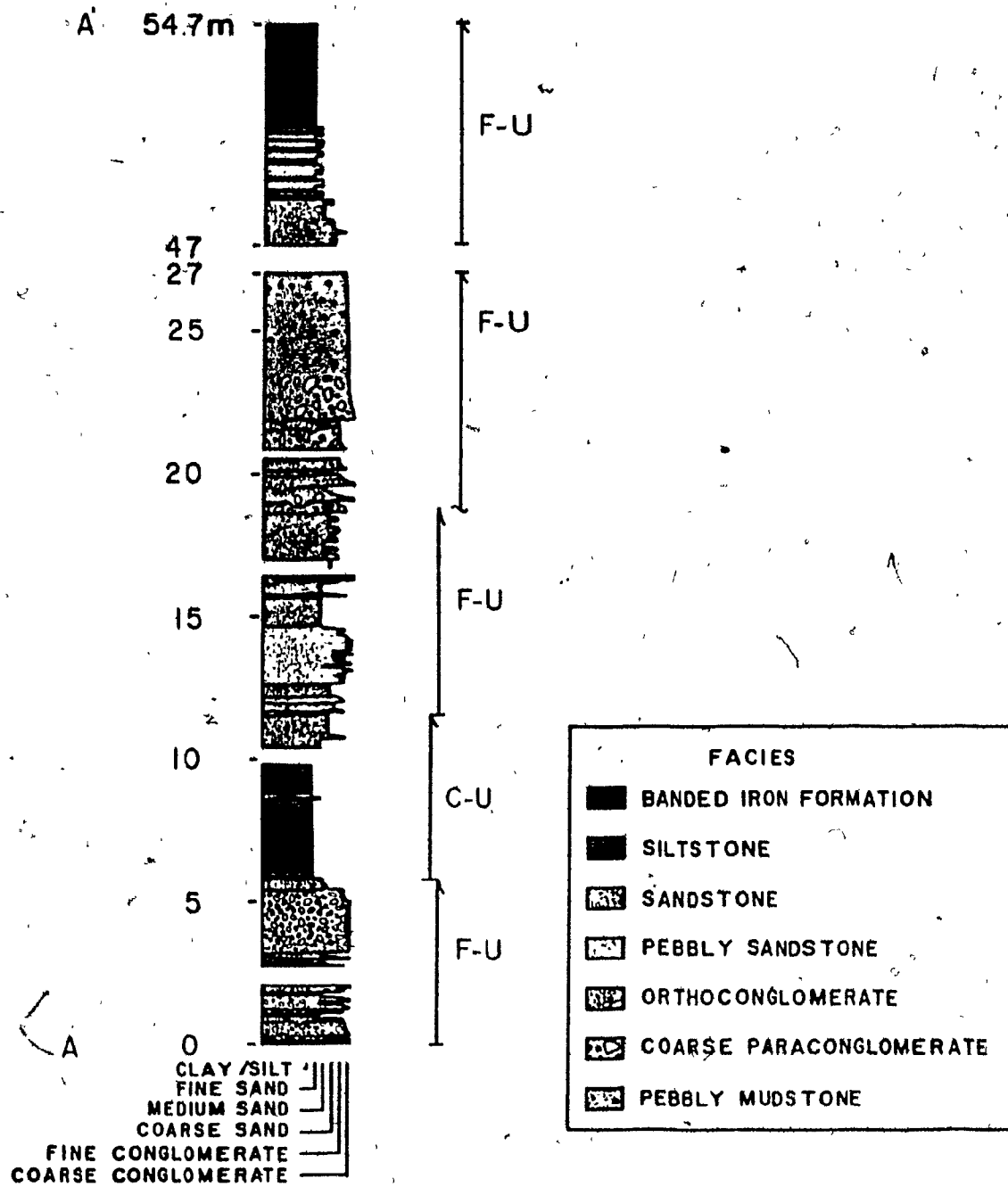


Figure 10

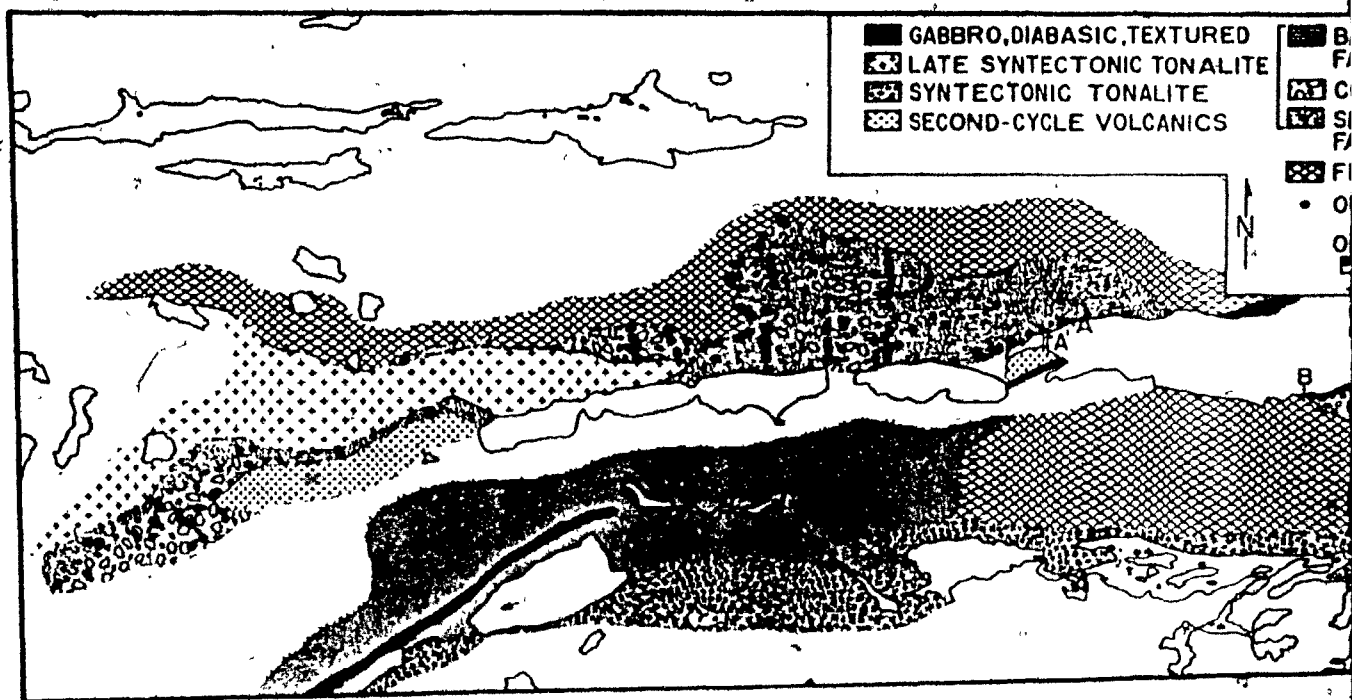


Figure 11 Facies map of the Unit 3 Metasediments. Sections A-A' and B-B' are shown for reference.

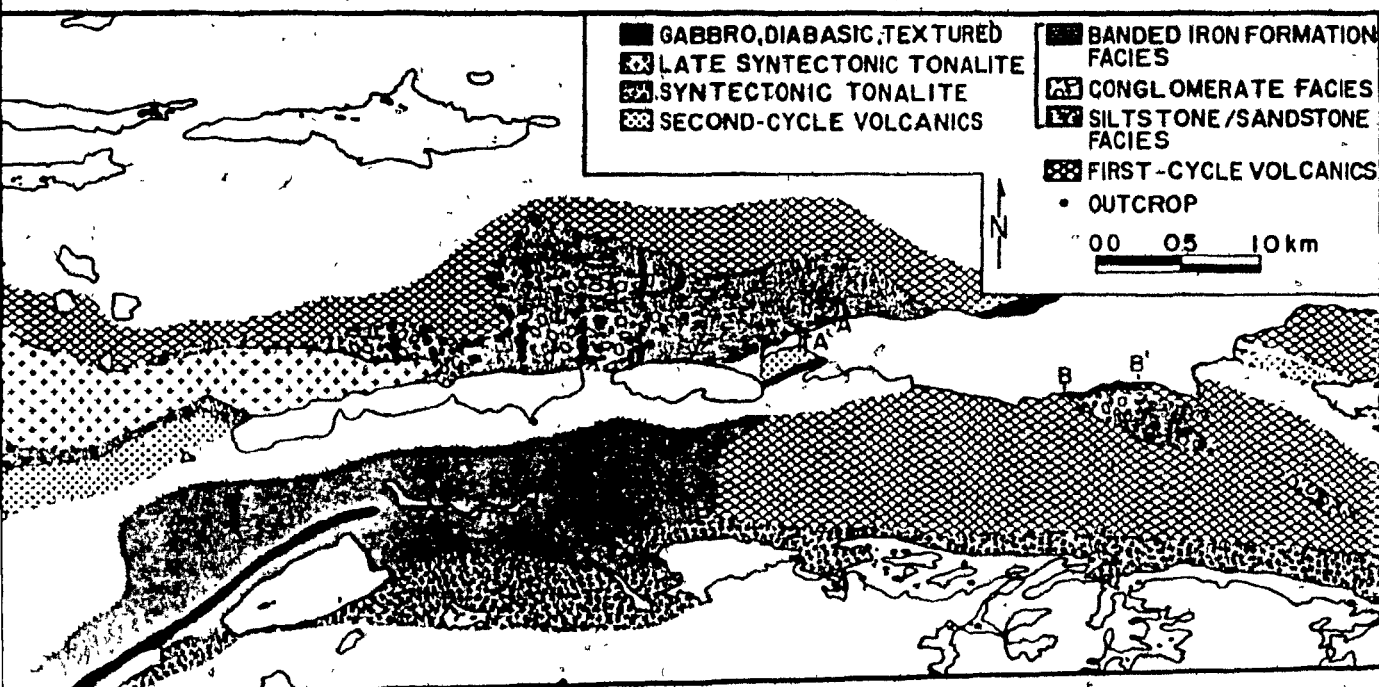


Figure 11 Facies map of the Unit 3 Metasediments.
 Sections A-A' and B-B' are shown for reference

The largest volume of clastic rocks in the Metasediments belongs to the siltstone-sandstone facies (Fig. 11). This facies is found throughout the clastic wedge, as laterally persistent deposits that are abruptly overlain by, grade up from, and have a sharp lateral transition into conglomerate-facies rocks. The siltstone-sandstone-facies rocks grade up into BIF-facies rocks of the basin-plain facies association. The siltstone-sandstone-facies rocks are characterized by coarsening- and thickening-upward megasequences, and fining-upward megasequences when they are interbedded with conglomerate-facies rocks (Fig. 10). The coarsening- and thickening upward megasequences are interpreted to represent progradational deposition of clastic detritus on the smooth lobes of a submarine fan (c.f. Walker, 1984). The fining-upward megasequences that overlie the conglomerates may represent channel-fill deposition as a result of channel abandonment (c.f. Walker, 1984).

The conglomerate-facies rocks comprise lenses that are found throughout the western and central parts of the Metasediments (Fig. 11). Conglomerate-facies rocks are never vertically transitional into BIF-facies rocks. They are characterized by fining- and thinning-upward megasequences. The abundant conglomerate-facies rocks in the lower 27 m of the stratigraphic section measured in the north (Fig. 10), and in the lower 240 m of the southern section (Fig. 9) indicate that these rocks were deposited in a proximal basin (c.f. Mutti, 1972). The clast-supported conglomerates of the southern and northern sections are tentatively ascribed to the upper-fan

environment as is commonly the case for many modern submarine fans (Walker, 1984). The debris-flow conglomerates at the base of the section in the south (Fig. 9) are interpreted to have been deposited in a feeder channel to a submarine fan. Such debris-flow conglomerates are generally found in feeder channels to submarine fans (Walker, 1975, 1984).

The occurrence of thick, massive sandstones, and sandstones with >10 cm trough-type crossbedding, in the siltstone-sandstone-facies rocks are associated with channeled, conglomerate-facies rocks (Fig's. 9, 10) is interpreted here to be indicative of channel migration. These features could be easily mistaken for fluvial facies associations, but the stratigraphic context is diagnostic here, and similar deposits have been reported in other deep submarine clastic deposits (Winn et al., 1977; Chough et al., 1978).

Fine clastics of the siltstone-sandstone facies that are interbedded with and grade up from the proximal basin conglomerates in the southern and northern sections (Fig's. 9, 10), are characterized by the stacking of the following Bouma sequences: A, AB, BC, BCD, BD *. These rocks are interbedded with conglomerates of the upper fan environment, and probably represent a variety of depositional settings. A detailed facies

* A= massive or graded, B= sandy parallel laminations, C= rippled and/or convoluted, D= delicate parallel interlaminations of silt and mud, E(t)= mud introduced by the turbidity current, E(h)= the hemipelagic background mud of the basin (Walker, 1984).

analysis of a large number of stratigraphic sections would be required unequivocally to ascribe these rocks to particular depositional settings. The massive and pebbly sandstones that directly overlie clast-supported conglomerates probably represent within-channel deposition in the lower parts of the upper fan, or in the mid-fan region (c.f. Walker, 1984). The siltstone-sandstone-facies rocks that comprise coarsening-upward megasequences and are believed to have been deposited on the smooth lobes of a submarine fan are classic turbidites and contain BC and BCD sequences.

Simplified models of submarine fans are often characterized by an overall coarsening upward that is interpreted to indicate progradation of the fan (Walker, 1984). However, the upper reaches of the southern and northern sections are comprised of laminated shales and BIF-facies rocks of the basin-plain facies association indicating that the rate of subsidence was greater than that of deposition and the submarine fan grew in progressively deeper water conditions. The waning of clastic sediments into this basin with time could have been caused by a major regression or the lateral switching of the sediment supply to another main channel. It is not possible at present, given the limited sedimentological data, to choose between these two alternatives.

The presence of deep submarine volcanic rocks (unit 2), and sedimentary rocks of resedimented facies association, suggests that the minimum depth of the basin during the emplacement and

deposition of the First-Cycle* Volcanics and overlying Metasediments was below maximum storm wave base* (in order to preserve primary sedimentary textures that develop as a result of turbidity currents) for the Metasediments (ca. 200m) and at least 1 km for the First-Cycle Volcanics (c.f. Jones, 1969).

4.3.2 Provenance of the Metasediments

The provenance of unit 3 sediments can be treated from two viewpoints: the provenance of the coarse clastic fraction in conglomerates, and the provenance of sandstones. Both the coarse clastic and fine clastic fractions of these sediments reflect a provenance of intrabasinal and extrabasinal origin.

There are two important source terranes for conglomerates in the sedimentary rocks of unit 3. The BIF and volcanic detritus in the western conglomerates and at the base of the section in the southern limb of the Chain Lakes syncline are similar in composition to basinal rocks that underlie them. The original site of deposition for these sedimentary rocks must have been somewhere to the west, since the southern fault block has been transported tectonically eastward. In the case of the debris-flow conglomerates in the southern limb of the Chain

* Although maximum storm wave base is an abstract concept in that it depends on the prevailing weather and geometry of the basin (amongst other factors), the maximum depths at which sediment has been observed to have been disturbed by storm processes, that does not include density currents triggered by storm activity, is on the coast of Washington and Oregon at ca. 200 m (Komar et al., 1972).

Lakes syncline this intrabasinal provenance appears to be the main provenance in the early stages of basin fill. The largest volume of conglomerates in unit 3 contain clasts of predominantly tonalitic ^{COMPOSITION} indicating an extrabasinal source. The volume of tonalitic detritus increases markedly up section in the southern limb of the Chain Lakes syncline, and the ratio of intrabasinal to extrabasinal clasts decreases from west to east in the northern limb. The textures of the tonalites indicate that the source region was probably a mature crystalline terrane. The occurrence of acid volcanic detritus in conglomerates in the northern limb of the Chain Lakes syncline suggests that this source terrane may have contained consanguineous volcanic rocks, although their scarcity indicates a predominantly relatively dissected crystalline terrane.

Whereas the provenance of the clasts in conglomerates can be readily determined, the sandstones pose a particular problem, since these rocks have been altered and recrystallized during secondary processes. Only the least deformed and recrystallized samples of sandstone are considered here.

Immature subarkoses and arkoses are composed predominantly of angular quartz, subangular plagioclase, lithic plutonic grains composed of plagioclase and quartz, and rare microcline. Their matrix is rich in sericite, quartz and secondary carbonates. The source of these rocks was probably dominated by an extrabasinal terrane of tonalitic composition.

Immature lithic arenites reflect a mixed provenance that includes extrabasinal and possible intrabasinal sources. The tonalitic rock fragments, abundant plagioclase, and rare felsic volcanic rock fragments are derived from outside the basin, whereas basic volcanic and sedimentary rock fragments could represent finely comminuted debris of intrabasinal origin.

Thus the clast compositions in unit 3 may reflect the derivation of sediment from outside the basin, and are predominantly tonalitic. Coarse sedimentary detritus that may be of intrabasinal origin is found predominantly in the lower parts of the succession and in the western part of the map area. Finer clastic detritus of both intrabasinal and extrabasinal provenance is found in lenses throughout the section, but dominates the lower parts of the section in the northern limb of the Chain Lakes syncline. It appears that initial sedimentation in the basin contained an important component of intrabasinal clastic sediment, and that with time the basin was fed by sediment from outside. The intrabasinal origin of sediments in the lower parts of this unit is consistent with the fact that late-stage First-Cycle volcanic activity was contemporaneous with the early deposition of the Metasediments, as evidenced by the intercalation of these two units in the southern limb of the Chain Lakes syncline. With time, sedimentation may have been a result of the progressive uplift and unroofing of a crystalline terrane that bordered the depositional basin or, alternatively, the degradation and resedimentation of previously deposited

sediment of predominantly tonalitic composition.

4.4 Second-Cycle Volcanics

The abundance of volcanoclastic rocks, including epiclastic sandstones and conglomerates, as well as the presence of massive lava flows in the Second-Cycle Volcanics, suggest that these rocks were deposited and emplaced in shallower water than the underlying submarine fan and basin-plain facies rocks of unit 3. These rocks conformably overlie the Metasediments and thus the transition between the two must reflect a gradual upward-shoaling of the succession. The green argillites that comprise the base of the succession are crosscut by Neptunian dykes that are commonly interpreted to indicate rapid accumulation of sediment in submarine conditions.

The Second-Cycle Volcanics may have formed volcanic islands, since they represent centers of volcanic activity in shallow marine to subaerial conditions and conformably overlie sedimentary rocks of deep marine origin. There is no evidence of extrabasinal detritus in these rocks. In fact, the largest volume of this unit is comprised of epiclastic sedimentary rocks. The lack of volcanic detritus of intermediate composition in the underlying Metasediments indicates that there may have been a considerable hiatus between the First- and Second-Cycle Volcanics.

4.5 Summary

The supracrustal succession is believed to have been deposited and emplaced in a basin which was actively subsiding such that sedimentary and volcanic rocks were deposited in progressively deeper water conditions until the time of deposition of the lower most units in the Second-Cycle Volcanics. The Second-Cycle Volcanics may have been emplaced in shallower water conditions at a time when the rate of subsidence was less than that of deposition (Fig. 12). The paleoslope of the basin was probably east-dipping during the deposition and emplacement of the Lower Volcanoclastics and Metasediments, First-Cycle Volcanics and Metasediments. Thus, the source of sediment during the deposition of the Metasediments was toward the west, and is assumed to have been an uplifted plutonic highland. The supracrustal succession is believed to have formed on a continental crust of predominantly tonalitic composition. This interpretation is based on the provenance of the sedimentary rocks in the Lower Volcanoclastics and Metasediments and the Metasediments, and on the presence of metasedimentary xenoliths in the First-Cycle Volcanics and granitic xenoliths in the Second-Cycle Volcanics. Further evidence for an underlying early continental crust may exist in the western part of the La Grande belt (Lac Yasinski area, Fig. 1), where clastic sediments (including conglomerates) of tonalitic provenance occur at the base of the supracrustal succession which is believed to locally overlie a tonalitic basement (personal communication, B. Rivard, 1985).

Figure 12 Paleogeographic and depositional model for the Archean supracrustal succession in the central part of the La Grande belt. The hachured pattern represents an extended sialic crust underlying the succession. The Lower Volcanoclastics and Metasediments overlie this basement. The dotted and semicircular patterns represent massive (proximal) and pillowed (distal) First-Cycle Volcanics lava flows that have erupted onto submarine plains. Toward the west the First-Cycle Volcanics are overlain by resedimented sediments in submarine fans whereas toward the east the basinal facies is banded iron formation (shown by the fine stipled pattern in plan and fine ruled pattern in section). The youngest volcanic rocks (Second-Cycle Volcanics) are shown as partly emergent island volcanoes.

3

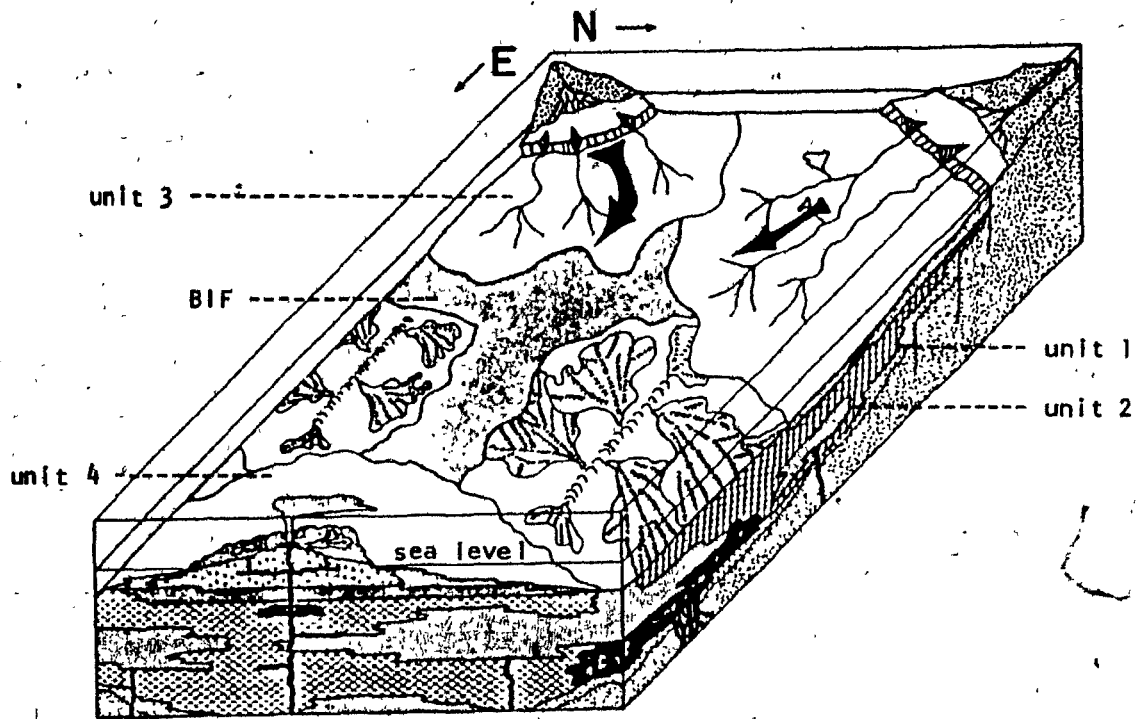


Figure 12

Chapter 5 Geochemistry of the Volcanic and Synvolcanic Intrusive Rocks

5.1 Introduction

This chapter concerns the geochemistry and petrology of the volcanic and intrusive rocks in the LG-3 area, and the intrusive rocks in the Lac Coutaceau area. It provides the basis for the petrogenetic models of Chapter 6. Forty-eight volcanic and intrusive rocks were analyzed for major and selected trace elements (Appendix B). Details of the sampling criteria, locations, sample preparation and analytical techniques are given in Appendix A. The data set contains 34 samples of the First-Cycle Volcanics (15 volcanic and 19 intrusive), 5 samples of the Second-Cycle Volcanics (4 volcanic and 1 intrusive) and 9 samples of dykes from the Lac Coutaceau area.

The volcanic rocks in the LG-3 area are classified on the basis of their SiO₂ weight % (normalized to 100% volatile-free) (c.f. Jolly, 1975; Gelinas et al., 1984). Volcanic rocks with SiO₂ <52% are termed 'basalts'; those with SiO₂ 52-57% are 'basaltic andesites' and those with SiO₂ 57-63% are 'andesites'. The chemical subdivision of these rocks is consistent with the qualitative colour-index classification scheme employed in the field and, at least in the case of the least deformed and recrystallized samples, with their petrography.

5.2 The First-Cycle Volcanics

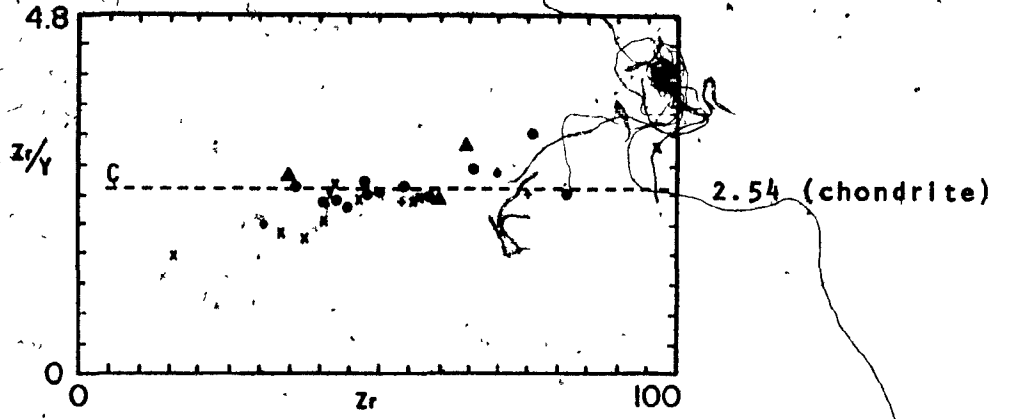
The First-Cycle Volcanics are composed, in decreasing order of abundance, of basalts, synvolcanic intrusives and basaltic andesites (3.2.1). All these rocks are recrystallized and only a few preserve relict primary textures (3.2.2.). Before discussing the primary (magmatic) chemistry of these rocks, the extent of secondary (post-magmatic) chemical remobilization must be evaluated.

To assess the extent of post-magmatic chemical alteration, it is necessary to identify elements that are relatively unsusceptible to secondary remobilization and compare their abundances with those of other elements. Zirconium and Y are particularly useful, since these elements have high field strengths (charge/radius) and are not usually transported in aqueous fluids of low F- and CO₂ activity (Pearce et al., 1979). Furthermore, these elements show systematic variations in unaltered volcanic rocks. Since Zr is more incompatible than Y in most igneous systems, changes in the Zr/Y ratio should reflect fractionation processes whereas equivalent increases in Zr or Y reflect enrichment processes resulting from fractional crystallization (Pearce et al., 1979, Ludden et al., 1984).

The Zr/Y ratio of the intrusive and extrusive rocks in the First-Cycle Volcanics is near chondritic (2.54) and increases slightly with increasing Zr (Fig. 13). These chemical variations are consistent with those of basic magmatic rocks that have

Figure 13 (a) Zr/Y and (b) $Mg / Mg + Fe$ (Mg#) versus Zr (ppm) for the First-Cycle Volcanics. Solid black circles are pillow basalts, solid black triangles are basaltic andesites, 'x' are pyroxene cumulate gabbro sills, open diamonds are diabasic gabbros, crosses are massive basalts and the open triangle is a GMP gabbro sill.

(a)



(b)

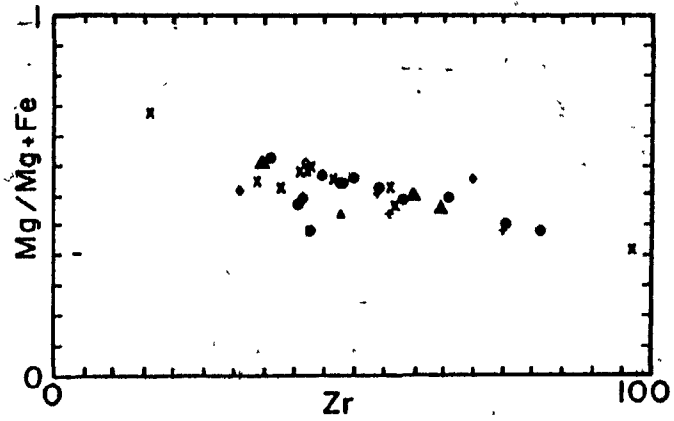


Figure 13

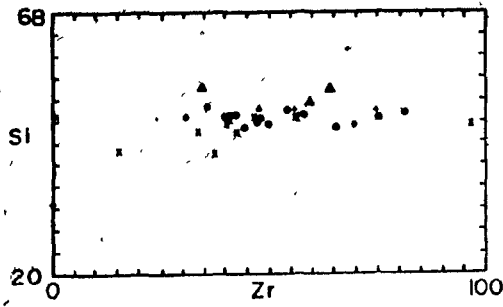
undergone low pressure fractionation (Pearce et al., 1979). Zirconium and Mg# ($Mg\% / (Mg\% + Fe\%)$) are good indices of magmatic differentiation in basic rocks and show a negative correlation in the First-Cycle Volcanics (Fig. 13b). The systematic trends of the Zr/Y ratio and Mg# versus Zr suggest that these rocks are for the most part comagmatic and that Zr, Y and the Mg# have not been affected by metasomatic processes.

The variations of Si, Ti, Al, Fe and, to a lesser extent Mg and Ca, abundances relative to Zr (Fig. 14); suggest that these elements have not been significantly remobilized. Sodium and K variations with Zr are very scattered (Fig. 14g and h). Studies of hydrothermal alteration of oceanic basalts by seawater suggest that Na and K are easily remobilized (Humphris et al., 1978; Mottl, 1983). Humphris (op. cit.) study on natural samples showed non-systematic variations in Na and K between altered rims of pillows and fresh cores. Mottl's experimental work on the batch-alteration of basalts by seawater at temperatures characteristic of the greenschist facies suggest that at low water-to-rock ratios Na is taken up by the rock (albitization), whereas at higher water-to-rock ratios it is leached. Thus, it seems likely that Na and K have been remobilized in the First-Cycle Volcanics by secondary processes and the present abundances of these elements are probably not representative of their primary abundances.

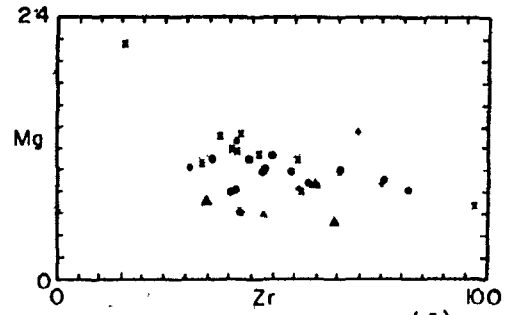
At a given Zr content, the basaltic andesites have higher Si and Al and lower Mg, Fe and Ca abundances than the other

Figure 14 (a) Si, (b) Ti, (c) Al, (d) Fe, (e) Mg, (f) Ca, (g) Na and (h) K (all in cation%) versus Zr (ppm) in the First-Cycle Volcanics. Symbols are as in Fig. 13.

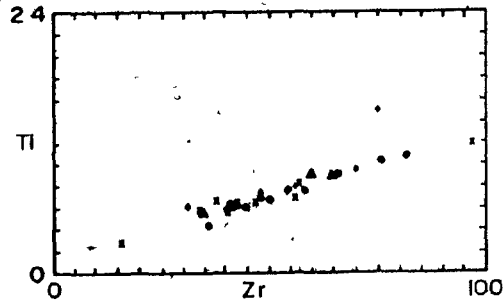
(a)



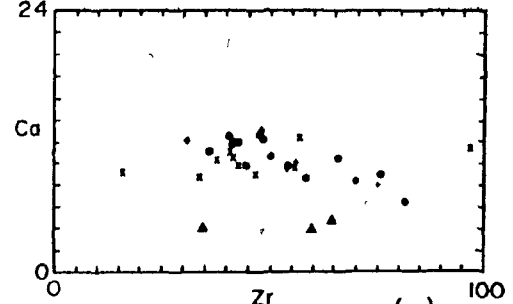
(e)



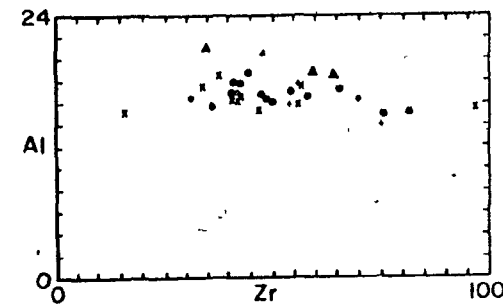
(b)



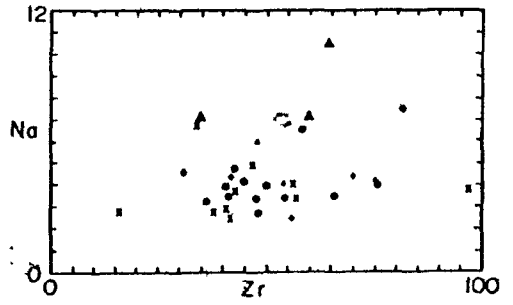
(f)



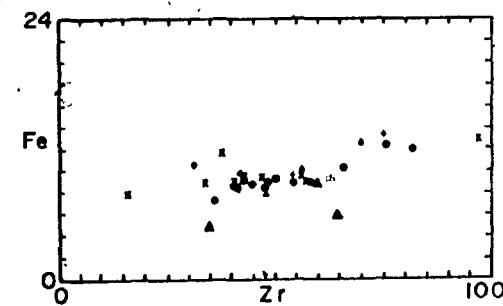
(c)



(g)



(d)



(h)

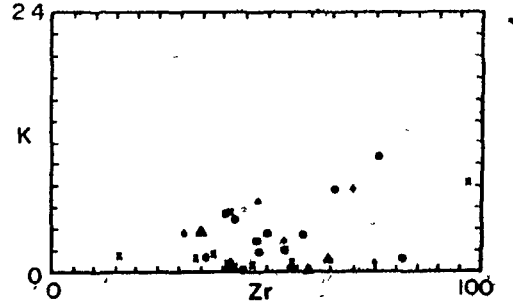


Figure 14

rocks in the First-Cycle Volcanics* (Fig. 14). The basaltic andesites have a high modal abundance of plagioclase (3.2.2) and the high Na and low Ca in these rocks suggest that the plagioclase was relatively sodic (Fig. 14).

With increasing differentiation (increasing Zr abundance), the basalts and synvolcanic intrusives in the First-Cycle Volcanics are characterized by: an increase in Ti, a slight increase in Si, and Fe, a constant Al abundance and decrease in Ca and Mg (Fig. 14). The most differentiated Fe-rich basalts occur throughout the First-Cycle Volcanics, but attain the highest Fe abundances in the upper part of the succession (see Appendix B for sample locations).

Pillowed basalts in the First-Cycle Volcanics contain phenocrysts (3.2.2) of plagioclase and possibly post-pyroxene pseudomorphs, whereas diabasic gabbros in the succession contain post-clinopyroxene pseudomorphs, plagioclase, titanomagnetite and granophyre. It is instructive to see what control these mineral phases exerted on the liquid line of descent. The continuous decrease in Mg and Ca (Fig. 14e and f) requires that the melt was saturated in a phase (or phases) that contains these components. Saturation of the melt with clinopyroxene could explain the decrease in Ca and Mg, whereas equilibration with olivine could explain a decrease in Mg alone. The

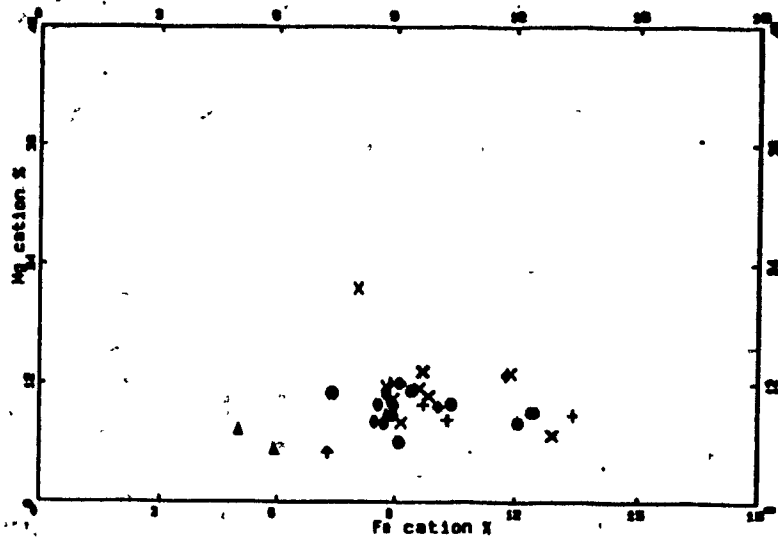
* The basaltic andesite with the lowest Zr, Ti and Fe is characterized by the highest Al, Si, Ni and Cr abundances, whereas its Mg content is intermediate between those of the other samples (Fig. 14, 16a and d).

tendency toward iron-enrichment in the most evolved basalts would require that the magma was saturated with a phase with low iron content, such as plagioclase (Fig 15a). The tendency toward increasing Fe and Ti with increasing differentiation suggests that the basaltic magma did not fractionate an Fe- and Ti-bearing phase (Fig. 14d, b, 15a and b). The presence of titanomagnetite in the basalts and in the interstices of differentiated gabbros probably reflects late-stage crystallization of these phases (3.2.2).

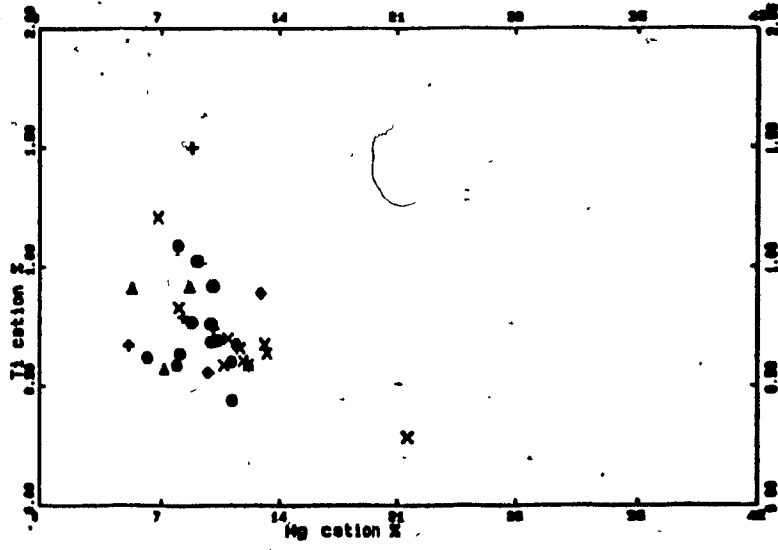
In Al-Si space, the basalts of the First-Cycle Volcanics exhibit a diffuse trend (Fig. 15c). The most iron-rich basalts plot at the low-Al and high-Si end of this spectrum, whereas the most magnesium-rich basalts have the lowest Si and highest Al abundances. The field for MORB basalts directly overlaps the compositional envelope of the First-Cycle Volcanics. This compositional envelope in Al-Si space corresponds to a two- or three-phase cotectic for many basaltic liquids that have fractionated along olivine-control lines until they became saturated with respect to plagioclase and perhaps clinopyroxene (Cox et al., 1979; Francis, 1983, ms. 1985). Plagioclase fractionation in Al-Si space drives the melt toward higher Si and lower Al. Similarly, in Ti-Mg and Mg-Fe space (Fig. 15b and a, respectively), plagioclase fractionation (either by the melting or crystallization of this phase) is marked by increasing Ti with decreasing Mg and an increase in Fe with decreasing Mg.

Figure 15 (a) Mg versus Fe, (b) Ti versus Mg and (c) Al versus Si (all in cation%) for the First-Cycle Volcanics. Symbols are as in Fig. 13. The dotted field in (c) is that of MORB (FAMOUS) glasses (Bryan, 1979).

(a)



(b)



(c)

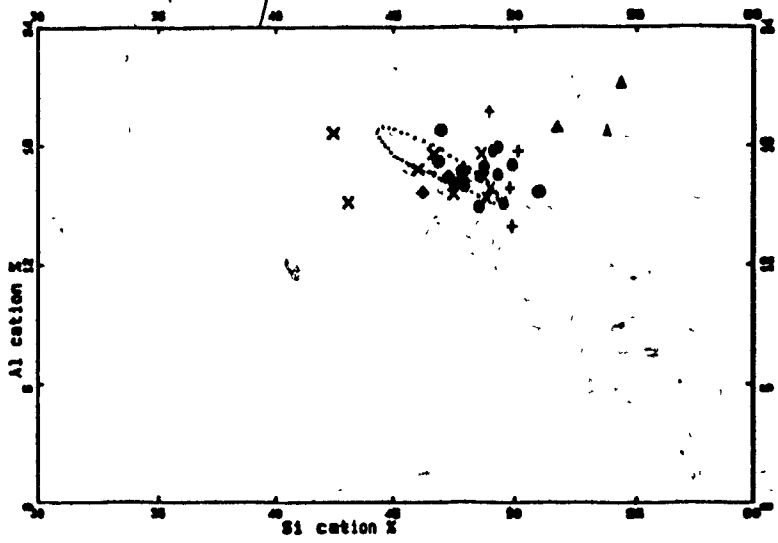


Figure 15

The basaltic andesites have higher Al and Si abundances than the basalts of the First-Cycle Volcanics (Fig. 15c). The abundance of microphenocrysts of plagioclase in these rocks (3.2.2) is consistent with their position in Al-Si space. Similarly, the one sample of GMP analyzed is displaced toward a higher Al abundance than the main cluster of data for the First-Cycle Volcanics (Fig. 15c).

With increasing Zr content the First-Cycle Volcanics are characterized by a continuous decrease in Ni and Cr (Fig. 16a and d). There is considerable scatter in Sr-Zr space, but overall Sr decreases in abundance relative to Zr (Fig. 16b). Phosphorus and V have a positive slope relative to Zr in the basalts of the First-Cycle Volcanics (Fig. 16c, e). Scandium shows little change in abundance with increasing Zr in the basalts (Fig. 16g).

Chondrite-normalized rare earth element (REE) abundances of the basalts in the First-Cycle Volcanics are flat and parallel, ranging from 7 to 16x chondrite (Fig. 17). The most magnesium-rich basalts have low chondrite-normalized REE abundances, whereas the most iron-rich basalts have high abundances. The $(La/Sm)_n$ and $(La/Yb)_n$ ratios show only a slight increase with increasing La abundance (Fig. 18a and b). These compositional relationships suggest that these elements were not greatly fractionated with respect to each other with increasing degrees of differentiation. The Zr/Y ratios of the basalts increase slightly with increasing Zr abundance (Fig. 13a), suggesting that

Figure 16 (a) Ni, (b) Sr, (c) P, (d) Cr, (e) V, (f) Y and (g) Sc versus Zr (all in ppm) for the First-Cycle Volcanics. Black circles are pillow basalts and triangles are basaltic andesites.

Figure 16

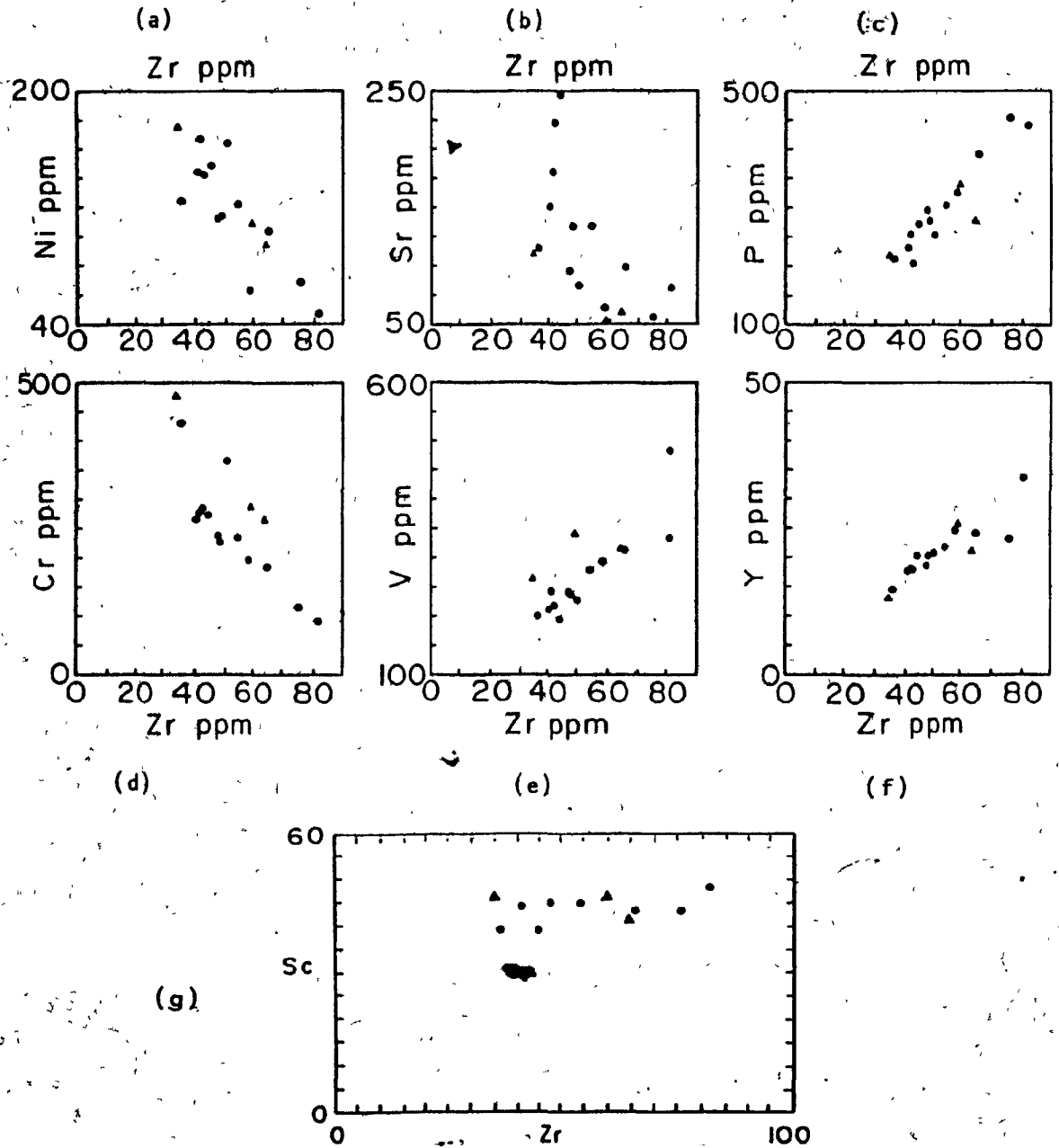


Figure 17 Chondrite normalized REE in the First-Cycle
Volcanics. Symbols are as in Fig. 16. Normalization factors
are those of the LEEDY chondrite (Hanson, 1980).

ROCK / CHONDRITE

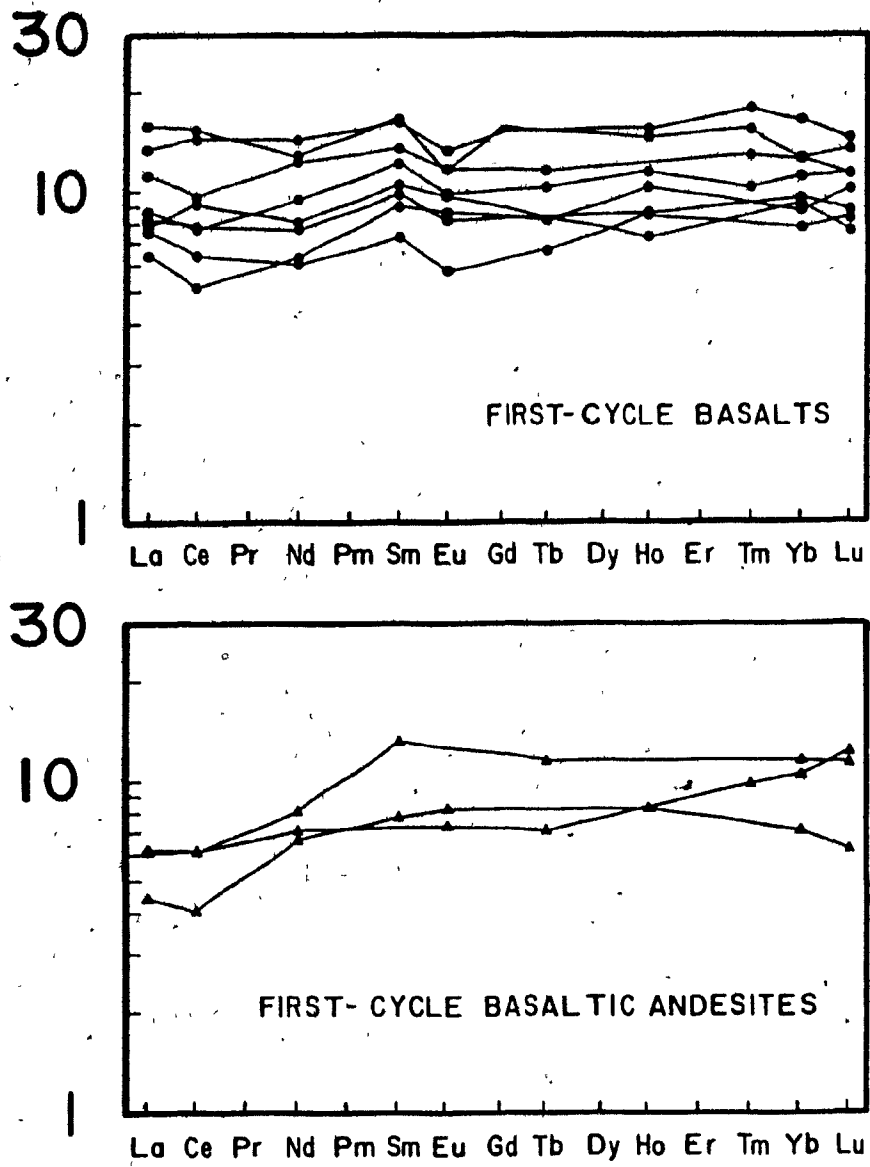
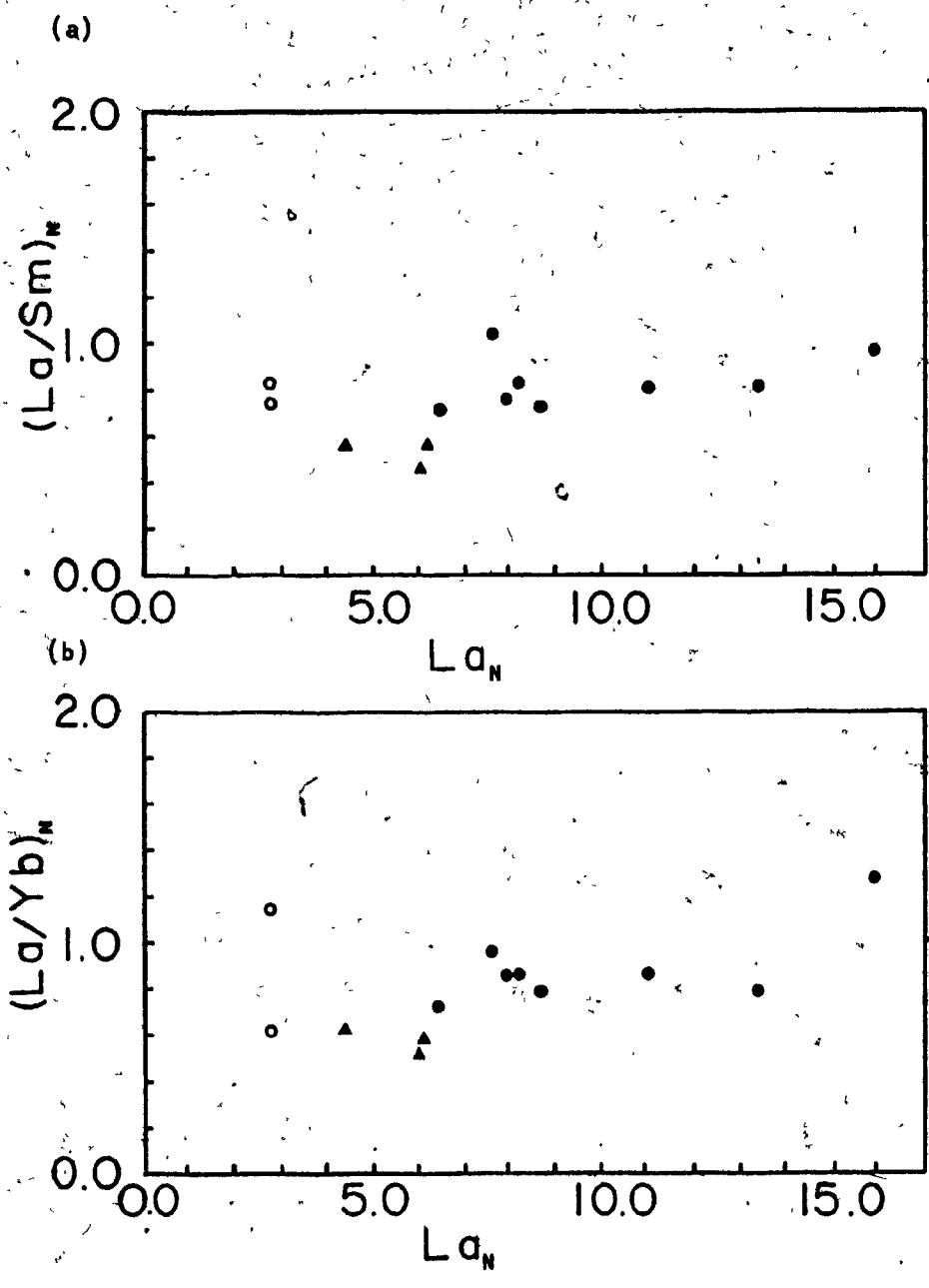


Figure 17

Figure 18 (a) $(La/Sm)_n$ and (b) $(La/Yb)_n$ versus $(La)_n$ for the First-Cycle Volcanics and Lac Geyer komatiites. Lanthanum and Samarium are normalized as per Fig. 17. Open circles are peridotitic komatiites (samples LG-315, LG-124, Stamatelopoulou-Seymour, 1982). Other symbols are as per Fig. 16.

Figure 18



there may have been some fractionation of these elements with increasing differentiation.

The basaltic andesites have ratios of Ni, Y, P, Sc and Sr to Zr similar to those of the basaltic rocks. However, they have higher Cr and V (Fig. 16). They have LREE depleted profiles and flat, unfractionated profiles from Sm toward the HREE (Fig. 17). The basaltic andesites are characterized by lower $(La/Sm)_n$ and $(La/Yb)_n$ ratios than the basalts (Fig. 18a and b). The Zr/Y ratios of two of the basaltic andesites are slightly higher than the basalts when compared at similar Zr abundances (Fig. 13a).

The Fe-enrichment with increasing differentiation in the First-Cycle Volcanics, as well as the low alkali and relatively low Ti abundances, are characteristic of low-K tholeiites. The First-Cycle Volcanics are similar to the Th1 Archean tholeiites * of Condie (1981, Table 3, this thesis). They have similar SiO_2 , TiO_2 , FeO, MgO, Na_2O , P_2O_5 and MnO abundances but slightly higher Al_2O_3 and lower CaO and K_2O . They have very similar trace element ratios (Ti/V , Zr/Y, Ti/V , $(La/Sm)_n$, Eu/Eu^* and $(Yb/Gd)_n$), although Cr, V and REE abundances are lower. Of average modern volcanic suites the First-Cycle high-magnesium basalts are closest in major- and trace-element composition to MORB (Table 3). Some notable differences between LG-3 basalts

* Type Th1 tholeiites are characterized by flat REE profiles (ca. 10x chondrite) with or without small Eu anomalies. Type Th2 tholeiites are characterized by enriched LREE and sloping REE profiles. Th1 differs from Th2 in its higher TiO_2 , K_2O , P_2O_5 , V, Zr, Sr, Y and Zr/Y and its lower CaO, Cr, FeO/Fe₂O₃ and Ti/Zr (Condie, 1981, Table 3-7).

Table 3 Comparison of Analyses (First-Cycle Volcanics)

	Archean		LG-3			Modern			
	1	2	3	4	5	6	7	8	9
S102	50.2	49.5	50.37	52.76	51.57	49.8	51.1	50.2	50.3
T102	0.94	1.49	0.86	1.54	0.41	1.5	0.83	1.0	2.2
A1203	15.5	15.2	17.16	13.66	9.73	16.0	16.1	17.7	14.3
FeO(*)	10.7	11.6	11.28	15.38	8.94	9.29	9.99	9.80	12.4
MgO	7.53	6.82	7.91	5.75	15.98	7.5	5.1	5.4	5.9
CaO	11.6	8.79	9.77	6.37	10.71	11.2	10.8	9.8	9.7
Na2O	2.15	2.70	2.32	4.08	1.54	2.8	2.0	2.7	2.5
K2O	0.22	0.69	0.02	0.10	0.56	0.14	0.30	0.9	0.8
P2O5	0.10	0.17	0.06	0.09	0.09	0.20	0.15	0.2	0.16
MnO	0.22	0.18	0.21	0.25	0.19	0.17	0.17	0.2	0.2
H2O	1.62	2.04				1.3	0.50	0.70	0.65
LOI			4.52	2.06	4.16				
CaO/A1203	0.75	0.58	0.56	0.46	1.10	0.70	0.67	0.55	0.68
Mg#(**)	0.41	0.36	0.41	0.27	0.64	0.44	0.33	0.36	0.32
Cr	490	250	272	90	1558	300	50	50	100
Ni	140	125	148	47	430	100	25	50	100
V	260	365	195	482	138	300	270	150	300
Zr	53	135	45	81	42	100	60	100	200
Ba	80	90	41	88	180	11	60	100	200
Sr	100	190	246	80	157	135	225	300	350
La	3.6	13	2.6	4.2	15.0	3.5	3.9	9.2	27
Ce	9.2	30	6.4	11.8	35.6	12	7	25	140
Nd	6.6	17	4.6	8.6	17.5	11	6	15	61
Sm	2.0	4.0	1.9	3.1	3.41	3.9	2.2	3.8	8.2
Eu	0.73	1.3	0.59	0.96	0.76	1.5	0.9	1.3	2.0
Gd	2.6	3.8				6.2	2.5	4.5	6.5
Yb	1.9	2.2	2.0	3.50	0.79	3.0	2.0	2.5	2.5
Lu	0.31	0.38	0.29	0.48	0.07	0.3	0.3	0.5	0.4
Y	20	30	20	34	9	30	20	23	30
Ti/Zr	106	66	114	114	58	90	83	60	66
Zr/Y	2.7	4.5	2.3	2.4	4.6	3.3	3.0	4.3	6.7
Ti/V	22	24	26	19	18	30	18	40	44
(La/Sm) _n	0.99	1.8	0.83	0.82	2.68	0.49	0.97	1.3	1.8
Eu/Eu*	0.96	1.0				0.92	1.2	1.0	0.85
(Yb/Gd) _n	0.91	0.73				0.60	1.0	0.69	0.48

- 1 average Archean tholeiite (Condie, 1981, Table 3-7, type Th1)
 2 average Archean tholeiite (Condie, 1981, Table 3-7, type TH2)
 3 First-Cycle pillowed plagioclase-phyric basalt (83-216)
 4 First-Cycle pillowed basalt (83-158)
 5 Second-Cycle basalt (83-285c)
 6 average MORB (Condie, 1981, Table 3-7)
 7 average arc tholeiite (Condie, 1981, Table 3-7)
 8 average calc-alkaline tholeiite (Condie, 1981, Table 3-7)
 9 average continental rift tholeiite (Condie, 1981, Table 3-7)
 * (total iron recalculated as FeO) ** (Mg# = MgO / MgO + FeO*)
 La/Sm and La/Yb are normalized to Leedy chondrite (Hanson, 1980)

and MORB are: lower TiO₂, CaO in the former and lower (La/Sm)_n, Ti/Zr and higher Zr/Y, V and REE abundances in the latter (Table 3).

5.3 Second-Cycle Volcanics and the Lac Coutaceau Dykes

The Second-Cycle Volcanics are composed of basalt, basaltic andesite, andesite and an intrusive plug of norite. Five samples were collected for chemical analysis; three from the top, middle and near the base of one flow (Appendix B), one from an adjacent flow and one from a noritic plug in the eastern part of the map area (Appendix B). The three samples from one flow range in composition from basaltic andesite at the top and center to basalt at the base of the flow.

Silicon, Ti, Al, Mg, Fe and Ca in the extrusive rocks of the Second-Cycle Volcanics define well developed linear variations with Zr, whereas, Na and K display more scatter (Fig 19). These compositional variations suggest again that, with the exception of Na and K, these elements have not been significantly remobilized by secondary processes. Silicon, Al and Na increase, whereas Mg, Fe and Ca decrease and Ti and K show little change in abundance with increasing Zr in the Second-Cycle Volcanics (Fig. 19). The First- and Second-Cycle Volcanics have distinctly different chemical compositions. The Second-Cycle Volcanics have higher Si, Mg and Na and lower Ti, Al, Fe and Ca abundances than the First-Cycle Volcanics (compare Figures 19, 14 and Table 3).

Figure 19 (a) Si, (b) Ti, (c) Al, (d) Fe, (e) Mg, (f) Ca, (g) Na and (h) K (all in cation%) versus Zr (ppm) for the Second-Cycle Volcanics and Lac Coutaceau dykes. Black diamonds are basaltic andesites and andesites and the cross is a norite plug that intrudes the Second-Cycle Volcanics. The open triangles are Lac Coutaceau dykes.

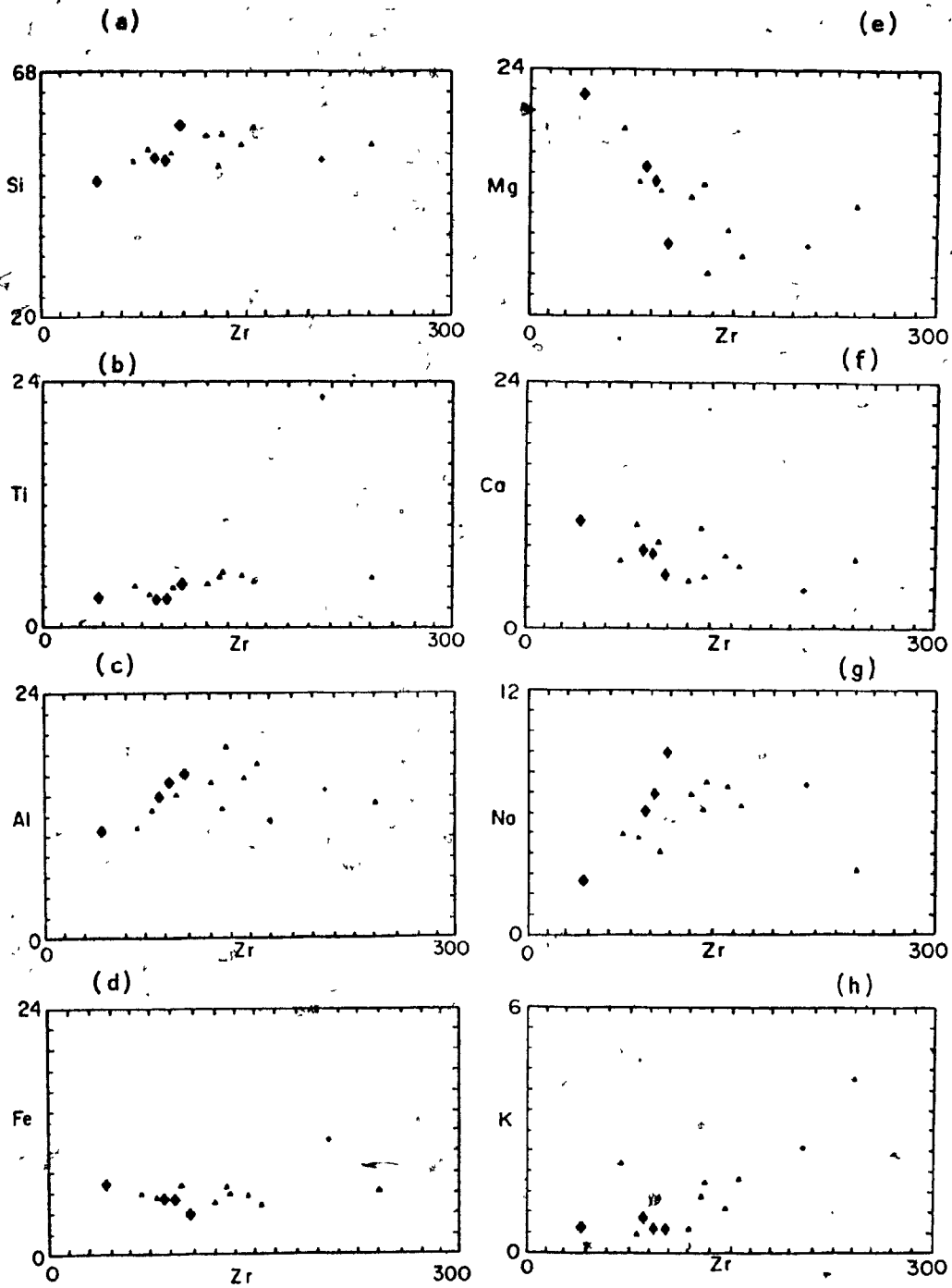


Figure 19

The noritic plug in the eastern part of the map area does not lie on the main trend of chemical variation of the extrusive rocks of the Second-Cycle Volcanics (Fig. 19). This rock has higher Zr, Ti, Fe and lower Ca abundances than the extrusive rocks. The abundance of titanomagnetite in this rock (3.4.2), and the high Ti and Fe concentrations relative to the extrusive rocks, suggest that titanomagnetite is a cumulate phase.

The Lac Coutaceau diorite dykes are chemically very similar to the extrusive rocks of the Second-Cycle Volcanics (Fig. 19). The dykes may have been feeders to Second-Cycle lava flows, especially since both suites were emplaced relatively late in the history of the greenstone belt (although the Lac Coutaceau dykes crosscut the supracrustal succession, whereas the Second-Cycle Volcanics comprise the top of the supracrustal pile).

The Lac Coutaceau diorite dykes are characterized by increasing Si, Al and Na, decreasing Mg and Ca and little change in Ti, Fe and K with increasing Zr abundance (Fig. 19). The compositional trends of the Lac Coutaceau dykes overlap the trends in the Second-Cycle Volcanics and extend to higher Zr abundances.

In Mg-Fe space, the Second-Cycle Volcanics define an iron-depletion trend with decreasing Mg. The Lac Coutaceau dykes overlap this trend at high Mg contents and evolve to lower decreasing Mg at constant Fe abundance (Fig. 20a). Both suites

are characterized by increasing Si and Al, decreasing Ca and a relatively low, constant abundances of Ti with decreasing Mg (Fig. 20, 21). The increase in Al with decreasing Mg suggests that these rocks were saturated with a magnesium-bearing phase (or phases) (Fig. 21b).

In Al-Si space (Fig. 20c), the Second-Cycle Volcanics and Lac Coutaceau dykes correlate positively. The continuous positive slope in Al-Si space and lack of Fe-enrichment suggests that these rocks did not fractionate an appreciable amount of plagioclase, since this phase would have decreased the Al abundance with increasing Si (Fig. 20c). Thus, the decrease in Ca abundance with decreasing Mg abundance (Fig. 21a) must be due in a large part to some other Ca-bearing phase, such as clinopyroxene.

It is unlikely that clinopyroxene alone could account for the major element variations of these rocks, especially in light of the large range in Mg over which these rocks have evolved. In principle the fractionation of olivine and/or orthopyroxene could account for the variation of Fe, Ti, Al and Si relative to Mg (Fig. 20 and 21) and indeed on the basis of these elements alone it is not possible to choose a unique fractionation scheme. However, Al-Si variations (Fig. 20c) are more consistent with an olivine control line, since this phase plots at 33.3% Si which is very close to the Si intercept (29% Si, at 0% Al) calculated by linear extrapolation. The nature of the phases

Figure 20 (a) Mg versus Fe, (b) Ti versus Mg and (c) Al versus Si (all in cation%) for the Second-Cycle Volcanics and Lac Coutageau dykes. Symbols are as in Fig. 19. Olivine (OLIV) and Al-free orthopyroxene (OPX) are shown for reference in Fig. 20c.

Figure 20

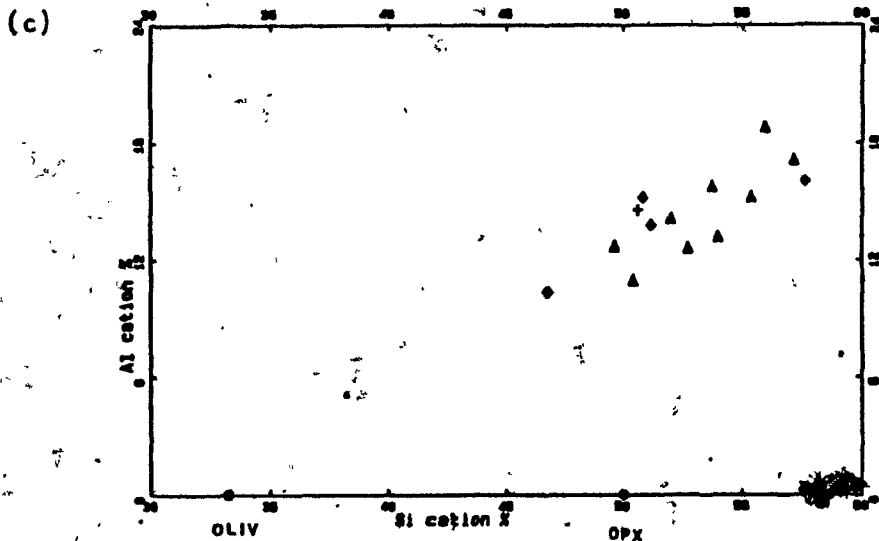
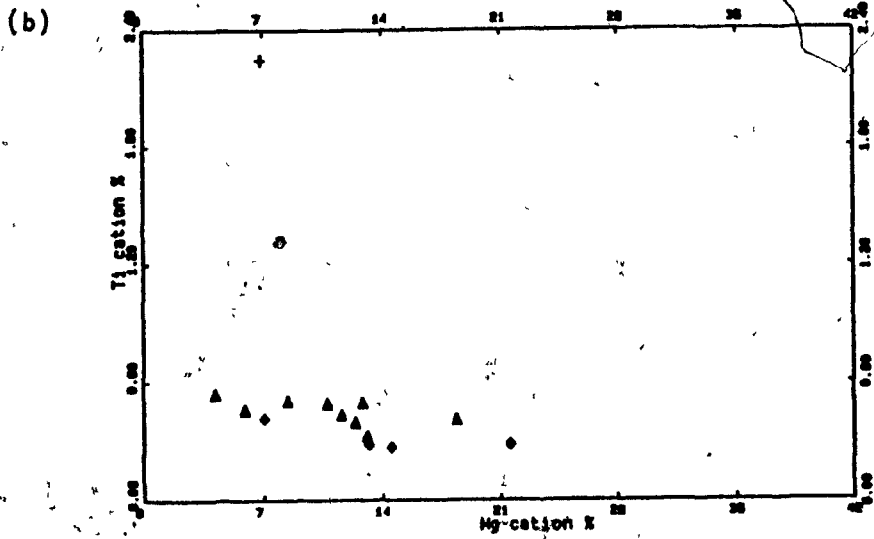
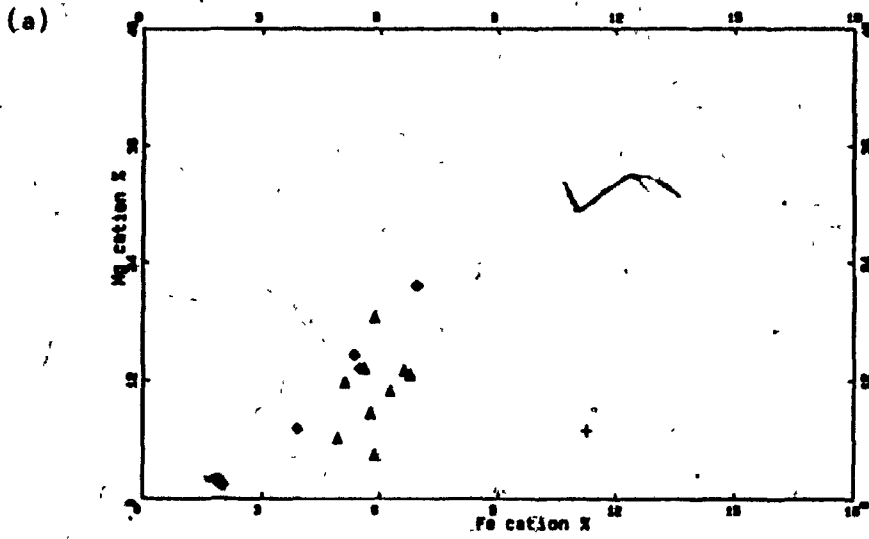
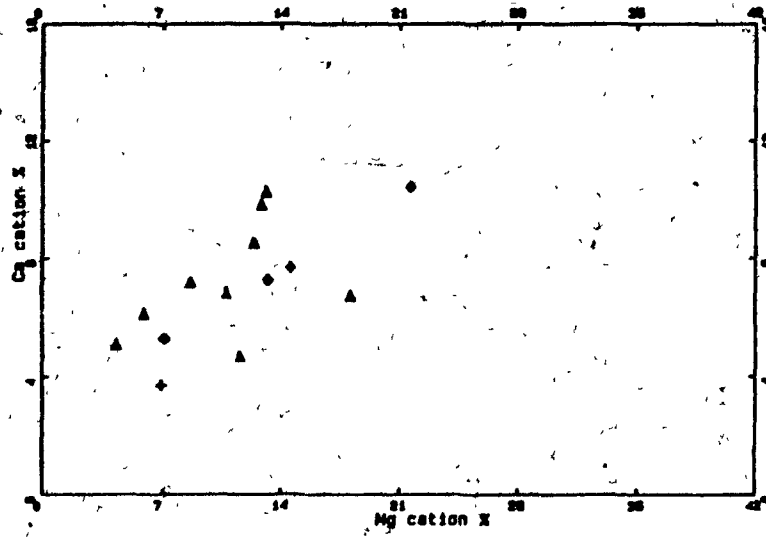


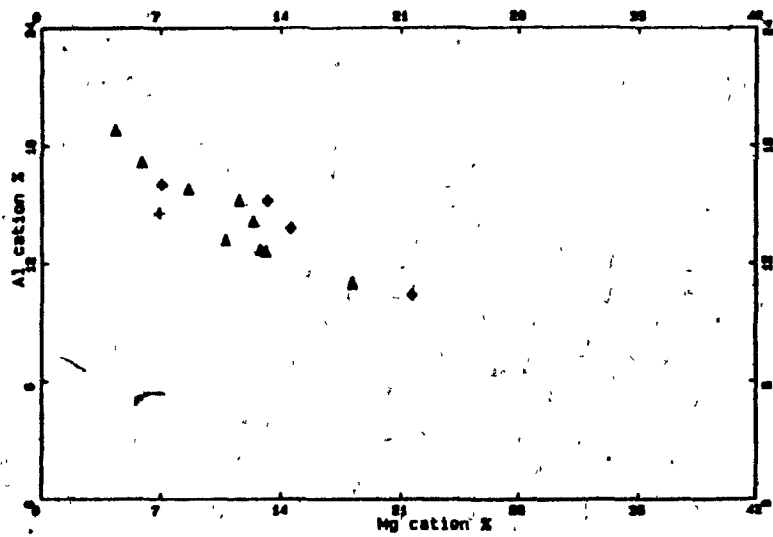
Figure 21 (a) Ca, (b) Al and (c) Si versus Mg (all in cation%) for the Second-Cycle Volcanics and Lac Coutageau dykes. Symbols are as in Fig. 19.

Figure 21

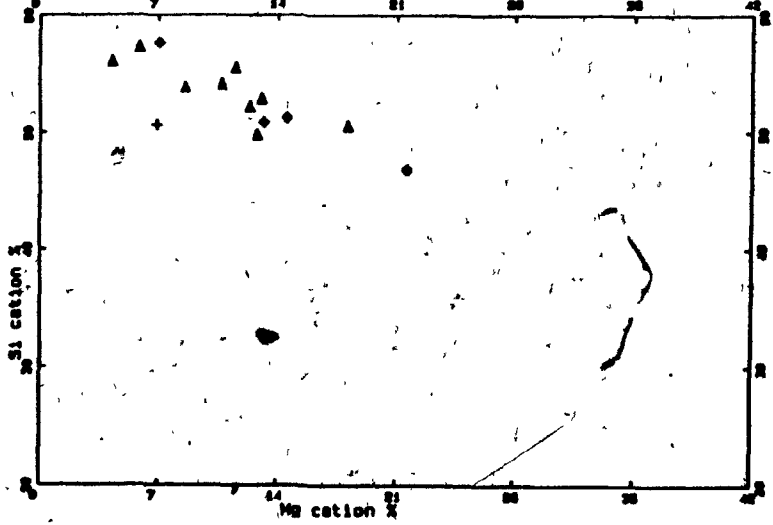
(a)



(b)



(c)



which controlled the evolution of this suite will be examined in more detail in chapter 6.

There is little change in Y with increasing Zr in the Second-Cycle Volcanics and Lac Coutaceau dykes (Fig. 22a). Phosphorus, and to a lesser extent Ti, increase with increasing Zr abundance (Appendix B and Fig. 19b). Chromium, Ni and Sc all decrease with increasing Zr with three- and two- orders of magnitude change in Cr and Ni respectively, and a three-fold decrease in Sc accompanying a four-fold increase in Zr (Fig. 22 b, c and d).

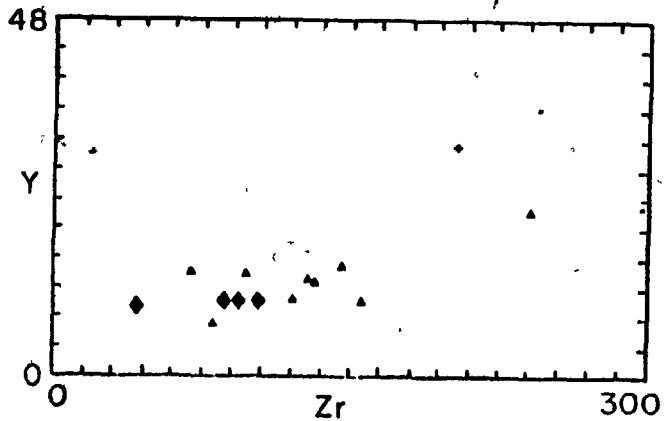
The chondrite-normalized patterns of both the Second-Cycle Volcanics and Lac Coutaceau Dykes are characterized by high abundances of LREE (up to 100x chondrite) and low abundances of HREE (as low as 2x chondrite, Fig. 23). The chondrite-normalized middle and heavy REE have slightly flatter slopes relative to the light REE. The $(La/Sm)_n$ and $(La/Yb)_n$ ratios of both suites increase with increasing La abundance (Fig. 24c and b). The scatter in the $(La/Yb)_n$ versus $(La)_n$ diagram (Fig. 24b), is probably due in part to analytical uncertainties at these low levels of HREE (see Appendix A). The Zr/Y ratio increases in both suites with increasing Zr abundance (Fig. 24a). In general the REE correlate positively with increasing Zr and Si (Appendix B).

The Second-Cycle Volcanics and Lac Coutaceau dykes have few Archean or Modern analogues in terms of their chemical

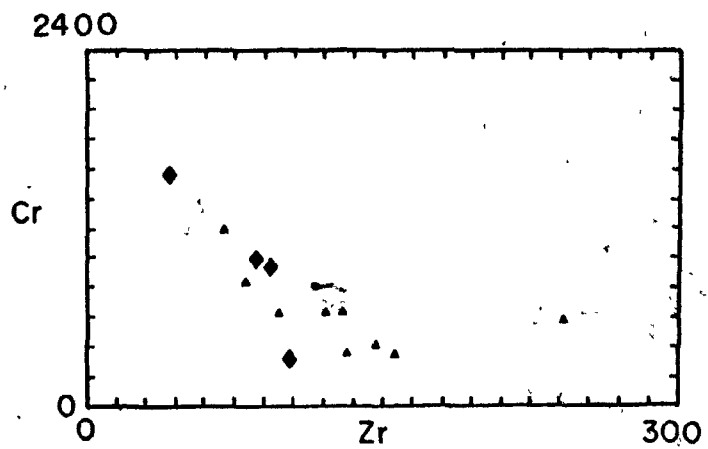
Figure 22 (a) Y, (b) Cr, (c) Ni and (d) Sc versus Zr (all in ppm) for the Second-Cycle Volcanics and Lac Coutaceau dykes. Symbols are as in Fig. 19.

Figure 22

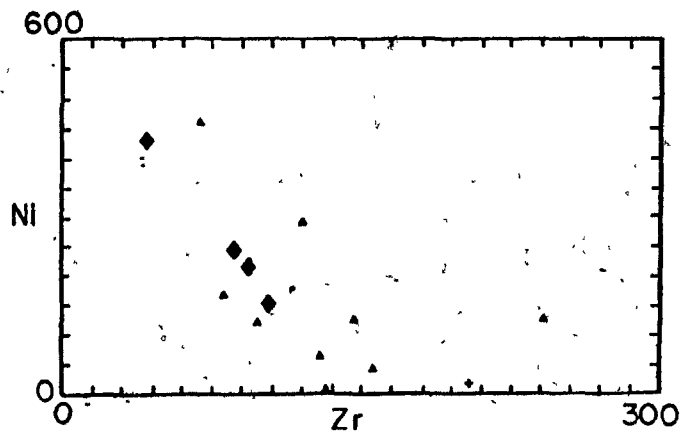
(a)



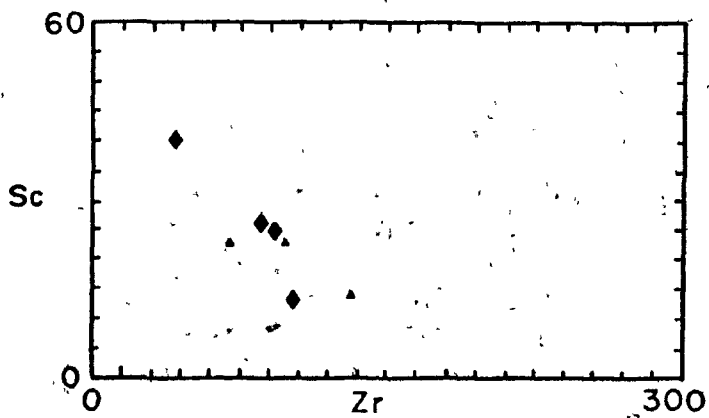
(b)



(c)



(d)



**Figure 23 Chondrite normalized REE in the Second-Cycle
Volcanics and Lac Coutaceau dykes. Normalizing factors are as
in Fig. 17. Symbols are as in Fig. 19.**

ROCK / CHONDRITE

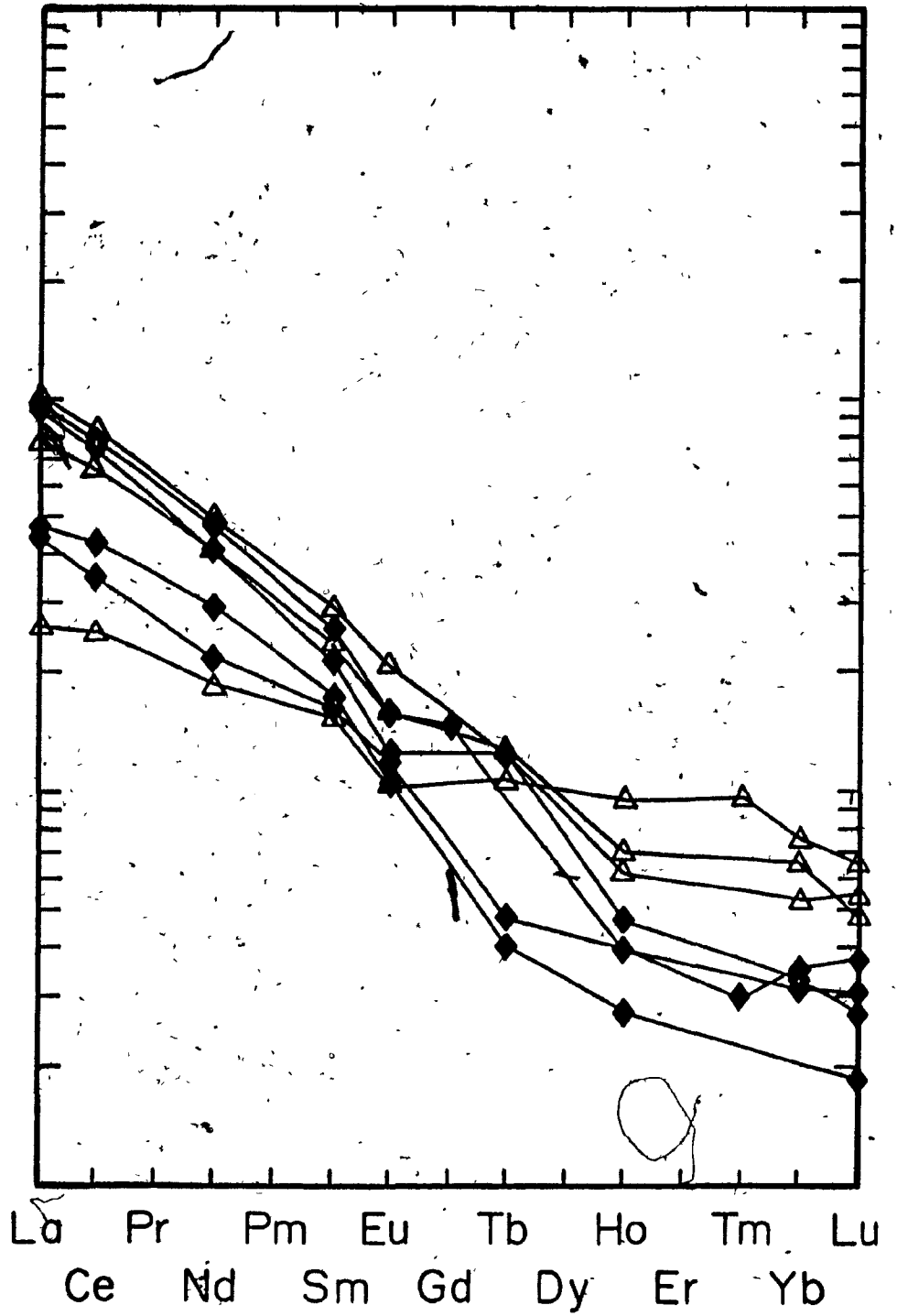


Figure 23

Figure 24: (a) Zr/Y versus Zr (all in ppm), (b) $(La/Yb)_n$ and (c) $(La/Sm)_n$ versus $(La)_n$ for the Second-Cycle Volcanics and Lac Coutaceau dykes. Normalizing factors for (b) and (c) are as in Fig. 17. Symbols are as in Fig. 19.

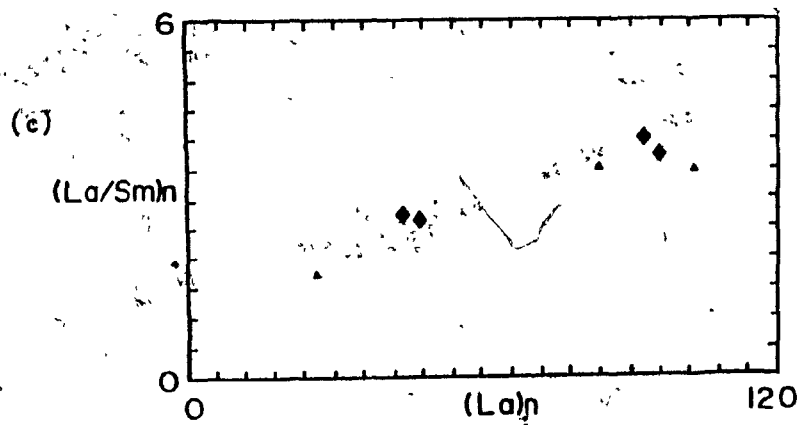
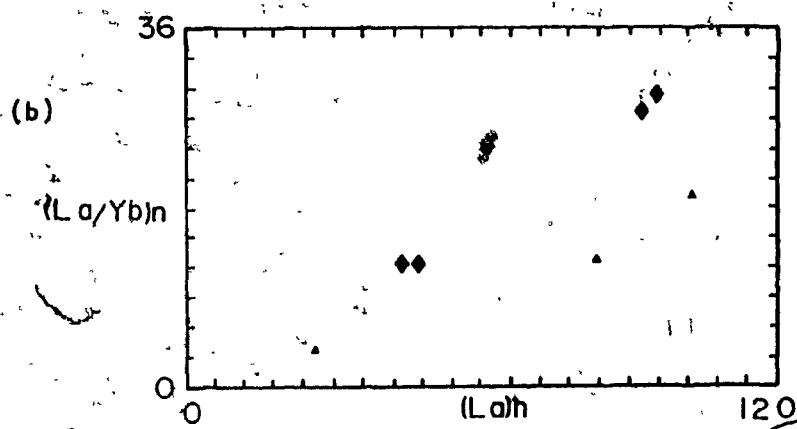
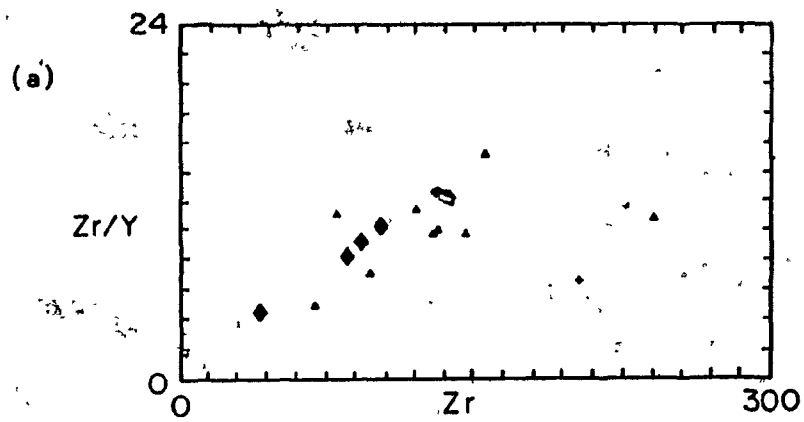


Figure 24

composition (Table 4). When compared with Type 1 * Archean andesites (Condie, 1981), the Second-Cycle and Coutaceau rocks at similar SiO₂ abundances (Table 4, #2 and #3) have: lower TiO₂, Al₂O₃, FeO*, Y, HREE and Zr abundances and higher MgO, CaO, K₂O, Cr, Ni, LREE, Zr/Y, (La/Sm)_n and (La/Yb)_n. Similarly, the least differentiated members of the Second-Cycle-Coutaceau suite (eg. Table 4, #1) are different from type BK1 average basaltic komatiites ** (Table 4, #5) at similar SiO₂ abundances. In particular, the basaltic komatiites have higher TiO₂, Al₂O₃, FeO*, CaO and Ti/Zr and lower MgO, Mg#, Cr, Ni, (La/Sm)_n, (La/Yb)_n and Zr/Y. The only modern volcanic rocks which have chemical compositions similar to those of the Second-Cycle Volcanics and Lac Coutaceau Dykes are boninites (Table 4, #8). When compared at similar SiO₂ abundances (eg. Table 4, #3 and #8) the boninites have: lower TiO₂, Al₂O₃, CaO, K₂O, CaO/Al₂O₃, Zr, Y, Sr, REE, (La/Sm)_n and (La/Yb)_n and higher MgO, Cr, Ni and Zr/Y than the Lac Coutaceau Dykes and Second-Cycle Volcanics.

* Type 1 andesites: high FeO, MgO, Ni, Cr, Zn and low K₂O, Rb and Ba relative to other Archean andesites and which have LREE enrichment in the order of 50 x chondrite. Type 2 andesites: notably enriched in LREE (ca. 200X chondrites) negligible europium anomalies. Type 3 andesites: flat REE patterns (ca. 20-30x chondrites), negative europium anomalies, low Y and Sr relative to types 1 and 2. (Condie, 1981, Table 3-9).

** BK exhibits flat to very slightly enriched LREE, BK2 exhibits slightly depleted LREE and BK3 strongly depleted LREE (Condie, 1981).

Table 4 Comparison of Analyses (Second-Cycle Volcanics).

	Archean						Modern		
	1	2	3	4	5	6	7	8	9
SiO ₂	49.79	54.02	55.43	58.98	50.5	56.7	56.20	54.52	53.80
TiO ₂	0.40	0.40	0.55	0.75	0.60	0.92	0.13	0.23	0.31
Al ₂ O ₃	9.39	13.69	12.70	16.75	11.0	14.0	10.57	9.36	11.40
FeO(*)	8.81	6.94	8.62	7.36	10.60	9.07	8.05	6.99	7.47
MnO	0.18	0.13	0.17	0.10	0.20		0.16	0.27	0.16
MgO	15.43	9.42	8.88	3.03	10.2	5.4	11.19	14.62	12.54
CaO	10.34	7.20	8.42	4.97	11.8	6.6	7.44	3.55	8.73
Na ₂ O	1.49	3.78	2.28	4.11	1.87	3.4	1.54	1.93	1.30
K ₂ O	0.54	0.48	1.14	1.44	0.17	0.67	0.40	0.41	0.15
P ₂ O ₅	0.09	0.21	0.30	0.34	0.06		0.02	0.03	0.02
H ₂ O(total)					2.4	3.0	3.95	7.62	3.79
LOI	4.16	4.34	1.56	1.69					
CaO/Al ₂ O ₃	1.10	0.53	0.66	0.30	1.10	0.47	0.70	0.38	0.77
Mg# (* *)	0.64	0.58	0.51	0.29	0.49	0.37	0.58	0.68	0.63
Cr	1558	935	870	334	920	125	695	1100	960
Ni	430	217	122	<1	360	70	194	400	268
V	138	120			250		181	105	204
Zr	42	93	97	132	33	150	20	63	18
Ba	180	166			20	230	30	54	12
Sr	157	572	337	669	100	278	61	325	62
La	15.0	30.4	26.57	32.6	3.0	13	0.82	4.40	0.88
Ce	35.6	64.2	55.13	70.6	7.9	31	1.79	10.39	2.22
Nd	17.5	28.0	23.90	29.7	5.2	17	1.20	5.37	1.91
Sm	3.41	4.98	4.60	5.75	1.6	3.6	0.35	1.27	0.73
Eu	0.76	1.11	1.09	1.41	0.55	1.1	0.11	0.39	0.27
Gd		3.83			2.0	3.6	0.40	1.28	0.96
Yb	0.79	0.68	1.38	1.12	1.5	1.8	0.52	0.75	1.04
Lu	0.07	0.10	0.19	0.14	0.23	0.3			
Y	9	10	14	13	17	25	5	7	9
Ti/Zr	58	66	34	34	109	37	39	22	103
Zr/Y	4.6	4.5	7.1	11.	1.9	6.0	4.0	9.0	2.0
Ti/V	18	20			14		4.3	13	9.1
(La/Sm) _n	2.6	3.7	3.5	3.5	1.1	2.2	1.4	2.1	0.73
(La/Yb) _n	12.5	29.5	12.7	19.2	1.3	4.8	1.0	3.5	0.56

- 1 Second-Cycle basalt 83-285c
- 2 Second-Cycle basaltic andesite 83-285a
- 3 Lac Coutaceau diorite dyke 82-493
- 4 Lac Coutaceau diorite dyke 82-496
- 5 average basaltic komatiite (Condie, 1981 Table 3-4 type BK1)
- 6 average Archean andesite (Condie, 1981 Table 3-9 type I)
- 7 boninite Bonin islands (Cameron et al., 1983 Table 2 #1)
- 8 boninite New Caledonia (Cameron et al., 1983 Table 2 #5)
- 9 boninite New Zealand (Cameron et al., 1983 Table 2 #8)
- * (total iron recalculated as FeO) ** (Mg# = MgO / MgO + FeO*)
- La/Sm and La/Yb are normalized to Leedy chondrite (Hanson, 1980)

Chapter 6 Petrogenesis of the Volcanic and Synvolcanic Intrusives

6.1 Introduction

In Chapter 5 it was seen that there are fundamental chemical differences between the two volcanic units in the LG-3 area. In this chapter, the petrogenetic significance of these differences is examined. The chemistry of the volcanic rocks in the LG-3 area is compared with that of other suites in the La Grande greenstone belt and petrogenetic models for the magmatic processes are developed and evaluated.

6.2.1 Petrogenesis of the First-Cycle Volcanics

The basalts and synvolcanic intrusives in the First-Cycle Volcanics comprise a chemical continuum and thus were probably related to a common parental magma by a similar petrological process(es). The best estimate of magmatic liquid compositions in the First-Cycle Volcanics is that of the pillow basalts. The most magnesium-rich basalts in this suite have 10.94% Mg and 8.74% Fe (Fig. 15a). These high-Mg basalts do not lie in the possible field of compositions that could have been in equilibrium with an upper mantle of pyrolite composition (c.f. Hanson et al., 1978). Thus, it would appear that the basalts in the First-Cycle Volcanics are not primary.

The lack of fractionation between the light and heavy REE

and the relatively large change in the abundance of compatible elements (such as Ni, Cr and Sr) compared with that of incompatible elements (such as Zr) with increasing differentiation suggests that the basalts in the First-Cycle Volcanics have evolved by fractional crystallization from more primitive parents (c.f. Arth, 1976). The decrease in Ca, Mg and lack of increase in Sc with increasing differentiation could reflect fractionation of clinopyroxene. Similarly, the decrease in Ca, Al, Sr and Eu and increase in Fe are consistent with the presence of plagioclase in the fractionating assemblage. The decrease in Cr abundance with increasing fractionation may reflect the fractionation of small quantities of a Cr-bearing spinel. Plagioclase is found in both the extrusive and intrusive rocks, whereas clinopyroxene can only be identified with reasonable certainty in the intrusive rocks, although phenocrysts may have occurred in the basalts (3.2.2). Chromite has been found in synvolcanic peridotite sills in the western part of the La Grande belt (Rivard et al., 1984).

The decrease in Ni with increasing differentiation suggests that olivine or orthopyroxene may have formed part of the fractionating assemblage. Although magmatic sulphides have very high partition coefficients for Ni, this phase is not invoked to explain the variations in the First-Cycle Volcanics, since magmatic sulphides have not been reported from the La Grande belt. Olivine is favoured over orthopyroxene since it has been reported as a phenocryst phase in komatiites and as a

cumulate phase in synvolcanic-high-level peridotitic sills in other parts of the La Grande belt, whereas orthopyroxene has not (Stametolopoulou-Seymour, 1982; Rivard et al., 1984).

A least-squares mixing program (Wright et al., 1970) using the major element abundances of an Mg-rich basalt (sample 216-83, Appendix B) as parent and an Fe-rich basalt as daughter (sample 158-83, Appendix B) was used to test the viability of fractional crystallization to reproduce the trend of Fe-enrichment in the basalts (Table 5). Various phase assemblages were tested including orthopyroxene - plagioclase - clinopyroxene, olivine - plagioclase, and clinopyroxene - plagioclase. The most satisfactory model (Table 5) has acceptably low residuals and indicates that 49% fractionation of plagioclase, olivine and clinopyroxene, in the proportions 62:20:18, could reproduce the Fe-enrichment trend in the basalts. The olivine composition required (Fo 71) is intermediate between those olivines which would coexist with the parent (Fo 81) and the daughter (Fo 68), using a distribution coefficient ($K_d = \text{Mg/Fe olivine} / \text{Mg/Fe liquid}$) of 0.30 with total iron calculated as FeO (c.f. Roeder et al., 1970). The pyroxene employed in the calculation is an average of high-Ca clinopyroxene phenocrysts taken from a tholeiitic basalt from Hawaii (Fodor et al., 1975) of similar chemical composition to the Mg-rich basalt parent (216-83).

It is possible to test whether the fractionation of olivine, plagioclase and clinopyroxene from an Mg-rich basalt to

Table 5 Fractional Crystallization Calculation, Fe-Enrichment in the First-Cycle Volcanics
HIGH-Mg BASALT = Fe-RICH BASALT + PLAG + OLIV + CPX

ELEMENT (wt%)	DAUGHTER	OLIV	CPX	PLAG	PROPOSED PARENT	CALCULATED PARENT	RESIDUALS	
SiO ₂	52.77	37.45	52.90	48.98	50.41	50.14	0.27	
Al ₂ O ₃	13.66		2.67	32.75	17.17	17.08	0.09	
FeO	15.38	28.01	6.24		11.28	11.22	0.06	
MgO	5.75	34.55	17.34		7.91	7.87	0.04	
CaO	6.37		18.92	15.59	9.77	9.60	0.17	
Na ₂ O	4.08			2.68	2.32	2.91	0.59	
TiO ₂	1.54		0.72		0.86	0.86		
WT PROP. 51.53					9.81	8.73	29.95	$\sum(\text{RESIDUALS})^2 = 0.46$
% CRYSTALLIZATION = 48.47%					PLAG:OLIV:CPX = 62:20:18			
Fo = 70.6					En = 50.3 An = 82			
					Fs = 10.2			
					Wo = 39.5			

These calculations were performed with the mineral distribution program of Wright and Doherty (1970). SiO₂, Al₂O₃, FeO, and MgO were weighted 5, CaO and Na₂O were weighted 1 and TiO₂ was weighted 30. Olivine and plagioclase were entered as end-members and their compositions were determined by the calculation. The clinopyroxene is a high Ca clinopyroxene phenocryst from a tholeiitic basalt from Hawaii (average from Fodor and Keil, 1975). The daughter rock is an Fe-enriched pillow basalt from the First-Cycle Volcanics (TS-158-83). The proposed parent is an Mg-rich pillow basalt from the First-Cycle Volcanics (TS-216-83). The calculation uses a least-squares mixing algorithm that adds in this case the mineral phases back into the daughter liquid composition to produce the parent composition. The difference between the proposed parent and calculated parent is shown as a residual. An arbitrary sum of the squares of the residuals = 1 was chosen as an upper cut-off limit in the first step toward determining the acceptability of a particular model.

produce the Fe-rich basalt can reproduce the variation in incompatible trace element concentrations, such as the REE, Zr, Ti and P. Two approaches are taken here. In model 1, bulk mineral-liquid partition coefficients for the trace elements are calculated (Table 6a, Fig. 25) using published mineral-liquid partition coefficients weighted for the proportions of mineral phases calculated from the least-squares calculation (Table 5). In model 2, bulk partition coefficients are calculated from the slope of log (trace element) versus log (hygromagmatophile element (La)) variations (c.f. Allegre et al., (1977) (Table 6b). Both models successfully reproduce the abundance of incompatible trace elements observed in the differentiated Fe-rich composition for 49% crystallization when calculated using the Rayleigh fractional crystallization equation (Table 6, Fig. 25). Thus, it would appear that fractional crystallization of olivine, plagioclase and clinopyroxene from Mg-rich parent basalts can reproduce the major and trace element compositions of the Fe-rich basalts.

The proportions of plagioclase, olivine and clinopyroxene (62:20:18 respectively, Table 5) used in the model, are within the limits (50:15:30 to 60:20:20) that can crystallize from a basalt to produce tholeiitic differentiates as determined by Biggar (1983). Experimental studies on natural and basaltic analogue systems of low-K tholeiites indicate that basaltic liquids are multiply saturated with plagioclase, olivine and clinopyroxene at pressures of less than 10 Kb, since the phase volumes of clinopyroxene increase and olivine and plagioclase

**Table 6a (Model 1) Rayleigh Fractional Crystallization Calculation (Trace Elements) Fe-Enrichment in the the First-Cycle Volcanics
HIGH-Mg BASALT = Fe-RICH BASALT + PLAG + OLIV + CPX**

ELEMENT	Co	C1	Kplag	Koliv	Kcpx	(1-F)100
Ni	148	47	0.04	19.73	2.0	40%
Cr	272	90	0.01	0.20	10	71%
Ti	5171	9260	0.01	0.024	0.47	49%
Y	20	34	0.03	0.01	0.5	45%
Zr	45	81	0.01	0.01	0.10	49%
Sc	39	47	0.017	0.265	4.05	59%
Ce	6.41	11.85	0.10	0.001	0.10	49%
Sm	1.90	3.13	0.07	0.002	0.26	43%
Eu	0.593	0.960	0.30	0.002	0.20	47%
Yb	2.01	3.50	0.03	0.002	0.28	45%

Fractionation was modelled using the Rayleigh expression

$$C1 / Co = (F) \exp (D-1)$$

where:

C1= concentration (ppm) in the daughter (TS-158-83)

Co= concentration (ppm) in the parent (TS-216-83)

D= bulk distribution coefficient, where $D = \sum wK$ and w = weight proportion of individual minerals and K is the mineral-liquid partition coefficient

F = proportion of original liquid remaining

Mineral-liquid partition coefficients were taken from, 1, Cox et al., 1979; 2, Pearce et al., 1979; 3, Irving, 1978. Mineral proportions are taken from the mineral distribution calculation in Table 6 where plagioclase:olivine:clinopyroxene = 62:20:18.

**Table 6b (Model 2) Rayleigh Fractional Crystallization Calculation (Trace Elements) Fe-Enrichment in the First-Cycle Volcanics
HIGH-Mg BASALT = Fe-RICH BASALT + PLAG + OLIV + CPX**

ELEMENT	C1	Co	B	r	(D = B-1)	(1-F)100
Nd	8.58	4.62	0.92	0.97	0.081	49%
Sm	3.13	1.90	0.84	0.90	0.165	45%
Eu	0.96	0.593	0.64	0.74	0.362	53%
Yb	3.50	2.01	0.67	0.85	0.327	56%
Y	34	20	0.62	0.77	0.376	57%
Zr	81	45	0.88	0.93	0.120	49%
P	440	270	0.86	0.94	0.140	43%
Sc	47	39	0.07	0.30	0.93	93%
Cr	272	90	-1.40	-0.87	2.40	55%
Ni	47	148	-1.08	-0.85	2.08	65%
Ti	9260	5171	0.88	0.87	0.125	49%
V	482	195	0.82	0.83	0.177	67%

Fractionation was modelled using the same equation as in Table 6a. However the bulk partition coefficient is calculated graphically (c.f. Allegre et al., 1977) by using the slope (B) from a log hygromagmatophile (La) versus log trace element plot and the relation $D = (B-1)$. The correlation coefficient (r) is given for the log hygromagmatophile versus log trace element plots. All other symbols as well as the parent and daughter liquid compositions are as in Table 6a.

Figure 25 Results of Rayleigh fractional crystallization model calculations for Fe-enrichment in the basalts of the First-Cycle Volcanics. High-Mg basalt = Fe-rich basalt + plag + cpx + oliv (Model 1, Table 6a, Model 2, Table 6b).

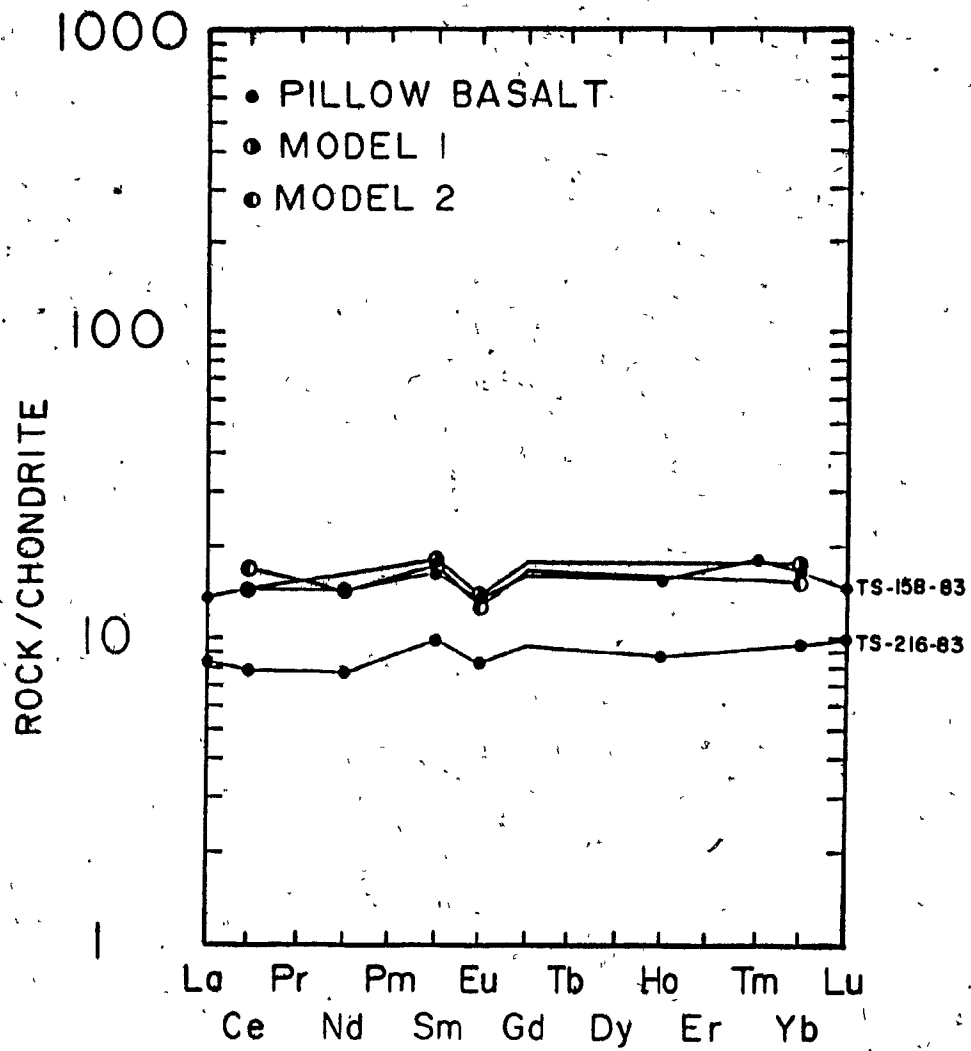


Figure 25

decrease with increasing pressure (Grove et al., 1983; Biggar, 1983; Bender, 1978; Grove et al., 1984). That the basalts in the First-Cycle Volcanics were multiply saturated in olivine, plagioclase and clinopyroxene at pressures less than 10Kb can be seen by plotting the basalts in isomolar (Elthon et al., 1983) projections in the olivine, clinopyroxene, plagioclase and silica tetrahedron (Fig. 26).

Even though it is possible to reproduce numerically the Fe-enrichment within the First-Cycle Volcanics it is important to note that the fractionation scheme proposed here is not necessarily a unique solution. Francis (Nature, 1985 ms.) has pointed out that picritic magmas can reproduce the spectrum of liquid compositions observed in the Tertiary Baffin island basaltic lavas by a combination of fractional and equilibrium crystallization of olivine. Thus the spectrum of liquid compositions observed in a region need not represent a liquid line of descent since each individual liquid composition could have evolved directly from picritic liquids without becoming saturated in olivine, plagioclase and clinopyroxene (Francis, op. cit.). Furthermore, the modelling done here does not preclude open-system processes.

6.2.2 The First-Cycle Volcanics and Mafic Magnetism in the La Grande Greenstone Belt

There is a broad consensus that most Archean tholeiitic basalts have undergone some degree of low-pressure fractionation

Figure 26 (a) clinopyroxene and (b) plagioclase projections in the isomolar, haplobasaltic quaternary system plagioclase, olivine, silica and clinopyroxene for the First-Cycle Volcanics. Symbols are as in Fig. 16. Pseudo-cotectic fields are taken from Elthon et al. (1983) and are based on high pressure phase equilibria studies of a high-magnesia basalt from the Tortuga Ophiolite.

(Hawkesworth et al., 1977; Nisbet et al., 1977; Jolly, 1978, 1980; Jahn et al., 1980; Thurston et al., 1983; Stamatelopoulou-Seymour et al., 1983; Ludden et al., 1984). However, there is less agreement on the chemical composition of the parental magmas. Komatiites are the least-differentiated basic magmas found in Archean greenstone belts and are often intercalated with tholeiitic basalts (Pyke et al., 1973; Arndt et al., 1977; Nisbet et al., 1977; Hawkesworth et al., 1977; Arndt et al., 1979; Jahn et al., 1980; Basaltic Volcanism Study Project, 1981; Condie, 1981; Stamatelopoulou-Seymour, 1982; Stamatelopoulou-Seymour et al., 1983). Despite the close spatial association of komatiites and tholeiitic basalts, it is uncertain whether the basalts represent the low pressure fractionated products of komatiites (Stamatelopoulou-Seymour, 1982; Nisbet et al., 1977; Nisbet, 1982; Hawkesworth et al., 1977) or alternatively, whether the parental magma to the basalts is distinct from the komatiites (Arndt et al., 1977, Arth et al., 1977; Jahn et al., 1980; Basaltic Volcanism Study Project, 1981; Condie, 1981). Key arguments for the second viewpoint are that there is commonly a distinct compositional gap between komatiites and basaltic komatiites at 18% MgO (Arndt et al., 1982) and that there are distinct differences in the trace element variations (in particular LREE) between the komatiites and tholeiites in some volcanic provinces (Arth et al., 1977; Jahn et al., 1980; Nesbitt et al., 1980). The relationship between komatiites and basalts is further complicated by recent evidence suggesting that komatiitic magmas may have been able to assimilate continental crust (Huppert et

al., 1984, Huppert et al., 1985). Their trace element contents may then reflect less their source than the crustal conduit through which they have passed.

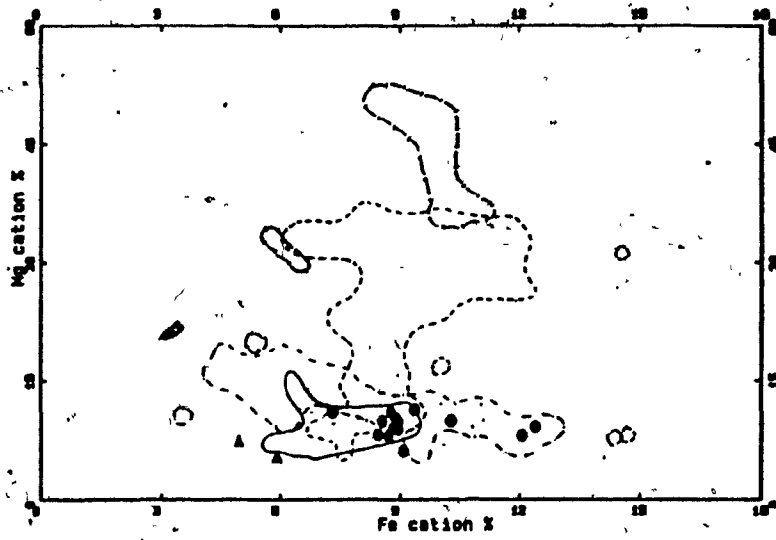
Although earlier work on the La Grande lavas referred to a compositional gap at 18% MgO between the komatiites and basalts (Stamatelopoulou-Seymour, 1983), recent work (Stamatelopoulou-Seymour, unpublished) has revealed that there are lavas that span this compositional gap (Fig. 27a). The basalts in the First-Cycle Volcanics and in the Lac Guyer area (Stamatelopoulou-Seymour, 1982; Liu, 1985) have near-chondritic Zr/Y and Ti/Zr ratios (ca. 2.5, 107 respectively, Nesbitt et. al., 1980) that increase slightly with increasing Zr (Fig 29b, a). The Zr/Y versus Zr variations in the komatiitic rocks from Lac Guyer are very similar to those in the basalts, but there is considerable scatter in the Ti/Zr variations (Fig. 29). Similarly (La/Sm)_n versus La variations in the komatiites (albeit for the few samples available) are similar to those in the basalts, whereas (La/Yb)_n versus La variations display more scatter (Fig. 18). The scatter in (La/Yb)_n versus La may be the result of analytical uncertainty at low abundances of Yb such as in the komatiites, or alternatively, as suggested by Stamatelopoulou-Seymour et. al. (1983) may reflect different residual phases in the source region of the pyroxenitic and peridotitic komatiites.

The similar trace element characteristics (Fig.18, 29) of the basalts and komatiites indicate that these rocks may be

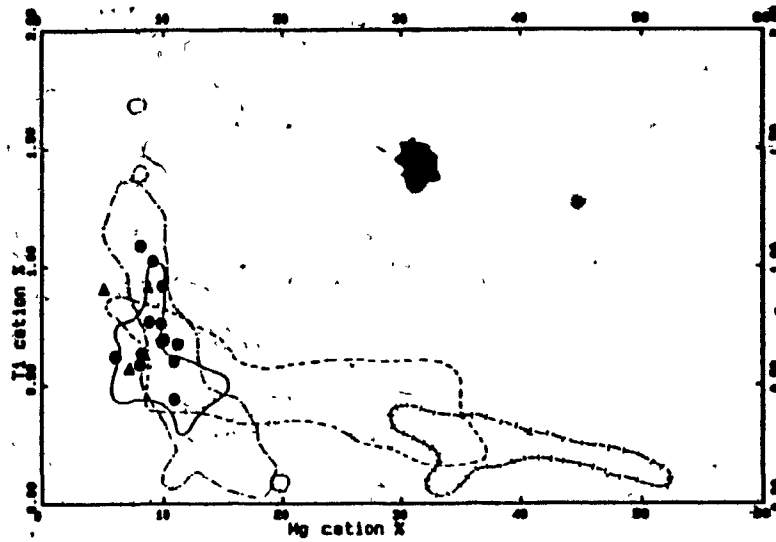
Figure 27 (a) Mg versus Fe, (b) Ti versus Mg and (c) Si versus Mg (all in cation%) for lavas of the First-Cycle Volcanics and from other parts of the La Grande greenstone belt. Individual samples have symbols as in Fig. 16. Solid line field and dash-dot field include lavas from the Lac Yasinski area and gabbros from the Lac Menarik intrusive respectively (B. Rivard, personal communication, 1985), dashed pattern includes peridotitic, pyroxenitic and basaltic komatiites as well as basalts from the Lac Guyer area (Stamatelopoulou-Seymour, 1982) and dash-bar and dotted patterns are komatiites and basalts respectively from south of Lac Guyer (Liu, 1985).

Figure 27

(a)



(b)



(c)

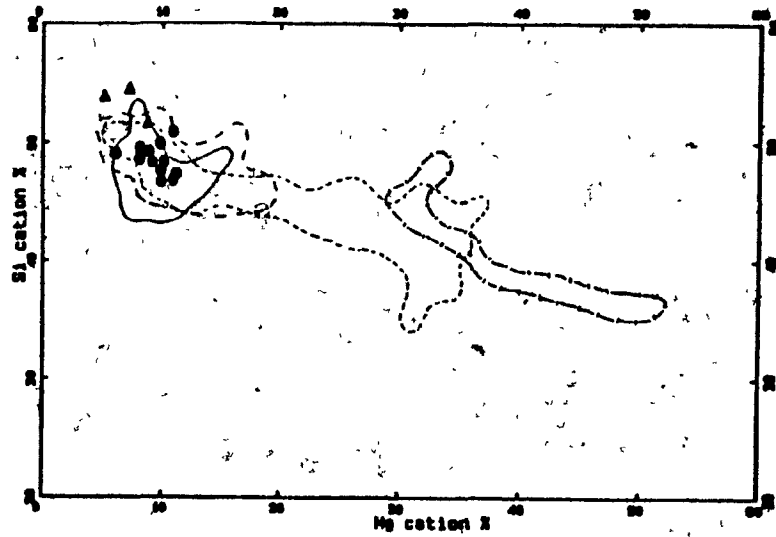
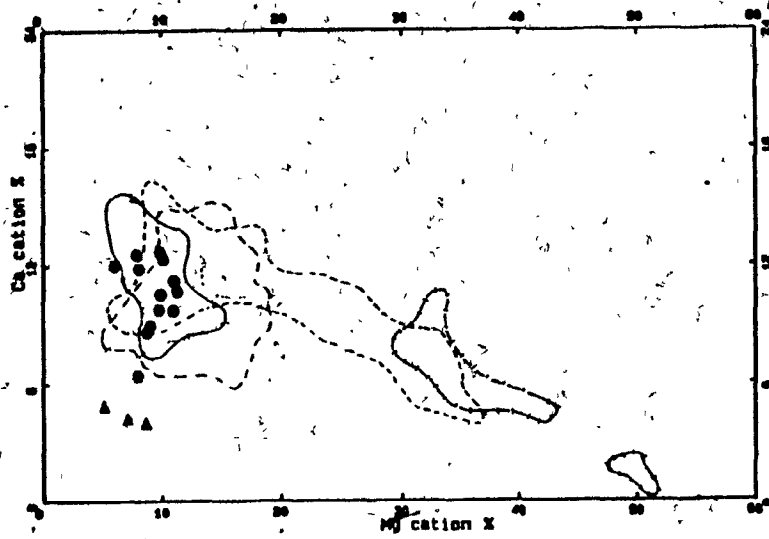


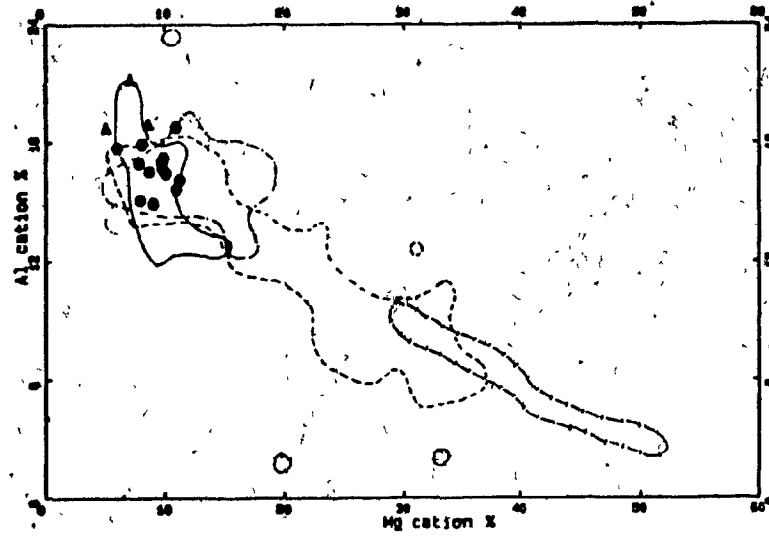
Figure 28 (a) Ca versus Mg, (b) Al versus Mg and (c) Al versus Si (all in cation%) for lavas of the First-Cycle Volcanics and from other parts of the La Grande greenstone belt. Symbols are as in Fig. 27. Olivine and Al-free orthopyroxene are shown in Fig. 28c for reference.

Figure 28

(a)



(b)



(c)

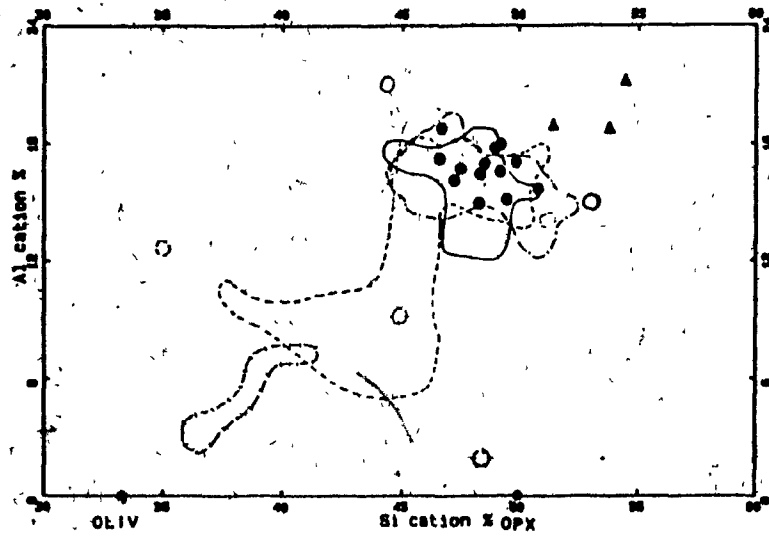


Figure 29 (a) Ti/Zr and (b) Zr/Y versus Zr (all in ppm) for lavas of the First-Cycle Volcanics and from other parts of the La Grande greenstone belt. Solid circles and triangles are pillow basalts and basaltic andesites of the First-Cycle Volcanics, diamonds and open circles are basalts and komatiites respectively from the Lac Guyer area (Stamatelopoulou-Seymour, 1982) and open circles and triangles are basalts and komatiites respectively from south of Lac Guyer (Liu, 1985).

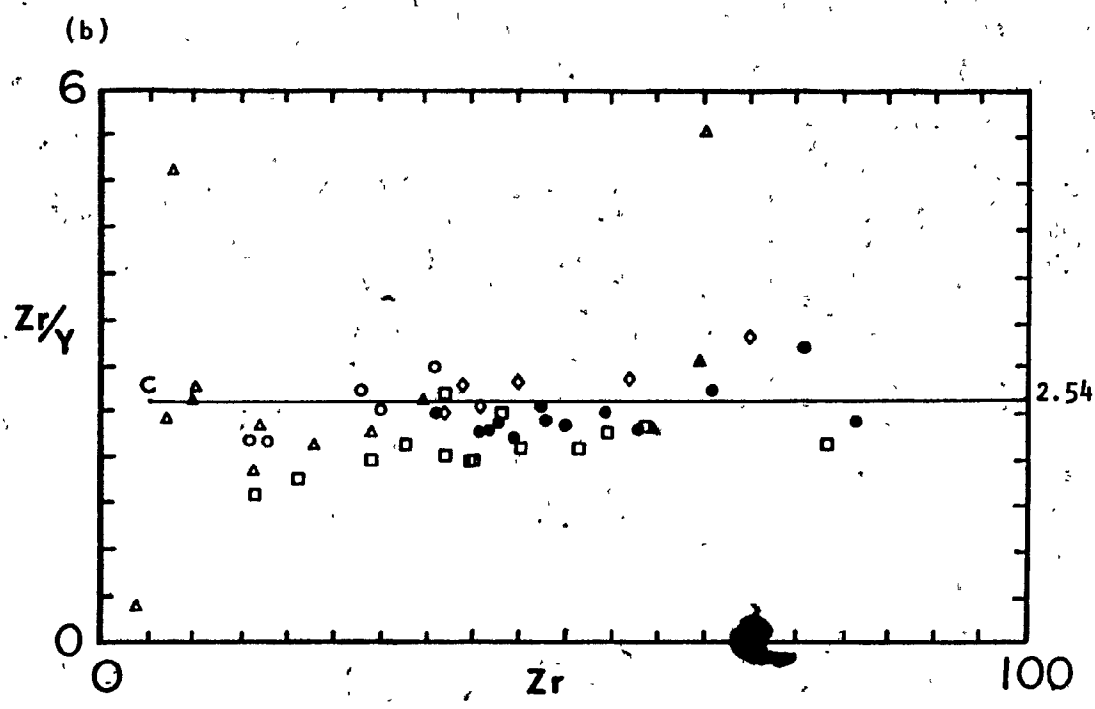
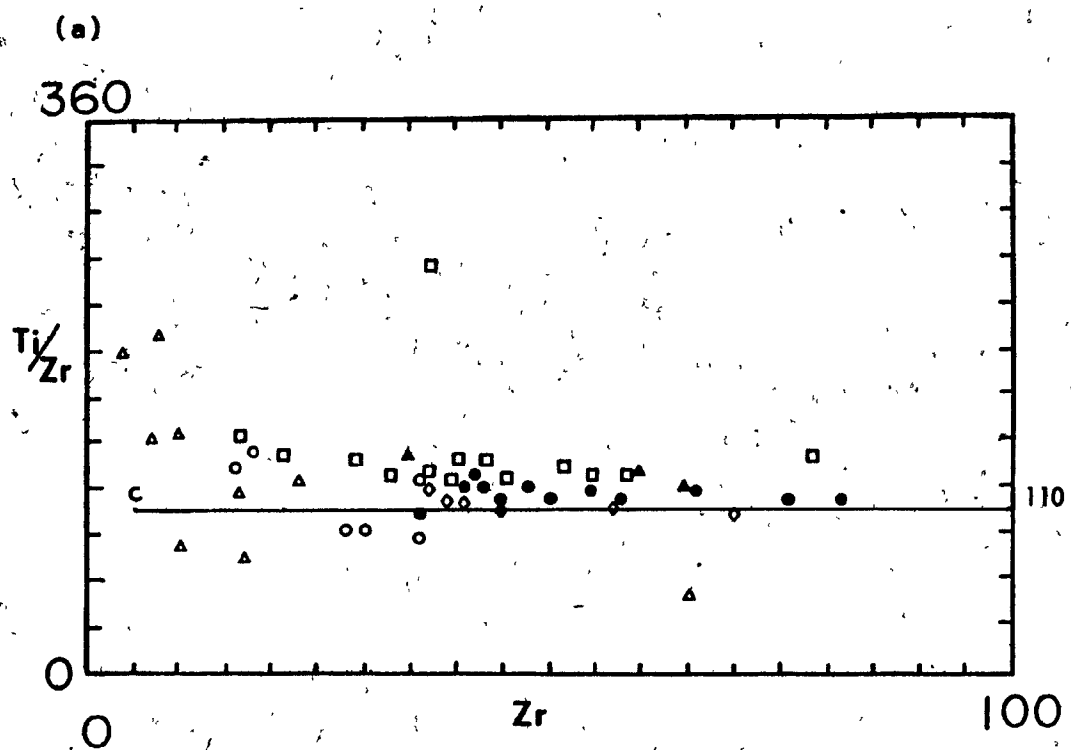


Figure 29

genetically related (c.f. Stamatelopoulou-Seymour, 1982, Stamatelopoulou-Seymour et. al., 1983). Stamatelopoulou-Seymour (op. cit.) has suggested that the primary control on compositional variations in the komatiites may be different degrees of partial melting, whereas the basalts in the Lac Guyer area may have evolved from basaltic komatiite parents by fractional crystallization of olivine, clinopyroxene and orthopyroxene (Stamatelopoulou-Seymour et al., 1983, 1985 (m.s.)).

Early saturation of high Mg-basalts and basaltic komatiites in orthopyroxene and olivine is evidenced in their compositional variations in Al-Si space (Fig. 28c). It is unlikely that equilibration with olivine alone could account for the steep positive slope of the basaltic komatiites and thus it seems likely that these liquids were on an orthopyroxene-olivine control line. The coexistence of orthopyroxene and olivine in the basaltic komatiites requires that these liquids last equilibrated at pressures in the vicinity of 10-20 kb (O'Hara, 1968; Yoder, 1976; Elthon et. al., 1984). Stamatelopoulou-Seymour (1983) has pointed out that the large decrease in the concentration of compatible trace elements (Ni, Cr) as opposed to incompatible elements (Zr) suggests that the basaltic komatiites evolved by fractional crystallization to produce basaltic daughter liquids. Thus, if basaltic komatiites were the parental magmas to basalts within the La Grande belt such as the First-Cycle Volcanics, then it follows from the previous discussion that these magmas must have undergone a polybaric

fractionation history. In short, the petrogenesis of these lavas was characterized by early high-pressure fractional crystallization followed by subsequent accumulation of the derivative magmas in shallow subcrustal magma chambers in which the magmas equilibrated with a low pressure assemblage.

The First-Cycle basalts and basalts collected south of Lac Guyer (Liu, 1985) have a tendency to increase in Fe, Ti and Si and decrease in Ca and Al with increasing differentiation (Fig. 27a-c, 28a and b). These compositional variations are consistent with the fractional crystallization at low pressures of olivine, clinopyroxene and plagioclase with or without Cr-spinel (this study), or as suggested by Liu (op.cit), by a combination of equilibrium and fractional crystallization of the same assemblage. On the other hand the Lac Guyer basalts (Stamatelopoulou-Seymour et al., 1983, Fig. 27a) and Lac Yasinski basalts (Rivard et al., 1984, 1985) appear to have constant Fe abundances with increasing differentiation. The compositional variations of these lavas appears to have been controlled by the fractional crystallization of assemblages that lack plagioclase as evidenced by the small changes in Ti and Al and decrease in Fe relative to Mg (Fig. 27 and 28, c.f. Stamatelopoulou-Seymour et al., 1983; Rivard et al., 1984). It would thus appear that although the basalts of the La Grande greenstone belt may have evolved from a similar komatiitic parent, there are significant differences in the nature of the high-level magmatic processes that account for the spectrum of

compositions amongst these rocks.

The gabbroic high level intrusives in the La Grande belt (including First-Cycle Volcanic gabbro sills and gabbroic dykes associated with the Lac Menarik intrusive, Rivard et. al., 1984, 1985) lie along Fe-enrichment trends similar to those in the First-Cycle basalts and basalts south of Lac Guyer (Fig. 27a). The compositional variations as well as the cumulate textures in some of these rocks (3.2.1) suggest that these intrusives may represent the high-level magma chambers in which Fe-enriched basalts evolved. The formation of basaltic magmas with relatively constant Fe abundances may be a result of problems of nucleation kinetics (Rivard et. al., 1985). However, if the constant-Fe lavas evolved from gabbroic liquids which were saturated in plagioclase as well as olivine and clinopyroxene, then the control on Fe-depletion is more likely related to the ability of plagioclase to separate from the melt.

A number of workers have pointed out that plagioclase may be bouyant in some tholeiitic liquids (Campbell et. al., 1978; Bedard et al., 1983). Indeed the presence of large megacrysts and glomeroporphyritic clusters of plagioclase in sills (3.2.1) in proportions greater than those required to produce the Fe-enrichment in the gabbros and basalts suggests that this phase may be accumulating or floating in these rocks. Phinney et. al. (1984) have found that large plagioclase megacrysts in volcanic flows and basaltic dykes and or sills have a unique shape (equidimensional) and composition (An 80-85) in many Archean

greenstone belts and are out of equilibrium with the host basaltic liquids whose trends indicate fractionation dominated by augite and plagioclase (An 50-65 lath-shaped). They have suggested that these megacrysts were crystallized from more primitive liquids and were subsequently incorporated by more fractionated liquids and transported to the surface or near-surface. The lack of complementary mafic megacrysts in flows has been interpreted as a result of ponding of high density melts in the lower crust or at the crust-mantle boundary, followed by sinking of mafics and floating of plagioclase that could be later entrained in upward surges of less dense magma (Phinney et. al., op.cit.). Although compositional data are lacking for megacrystic and phenocryst plagioclase in GMP sills and pillow lavas in the First-Cycle Volcanics, Phinney's explanation of these relationships may apply in the case of the La Grande belt, since the plagioclase megacrysts are found in both flows and intrusives in this terrane and the megacrysts commonly occur in gabbroic matrices which contain lath-shaped crystals enclosed in augite.

The differences between the constant-Fe and Fe-enriched lavas in the La Grande belt may be related to the buoyancy of plagioclase in basaltic melts. Fe-enriched lavas may have fractionated plagioclase either by attaining a density contrast sufficient for the plagioclase to sink or alternatively, by separating crystal from melt by some form of flowage differentiation in narrow sills (Bhattacharji et al., 1964;

Komar, 1972, 1976; Barriere, 1976). Lavas of constant-Fe may have had difficulty nucleating plagioclase or alternatively crystals of plagioclase may have been buoyant in the melt and carried to the surface.

6.3.1 Petrogenesis of the Second-Cycle Volcanics and Lac Coutaceau Dykes

In Chapter 5 it was demonstrated that the Second- and First-Cycle Volcanics could not have been comagmatic. Furthermore, the Lac Coutaceau dykes were shown to be probable chemical analogues of Second-Cycle magmas. In this section the question of their ultimate origin and their role in the petrogenetic history of the La Grande belt is addressed.

The systematic variation in major and trace element compositions within one flow of the Second-Cycle Volcanics can be attributed to differential crystal accumulation within the flow (5.3). Similarly, the large variation in compatible trace elements (Ni, Cr) versus incompatible elements (Zr) in the Second-Cycle Volcanics and Lac Coutaceau dykes can be attributed to the fractional crystallization of Ni- and Cr-bearing phases (Fig. 22b and c). However, fractional crystallization of Ni- and Cr-bearing phases such as olivine and clinopyroxene and or Cr-bearing spinel alone cannot account for the increase in incompatible trace element ratios (Zr/Y, La/Sm, La/Yb) with increasing differentiation in the Lac Coutaceau and Second-Cycle suites (Fig. 24). Several petrological processes could account

for this type of variation in trace element ratios including: different degrees of partial melting, open system fractional crystallization, magma mixing and contamination. Different degrees of partial melting cannot be invoked since this process could not account for the compatible element variations. There is no field evidence in support of magma mixing, although there is ample evidence of at least physical contamination of the magma as evidenced by the presence of xenoliths in both the Second-Cycle and Lac Coutaceau suites (3.4.1, 3.5.1). The possibility of contamination of the Second-Cycle and Lac Coutaceau parental magma(s) is therefore worth considering further.

The high Mg# of some of the Lac Coutaceau dykes (0.76) and the high Ni and Cr abundances suggest that some of these high-Mg magmas may have been in equilibrium with the upper mantle (Hanson et al., 1978). Similar magma compositions are attained by some of the komatiites in the La Grande belt. The Second-Cycle and Lac Coutaceau suites, however, extend to higher Si and Al, maintain constant Ti with decreasing Mg and are characterized by decreasing Ca and Fe with increasing differentiation (Fig. 20 and 21). At similar Mg abundances this suite is characterized by much higher LREE and Zr abundances than the komatiites (5.3).

The major element and compatible element (Ni and Cr) variations of the Second-Cycle and Lac Coutaceau suite are

consistent with these rocks having fractionally crystallized olivine and clinopyroxene. Furthermore, at least on the basis of these elements this suite could have been derived from komatiite-like melts. The decrease in Fe with increasing differentiation (decreasing Mg) could be explained by the equilibrium crystallization of olivine, since this process leads to lower Fe abundances after larger degrees of fractionation (c.f. Hanson et al., 1978). However, the fractionation of olivine and clinopyroxene cannot explain the trace element abundances in the Second-Cycle and Lac Coutaceau suite.

It is possible that a komatiitic magma interacted with a sialic crust to produce the Second-Cycle and Lac Coutaceau suites. Evidence for this process is only indirect, komatiites are found near the top of the supracrustal succession exclusively in the eastern part of the La Grande belt (2.1, Stamatelopoulou-Seymour, 1982; Liu, 1985) whereas the Second-Cycle Volcanics and Lac Coutaceau dykes are late-stage magmas that contain crustal xenoliths and are the highest-Mg magmas reported from the central and western parts of the belt. In order to see if this hypothesis is consistent with the chemical variations in the Second-Cycle and Lac Coutaceau suite it is necessary to estimate the composition of the proposed contaminant.

Although there may have been considerable heterogeneity in the composition of the sialic crust a reasonable estimate of the bulk composition of the crust underlying the La Grande

greenstone belt is that of a tonalite. This estimate is based on the composition of xenoliths in the volcanic and intrusive rocks, the provenance of sedimentary rocks in the supracrustal succession and the composition of the granitoid basement intruded by the Lac Menarik intrusive (Rivard et al., 1984, 1985). Stamatelopoulou-Seymour (1982) has suggested that the rhyolites and rhyodacites found in the Lac Guyer area are the extrusive equivalents of granodioritic-tonalitic intrusives in this area. Therefore, the rhyolites provide us with a crude estimate of the composition of a partial melt of the crust that may have reacted with the komatiitic melt.

In order to test the viability of assimilation fractional crystallization a least-squares mixing program was used to test combinations of fractionating phases that would have to be added to a derivative liquid to produce a mixture of the parental liquid and the contaminant (adapted after Wright et al., 1970). This technique is at best an approximate one in that it does not account for the expected continuous compositional variation of some of the fractionating phases. The following crystallizing assemblages were tested: * KOM + RHY = OLI + DAU, = OLI + CPX + DAU, = OLI + CPX + PLAG + DAU, = OPX + OLI + CPX + PLAG + DAU, OPX + CPX + PLAG + DAU. Amongst these models the best residuals were calculated for the assemblage containing OPX + CPX + PLAG + DAU (Table 7). The OLI + CPX + DAU assemblage had relatively low

* where komatiite = KOM, rhyolite = RHY, olivine = OLI, clinopyroxene = CPX, plagioclase = PLAG, orthopyroxene = OPX and daughter = DAU.

Table 7 Assimilation Fractional Crystallization Model Using A Least Squares Mixing Calculation for the Second-Cycle Volcanics

KOMATIITE + RHYOLITE (CONTAMINANT) = ANDESITE + OPX + CPX + PLAG

ELEMENT	ENSTA	FERRS	CPX	PLAG	ANDES	CONTAM	PROP. CALC. KOMAT	RESIDUE KOMAT	
SiO2	59.84	45.35	52.83	43.20	63.29	76.46	49.11	49.17	-0.06
Al2O3			2.55	36.65	14.90	14.20	7.38	7.39	0.00
FeO		54.45	5.95		5.14	0.66	10.40	10.41	0.00
MgO	40.16		18.53		5.19	0.18	23.95	23.96	-0.01
CaO			19.83	20.17	5.41	2.16	8.36	8.41	-0.04
Na2O			0.12		5.09	5.47	0.38	0.44	-0.05
K2O					0.50	0.85	0.10	-0.09	0.20
TiO2			0.21		0.61	0.06	0.35	0.36	0.00

WT. PRO. 44.21 12.44 18.55 13.39 54.77 -43.33 $\sum(\text{RESIDUALS})^2 = 0.05$

% CRYSTALLIZATION = 45% % ASSIMILATION 43%

(ENSTA 78 : CPX : PLAG (AN=100)) = 64 : 21 : 15

ENSTA = ENSTATITE, FERRS = FERROSILITE, CPX = CLINOPYROXENE, PLAG = PLAGIOCLASE, ANDES = ANDESITE, CONTAM = CONTAMINANT, PROP. KOMAT = PROPOSED PARENT, CALC. KOMAT = CALCULATED PARENT

These calculations were performed with the mineral distribution program of Wright and Doherty (1970). SiO2, CaO, Na2O and K2O were weighted 1, Al2O3 and MgO were weighted 3, FeO was weighted 10 and TiO2 was weighted 50. The parent magma is a peridotitic komatiite (LG-315) and the contaminant is a rhyolite (LG-306C) both analysis are of volcanic rocks from the Lac Guyer area, (Stamatelopoulou-Seymour, 1982). The derivative lava composition is an andesite from the Second-Cycle Volcanics (TS-283-85). Orthopyroxene and plagioclase compositions were determined by the program by mixing end members, whereas the clinopyroxene analysis is taken from Stamatelopoulou-Seymour (1982). The calculation uses a least-squares mixing algorithm that combines the mineral and daughter compositions to produce a mixture of contaminant and komatiite. An arbitrary sum of the squares of the residuals = 1 was chosen as an upper cut-off limit in the first step toward determining whether a particular model was acceptable.

residuals with the exception of Na, but the solution of this model did not use the contaminant. The OPX + CPX + PLAG + DAU model requires slightly greater degrees of crystallization than contamination (Table 7).

The abundance of plagioclase in the fractionating assemblage (Table 7) is very low and thus consistent with the increase in Si and Al with increasing differentiation in the Second-Cycle Volcanics and Lac Coutaceau suite (Fig. 20c). If assimilation of tonalitic material was involved in the fractionation history of these magmas than the modelling predicts orthopyroxene and not olivine would be on the liquidus. An OPX control line may be masked in Al-Si space by the presence of a rhyolitic contaminant which causes the liquid line of descent to tend toward higher Si contents (Fig. 20c). This is consistent with the fact that increases in the silica activity of a melt saturated with olivine should force the crystallization of orthopyroxene. Evidence for the presence of orthopyroxene is found in the high level noritic plug that intrudes the Second-Cycle Volcanics (3.4.2).

It is necessary to test whether the favoured assimilation fractional crystallization (AFC) model favoured above (OPX + CPX + PLAG, Table 7) can account for the trace element composition of the daughter liquid. This can be done with the Depaulo (1981) AFC equation (Table 8) using the parent and contaminant trace element abundances (C_m , Ca), and calculating the bulk partition coefficient (D) by using weighted proportions of minerals (from

**Table 8 Assimilation Fractional Crystallization Calculation
Using the DePaulo Equation.**

KONATIITE + RHYOLITE (CONTAMINANT) = ANDESITE + CPX + PLAG + OPX

ELEMENT	Ma	Mc	Cm	Cmo	Ca	F	Kplag	Kopx	Kcpx	D	Cm*
Ce	43.3	88.6	28.5	5.02	39.7	0.55	0.10	0.003	0.10	0.038	39.1
Sm	43.3	88.6	3.1	0.81	2.74	0.55	0.07	0.010	0.26	0.165	3.15
Eu	43.3	88.6	0.86	0.21	0.48	0.55	0.30	0.013	0.20	0.095	0.69
Yb	43.3	88.6	0.73	1.07	0.40	0.55	0.03	0.05	0.28	0.095	2.03
Ti	43.3	88.6	3635	2360	299	0.55	0.04	0.1	0.30	0.133	3887
Zr	43.3	88.6	103	18	65	0.55	0.01	0.03	0.10	0.042	81
Y	43.3	88.6	10	9	16	0.55	0.03	0.2	0.50	0.238	23

Fractionation was modelled using the equation:

$$Cm/Cmo = F^{-z} + ((r)/(r-1))Ca/(zCmo)(1-F^{-z})$$

where $z = (r + D - 1)/(r - 1)$ and $r = Ma/Mc$

Ma = rate at which wallrock is assimilated (% assimilation Table 7)

Mc = rate at which fractionating phases are effectively being removed (% crystallization Table 7)

Cm = concentration (ppm) of trace element in magma

Cmo = concentration (ppm) of trace element in original magma

Ca = concentration (ppm) of trace element in wallrock

F = mass of the magma as a fraction of the original mass

D = bulk solid/liquid partition coefficient for the element between the fractionating mineral phases and the magma

Cm* = calculated concentration (ppm) of trace element in magma

The proportion of minerals used in calculating D as well as the factor F are taken from Table 7. The mineral liquid partition coefficients are taken from the following references (1) Cox et al., 1979; (2) Pearce et al., 1979. Parent magma (original magma), contaminant (wallrock) and derivative magma (magma) are the same as in Table 7. The equation used here is taken from DePaulo (1981). The results of this calculation are shown graphically in Fig. 30.

Figure 30 Results of the assimilation fractional crystallization calculation, komatiite + rhyolite = opx + cpx + plag + andesite (Second-Cycle lavas). Dark square is a peridotitic komatiite (LG-315), open square is the contaminant rhyolite (LG-306c), the black diamond is the derivative andesite (TS-283-83) and the model value is shown as an open hexagon. The normalizing factors are taken from Hanson (1980) and Sun et al. (1977).

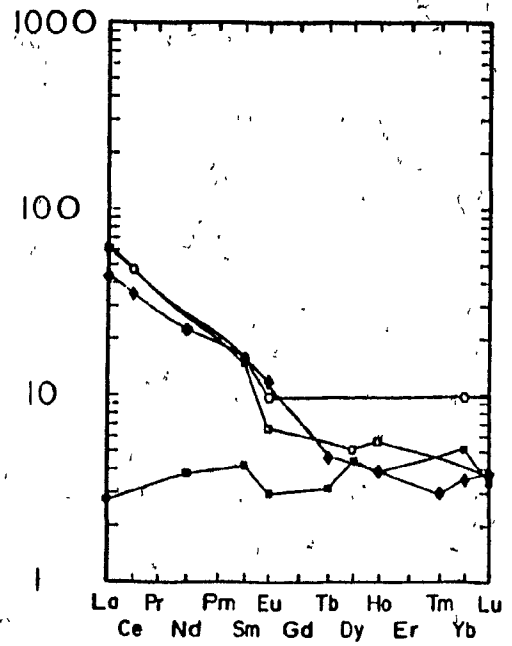
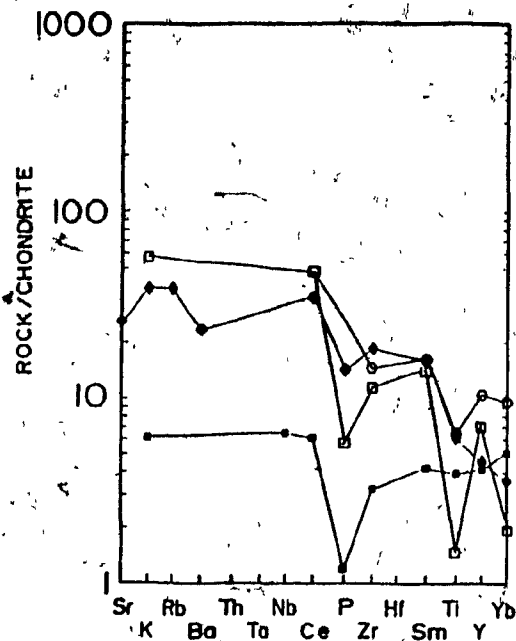


Figure 30

the least-squares calculation) and published mineral-liquid partition coefficients. The results of this analysis show that this model could explain the abundances of Ce, Sm, Eu, Zr and Tl, but overestimates the abundances Y and Yb (Fig. 30).

The overestimate of Y and Yb may be due a number of factors, including a poor choice of contaminant or parental magma, selective exclusion of these elements by retention in a refractory residue during melting, crystallization of a minor phase that preferentially partitions these elements, or alternatively, the contamination process may have been one of selective diffusion of cations (c.f. Watson, 1982; Watson et al., 1984). The first possibility is thought to be the most likely since there is no evidence to warrant the latter. Despite the success of a contamination model, open system fractional crystallization cannot be excluded as a possible process to account for these rocks. Since there are few data available to constrain modelling of open system fractional crystallization it is not, however, treated further.

It would seem then that the bulk of field and chemical data on the Second-Cycle Volcanics and Lac Coutaceau dykes are consistent with a model in which these rocks were derived by the contamination of a komatiitic magma by a tonalitic crust. It is interesting to note that a number of recent workers have predicted that komatiitic magmas in the Archean may have had a great capacity for the assimilation of wallrocks by virtue of their high liquidus temperatures and probable turbulent state in

the near surface environment, which could have provided a constant heat flux at the zone of melting and assimilation (Huppert et al., 1984, Huppert et al., 1985).

The two-volcanic cycles studied in the central part of the La Grande belt are believed to record the progressive effects of interaction between a komatiitic magma and the continental crust. The komatiitic magmas are believed to have undergone a polybaric fractionation history. Initially, rising komatiitic magmas were forced to fractionate olivine and orthopyroxene at relatively deep crustal levels. The residual basaltic komatiites then rose to shallower depths where they are believed to have fractionated at low-pressures to produce basaltic daughter liquids. With time, and perhaps continued rifting (see 7.2), komatiitic magmas were erupted in the eastern part of the La Grande belt whereas toward the west these magmas may have been forced to interact with the continental crust to produce contaminated siliceous differentiates.

Chapter 7 The Tectonic Evolution of the La Grande Greenstone Belt

7.1 Archean Tectonics

All models of Archean crustal evolution are closely allied to, and depend upon, the earth's thermal history. Heat flow in the Archean is generally thought to have been higher than at present, as a result of the greater abundance of long-lived radioactive nucleides and whole-earth post-accretionary cooling. Most estimates for radiogenic heat production in the Archean (2.6 Ga) are between 2 and 3 times the present (Wasserburg et al., 1964; O'Nions et al., 1978). However, the range of estimates of Archean global heat loss, which is a function of the relative proportions of whole-earth cooling and heat production, is large.

Prior to the recognition of plate tectonics most investigators assumed that heat transport by conduction was the principal means by which heat was transported through the earth (Lubimova, 1958). However, it is now clear that convective heat transport through the creation of oceanic lithosphere at spreading centers and its recirculation through subduction is a very effective means of dissipating heat (Bickle, 1978; Sclater et al., 1980). Consequently, many workers have considered convective heat transport mechanisms when modelling the earth's thermal history (eg. McKenzie et al., 1975; Bickle, 1978; Campbell et al., 1984).

A number of investigators have argued that since calculated geotherms in Archean high-grade terranes are not significantly higher than modern continental geotherms, the heat transport in the Archean must have been accommodated through greater heat loss from oceanic basins (Bickle, 1978; Burke et al., 1978). A greater heat loss from the Archean ocean basins could have been effected by higher rates of spreading and/or greater lengths of mid-oceanic ridge (Bickle, 1978). Hoffman et al. (1984) have extended these arguments to the early Proterozoic, and have suggested that the Wilson cycle operated faster during the Proterozoic, as evidenced in the formation and destruction of the short-lived 1.9 Ga continental margin of the Wopmay Orogen, Canada.

The principal objections to plate tectonics in the Archean (Baer, 1981) are that the higher mean temperatures of the Archean mantle would have inhibited the development of density contrasts between the cool oceanic lithosphere and the underlying asthenosphere sufficiently large for the spontaneous subduction of oceanic plates. Baer (op cit.) has also argued that the higher mean temperature of the Archean mantle would have decreased the stability field of eclogite. Thus, even if subduction could be initiated, it would be difficult to maintain, due to the decrease in the slab-pull force, which is aided by the density increase accompanying the basalt-eclogite transformation. However, assuming the earth did not expand it

seems unlikely that there was no subduction during the Precambrian in light of the probable higher rates of sea-floor spreading at that time (Bickle et al., 1978; Burke et al., 1979). Hynes (1982) has argued that during the Proterozoic all oceanic tectosphere was subducted young, because of its inherent instability at the earth's surface. Nisbet et al. (1983) and Arndt (1983) have argued that Archean oceanic crust was probably komatiitic in composition and thus by virtue of its high density may have subducted spontaneously with cooling.

In this chapter the tectonic setting of the La Grande greenstone belt is discussed in light of contemporary ideas on Archean crustal evolution. Model calculations show that the La Grande belt may have developed in a passive continental rifting environment. The amount of stretching required for the lithosphere, to produce the observed subsidence, is similar in magnitude to extension factors calculated in similar Modern tectonic environments.

7.2 The Tectonic Setting of the La Grande Greenstone Belt

In Chapter 4, various evidence was presented which favors formation of the La Grande belt on sialic crust. It is not possible from the available data to determine whether this underlying continental crust was in the interior or on the margin of a large stable cratonic land mass or, alternatively, a small continental nucleus (analogous to a mature arc complex).

A number of lines of evidence favor a model in which the La Grande greenstone belt developed in an extensional tectonic environment. Sialic crust acts as a density barrier to primitive basic magmas such as komatiites (Francis et al., 1983). In order to overcome this density barrier, basic magmas must either cool and consequently fractionate to less dense compositions or, alternatively, the sialic crustal barrier must be thinned to a level permitting the buoyant upwelling of hot, unfractionated basic magmas (c.f. LePichon et al. 1982). The extrusion of large volumes of compositionally uniform, relatively evolved, basaltic magmas requires large-volume subcrustal magma chambers in which dense, primitive magmas can collect and fractionate to less dense compositions before eruption. The development of large subcrustal magma chambers and the ultimate failure of the sialic density barrier is most likely to occur in an extensional tectonic environment in which the continental lithosphere is thinned. The extension of continental lithosphere is accompanied by the passive upwelling of the asthenosphere, thus permitting the generation by adiabatic melting of a large volume of basaltic magma, and ultimately leading to the eruption at surface of these unfractionated magmas when the density barrier is breached.

The occurrence of primitive komatiitic lavas overlying a large volume of basaltic lavas in the eastern part of the La Grande greenstone belt, as well as the fact that the volcanosedimentary succession appears to have accumulated in a

subsiding basin which became progressively deeper with time, is consistent with its derivation in an extensional tectonic environment. Initially, the komatiitic magmas were forced to pool in large subcrustal magma chambers and cool to form basaltic daughter liquids that periodically erupted. Stamatelopoulou-Seymour (1982) has suggested that the felsic volcanics found near the base of the Lac Guyer succession in the eastern part of the La Grande belt, may have formed by partial melting of sialic crust at a time when komatiitic were forced to pool and fractionate in subcrustal magma chambers. Ultimately, lithospheric extension resulted in the failure of the crustal density barrier and the consequent eruption of komatiitic lavas.

Liu (1985) suggested that the La Grande greenstone belt developed as a result of a westwardly propagating rift. This suggestion was based on the restriction of komatiites to the eastern part of the belt (suggesting greater rifting in the east) and on an apparent eastward increase in pressure at which basalts from the La Grande belt equilibrated on the three-phase cotectic (plagioclase-olivine-clinopyroxene) indicating an initially thicker crust in the east where rifting would have commenced. The apparent increase in basin-depth from west to east in the LG-3 area is consistent with this westwardly propagating rift model. However, a larger, more complete data-set of the basalts in the La Grande belt reveals considerable scatter on the projections used by Liu (1985) (isomolar plot), so that an eastward displacement toward higher pressure cotectics must be considered uncertain at this stage.

7.3 A Model of Passive Rifting in the La Grande Greenstone Belt

The extent to which the continental lithosphere may have been stretched to produce the subsidence recorded by the deposition and emplacement of the Lower Volcanoclastics and Metasediments, First-Cycle Volcanics and Metasediments in the central part of the La Grande belt can be calculated if a number of assumptions are made. McKenzie (1978) and Royden et. al. (1980) describe the theory behind instantaneous thermal stretching of continental lithosphere. Two stages of subsidence occur as a result of isostatic compensation of continental lithosphere that has been rapidly extended. In the first stage, termed initial subsidence, immediate elevation changes occur to return the stretched lithosphere to isostatic equilibrium. The second stage of subsidence, termed thermal subsidence, occurs as a result of conductive cooling of the lithosphere; and its effects are delayed due to the relatively low thermal diffusivity of the continental lithosphere. The initial subsidence stage corresponds to a period of high heat flow and may be accompanied by magmatic activity, whereas the thermal subsidence stage is characterized by a diminishing heat flow and may be characterized by the development of a sedimentary basin. It is the initial subsidence phase that is believed to have been responsible for the deposition and emplacement of the lower three units in the central part of the La Grande belt.

In order to determine the extent to which the lithosphere must have been deformed to account for the formation of the basin into which the units 1 to 3 accumulated, it is necessary to make a number of assumptions. The maximum (not corrected for minor folding) thickness of units 1 to 3 is 4.35 km (unit 1 = 0.75 km, unit 2 = 3.1 km, unit 3 = 0.5 km) and the weighted mean density of this pile not corrected for compaction is 2.8 gm cm⁻³ (assuming that the mean density of unit 1 = 2.5 gm cm⁻³, unit 2 = 2.9 gm cm⁻³ and unit 3 = 2.7 gm cm⁻³). In the simplest case the initial subsidence corrected for loading is given by (after Nisbet 1984):

$$S_i = 4.35((\rho_m - \rho_s)/\rho_m - \rho_w) = 0.93 \text{ km} \quad 7.1$$

This estimate is consistent with the amount of water that is believed to have existed in the basin during the eruption of the First-Cycle Volcanics and deposition of the Metasediments (4.2, 4.3.1).

The choice of parameters is not straightforward when modelling lithospheric deformation during the Archean. Certain parameters such as the thermal diffusivity, thermal expansion coefficient, average crustal and mantle densities were probably similar to modern values, since a large proportion of the earth's present continental land mass had segregated by 2.5 billion years ago and thus the crust and upper mantle were probably of broadly similar composition to the present. Similarly, Nisbet (1984), based on several lines of evidence,

has suggested that crustal thicknesses during the Archean in southern Africa may have been in the order of 35 km. For the sake of simplicity the same estimate is used here. A considerable amount of uncertainty lies in estimates of the thickness and temperature at the base of the slab. McKenzie et al. (1975, 1980) have estimated that the continental lithosphere at 2.5 Ga was approximately 80 km thick and its base was defined by the 1394°C isotherm. Nisbet (1984), on the other hand, has suggested that the temperature at the base of the slab may have been as high as 1700°C, since this estimate must account for the minimum temperature of eruption of komatiitic melts at 1650°C or more which rose adiabatically from a convecting region in the upper mantle. It will be shown here that the choices of thickness of lithosphere and temperature at the base of the lithosphere produce only second-order changes to estimates of the lithospheric extension factor. The approach taken here is to solve for the initial elevation change for a variety of uniform extension factors using both McKenzie's and Nisbet's estimates of the temperature at the base of the slab (Fig. 31).

To calculate the lithospheric extension factor which can account for the initial subsidence of the lower three units in the central part of the belt (given by 7.1) it is necessary to combine expressions for thermal expansion (E1, 7.3) with those for elevation changes due to crustal thinning or replacement (E2, 7.4) (equations are from Royden et al. 1980, parameters defined in Table 9). Elevation changes associated with thermal

Figure 31 The results of instantaneous lithospheric thinning calculations. (a) temperature (T) at the base of the slab, (b) lithospheric thickness (A), (c) crustal thickness (t_c), and (d) uniform extension factors versus initial elevation change ($E_1 + E_2$). The curves were calculated using the equations in chapter 7.

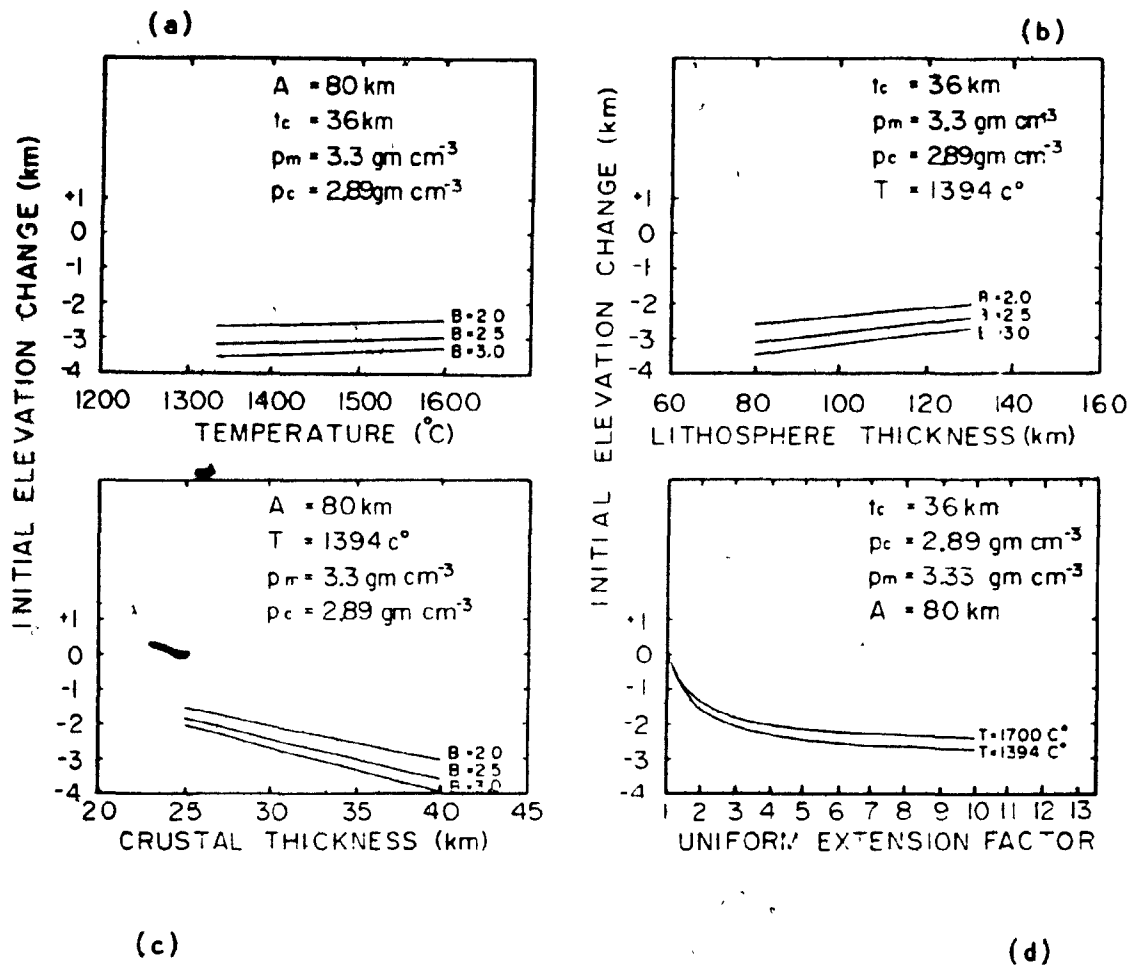


Figure 31

expansion are proportional to the amount of heat added to the lithosphere (7.2). Where $\Delta H=1$ is 'total oceanization', or non-equilibrium heat input at a mid ocean ridge. $\Delta H=0$ represents a stable thermal equilibrium in the lithosphere (cold continent) and is given by

$$\Delta H = (1 - (1/\beta)) + ((y^2/a^2) - (2y/a)((1/\delta - 1/\beta)), (1-\gamma) + \gamma \quad 7.2$$

and thus

$$E1 = (T_c \cdot \alpha \cdot \Delta H) / (2(1 - \alpha T_c)) \quad 7.3$$

The result of (7.3) is added to that of (7.4) the elevation change due to crustal thinning or replacement (E2)

$$E2 = -((\rho_m - \rho_c) / (\rho_m (1 - \alpha T_c))) t_c (1 - 1/\delta + \gamma/\delta) \times (1 - (T_c \alpha t_c) / 2a) \text{ where } y \geq t_c \quad 7.4.1$$

$$E2 = -((\rho_m - \rho_c) / \rho_m (1 - \alpha T_c)) y (1 - 1/\delta + \gamma/\delta) (1 - (\alpha T_c y / 2a)) + (t_c - y) \times (1 - 1/\beta + \gamma/\beta) (1 - (\alpha T_c / 2a)(y + t_c) \text{ where } y \leq t_c \quad 7.4.2$$

Positive values of $E1 + E2$ indicate uplift, negative values subsidence. For the sake of simplicity the lithosphere is assumed to deform uniformly ($\delta = \beta$). By replacing $E1 + E2$ by the amount of subsidence calculated from (7.1) and using parameters specified in Table 9 it is possible to calculate the lithospheric extension factor (Fig. 31).

Table 9 Parameters Used in the Calculations

ρ_m	density of the mantle	3.3 gm.cm ⁻³
ρ_c	mean density of the crust	2.89 gm.cm ⁻³
ρ_w	density of water	1.00 gm.cm ⁻³
ρ_s	density of the sedimentary pile	2.8 gm.cm ⁻³
α	thermal expansion coefficient	$3.2 \times 10^{-6} \text{ } ^\circ\text{C}^{-1}$
a	thickness of the lithosphere	80 km
T_1	temperature at the bottom of the plate model	a) 1394 ^o C, b) 1700 ^o C
κ	thermal diffusivity	0.0075 cm ² /s
δ	extension factor from surface to depth y	
β	extension factor from depth y to base of slab	
y	equal to the crustal thickness (t_c)	36 km
γ	fraction of lithosphere occupied by dykes	0
t_c	original thickness of the crust	36 km

Both models of the initial subsidence (1394^o C and 1700^o C isotherms defining the base of the slab) require very similar extension factors (approximately 1.5) to produce the 0.93 km of subsidence (corrected for loading) recorded by the protorift succession in the central part of the La Grande belt (Fig. 31). Because the thermal expansion coefficient is very small, changes in the temperature at the base of the slab do not greatly affect the estimate of $E_1 + E_2$ (Fig. 31). Similarly, $E_1 + E_2$ is not greatly affected by varying the estimated lithosphere thickness. On the other hand, $E_1 + E_2$ is quite sensitive to the estimated crustal thickness (Fig. 31).

The extension factor calculated for the central part of the La Grande belt (1.5) is very similar to that calculated by Royden et al. (1980) for the crustal extension in a number of locations on the eastern margin of Canada, (1.3-2.0) and the extension factors estimated for the Aegean Sea from seismic refraction studies (2); see Makris et al. (1977) and in the

North Sea (1.5 see McKenzie, 1978). Perhaps more significant is the fact that two Archean protorift successions are believed to have undergone similar degrees of extension (Witwatersrand = 1.3 and Beilingsboon Upper Greenstones = 1.6 Nisbet, 1984).

The deformation of the lithosphere during rifting need not have been purely plastic. Indeed it is possible that the presence of coarse clastic sediments of toialitic provenance in the higher levels of the supracrustal succssion (Metasediments) may be due to rapid uplift and unroofing of the basement in geanticlines on both sides of the greenstone belt (M. Liu, personal communication, 1985). The geanticlines may have formed in response to flexural deflection of the lithosphere as a result of loading of the lithosphere by volcanic and sedimentary rocks.

A consequence of invoking instantaneous lithospheric extension models to explain continental rifts throughout the earth's history is that one may expect the volume of magmatic activity in protorift regions to have diminished with time for similar degrees of extension. This is due to the decrease in temperature at the base of the continental lithosphere with time, as suggested by models of the earth's thermal history (McKenzie et al., 1975, 1980; Campbell et al., 1984). Higher temperatures at the base of the slab place the geothermal gradient closer to the peridotite solidus so that with lithospheric thinning and asthenospheric rise, greater degrees

of adiabatic melting may have been expected in the past (c.f. Sleep et al., 1982). In light of this it would be interesting to compare Archean, Proterozoic and Phanerozoic rift margins for evidence of early magmatic activity prior to crustal failure and the development of oceanic crust.

Chapter 8 Conclusions

8.1 Summary and Conclusions

The La Grande greenstone belt is believed to have been the site of an Archean continental rift. There are four lines of evidence that suggest that continental crust floored the rift basin in the central and western parts of the greenstone belt: a) the granitic provenance of clastic sediments in the succession, b) the occurrence of granitic and metasedimentary xenoliths in both the early and late eruptive products, c) indirect evidence in the western part of the La Grande belt for a tonalitic basement underlying the supracrustal pile (Rivard et al., 1985), and d) The bimodal character of volcanic rocks in the eastern part of the La Grande belt which attest to early silicic magmatism that may have been produced by partial melting of sialic crust followed by subsequent mafic volcanism including primitive komatiites and their fractionated products which may have erupted when the crustal barrier was breached. Sedimentological data indicate that in the central part of the belt the basin deepened toward the east. Furthermore, the restriction of komatiites to the eastern part of the belt may reflect a more protracted rifting history there, which ultimately led to the eruption of dense primitive magmas through a thinner lithosphere. The results of the present work are consistent with an earlier suggestion that the rifting was westward propagating (Liu, 1985).

In the La Grande greenstone belt volcanic activity was episodic, and individual episodes were probably extensive and prolonged. Early volcanic activity may have occurred in a shallow water environment as evidenced by the accumulation in the central part of the belt of mafic pyroclastic and epiclastic rocks interbedded with immature terrigenous clastic sediments. Continued subsidence resulted in the eruption and accumulation of tholeiitic basalts. This volcanic activity is believed to have been characterized by high effusion rates and the eruption of lavas from fissures on submarine lava plains. The restricted chemical variation of these basalts and evidence of their having last equilibrated at relatively low pressures are compatible with their derivation from large, shallow, subcrustal magma chambers. The parental magmas to the basalts may have been komatiitic as suggested by some earlier workers (Stamatelopoulou-Seymour, 1982). The continental crust may have acted as a density barrier to these komatiitic magmas and forced them to fractionate in subcrustal magma chambers.

Toward the end of the main period of basaltic volcanism a blanket of resedimented coarse clastic sediments of tonalitic provenance was deposited within the basin. These clastic sediments were transported eastward, parallel to the tectonic strike of the basin. The presence of similar clastic sediments high in the succession throughout the La Grande belt may reflect the uplift and unroofing of a tonalitic basement on marginal geanticlines of the greenstone belt. These geanticlines may have

formed as a result of the flexural rigidity of the deforming lithosphere.

Komatiitic lavas occur high in the succession in the eastern part of the belt whereas in the central part of the greenstone belt, komatiitic magmas may have assimilated a silicic contaminant to produce basaltic andesites and andesites characterized by high magnesium and compatible-trace-element compositions and LREE-enriched trace element compositions. These features indicate that crustal failure may have occurred as a result of protracted lithospheric thinning in the east, whereas in the central and western parts of the belt, in front of the propagating rift, the lithosphere did not thin to comparable extents.

Lithospheric extension factors in the order of 1.5 have been calculated for the central, initial subsidence phase, assuming uniform instantaneous extension of the continental lithosphere. Extension factors of this magnitude have been calculated for the Archean Belingwe and Witwatersrand successions as well as a number of sedimentary basins on the east coast of North America and the North Sea.

8.2 Recommendations for Future Work

The following are recommendations for future work.

- 1) A palinspastic reconstruction of a shallow water clastic facies at the base of the succession could serve to elucidate

the geometry of the rift basin. There are several indications that the rift basin was shallower toward the west and an unconformity between the greenstone belt and its basement may be found there.

2) It is necessary to examine sedimentary units throughout the La Grande belt with an emphasis on determining paleocurrent directions and the provenance of the sediments.

3) A more thorough examination of the La Grande belt is required to determine the disposition of shallow- and deep-water clastic and volcanic facies. This could serve to test the suggestion made here that the basin underwent a prolonged period of subsidence.

4) More detailed mapping and geochemical analyses of volcanic rocks are required in the central and western parts of the La Grande belt in order to determine the extent of the Second-Cycle Volcanics.

REFERENCES

- ALLEGRE, C.J., TREUIL, M., MINSTER, J-F., MINSTER, B., ALBAREDE, F., 1977, Systematic use of trace elements in igneous processes. Part 1: fractional crystallization processes in volcanic suites; *Contrib. Mineral., Petrol.*, V. 60, p. 57-75.
- AHMEDALI, T., 1983, X-ray fluorescence procedures, circular 1; Department of Geological Sciences (McGill University), Geochemical Lab Circular.
- ANHAEUSSER, C.R., 1971, Cyclic volcanicity and sedimentation in the evolutionary development of Archean greenstone belts of shield areas; *Geol. Soc. Aust., Spec. Publ.*, 3, p. 57-70.
- ARNDT, N.T., 1977, Ultrabasic magmas and high-degree melting of the mantle; *Contrib. Min. Petrol.*, V. 64, p. 205-221.
- , N.T., NALDRETT, A. J., PYKE, D.R., 1977, Komatiitic and iron-rich tholeiitic lavas of Munro Township, northeast Ontario; *J. Petrol.*, V. 18, p. 319-369.
- , N.T., FRANCIS, D., HYNES, A.J., 1979, The field characteristics and petrology of Archean and Proterozoic komatiites; *Can. Mineral.*, V. 17, p. 147-163.
- , N.T., NISBET, E.G., 1982, Komatiites; George Allen and Unwin Ltd., London, 526 pages.
- , 1983, Role of a thin, komatiite-rich oceanic crust in the Archean plate-tectonic process; *Geology*, V. 11, p. 372-375.
- ARTH, J.G., 1976, Behaviour of trace elements during magmatic processes - a summary of theoretical models and their application *J. Res. U.S.G.S.* V. 41, p. 41-47.
- , ARNDT, N.T., NALDRETT, A.J., 1977, Genesis of Archean komatiites from Munro Township, Ontario: trace-element evidence; *Geology*, V. 5, p.590-594.
- AVRAMTCHEV, L., 1983, Cartes des gites mineraux du Quebec, Region de la Baie James, Ministere de l'energie et des Ressources du Quebec, DPV-940.
- BALLARD, R.D., HOLCOMB, R.T., VAN ANDEL, T.H., 1979, The Galapagos rift at 86 W.3: Sheet flows, collapse pits, and lava lakes of the Rift Valley; *J. Geophys. Res.*, V. 84, p. 5407-5422.
- BARAGAR, W.R.A., 1984, Pillow formation and layered flows in the Circum-Superior Belt of eastern Hudson Bay; *Can. J. Earth Sci.*, V. 21, p. 781-792.

- BARRIERE, M.**, 1976, Flowage differentiation: limitations of the "Bagnold effect" to the narrow intrusions; *Contrib. Mineral. Petrol.*, V. 55, p. 139-145.
- BARTON Jr., J.M.**, 1981, The pattern of Archaean crustal evolution in Southern Africa as deduced from the evolution of the Limpopo mobile belt and the Barberton granite-greenstone terrain; *Spec. Publs. Geol. Soc. Aust.*, 7, p. 21-31.
- BASALTIC VOLCANISM STUDY PROJECT**, 1981, Basaltic volcanism on the terrestrial planets; Pergamon Press Inc., New York, 1286 pages.
- BAER, A.J.**, 1981, Geotherms, evolution of the lithosphere and plate tectonics; *Tectonophys.*, V.72, p. 203-227.
- BEDARD, J.H., FRANCIS, D.M., HYNES, A.J., NADEAU, S.**, 1984, Fractionation in the feeder system at a Proterozoic rifted margin; *Can. J. Earth Sci.*, V. 21, p. 489-499.
- BENDER, J.F., HODGES, F.N., BENCE, A.E.**, 1978, Petrogenesis of basalts from the project Famous area: experimental study from 0 to 15 kbars; *Earth Planet. Sci. Lett.*, V. 41, p. 277-302.
- BERGERIOUX, C., KENNEDY, G., ZIKOVSKY, L.**, 1979, Use of the semi-absolute method in neutron activation analysis; *J. Radio-analyt. Chem.*, V. 50, p. 229-234.
- BHATTACHARJI, S., SMITH, C.H.**, 1964, Flowage differentiation; *Science*, V. 145, p. 150-153.
- BICKLE, M.J., MARTIN, A., NISBET, E.G.**, 1975, Basaltic and peridotitic komatiites and stromatolites above a basal unconformity in the Belingwe greenstone belt, Rhodesia; *Earth Planet. Sci. Lett.*, V. 27, p. 155-162.
- , 1978, Heat loss from the earth: a constraint on Archean tectonics from the relation between geothermal gradients and the rate of plate production; *Earth Planet. Sci. Lett.*, V. 40, p. 301-315.
- , **BETTENAY, L.F., BOUTLER, C.A., GROVES, D.I., MORANT, P.**, 1980, Horizontal tectonic interaction of an Archean gneiss belt and greenstones, Pilbara block, Western Australia; *Geology*, V. 8, p. 525-529.
- , **ERIKSSON, K.A.**, 1982, Evolution and subsidence of early Precambrian sedimentary basins; *Phil. Trans. R. Soc. Lond.*, ser. 305, p. 225-247.
- BIGGAR, G.M.**, 1983, Crystallization of plagioclase, augite, and olivine in synthetic systems and tholeiites; *Mineral. Mag.*, V. 47, p. 161-176.

- BROOKS, C., LUDDEN, J., PIGEON, Y., HUBREGTSE, J.J.M.W., 1982, Volcanism of shoshonite to high-K andesite affinity in an Archean arc environment, Oxford Lake, Manitoba; *Can. J. Earth Sci.*, V. 19, p. 55-67.
- BRYAN, W.B., 1972, Morphology of quench crystals in submarine basalts; *J. Geophys. Res.*, V. 77, p. 5812-5819.
- , 1979 Regional variation and petrogenesis of basalt glasses from the FAMOUS arc, Mid-Atlantic Ridge and Kane Fracture Zone, *J. Geophys. Res.*, V. 86, p. 11815-11836.
- BURKE, K., KIDD, W.S.F., 1978, Were Archean continental geothermal gradients much steeper than those of today?; *Nature*, V.272, p. 240-241.
- CAMERON, W.E., McCULLOCK, M.T., WALKER, D.A., 1983, Boninite petrogenesis: chemical and Nd-Sr isotopic constraints; *Earth Planet. Sci. Lett.*, V. 65, p. 75-89.
- CAMPBELL, I.H., ROEDER, P.L., DIXON, J.M., 1978, Plagioclase buoyancy in basaltic liquids as determined with a centrifuge furnace; *Contrib. Mineral. Petrol.*, V. 67, p. 369-377.
- , 1984, Mantle convection and early crustal evolution; *Precamb. Res.*, V. 15, p. 15-56.
- CHOUGH, S., HESSE, R., 1978, Submarine meandering talweg and turbidity currents flowing for 4000 km in the Northwest Atlantic Mid-Ocean Channel, Labrador Sea; *Geology*, V. 4, p. 529-533.
- CIESIELSKI, A., 1984, Geologie de La Grande Riviere (Chissassibi-LG3) sous province de la Baie James, Quebec; *Geol. Surv. Canada*, open file Map 379.
- CONDIE, K.C., 1980, Origin and early development of the earth's crust; *Precamb. Res.*, V. 11, p. 183-197.
- , 1981, Archean greenstone belts; Elsevier, Amsterdam, 432 pages.
- , Hunter, D.R., 1976, Trace element geochemistry of Archean granitic rocks from the Barberton region, South Africa; *Earth Planet. Sci.*, V. 29, p. 389-400.
- COX, K.G., BELL, J.D., PANKHURST, R.J., 1979, The interpretation of igneous rocks; George Allen and Unwin, London, 450 pages.
- DePAULO, D.J., 1981, Trace element and isotopic effects of combined wallrock assimilation and fractional crystallization; *Earth Planet. Sci. Lett.*, V. 53, p. 189-202.
- DIMROTH, E., 1975, Paleo-environment of iron-rich sedimentary rocks; *Geolog. Rundsch.*, V. 64, p. 751-767.

- , COUSINEAU, P., LEDUC, M., SANSCHAGRIN, Y., 1978, Structure and organization of Archean subaqueous basalt flows, Rouyn-Noranda area, Quebec, Canada; Can. J. Earth Sci., V. 15, p. 902-918.
- , E., IMREH, L., ROCHELEAU, M., GOULET, N., 1982, Evolution of the south-central part of the Archean Abitibi belt, Quebec. part I: stratigraphy and paleogeographic model; Can. J. Earth Sci., V. 19, p. 1729-1758.
- , 1983a, Evolution of the south-central segment of the Archean Abitibi belt, Quebec. part II: tectonic evolution and geochemical model; Can. J. Earth Sci., V. 20, p. 1355-1373.
- , 1983b, Evolution of the south-central segment of the Archean Abitibi belt, Quebec. part III: plutonic and metamorphic evolution and geotectonic model; Can. J. Earth Sci., V. 20, p. 1374-1388.
- , 1984, Paleogeography, isostasy and crustal evolution of the Archean Abitibi belt: a comparison between the Rouyn-Noranda and Chibougamau-Chapais areas; in: Chibougamau-Stratigraphy and Mineralization, Guha, J., Chown, E.H., ed., CIM Spec. Vol. 34, p. 73-91.
- EADE, K.E., 1966, Fort George river and Kaniapiskau river (west-half) map-areas, New Quebec; Geol. Surv. Canada memoir 339.
- , HEYWOOD, W.W., 1957, Preliminary map, Sakami lake area, New Quebec; Geol. Surv. Can. map 23-1957.
- EKSTROM, R., 1960, Report of exploration in the Corvette Lake-La Grande River area, New Quebec; Tyrone Mines Ltd., June-October, 1959, ministere des Richesses naturelles, GM-10515.
- ELTHON, D., 1983, Isomolar and isostructural pseudo-liquidus phase diagrams for oceanic basalts; Amer. Mineral., V. 68, p. 506-511.
- , Scarfe, C.M., 1984, High-pressure phase equilibria of a high-magnesia basalt and the genesis of primary oceanic basalts; Amer. Mineral. V. 69, p. 1-15.
- ERIKKSON, K.A., 1978, Alluvial and destructive beach facies from the Archean Moodies Group, Barberton Mountainland, South Africa; in: Fluvial Sedimentology, Miall, A.D., ed., Can. Soc. Petrol. Geol. Mem. 5, p. 287-316.
- , 1980, Transitional sedimentation styles in the Moodies and Fig Tree Groups, Barberton Mountainland: evidence favouring on Archean continental margin; Precamb. Res., V. 12, p. 141-160.

- , 1981, Archean platform to trough sedimentation in the east Pilbara block, Australia; Spec. Publ. Geol. Soc. Aust., 7, p. 235-244.
- , 1982, Geometry and internal characteristics of Archean submarine channel deposits, Pilbara Block, Western Australia; J. Sed. Petrol., V. 52, p. 383-393.
- FISHER, R.V., SCHMINKE, H.-U., 1984, Pyroclastic rocks, Springer Verlag, New York, 528 pages.
- FODOR, R.V., KEIL, K., 1975, Contributions to the mineral chemistry of Hawaiian rocks, IV. Pyroxenes in rocks from Haleakola and West Main volcanoes; Contrib. Mineral. Petrol., v. 50, p. 173-195.
- FOLK, R., 1968, Petrology of sedimentary rocks; Austin Tex., Hemphills Bookstore, 170 pages.
- FOUQUES, J.P., SCHUMACHER, F., 1979, Rapport de synthese du permis SES, Seru Nucleaire, Eldorado Nucleaire, SDBJ, 26 pages.
- FRANCIS, D.M., LUDDEN, J., HYNES, A., 1983, Magma evolution in a Proterozoic rifting environment; J. Petrol., V. 24, p. 556-582.
- FRITH, R., FRITH, R.A., DOIG, R., 1977, The geochronology of the granitic rocks along the Bear-Slave structural province boundary, northwest Canadian Shield; Can. Jour. Earth Sci., V. 14, p. 1356-1373.
- 3 FYFE, W.S., 1974, Archean tectonics; Nature, V. 249, p. 338.
- GARIEPY, C., 1980, Analyse des terres-rares et de quelques elements en trace par activation neutronique; Laboratoire de Geochemie, Department de Geologie, Universite de Montreal, 32 pages.
- GELINAS, L., BROOKS, C., 1974, Archean quench texture tholeiites; Can. J. Earth Sci., V. 11, p. 324-340.
- GELINAS, L., TRUDEL, P., HUBERT, C., 1984, Chemostratigraphic division of the Blake river Group Rouyn-Noranda area, Abitibi, Quebec; Can. J. Earth Sci., V. 21, p. 220-231.
- GLICKSON, A.Y., 1971, Archean geosynclinal sedimentation near Kalgoorlie, Western Australia; Geol. Soc. Aust., Spec. Publ., 3, p. 443-460.
- , 1972, Early Precambrian evidence of a primitive ocean crust and island nuclei of sodic granite; Geol. Soc. Am. Bull., V83, p. 3323-3344.

- , 1976, Earliest Precambrian ultramafic-mafic volcanic rocks: Ancient oceanic crust or relic terrestrial maria?; *Geology*, V. 4, p. 201-206.
- GOODWIN, A.M., RIDLER, R.H., 1970, The Abitibi orogenic belt; *Geol. Surv. Can. Paper*, 70-40, p. 1-30.
- , 1972, The Superior province; in: Variations in tectonic style, Price, R.A., Douglas, R.J.W., ed., *Geol. Assoc. Can., Spec. Paper*, 11, p. 527-624.
- GREELEY, R., 1982, The Snake River plain, Idaho,: Representative of a new type of volcanism; *J. Geophys. Res.*, V. 87, p. 2705-2712.
- GRENON, A., ROY, D.W., SHARMA, K.N.M., 1977, Rejet net probable de la faille de LG-3 et identification de structures en domes et bassins territoire du Nouveau-Quebec, Quebec; *Can. J. Earth Sci.*, V. 14, p. 500-504.
- GROVE, T.L., BAKER, M.B., 1984, Phase equilibrium controls on the tholeiitic versus calc-alkaline differentiation trends; *J. Geophys. Res.*, V. 89, p. 3253-3274.
- HANSON, G.N., LANGMUIR, C.H., 1978, Modelling of major elements in mantle-melt systems using trace element approaches; *Geochim. Cosmochim. Acta*, V. 42, p. 725-741.
- , 1980, Rare earth elements in petrogenetic studies of igneous systems; *Ann. Rev. Earth Planet. Sci.*, V. 8, p. 371-406.
- HAWKESWORTH, C.J., O'NIONS, R.K., 1977, The petrogenesis of some Archean volcanic rocks from southern Africa; *J. Petrol.*, V. 18, p. 487-520.
- HOFFMAN, P., BOWRING, S.A., 1984, Short-lived 1.9 Ga continental margin and its destruction, Wopmay origin, northwest Canada; *Geology*, V. 12, p. 68-72.
- HUMPHRIS, S.E., THOMPSON, G., 1978, Hydrothermal alteration of oceanic basalts by sea water; *Geochim. Cosmochim. Acta*, V. 42, p. 127-136.
- HUPPERT, H.E., SPARKS, R.S.J., TURNER, ARNDT, N.T., 1984, Emplacement and cooling of komatiite lavas; *Nature*, V. 398, p. 19-22.
- , 1985, Cooling and contamination of mafic and ultramafic magmas during ascent through continental crust; *Earth Planet. Sci. Lett.* V. 74, p. 371-386.
- HUNTER, D.R., 1974, Crustal development in the Kaapvaal craton, I. The Archean; *Precamb. Res.*, V. 1, p. 259-294.

- HUTCHINSON, C.S., 1974, Laboratory handbook of petrographic techniques; John Wiley and Sons, New York, 527 pages.
- HYDE, R.S., WALKER, R.G., 1977, Sedimentary environments and the evolution of the Archean greenstone belt in the Kirkland lake area, Ontario; in: Report of Activities, Part a, Geol. Surv. Can., paper 77-1a, p. 185-190.
- HYNES, A.J., 1982, Stability of the oceanic tectosphere-a model for early Proterozoic intercratonic orogeny; Earth Planet. Sci. Lett., V. 61, p. 333-345.
- IRVING, A.J., 1978, A review of experimental studies of crystal/liquid trace element partitioning; Geochim. Cosmochim. Acta, V. 42, p. 743-770.
- JAHN, B.-M., AUVRAY, B., BLAIS, S., CAPDEVILA, R., CORNICHE, J., VIDAL, F., HAMEURT, J., 1980, Trace element geochemistry and petrogenesis of Finnish greenstone belts; J. Petrol., V. 21, p. 201-44.
- JOLLY, W.T., 1975, Subdivision of the Archean lavas of the Abitibi area from Fe-Mg-Ni-Cr relations; Earth Planet. Sci. Lett., V. 27, p. 200-210.
- JOLLY, W.T., 1980, Development and degradation of Archean lavas, Abitibi area Canada, in light of major element chemistry; J. Petrol., V. 21, p. 323-363.
- JONES, J.G., 1969, Pillow lavas as depth indicators; Amer. J. Sci., V. 267, p. 181-195.
- KOMAR, P.D., NEUDECK, R.H., KULM, L.D., 1972, Observations and significance of deep water oscillatory ripple marks on the Oregon continental shelf; in: Shelf Sediment Transport: Process and Pattern, Swift, D.J.P., Duane, D.B., Pilkey, O.H., ed., Dowden, Hutchinson and Ross, Stroudsburg, p. 601-619.
- , 1972, Mechanical interactions of phenocrysts and flow differentiation of igneous dikes and sills; Geol. Soc. Amer. Bull., V. 83, p. 973-988.
- , 1976, Phenocryst interactions and the velocity profile of magmas flowing through dykes or sills; Geol. Soc. Amer. Bull., V. 87, p. 1336-1342.
- LAJOIE, J., 1984, Volcaniclastic rocks; in: Facies Models Second Edition, Geoscience Canada, Reprint ser. 1, Walker, R.G., ed., p. 39-52.
- LANGFORD, F.F., MORIN, J.A., 1976, The development of the Superior Province of northwestern Ontario by merging island arcs; Amer. J. Sci., V. 276, p. 1023-1034.

- LANGMUIR, C.H., HANSON G.N., 1980, An evaluation of major element heterogeneity in the mantle sources of basalts; *Phil. Trans. R. Soc. Lond.*, V. 297A, p. 383-407.
- LAROSE, P.Y., 1975, Carte Geologique, N.T.S. 33G/12, Groupe minier SES.
- LePICHON, X., ANGELIER, J., SIBUET, J-C, 1982, Plate boundaries and extensional tectonics; *Tectonophys.*, V. 81, p. 239-256.
- LIU, M., 1985, Migmatization and volcanic petrogenesis in the La Grande greenstone belt, Quebec; Masters thesis, unpubl., McGill University, Montreal, Quebec, 87 pages.
- LONSDALE, P., 1977, Abyssal pahoehoe with lava coils at the Galapagos Rift; *Geology*, V. 5, p. 147-152.
- LOWDON, J.A., 1960, Age determinations by the Geological Survey of Canada, Report 1, Isotopic ages; *Geol. Surv. Can. paper* 60-17.
- LUBIMOVA, E.A., 1958, Thermal history of the earth with consideration of the variable thermal conductivity of the mantle; *Geophysics*, V. 1, p. 115-134.
- LUDDEN, J.N., GELINAS, L., TRUDEL, P., 1982, Archean metavolcanics from the Rouyn-Noranda district, Abitibi greenstone belt, Quebec. 2. mobility of trace elements and petrogenetic constraints; *Can. J. Earth Sci.*, V. 19, p.2276-2287.
- , FRANCIS, D., ALLARD, G., 1984, The geochemistry and evolution of the volcanic rocks of the Chibougamau region of the Abitibi metavolcanic belt; in: *Chibougamau-Stratigraphy and Mineralization*, Guha, J., Chown, E.H., ed., *CIM Spec. V. 34*, p. 20-34.
- MACGREGOR, A.M., 1951, Some milestones in the Precambrian of southern Rhodesia; *Trans. Geol. Soc. S. Afr.*, V. 54, p. 27-71.
- MAKRIS, J., VEES, R., 1977, Crustal structure of the Aegean Sea and the islands of Evia and Crete, Greece, obtained by seismic refraction experiments; *J. Geophys.*, V. 41, p. 329-340.
- MATHEWS, P.E., 1967, The pre-Karoo formations of the White Umfolozi inlier, northern Natal; *Trans. Geol. Soc. S. Afr.*, 71, p. 39-63.
- McKENZIE, D.P., WEISS, N., 1975, Speculations on the thermal and tectonic history of the earth; *J. R. Astron. Soc.*, V. 42, p. 131-174.

- , 1978, Some remarks on the development of sedimentary basins; *Earth Planet. Sci. Lett.*, V. 40, p. 25-32.
- , WEISS, N., 1980, The thermal history of the earth; in: *The Continental Crust and its Mineral Deposits*, Strangway, D.W., ed., *Geol. Assoc. Can.*, spec. paper 20, 575-590.
- , NISBET, E., SCLATER, J.G., 1980, Sedimentary basin development in the Archean; *Earth Planet. Sci. Lett.*, V. 48, p. 35-41.
- MOORBATH, S., 1975, Evolution of Precambrian crust from strontium isotopic evidence; *Nature*, V. 254, p. 395-396.
- MOORE, J.G., 1965, Petrology of deep-sea basalt near Hawaii; *Amer. J. Sci.*, V. 251, p. 169-191.
- MOTTL, M.J., 1983, Metabasalts, axial hot springs, and the structure of hydrothermal systems at mid-ocean ridges; *Geol. Soc. Amer. Bull.*, V. 94, p. 161-180.
- MUTTI, E., RICCI-LUCCI, F., 1972, Le Torbiditi dell'-Appennino settentrionale: introduzione all'analisi di facies; *Soc. Geol. Italiana Mem.* 11, p. 161-199, English trans. by T.H. Nilsen, 1978, *International Geology Rev.*, V. 20, p. 125-166; AGI reprint ser. 3.
- NESBITT, R.W., SUN, S.-S., 1980, Geochemical features of some Archean and post-Archean high-magnesian-low-alkali liquids; *Phil. Trans. R. Soc. Lond.*, ser. A297, p. 365-381.
- NISBET, E.G., BICKLE, M.J., MARTIN, A., 1977, The mafic and ultramafic lavas of the Belingwe greenstone belt, Rhodesia; *J. Petrol.*, V. 18, p. 521-566.
- , WALKER, D., 1982, Komatiites and the structure of the Archean mantle; *Earth Planet. Sci. Lett.*, V. 60, p. 105-113.
- , FOWLER, C.M.R., 1983, Model for Archean plate tectonics; *Geology*, V. 11, p. 376-379.
- , 1984a, Gold in the Upper Greenstones of the Belingwe greenstone belt: a model; in: *Gold'82: The geology, geochemistry and genesis of gold deposits*, ed., Foster, R.P., *Geol. Soc. Zimbabwe, Spec. Publ.*, 1, p. 583-593.
- , 1984b, The continental and oceanic crust and lithosphere in the Archean: isostatic, thermal and tectonic models; *Can. J. Earth Sci.* V. 21, p. 1426-1441.
- NORMARK, W.R., 1976, Delineation of the main extrusion zone of the East Pacific Rise at latitude 21 N; *Geology*, V. 4, p.

681-685.

- O'HARA, M.J., 1968, The bearing of phase equilibria studied in synthetic and natural systems on the origin and evolution of basic and ultrabasic rocks; *Earth Sci. Rev.*, V. 4, p. 69-133.
- O'NIONS, R.K., EVENSEN, N.M., HAMILTON, P.J., CARTER, S.R., 1978, Melting of the mantle past and present: isotopic trace element evidence; *Phil. Trans. R. Soc. Lon.*, ser. A288, p. 547-559.
- PEARCE, J.A., NORRY, M.J., 1979, Petrogenetic implications of Ti, Zr, Y and Nb variations in volcanic rocks; *Contrib. Mineral. Petrol.*, V. 69, p. 33-47.
- PEARCE, T.H., 1974, Quench plagioclase from some Archean basalts; *Can. J. Earth Sci.*, V. 11, p. 715-719.
- PHINNEY, W.C., MORRISON, D.A., MACZUGA, D.E., 1984, Calcic plagioclase megacrysts: Implications for wide-spread formation of cumulates in Archean crust; Abstracts with Programs, *Geol. Soc. Amer.*, annual meeting, Reno, Nevada.
- PINCUS, H., 1955, Some vector and arithmetic operations on two-dimensional orientation variates, with applications to geological data; *J. Geology*, V. 64, p. 533-557.
- PYKE, D.R., NALDRETT, A.J., ECKSTAND, O.R., 1973, Archean ultramafic flows in Munro township, Ontario; *Geol. Soc. Amer. Bull.*, V. 84, p. 955-978.
- RAMSAY, J.G., 1965, Structural investigations in the Barberton Mountain Land, eastern Transvaal; *Trans. Geol. Soc. S. Afr.*, V. 66, p. 353-401.
- RIVARD, B., FRANCIS, 1984, Preliminary models for basalt evolution in the La Grande Greenstone belt; in: *Chibougamau-Stratigraphy and Mineralization*, Guha, J., Chown, E.H., ed., *CIM Special Vol. 34*, p. 48-56.
- , 1985, Petrochemistry of a layered Archean magma chamber and its relation to models of basalt evolution; in: *Program with Abstracts*, *Geol. Assoc. Can.-Miner. Assoc. Can.* annual meeting, Fredericton, New Brunswick.
- ROEDER, P.L., EMSLIE, R.F., 1970, Olivine-liquid equilibrium; *Contrib. Mineral. Petrol.*, V. 29, p. 275-289.
- ROYDEN, L., KEEN, C.E., 1980, Rifting process and thermal evolution of the continental margin of eastern Canada determined from subsidence curves; *Earth Planet. Sci. Lett.*, V. 51, p. 343-361.
- SCHROEDER, B., THOMPSON, G., SULANOWSK, M., LUDDEN, J.N., 1980,

Analysis of geologic materials using an automated x-ray fluorescence system; X-ray spectrometry; V. 9, p. 198-205.

SCLATER, J.G., JAUPART, C., GALSON, D., 1980, The heat flow through oceanic and continental crust and the heat loss of the earth; Rev. Geophys. Space Phys., V. 18, p. 269-311.

SCUMACHER, F., FOUQUE, J.P., 1978, Geologie du permis SES, map Groupe minier SES.

SHARMA, K.N.M., 1977, Region de La Grande Riviere area; Ministere des Richesses Naturelles, Quebec, rapport geologique 184, 75 pages.

SKULSKI, T., HYNES, A., FRANCIS, D., 1984, Stratigraphic and lithochemical characterization of cyclic volcanism in the LG-3 area, La Grande River greenstone belt, Quebec; in: Chibougamau-Stratigraphy and Mineralization, Guha, J., Chown, E.H., ed., CIM Special Vol. 34, p. 57-72.

-----, LIU, M., HYNES, A., 1985, Continental rifting in the Archean La Grande greenstone belt, central Quebec, in: Program with Abstracts, Geol. Assoc. Can. - Miner. Assoc. Can., annual meeting, Fredericton, New Brunswick.

SLEEP, N.H., WINDLEY, B.F., 1982, Archean plate tectonics: constraints and inferences; J. Geology, V. 90, p. 363-379.

SMITH, T.E., LONGSTAFFE, F.J., 1974, Archean rocks of shoshonitic affinities at Bijou point, northwestern Ontario; Can. J. Earth Sci., V. 11, p. 1407-1413.

SPRY, A., Metamorphic textures; Pergamon Press, Oxford, 350 pages.

STAMATELOPOULOU-SEYMOUR, K., 1982, Volcanic petrogenesis in the Lac Guyer greenstone belt, James Bay area, Quebec. Phd thesis, unpubl., McGill University, Montreal, Quebec, 304 pages.

-----, K., FRANCIS, D., LUDDEN, J., 1983, The petrogenesis of the Lac Guyer komatiites and basalts and the nature of the komatiite-komatiitic basalt compositional gap; Contrib. Mineral. Petrol., V. 84, p. 6-14.

SUN, S., NESBITT, R.W., 1977, Chemical heterogeneity of the Archean mantle, composition of the earth and mantle evolution, Earth Planet. Sci. Lett., V. 35, p. 429-448.

TARNEY, J., DALZIEL, I.W.D., DEWIT, M.J., 1976, Marginal basin 'Rocas Verdes' complex from s. Chile: a model for Archean greenstone belt formation; in: The Early History of the Earth, Windley, B.F., ed., Proc. NATO Symp., Univ. Leicester, p. 131-146.

- TEAL, P.R., WALKER, R.G., 1977, Stratigraphy and sedimentology of the Archean Manitou Group, northwestern Ontario; in: Report of Activities, Part A., Geol. Surv. Can., paper 77-1a, p.181-184.
- THURSTON, P.C., FRYER, B.J., 1983, The geochemistry of repetitive cyclical volcanism from basalt through rhyolite in the Uchi-Confederation greenstone belt, Canada; Contrib. Min. Petrol., V. 83, p. 204-226.
- TREMBLAY, M., 1982, Rapport d'exploration 1982 digues TA-26A et TA-26B travaux d'exploration-plan, map, Societe d'energie de la Baie-James.
- TURNER, C.C., WALKER, R.G., 1973, Sedimentology, stratigraphy, and crustal evolution of the Archean greenstone belt near Sioux Lookout, Ontario; Can. J. Sci., V. 10, p. 817-845.
- WALKER, R.G., PETTIJOHN, F.J., 1971, Archean sedimentation : analysis of the Minnitakibasin, northwestern Ontario, Canada; Geol. Soc. Amer. Bull., V. 82, p. 2099-2130.
- , 1975, Generalized facies models for resedimented conglomerates of turbidite association; Geol. Soc. Amer. Bull., V. 86, p.737-748.
- , 1978, Turbidites and associated coarse clastic deposits, in: Facies models, Geoscience Canada, Reprint ser. 1, Walker, R.G., ed., p. 91-104.
- , 1984, Turbidites and associated coarse clastic deposits; in: Facies Models second edition, Geoscience Canada, Reprint ser. 1, Walker, R.G., ed., p. 171-188.
- WASSERBURG, G.J., MACDONALD, G.J.F., HOYLE, F., FOWLER, W.A., 1964, Relative contributions of uranium, thorium and potassium to heat production in the earth; Science, V 143, p. 465-467.
- WATSON, E.B., 1982, Basalt contamination by continental crust: some experiments and models; Contrib. Mineral. Petrol., V. 80, p. 73-87.
- , JUREWICZ, S.R., 1984, Behavior of alkalis during diffusive interaction of granitic xenoliths with basaltic magma; J. Geology, V. 92, p. 121-131.
- WILLIAMS, D.A.C., FURNELL, R.G., 1979, Reassessment of part of the Barberton type area, South Africa; Precam. Res., V. 9, p. 325-347.
- WILLIAMS, H.R., 1977, African Archean mobile belts and granite-greenstone terrane; Nature, V. 266, p. 163-164.

WILSON, J.F., BICKLE, M.J., HAWKSWORTH, C.J., MARTIN, A.,
NISBET, E.G., ORPEN, J.L., 1978, Granite-greenstone terrains
of the Rhodesian Archean craton; *Nature*, v. 271, p. 23-27.

WINDLEY, B.F., 1973, Crustal development in the Precambrian;
Phil. Trans. R. Soc Lond. ser. A, 273, p. 321-341.

-----, 1977, *The evolving continents*; J. Wiley and Sons,
New York, N.Y., 385 p.

WINN, R.D., DOTT, R.H., 1977, Large-scale traction-produced
structures in deep-water fan-channel conglomerates in
southern Chile; *Geology*, V. 5, p. 41-44.

WRIGHT, T.L., DOHERTY, P.C., 1970, A linear programming and
least squares computer method for solving petrologic mixing
problems; *Bull. Geol. Soc. Am.*, V. 81, p. 1955-2008.

YODER, H.S., 1976, *Generation of basaltic magma*; National
Academy of Sciences, Washington, D.C., 265 pages.

Appendix A Analytical Methods, Sampling Criteria and Preparation

The whole rock samples collected from extrusive and intrusive rocks in the study area were chosen carefully to avoid analyzing samples which may have undergone appreciable secondary alteration. Pillow lavas collected from the First-Cycle Volcanics were sampled at their margins so that 50-100 grams of microcrystalline lava could be analyzed approximately 5-10 cm from the margin of the pillow. This ensured a uniformed sampling procedure and also it is believed that these portions of pillows are least likely to have undergone redistribution of phenocrysts. A petrographic description and location of all samples analyzed and used in this thesis is given in A2.4. Total volatile contents were determined by using the loss on ignition technique. Analysis which summed to less than 99.0% and more than 101.0% were rejected (dry total + LOI).

The major elements (as well as Ni, Cr, Sr, Ba and V) and trace elements (Zr and Y) were analyzed by x-ray fluorescence using glass beads and pressed powder discs respectively, at the Department of Geological Sciences, McGill University.

All samples analyzed by x-ray fluorescence at McGill University were obtained using a Phillips PW 1400 spectrometer with a 100 KV generator *. Major element standardization was achieved by comparing net peak counts-per-second corrected for mass absorption with a calibration line derived from 18

international reference materials. The precision is 0.2% (absolute).

Trace elements obtained at McGill University were determined from peak- and five background-counts per second. The background data were used to calculate a best-fit background curve of the form

$$C = a + b \exp(t) + c \exp(2t) + d \exp(3t) + e \exp(4t)$$

where C is the background and t is the value of 2θ . Since some of the background positions are subject to interference, empirical corrections (based on diluted "spike tests") were applied to the backgrounds, using the net peaks for elements at lower 2θ positions. Several successive background curves were calculated, incorporating net peaks of elements with progressively lower 2θ positions. Empirical interference corrections were also applied to the peaks. Net peaks were corrected for mass absorption using mass absorption coefficients from the major element analyses. Standardization of the trace element was achieved by comparing with calibration lines from a set of diluted spikes. This calibration was preferred over that based on international standards, because there is considerable inhomogeneity in many of the international standards at the levels of concern in this study. Nevertheless, variations between the spike-derived calibrations and those using an international standard data-set are less than 5% in all cases.

* The analytical procedure for analysis by x-ray fluorescence obtained at McGill University is adapted after Liu, 1985. Further details of the analytical procedure can be found in Ahmedali (1983).

Chromium analysis from the Lac Coutaceau dykes was obtained at the Université de Montréal, GINNA laboratory by x-ray fluorescence using pressed powder discs. Calibration techniques and mass-absorption corrections and precisions of analysis are described in Schroeder et. al., (1980).

The REE , Sc, Th, Ta, U, and Hf were analyzed by instrumental neutron activation analysis at the GINNA laboratory. The samples were irradiated in a SLOWEPOKE II reactor for 2 hours in a neutron flux of 10 n/cm/sec and counted over a period of 1 month using Ge detectors of 0.57 Kev. resolution at 122 Kev. and 1.8 Kev. resolution at 1.33 Kev. Details of the analytical technique can be found in Bergerioux et al. (1979) and Gariépy (1980). The precision of La, Sm, Eu, Yb, and Sc are estimated at less than 5% and 5-10% for Ce, Nd, Ho, Tb, Lu, U and Ta.

Appendix B

FIRST-CYCLE VOLCANICS

	PLBAS 338	PLBAS 158	PLBAS 330C	PLBAS 152	PLBAS 554	BSAND 451	BSAND 229	BSAND 452
SiO2	50.19	51.57	50.29	47.90	54.04	52.79	57.20	56.11
TiO2	0.96	1.51	0.81	1.35	0.62	1.24	0.79	1.25
Al2O3	14.95	13.35	14.90	12.56	14.12	16.40	18.83	16.53
Fe2O3	0.00	0.00	0.00	0.00	0.00	0.00	0.00	0.00
MgO	6.97	5.62	5.54	6.05	7.83	5.97	5.05	3.63
FeO	10.75	15.04	10.75	14.70	9.20	10.72	6.20	7.38
MnO	0.25	0.24	0.25	0.24	0.17	0.25	0.13	0.17
CaO	12.51	6.23	12.16	8.29	11.13	3.74	4.05	4.66
Na2O	1.85	3.99	2.08	2.01	1.76	3.73	3.87	5.63
K2O	0.24	0.10	0.44	0.83	0.11	0.02	0.31	0.10
P2O5	0.06	0.09	0.05	0.09	0.04	0.07	0.04	0.07
LOI	1.02	2.06	2.79	6.61	0.58	5.93	3.81	4.89
Total	99.75	99.80	100.06	100.63	99.60	100.86	100.28	100.42

CATION PROPORTIONS BASED ON 100 CATIONS

Si	47.59	49.49	48.55	48.31	50.90	51.53	54.43	53.77
Ti	0.68	1.09	0.59	1.02	0.44	0.91	0.57	0.90
Al	16.71	15.10	16.95	14.93	15.67	18.87	21.12	18.67
Fe3	0.00	0.00	0.00	0.00	0.00	0.00	0.00	0.00
Mg	9.85	8.04	7.97	9.10	10.99	8.69	7.16	5.18
Fe2	8.52	12.07	8.68	12.40	7.25	8.75	4.93	5.91
Mn	0.20	0.20	0.20	0.21	0.14	0.21	0.10	0.14
Ca	12.71	6.41	12.58	8.96	11.23	3.91	4.13	4.78
Na	3.40	7.42	3.89	3.93	3.21	7.06	7.14	10.46
K	0.29	0.12	0.54	1.07	0.13	0.02	0.38	0.12
P	0.05	0.07	0.04	0.08	0.03	0.06	0.03	0.06
Total	100.00	100.00	100.00	100.00	100.00	100.00	100.00	100.00

Ti	5815	9232	4975	8632	3776	7853	4915	7853
Zr	48.	82.	41.	76.	36.	60.	35.	64.
Y	19.	34.	18.	24.	15.	26.	13.	21.
Sc	45.00	48.00	44.00	43.00	39.00	46.00	46.00	41.00
V	243.	482.	212.	332.	200.	340.	264.	317.
Cr	237.	90.	265.	115.	431.	286.	475.	263.
Ni	112.	47.	144.	69.	123.	108.	174.	94.
P	296.	440.	231.	453.	213.	340.	218.	278.
Sr	98.	80.	150.	56.	115.	52.	110.	59.
Ba	0.	88.	157.	204.	12.	49.	83.	149.
La	2.50	4.22	2.03	5.03	2.40	1.90	1.39	1.96
Ce	7.41	11.85	4.19	12.50	5.20	5.08	3.27	5.03
Nd	4.83	8.58	3.77	7.64	3.58	4.89	3.97	4.25
Sm	2.04	3.13	1.73	3.16	1.40	2.52	1.50	2.15
Eu	0.69	0.96	0.62	0.86	0.42	1.25	0.60	0.53
Tb	0.60	0.97	0.40	0.52	0.33	0.57	0.27	0.35
Ho	0.53	1.15	0.74	1.09	0.63	1.51	0.61	0.81
Tm	0.48	0.54	0.16	0.47	0.32	0.43	0.31	0.30
Yb	1.95	3.50	1.86	2.68	1.65	2.42	1.47	2.19
Lu	0.25	0.48	0.32	0.43	0.27	0.37	0.20	0.40

PLBAS= PILLOW BASALT, BSAND= BASALTIC ANDESITE

Appendix B

FIRST-CYCLE VOLCANICS

	PLBASP 216	PLBASP 447A	PLBASP 18A	PLBASP 92B	PLBASP 426	PLBASP 330B	PLBASP 336B	PLBASP 336C
SiO ₂	48.47	48.58	51.83	49.88	50.66	50.09	49.19	51.11
TiO ₂	0.83	1.27	1.05	0.95	0.87	0.84	0.93	1.06
Al ₂ O ₃	16.51	15.20	15.02	14.38	15.66	15.40	14.21	14.58
Fe ₂ O ₃	0.00	0.00	0.00	0.00	0.00	0.00	0.00	0.00
MgO	7.61	6.91	6.83	7.02	5.63	4.18	7.85	6.13
FeO	10.85	12.75	11.10	10.96	10.35	11.11	11.64	11.09
MnO	0.20	0.22	0.23	0.27	0.30	0.25	0.21	0.25
CaO	9.40	10.25	9.46	11.87	11.39	11.48	10.37	8.37
Na ₂ O	2.23	1.86	1.81	1.42	1.83	2.50	2.14	3.49
K ₂ O	0.02	0.62	0.16	0.15	0.03	0.39	0.29	0.28
P ₂ O ₅	0.06	0.08	0.06	0.06	0.05	0.04	0.05	0.07
LOI	4.52	1.84	2.91	3.86	3.75	4.06	3.86	3.64
Total	100.70	99.58	100.46	100.82	100.52	100.34	100.74	100.07

CATION PROPORTIONS BASED ON 100 CATIONS

Si	46.78	46.69	49.89	48.37	49.23	48.97	47.33	49.21
Ti	0.60	0.92	0.76	0.69	0.64	0.62	0.67	0.77
Al	18.78	17.22	17.04	16.44	17.94	17.74	16.12	16.54
Fe ₃	0.00	0.00	0.00	0.00	0.00	0.00	0.00	0.00
Mg	10.95	9.90	9.80	10.15	8.15	6.09	11.26	8.80
Fe ₂	8.76	10.25	8.94	8.89	8.41	9.08	9.37	8.93
Mn	0.16	0.18	0.19	0.22	0.25	0.21	0.17	0.20
Ca	9.72	10.56	9.76	12.33	11.86	12.03	10.69	8.63
Na	4.17	3.47	3.38	2.67	3.45	4.74	3.99	6.51
K	0.02	0.76	0.20	0.19	0.04	0.49	0.36	0.34
P	0.05	0.07	0.05	0.05	0.04	0.03	0.04	0.06
Total	100.00	100.00	100.00	100.00	100.00	100.00	100.00	100.00

Ti	5155	7793	6450	5875	5396	5215	5755	6594
Zr	45.	66.	54.	48.	42.	43.	50.	58.
Y	20.	24.	22.	20.	18.	18.	21.	25.
Sc	39.00	43.00	45.00					
V	195.	313.	279.	237.	243.	219.	227.	294.
Cr	272.	183.	233.	226.	276.	283.	365.	196.
Ni	148.	103.	122.	114.	166.	142.	163.	63.
P	270.	392.	301.	270.	244.	196.	244.	288.
Sr	246.	99.	133.	134.	180.	221.	82.	64.
Ba	41.	177.	86.	23.	0.	169.	72.	186.
La	2.60	3.49	2.75					
Ce	6.41	8.02	6.28					
Nd	4.62	7.22	5.61					
Sm	1.90	2.64	2.32					
Eu	0.59	0.86	0.72					
Tb	0.25	0.58	0.50					
Ho	0.63	1.21	0.85					
Tm	0.00	0.39	0.31					
Yb	2.01	2.67	2.31					
Lu	0.29	0.37	0.36					

PLBAS = PILLOW BASALT, PLBASP = PLAGIOCLASE-PHYRIC BASALT

Appendix B

FIRST-CYCLE VOLCANICS

	MASBA 461	MASBA 186	MASBA 201	PYGAB 424A	PYGAB 427	PYGAB 428C	PYGAB 139	PYGAB 431
S102	50.52	50.58	52.03	50.60	49.87	48.16	50.61	47.84
T102	1.06	2.02	1.03	0.84	0.82	0.89	0.91	1.09
Al2O3	15.16	12.00	14.07	14.52	14.58	14.96	13.55	14.76
Fe2O3	0.00	0.00	0.00	0.00	0.00	0.00	0.00	0.00
MgO	5.63	6.00	6.95	8.19	8.43	9.30	8.03	5.36
FeO	12.24	16.11	12.02	10.90	11.21	12.04	11.84	10.79
MnO	0.23	0.26	0.18	0.22	0.20	0.23	0.21	0.25
CaO	9.52	7.61	9.33	10.41	10.86	9.57	8.76	11.33
Na2O	1.27	2.18	2.18	1.33	1.57	2.02	2.64	1.71
K2O	0.04	0.07	0.23	0.46	0.03	0.04	0.06	0.03
P2O5	0.06	0.09	0.07	0.05	0.05	0.05	0.06	0.05
LOI	5.01	3.06	1.99	2.65	2.82	3.69	3.78	7.67
Total	100.74	99.98	100.08	100.17	100.44	100.95	100.45	100.88

CATION PROPORTIONS BASED ON 100 CATIONS

S1	50.13	49.87	49.78	48.55	47.70	45.93	48.69	48.41
T1	0.79	1.50	0.74	0.61	0.59	0.64	0.66	0.83
Al	17.73	13.94	15.86	16.42	16.44	16.82	15.36	17.60
Fe3	0.00	0.00	0.00	0.00	0.00	0.00	0.00	0.00
Mg	8.33	8.82	9.91	11.71	12.02	13.22	11.51	8.08
Fe2	10.16	13.28	9.62	8.75	8.97	9.60	9.53	9.13
Mn	0.19	0.22	0.15	0.18	0.16	0.19	0.17	0.21
Ca	10.12	8.04	9.56	10.70	11.13	9.78	9.03	12.28
Na	2.44	4.17	4.04	2.47	2.91	3.74	4.92	3.36
K	0.05	0.09	0.28	0.56	0.04	0.05	0.07	0.04
P	0.05	0.08	0.06	0.04	0.04	0.04	0.05	0.04
Total	100.00	100.00	100.00	100.00	100.00	100.00	100.00	100.00

Ti	7900	10500	7400	6100	5900	6400	6600	8300
Zr	56.	75.	54.	42.	41.	43.	47.	57.
Y	24.	31.	23.	18.	20.	17.	20.	24.
Cr	261.	68.	199.	261.	235.	201.	272.	261.
Ni	85.	19.	75.	152.	131.	120.	85.	98.
P	296.	418.	309.	231.	235.	222.	266.	274.
Sr	103.	65.	123.	122.	138.	138.	123.	108.

MASBA= MASSIVE BASALT, PYGAB= PYROXENE CUMULATE GABBRO

Appendix B

FIRST-CYCLE VOLCANICS

	PYGAB 217	PYGAB 445A	PYGAB 542A	PYGAB 542B	PYGAB 379	DIGAB 341	DIGAB 55	DIGAB 447B
SiO ₂	50.42	48.58	49.41	43.70	46.18	50.19	49.68	47.97
TiO ₂	0.96	1.65	0.83	0.93	0.41	0.78	0.82	1.23
Al ₂ O ₃	13.91	13.58	15.86	16.38	13.86	14.24	14.74	13.81
Fe ₂ O ₃	0.00	0.00	0.00	0.00	0.00	0.00	0.00	0.00
MgO	7.44	4.67	7.48	9.08	15.59	6.81	8.52	8.96
FeO	12.02	15.75	11.37	14.72	10.20	12.53	11.50	14.61
MnO	0.21	0.23	0.18	0.25	0.18	0.24	0.18	0.28
CaO	9.38	11.08	8.65	10.04	9.17	11.28	10.27	7.49
Na ₂ O	2.17	1.98	3.72	1.44	1.52	2.29	2.23	2.16
K ₂ O	0.06	0.66	0.11	0.13	0.13	0.25	0.03	0.58
P ₂ O ₅	0.07	0.12	0.05	0.06	0.02	0.04	0.05	0.08
LOI	3.56	0.80	2.59	3.53	3.34	0.91	2.56	2.83
Total	100.20	99.10	100.25	100.26	100.60	99.56	100.58	100.00

CATION PROPORTIONS BASED ON 100 CATIONS

Si	48.83	47.25	46.53	42.21	42.88	47.68	47.07	46.12
Ti	0.70	1.21	0.59	0.68	0.29	0.56	0.58	0.89
Al	15.88	15.57	17.60	18.65	15.17	15.94	16.46	15.65
Fe ₃	0.00	0.00	0.00	0.00	0.00	0.00	0.00	0.00
Mg	10.74	6.77	10.50	13.07	21.58	9.64	12.03	12.84
Fe ₂	9.74	12.81	8.95	11.89	7.92	9.95	9.11	11.75
Mn	0.17	0.19	0.14	0.20	0.14	0.19	0.14	0.23
Ca	9.73	11.55	8.73	10.39	9.12	11.48	10.43	7.72
Na	4.07	3.73	6.79	2.70	2.74	4.22	4.10	4.03
K	0.07	0.82	0.13	0.16	0.15	0.30	0.04	0.71
P	0.06	0.10	0.04	0.05	0.02	0.03	0.04	0.07
Total	100.00	100.00	100.00	100.00	100.00	100.00	100.00	100.00

Ti	7000	10210	5900	6800	2900	5600	5800	8900
Zr	56.	97.	34.	38.	16.	31.	42.	70.
Y	24.	32.	18.	21.	10.	16.	18.	27.
Cr	198.	73.	489.	149.	899.	31.	235.	204.
Ni	76.	28.	89.	166.	391.	41.	129.	205.
P	305.	266.	227.	283.	104.	196.	244.	397.
Sr	163.	143.	142.	140.	100.	109.	93.	100.

PYGAB- PYROXENE CUMULATE GABBRO, DIGAB- DIABASIC GABBRO

Appendix B

FIRST-CYCLE VOLCANICS

GMPGA
418

SiO2	51.10
TiO2	0.93
Al2O3	17.52
Fe2O3	0.00
MgO	3.52
FeO	8.95
MnO	0.25
CaO	12.00
Na2O	3.00
K2O	0.47
P2O5	0.06
LOI	2.34
Total	100.14

CATION PROPORTIONS BASED ON 100 CATIONS

Si	48.80
Ti	0.67
Al	19.72
Fe3	0.00
Mg	5.01
Fe2	7.15
Mn	0.20
Ca	12.28
Na	5.55
K	0.57
P	0.05
Total	100.00

Ti	6700
Zr	48.
Y	20.
Cr	261.
Ni	137.
P	301.
Sr	105.

GMPGA= GLOMEROPORPHYRITIC PLAGIOCLASE GABBRO

Appendix B SECOND-CYCLE VOLCANICS

	ANDES 283	BSAND 285C	BSAND 285B	BASLT 285A	NORIT 537C
SiO2	60.28	49.79	54.85	54.02	52.04
TiO2	0.58	0.40	0.38	0.40	3.07
Al2O3	14.21	9.39	12.52	13.69	12.70
Fe2O3	0.00	0.00	0.00	0.00	0.00
MgO	4.95	15.43	10.46	9.42	4.75
FeO	4.90	8.81	6.85	6.94	13.81
MnO	0.09	0.18	0.13	0.13	0.20
CaO	5.16	10.34	7.68	7.20	3.55
Na2O	4.85	1.49	3.34	3.78	3.89
K2O	0.47	0.54	0.72	0.48	2.08
P2O5	0.14	0.09	0.20	0.21	0.79
LOI	5.03	4.16	3.32	4.34	3.15
Total	100.66	100.62	100.45	100.61	100.03

CATION PROPORTIONS BASED ON 100 CATIONS

Si	57.59	46.79	51.21	50.85	50.63
Ti	0.42	0.28	0.27	0.28	2.25
Al	16.00	10.40	13.78	15.19	14.56
Fe3	0.00	0.00	0.00	0.00	0.00
Mg	7.05	21.61	14.56	13.22	6.89
Fe2	3.92	6.92	5.35	5.46	11.24
Mn	0.07	0.14	0.10	0.10	0.16
Ca	5.28	10.41	7.68	7.26	3.70
Na	8.98	2.71	6.05	6.90	7.34
K	0.57	0.65	0.86	0.58	2.58
P	0.11	0.07	0.16	0.17	0.65
Total	100.00	100.00	100.00	100.00	100.00

Ti	3634	2457	2341	2457	22500
Zr	103.	42.	86.	93.	205.
Y	10.	9.	10.	10.	31.
Sc	13.	40.	26.	25.	
Cr	305.	1558.	983.	935.	43
Ni	153.	430.	245.	217.	17.
P	638.	392.	916.	960.	3591.
Sr	282.	158.	494.	572.	341
Ba	82.	180.	290.	166.	
La	13.90	15.00	29.35	30.37	
Ce	28.50	35.64	60.34	64.22	
Nd	13.70	17.52	24.18	28.00	
Sm	3.09	3.41	4.45	4.98	
Eu	0.87	0.76	0.96	1.11	
Tb	0.23	0.20	0.62	0.07	
Ho	0.29	0.20	0.34	0.29	
Tm	0.09	0.19	0.21	0.19	
Yb	0.73	0.79	0.70	0.68	
Lu	0.12	0.07	0.09	0.10	

ANDES = ANDESITE, BSAND = BASALTIC ANDESITE, BASLT = BASALT
 NORIT = NORITE

Appendix B

LAC COUTACEAU DYKES

	DIDYK 493	DIDYK 496	DIDYK 452	DIDYK 489	DIDYK 509	DIDYK 485	DIDYK 492	DIDYK 444
SiO2	55.43	58.98	54.71	57.19	52.68	56.79	60.69	58.17
TiO2	0.55	0.75	0.58	0.46	0.69	0.68	0.64	0.72
Al2O3	12.70	16.75	10.03	11.54	11.37	11.70	15.38	14.43
Fe2O3	0.00	0.00	0.00	0.00	0.00	0.00	0.00	0.00
MgO	8.88	3.03	13.27	9.54	9.14	7.61	4.23	6.17
FeO	8.62	7.36	7.60	7.24	8.40	7.88	6.26	7.44
MnO	0.17	0.10	0.16	0.14	0.15	0.12	0.09	0.12
CaO	8.42	4.97	6.76	10.33	9.66	6.65	6.02	7.21
Na2O	2.28	4.11	2.81	2.69	3.36	1.76	3.47	4.04
K2O	1.14	1.44	1.87	0.40	1.15	3.51	1.52	0.94
P2O5	0.30	0.34	0.23	0.21	0.50	1.29	0.27	0.36
LOI	1.56	1.69	2.36	0.91	2.49	1.67	0.96	0.94
Total	100.05	99.57	100.38	100.77	99.59	99.66	99.53	100.54

CATION PROPORTIONS BASED ON 100 CATIONS

Si	52.02	55.93	50.42	52.71	49.64	53.97	57.12	53.71
Ti	0.39	0.53	0.40	0.32	0.49	0.49	0.45	0.50
Al	14.05	18.72	10.89	12.53	12.63	13.10	17.06	15.70
Fe3	0.00	0.00	0.00	0.00	0.00	0.00	0.00	0.00
Mg	12.42	4.28	18.23	13.11	12.84	10.78	5.93	8.49
Fe2	6.77	5.84	5.86	5.58	6.62	6.26	4.93	5.75
Mn	0.14	0.08	0.12	0.11	0.12	0.10	0.07	0.09
Ca	8.47	5.05	6.67	10.20	9.75	6.77	6.07	7.13
Na	4.15	7.56	5.02	4.81	6.14	3.24	6.33	7.23
K	1.36	1.74	2.20	0.47	1.38	4.25	1.82	1.11
P	0.24	0.27	0.18	0.16	0.40	1.04	0.22	0.28
Total	100.00	100.00	100.00	100.00	100.00	100.00	100.00	100.00

Ti	3297	4496	3477	2757	4136	4076	3836	4316
Zr	129.	132.	69.	80.	129.	241.	46.	146.
Y	14.	13.	14.	7.	14.	22.	12.	15.
Sc	23.	14.	23.					
Cr	870.	334.	1694.	1089.	885.	596.	417.	551.
Ni	122.	41.	462.	169.	65.	127.	44.	417.
P	1309.	7376.	1003.	916.	2182.	5630.	1178.	1571.
Sr	337.	669.	24.	319.	710.	777.	139.	755.
La	26.57	32.58	8.37					
Ce	55.13	70.60	20.46					
Nd	23.90	29.71	10.76					
Sm	4.60	5.75	2.96					
Eu	1.09	1.41	0.76					
Tb	0.35	0.26	0.36					
Ho	0.50	0.44	0.70					
Tm	0.33	0.29	0.29					
Yb	1.38	1.12	1.56					
Lu	0.19	0.14	0.21					

DIDYK- DIORITE DYKE

Appendix B

LAC COUTACEAU DYKES

82445
DIDYK

S102	59.37
T102	0.61
Al2O3	13.77
Fe2O3	0.00
MgO	8.36
FeO	6.54
MnO	0.09
CaO	4.63
Na2O	3.82
K2O	0.50
P2O5	0.21
LOI	2.59
Total	100.58

CATION PROPORTIONS BASED ON 100 CATIONS

Si	55.32
Ti	0.43
Al	15.12
Fe3	0.00
Mg	11.61
Fe2	5.10
Mn	0.07
Ca	4.62
Na	6.90
K	0.59
P	0.17
Total	100.00

Ti	3600
Zr	121.
Y	11.
Cr	890.
Ni	293.
P	916.
Sr	460.

DIDYK* DIORITE DYKE

Appendix B Modal Composition of Granitic Intrusives

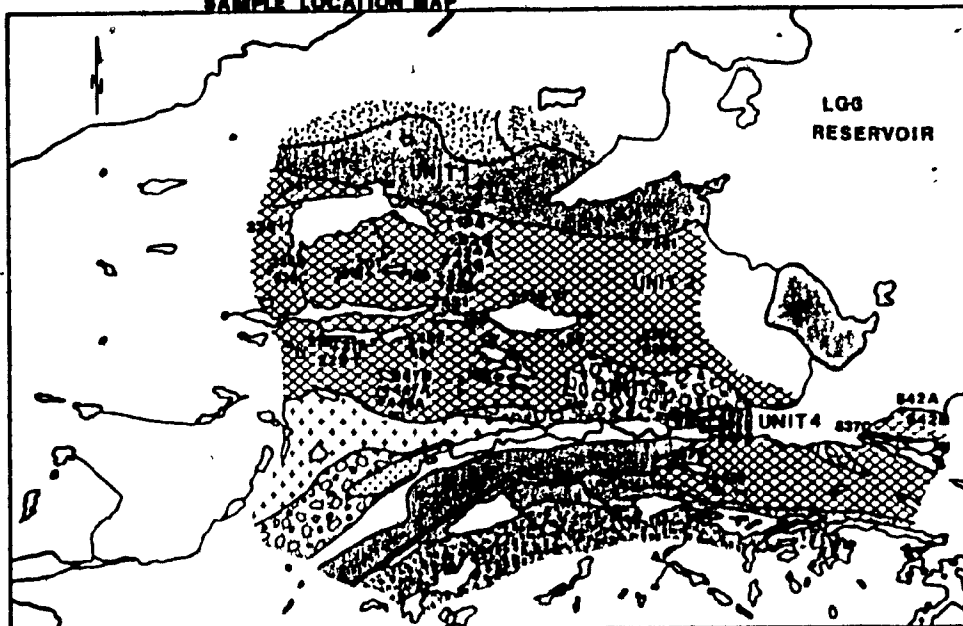
SAMPLE ROCK		COMPOSITION (%)				
NO.	NAME	PLAGIOCLASE	QUARTZ	BIOTITE	HORNBLende	GROUNDMASS
TS-x-83						
444	1	24				76
423	2	35	11			54
422	1	31	TR	2	1	66
330A	2	27	4	1	1	67
140	2	36	3	2		59
243	2	30	3	1	6	60
602F	2	36	6		1	57
445B	2	30	3		20	47
424B	1	17	TR			83
920	1	21		TR		79
301	3	23			1	76
443A	4	28	1	TR	18	53

ROCK NAMES AND INTRUSIVE TYPES

- 1 = LATE SYNTECTONIC PORPHYRITIC TRONDHJEMITE DYKE
- 2 = LATE SYNTECTONIC PORPHYRITIC TONALITE DYKE
- 3 = LATE SYNTECTONIC NORTHERN PORPHYRITIC TONALITE
- 4 = MIDDLE TONALITE PLUTON

Modal composition was determined by point counting. At least 2000 points were counted from each section.

SAMPLE LOCATION MAP



+ SAMPLE LOCATION (TS- ----83)

1:80,000

0 0.5 1 2 km

Appendix B Petrography of Analyzed Samples

TS-338-83 Pillow basalt,
-fine grained, hornblende, oligoclase, epidote, quartz, apatite and leucoxene, quartz + calcite + sericite pseudomorphs of plagioclase microphenocrysts, hornblende sheafs after glass?
-thin veins of calcite and epidote

TS-426-83 Pillow basalt,
-fine grained, hornblende, epidote, oligoclase, quartz and leucoxene, quartz + calcite pseudomorphs of plagioclase microphenocrysts, hornblende sheafs after glass?
-quartz and quartz + epidote veins

TS-158-83 Pillow basalt,
-medium grained, hornblende, oligoclase, chlorite and opaque, leucoxene after cruciform ilmenite

TS-216-83 Pillow basalt,
-medium grained, epidote, hornblende, quartz, chlorite, actinolite, albite, sericite and opaque
-quartz + calcite veins

TS-330C-83 Pillow basalt,
-fine grained, epidote, albite, actinolite, chlorite, quartz, opaque and leucoxene, swallow tail plagioclase microlites, microphenocrysts of plagioclase replaced by quartz and calcite, plumose actinolite after glass, calcite + quartz + chlorite after clinopyroxene
-thin epidote veins

TS-152-83 Pillow basalt,
-fine to medium grained, hornblende, quartz, chlorite, actinolite, epidote, albite and leucoxene after cruciform opaque.
-thin veinlets of calcite and quartz

TS-554-83 Pillow basalt,
-fine grained schist, hornblende, quartz, albite, epidote and leucoxene
-thin veins of quartz and quartz + epidote

TS-330B-83 Pillow basalt,
-fine grained, actinolite, chlorite, epidote, albite, leucoxene and opaques, swallow tail plagioclase microlites, chlorite + quartz after clinopyroxene?
-thin veinlets of calcite and chlorite

TS-447A-83 Plagioclase-phyric pillow basalt,
-medium grained groundmass, sparsely porphyritic, epidote, quartz, hornblende, chlorite, albite, leucoxene after cruciform ilmenite, plagioclase phenocrysts replaced by saussurite
-thin calcite veins

Appendix B Petrography of Analyzed Samples (continued)

- TS-18A-83 Plagioclase-phyric pillow basalt,
-fine to medium grained schist, hornblende, epidote, chlorite,
leucoxene and opaques
-thin veins of calcite.
- TS-336C-83 Plagioclase-phyric pillow basalt,
-fine grained groundmass, sparsely porphyritic, epidote, quartz,
hornblende, actinolite, albite, chlorite and leucoxene,
microphenocrysts of plagioclase and plumose actinolite after
primary glass
-thin epidote veinlets
- TS-336B-83 Glomeroporphyritic plagioclase pillow basalt,
-medium grained groundmass, glomeroporphyritic and megacrysts of
plagioclase, chlorite, epidote, calcite, hornblende, actinolite,
quartz, albite and leucoxene, plagioclase megacrysts are
replaced by calcite, chlorite and epidote
- TS-451-83 Massive basaltic andesite,
-fine to medium grained, pilotaxitic and microphenocrysts of
plagioclase, albite, chlorite, quartz, calcite and leucoxene
-thin veinlets of calcite
- TS-229-83 Massive basaltic andesite,
-fine to medium grained, pilotaxitic, microphenocrysts of
plagioclase, chlorite, albite, epidote, opaques and leucoxene
-thin veinlets of chlorite and calcite
- TS-452-83 Massive basaltic andesite,
-fine grained groundmass, pilotaxitic and microphenocrysts of
plagioclase, albite, chlorite, quartz, calcite, epidote,
leucoxene and opaques
-thin veinlets of calcite
- TS-283-83 Massive andesite,
-medium grained, chlorite, albite, epidote and leucoxene
-thin veinlets of calcite
- TS-285A-83 Massive basaltic andesite,
-medium grained, chlorite, albite, quartz, epidote, hornblende,
opaque and leucoxene (actinolite rims around hornblende)
-thin veinlets of calcite, quartz and chlorite
- TS-285B-83 Massive basaltic andesite,
-medium grained, hornblende, albite, epidote, quartz, apatite,
chlorite, actinolite, leucoxene and opaques
-thin veinlets of quartz and calcite
- TS-285C-83 Massive basaltic andesite,
-medium grained, hornblende (with rims of actinolite), calcite,
chlorite, albite, quartz and leucoxene
-thin veinlets of calcite and quartz

Appendix B Petrography of Analyzed Samples

TS-424A-83 Pyroxene cumulate gabbro sill,
-hornblende replaces clinopyroxene, medium grained, pyroxenes subophitically enclose plagioclase, hornblende, plagioclase, opaques, leucoxene, chlorite

TS-427-83 Pyroxene cumulate gabbro sill,
-hornblende replaces clinopyroxene, pyroxene subophitically encloses plagioclase, medium to fine grained, hornblende, plagioclase, epidote, leucoxene, chlorite, quartz, hematite, pyrite, opaques
-albite + quartz veins and chlorite veins

TS-428C-83 Pyroxene cumulate gabbro sill,
-medium grained hornblende replacement after clinopyroxene, pyroxene subophitically encloses plagioclase, hornblende, chlorite, plagioclase, quartz, hematite, epidote and calcite
-opaque veinlets

TS-139-83 Equigranular gabbro sill,
-hornblende replaces pyroxene, pyroxene subophitically encloses plagioclase, medium grained, hornblende, chlorite, epidote, plagioclase, quartz, opaques, leucoxene, calcite
-thin calcite veinlets

TS-445A-83 Glomeroporphyritic plagioclase gabbro,
-medium to coarse grained groundmass, glomerocrysts and megacrysts of plagioclase replaced by saussurite, hornblende, epidote, quartz, leucoxene, plagioclase, chlorite after hornblende
-thin chlorite veins

TS-542A-83 Gabbro sill,
-medium to coarse grained, pyroxene is replaced by hornblende, pyroxene subophitically encloses plagioclase, hornblende, chlorite (after hornblende), plagioclase, quartz, epidote, leucoxene and opaques
-thin veinlets of chlorite and quartz

TS-542B-83 Pyroxene cumulate gabbro,
-pyroxene is replaced by hornblende, pyroxene subophitically encloses plagioclase, hornblende (replaced in part by chlorite), plagioclase, quartz, opaques, calcite, epidote and apatite

TS-341-83 Fine grained gabbro,
-fine grained, hornblende, plagioclase, quartz, apatite and opaques, granophyric texture, cruciform opaques, pyroxene subophitically encloses plagioclase, interstitial quartz and magnetite

TS-447B-83 Pyroxene cumulate gabbro,
-fine grained groundmass, hornblende, epidote, plagioclase, opaques, quartz, chlorite, apatite and leucoxene

Appendix B Petrography of Analyzed samples

TS-418-83 Glomeroporphyritic and megacryst plagioclase gabbro,
-plagioclase megacrysts and glomerocrysts are replaced by
epidote, calcite, quartz and chlorite, hornblende, epidote,
opaques and quartz

-thin veinlets of calcite, quartz and epidote

TS-537C-83 Norite,

-medium grained plagioclase is subophitically enclosed by
orthopyroxene which is replaced by chlorite + magnetite and in
places hornblende, biotite replaces hornblende, granophyric
patches, abundant opaques and plagioclase (replaced by
saussurite)

-thin veinlets of chlorite and quartz

TS-55-83 Diabasic gabbro,

-fine grained, actinolite, epidote, quartz, albite, leucoxene
and opaques

TS-186-83 Massive basalt,

-fine grained, leucoxene after skeletal opaque, hornblende,
epidote, calcite, albite, quartz, chlorite and hematite

TS-201-83 Massive basalt,

-hornblende replaces clinopyroxene which subophitically encloses
saussuritized plagioclase, fine grained, hornblende, epidote,
chlorite, plagioclase, quartz, calcite and leucoxene

TS-431-83 Pyroxene cumulate gabbro,

-fine grained groundmass, plagioclase phenocrysts
(saussuritized), epidote, chlorite, actinolite, quartz, opaque,
albite and leucoxene

TS-217-83 Pyroxene cumulate gabbro,

-hornblende replaces pyroxene which subophitically encloses
saussuritized plagioclase, epidote, chlorite, hornblende,
albite, quartz, leucoxene and opaque.

TS-379-83 Pyroxene cumulate gabbro,

-hornblende porphyroblasts (after pyroxene?), medium grained,
hornblende, calcite, quartz, leucoxene, epidote, plagioclase and
chlorite

TS-485-82 Diorite dyke,

-fine grained foliated dyke, calcite, epidote, hornblende,
biotite, chlorite, quartz, microcline, plagioclase and opaque

TS-489-82 Diorite dyke,

-fine grained, hornblende, actinolite (rims around hornblende),
diopside, quartz, plagioclase, calcite, chlorite

TS-509-82 Diorite dyke,

-fine grained, epidote, plagioclase, pyrite, calcite,
hornblende and chlorite

Appendix B Petrography of Analyzed Samples

TS-496-82 Diorite dyke,
-fine grained, hornblende, saussuritized plagioclase, quartz,
opaques, calcite, zircon and chlorite after hornblende

TS-452-82 Diorite dyke,
-fine grained, weakly foliated, actinolite, biotite, chlorite
(after biotite), saussuritized plagioclase, calcite and quartz

TS-445-82 Diorite dyke,
-fine grained, hornblende with actinolite rims, biotite with
chlorite rims, quartz, porphyroblastic plagioclase, opaques,
zircon and calcite

TS-492-82 Diorite dyke,
-fine grained, foliated, hornblende with actinolite rims,
quartz, biotite, calcite, albite, zircon and magnetite

TS-444-82 Diorite dyke,
-fine grained, foliated, hornblende with actinolite rims,
epidote rims on pyrite, quartz, calcite, magnetite, plagioclase,
biotite and small xenoliths of granodiorite?

TS-493-82 Diorite dyke,
-fine grained, moderately foliated, hornblende with actinolite
rims, chlorite, plagioclase and quartz

Appendix C Plates

Plate 1 Deformed (D1) conglomerates in the Metasediments north of the Chain Lakes Fault. This highly deformed conglomerate contains clasts of tonalite that have been flattened into the S1 schistosity plane. The exposure is located on the north shore of Chain Lakes (Fig. 2) and is located within the hinge zone of the Chain Lakes Syncline (F1) (hammer is 90 cm. long).

Plate 2 Folded (F1) siltstones in the Lower Volcanoclastics and Metasediments. This sequence of isoclinally folded (F1) siltstones and slates occur on the shores of the LG-3 reservoir in the north-central part of the map area (lens cap is 5 cm in diameter).

Plate 3 Minor faults (D2) in the Lower Volcanoclastics and Metasediments. These minor strike-slip faults displace beds of lappilistone in an exposure NE of Sakami village in the north-central part of the map area.

Plate 4 F2 folds in the Lower Volcanoclastics and Metasediments. In this photograph, early, relatively tight, F1 folds, have been refolded by steeply plunging, relatively open, NNW-trending F2 folds. These rocks are siltstones and mafic epiclastic sandstones. They are exposed south of the Chain Lakes fault, in the south central part of the map area.

Plate 5 F2 box folds in the Second-Cycle Volcanics. In this photograph, late, F2, box folds refold earlier S0 and S1 fabrics developed in volcanoclastics. This exposure is found in the east central part of the map area, on the shore of the LG-3 reservoir.

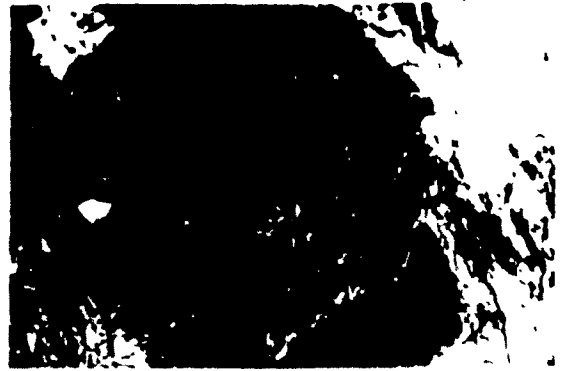
Plate 6 Mafic crystal tuff in the Lower Volcanoclastics and Metasediments. Thin beds of mafic crystal tuff occur in the north-central part of the map area on the southern shore of the LG-3 reservoir. Original pyroclasts are replaced by hornblende.

Plate 7 Bomb-sags in the Lower Volcanoclastics and Metasediments. The deformation of siltstones around these clasts of basalt are interpreted as bomb sags. This exposure is located on the southern shore of the LG-3 reservoir in the north-central part of the map area.

Plate 8 Banded iron formation in the Lower Volcanoclastics and Metasediments. Thin beds of banded iron formation occur interbedded with siltstones and mafic epiclastic sediments. This example is of an exposure in the north central part of the map area.



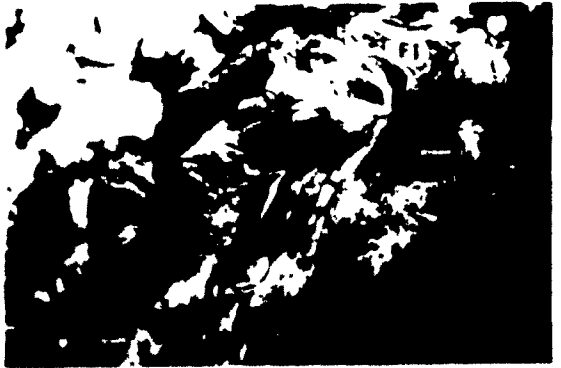
1



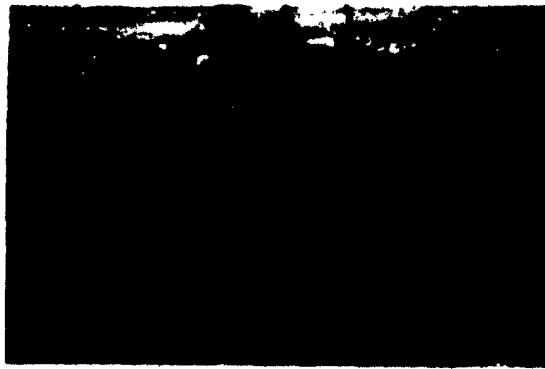
2



3



4



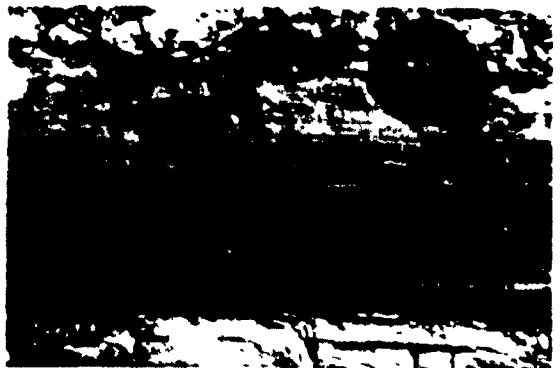
5



6



7



8

Appendix C Plates

Plate 9 Conglomerates in the Lower Volcanoclastics and Metasediments. Polymict orthoconglomerates occur in lenses in the north-central part of the map area. Some of the clasts are tonalitic in composition.

Plate 10 Pillowed basalts in the First-Cycle Volcanics. This pillowed basaltic lava flow is located in the central part of the map area, north of the Chain Lakes Fault. Note the absence of vesicles in these rocks.

Plate 11 Plagioclase megacrysts and glomerocrysts in pillow basalts from the First-Cycle Volcanics. Individual pillows of basalt commonly have sharp, dark-coloured, fine grained chilled margins. This exposure is from the same location as that in Plate 10. Note the presence of plagioclase megacrysts and glomerocrysts.

Plate 12 GMP gabbro sills in the First-Cycle Volcanics. This GMP gabbro is located in the central part of the map area, north of the Chain Lakes Fault.

Plate 13 Metasedimentary xenoliths in a gabbro sill in the First-Cycle Volcanics. This gabbro sill contains large metasedimentary crustal xenoliths. This exposure is in the east-central part of the map area, north of the Chain Lakes Fault.

Plate 14 Xenoliths in gabbro sills from the Lac Guyer area. Crustal xenoliths are also found in other parts of the La Grande belt, such as in this example taken south of Lac Guyer and north of the road to LG-4. Note the sharp boundaries between the tonalite xenoliths and their gabbroic host.

Plate 15 Normally graded siltstone-sandstone facies rocks in the Metasediments. Normally graded siltstone-sandstone facies rocks are shown here in these overturned beds exposed near the northern shore of the LG-3 reservoir, north of the Chain Lakes Fault.

Plate 16 Rhythmically bedded siltstones and sandstones in the Metasediments. In this exposure of siltstone-sandstone facies rocks in the northern fault block, siltstones grade up from sandstones and are interbedded in rhythmic successions. This outcrop is located in the central part of the map area.



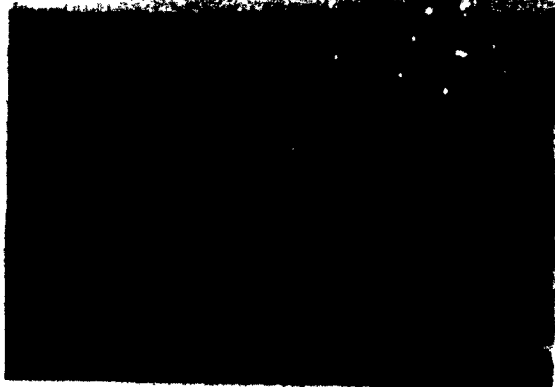
9



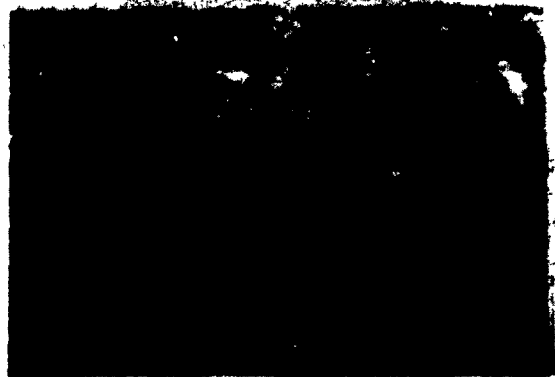
10



12



14



15



16

Appendix C Plates

Plate 17 Siltstone-Sandstone and Conglomerate facies rocks in the Metasediments. In this exposure of siltstone-sandstone and conglomerate facies rocks in the SE part of the map area (south shore of the LG-3 reservoir) massive sandstones grade up from conglomerate lenses.

Plate 18 Parallel laminated and trough-type crossbedding in the Metasediments. This exposure of siltstone-sandstone facies rocks shows interbedded parallel laminated sandstones and trough-type crossbedded sands. This outcrop is located on the south shore of the LG-3 reservoir in the SE part of the map area.

Plate 19 Large-scale trough crossbeds in the Metasediments. On the southern shore of the LG-3 reservoir in the SE corner of the map area, siltstone-sandstone facies rocks are characterized in places by large-scale trough to planar crossbedding.

Plate 20 Tonalite boulders in conglomerates in the Metasediments. Detail of a large boulder of tonalite in a paraconglomerate (same location as in Plate 1).

Plate 21 Channeling of conglomerates into underlying sandstones, Metasediments. This photograph shows inverted beds of conglomerate which have been deposited into a channel that cuts into underlying siltstone-sandstone facies rocks. This outcrop is located near the northern shore of the LG-3 reservoir in the central part of the map area (north of the Chain Lakes Fault).

Plate 22 BIF clasts in an orthoconglomerate in the Metasediments. Most conglomerate facies rocks in the Metasediments carry clasts of tonalitic composition, however in this case in the western part of the map area, north of the Chain Lakes Fault, the orthoconglomerate contains clasts of BIF as well.

Plate 23 Debris flow sub-facies conglomerates in the Metasediments. This conglomerate belongs to the debris flow sub-facies and is composed of large blocks of BIF in a comminuted matrix of similar mineralogical composition. It is exposed on the south shore of the LG-3 reservoir in the SE corner of the map area.

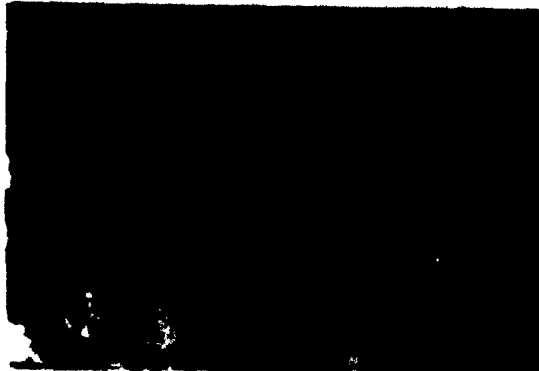
Plate 24 Shale/siltstone rip-up clasts in the Metasediments. This conglomerate exposed on the southern shore of the LG-3 reservoir in the SE corner of the map area is composed of angular shale/siltstone rip-up clasts.



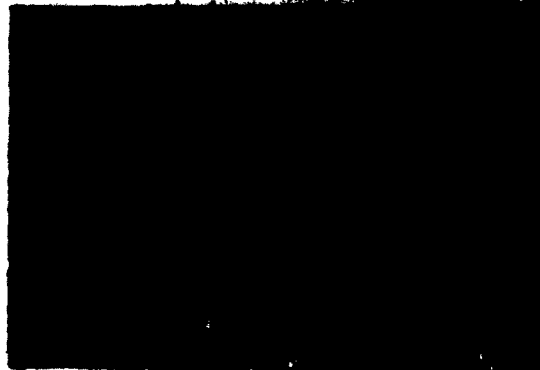
17



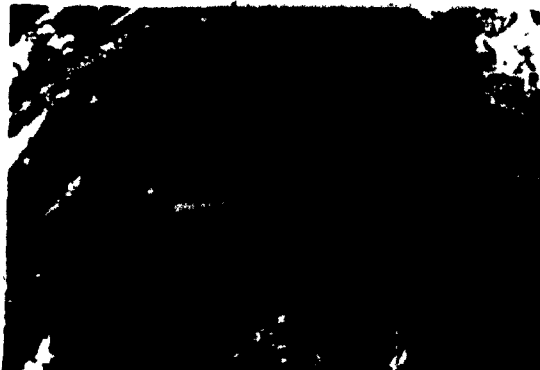
18



20



22



23



24

Appendix C Plates

Plate 25 Banded iron formation facies of the Metasediments. The banded iron formation facies consist, as in this example from the central part of the map area north of the Chain Lakes Fault, of wavy discontinuous laminae and thin beds of quartz and magnetite/hematite.

Plate 26 Xenoliths in gabbro sills in the Second-Cycle Volcanics. Thin gabbroic sills, such as this one in the northern fault block in the western part of the map area, intrude the Second-Cycle Volcanics and carry xenoliths of granitic composition.

Plate 27 Sandstone dykes in the Second-Cycle Volcanics. The argillites at the base of the Second-Cycle Volcanics, such as this example found in the northern fault block, in the western part of the map area, are crosscut by sandstone dykes.

Plate 28 Epiclastic sandstones in the Second-Cycle Volcanics. The epiclastic sandstones are characterized by a distinctive green and pale pink colour banding that facilitates their identification and correlation across large distances. This example is from the central part of the map area, in the northern fault block.

Plate 29 Intrusive contact of a syntectonic pluton. This exposure of the late syntectonic Northern Porphyritic Tonalite-Granodiorite intrudes the supracrustal succession and contains xenoliths of basalt.

Plate 30 Lac Coutaceau dyke intrusive into a tonalite pluton. The Lac Coutaceau dykes were intruded late in the history of the greenstone belt as evidenced here by the presence of a dyke intrusive into a tonalite pluton. In other places, tonalite-granodiorite dykes intrude the Lac Coutaceau dykes. This exposure is on the southern shore of the LG-2 reservoir, some 30 km west of the map area.

Plate 31 Lac Coutaceau dyke with basaltic xenolith. In those areas in which the Lac Coutaceau dykes intrude the greenstone belt, they carry unresorbed angular xenoliths of basalt. This exposure is located close to that of Plate 3.



25



26



27



28



29



30

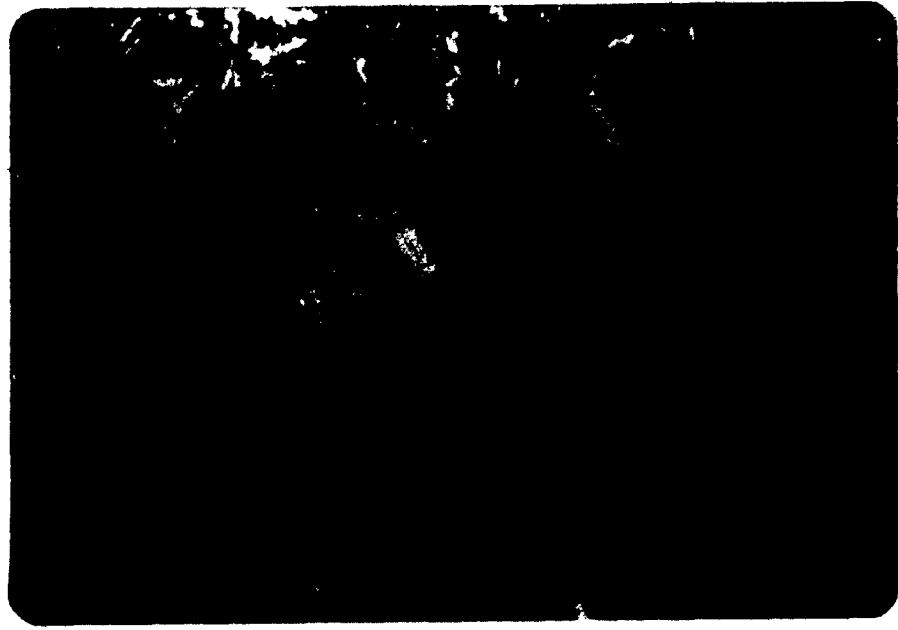


31

Appendix C Plates

Plate 32 Photomicrograph of the chilled margin of a pillowed basalt, First-Cycle Volcanics. This photomicrograph is of the chilled margin of a pillow basalt (TS-330c-83), found in the east-central part of the map area, north of the Chain Lakes Fault. Note the swallow-tail terminations of plagioclase microlites, and the replacement of primary glass by plumose actinolite. (plain light, field of view = 0.9 mm).

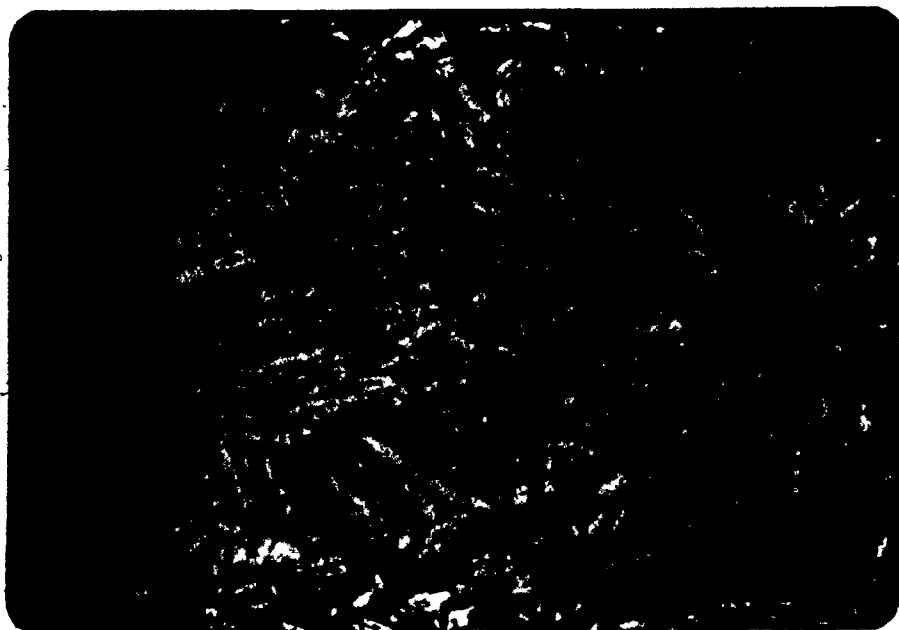
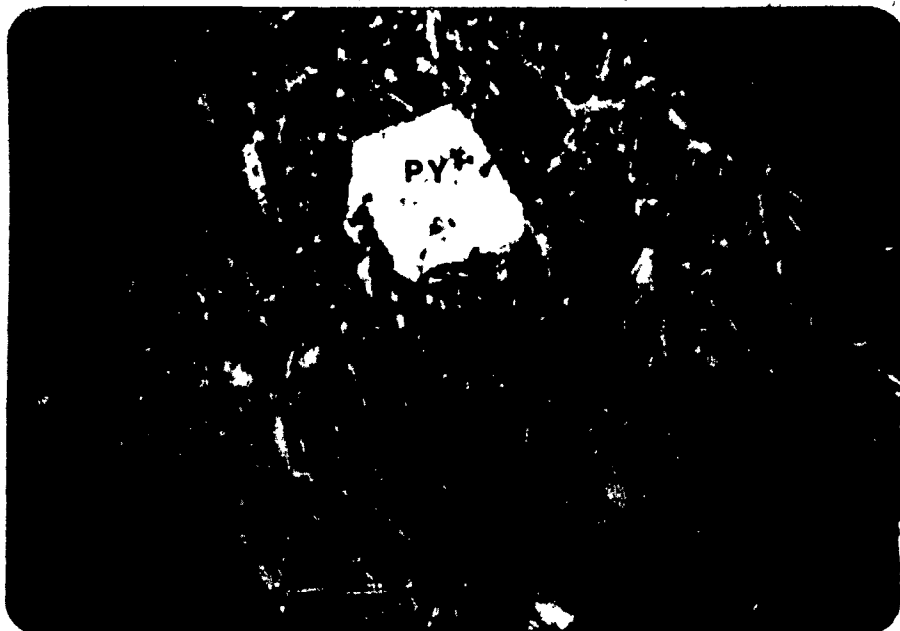
Plate 33 Photomicrograph of plagioclase phenocrysts in the chilled margin of a pillow basalt in the First-Cycle Volcanics. The chilled margins of some basalt pillows contain plagioclase phenocrysts (PL) such as in this example (TS-338-83) from the north central part of the map area (plain light, field of view = 3.6 mm).



Appendix C Plates

Plate 34 Pyroxene phenocrysts in the chill margin of pillow basalts in the First-Cycle Volcanics. The chilled margins of some basalt pillows contain equant pseudomorphs after pyroxene (PY). These are replaced by calcite and quartz. This sample (TS-330c-83) is from the same locality as that in Plate 15 (plain light, field of view = 3.6 mm).

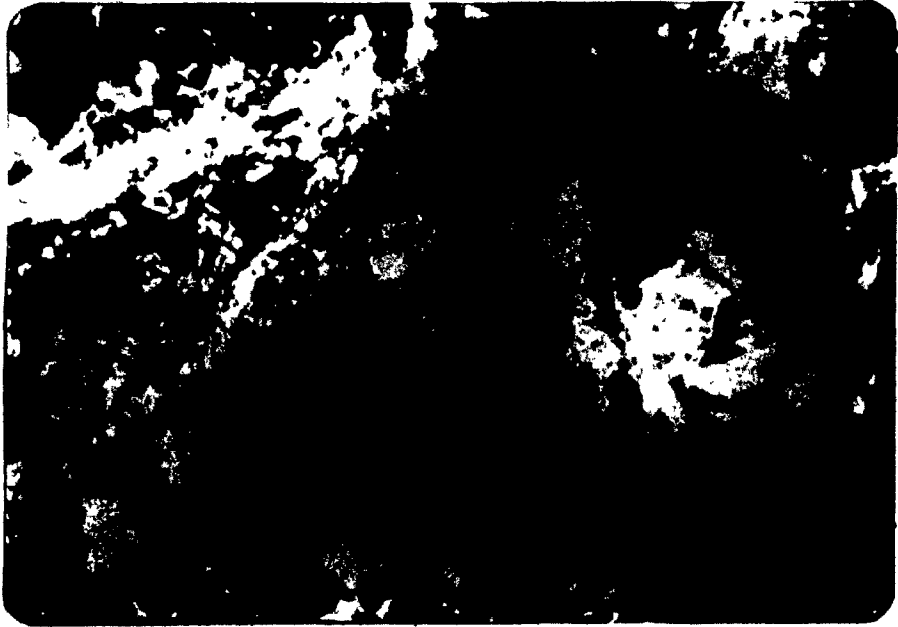
Plate 35 Photomicrograph of a basaltic andesite in the First-Cycle Volcanics. This photomicrograph of a basaltic andesite (TS-452-83) shows plagioclase microlites and microphenocrysts which have a pilotaxitic texture. This sample is located north of the Chain Lakes Fault in the central part of the map area. (plain light, field of view is 3.6 mm).



Appendix C Plates

Plate 36 Photomicrograph of a diabasic gabbro from the First-cycle Volcanics. The most differentiated gabbros in the First-Cycle Volcanics are characterized by abundant modal magnetite and the presence of interstitial granophyric patches (GR) such as is shown in this photomicrograph of a sill (TS-617-83) from the southern part of the map area. Clinopyroxene has been replaced by hornblende (HB) (crossed nicols, field of view = 3.6 mm).

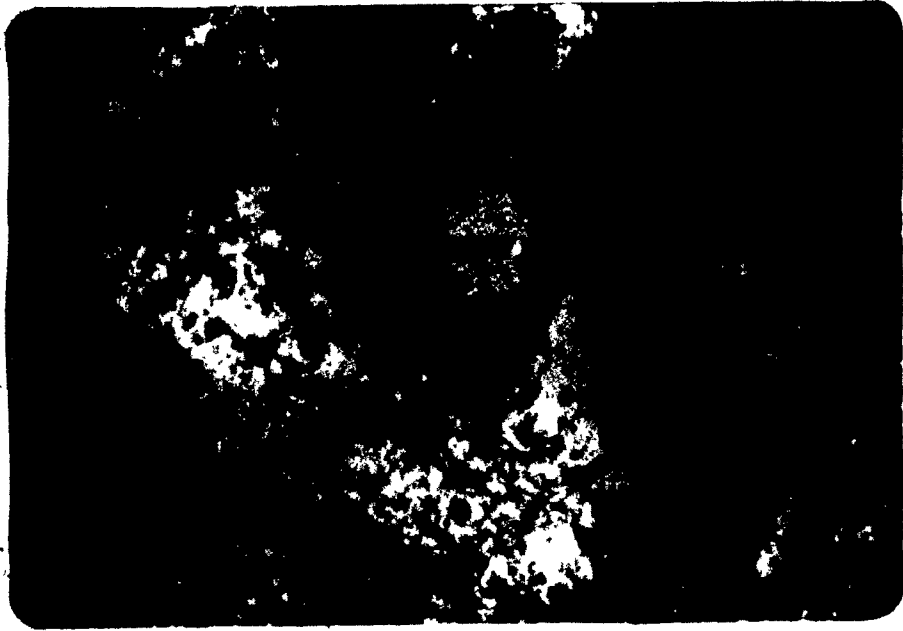
Plate 37 Photomicrograph of a subarkose in the Metasediments. Subarkoses are generally comprised of, as in the case of this example from the central part of the map area, angular quartz and lithic grains of tonalite (crossed nicols, field of view = 3.6 mm).



Appendix C Plates

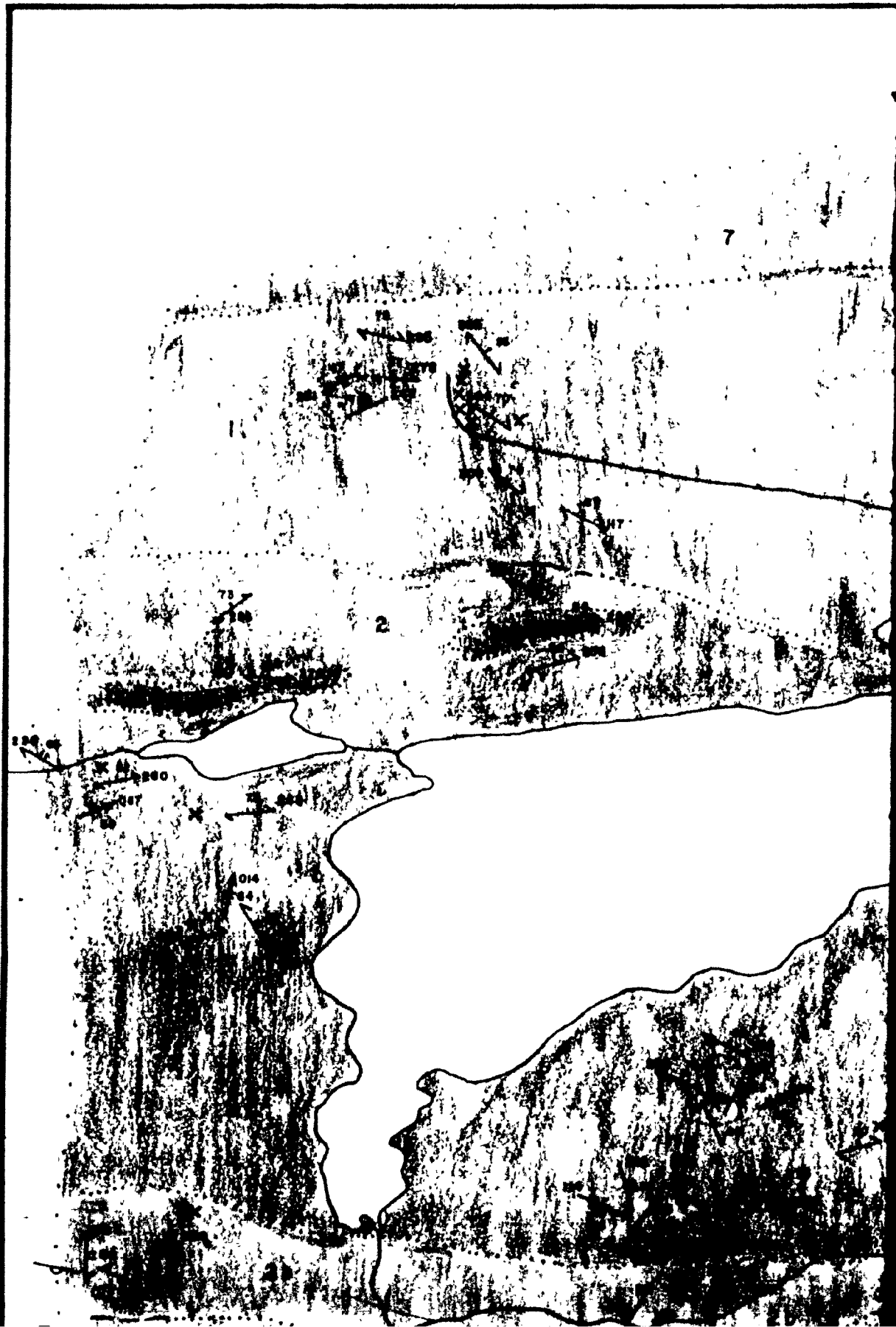
Plate 38 Photomicrograph of a norite in the Second-Cycle Volcanics. The noritic plug that intrudes the Second-Cycle Volcanics in the eastern part of the map area on the shores of the LG-3 reservoir, is characterized by orthopyroxene pseudomorphed by idiomorphic chlorite and magnetite (OPX). The orthopyroxene is subophitically enclosed by plagioclase (PL) laths (plain light, field of view = 3.6 mm). (sample TS-537-C-83)

Plate 39 Photomicrograph of a norite in the Second-Cycle Volcanics. The same norite as in Plate 36 contains primary hornblende (HB) with biotite (BI) reaction rims. Note the large apatite crystals (AP). (crossed nicols, field of view is 0.9 mm).



76° 05'

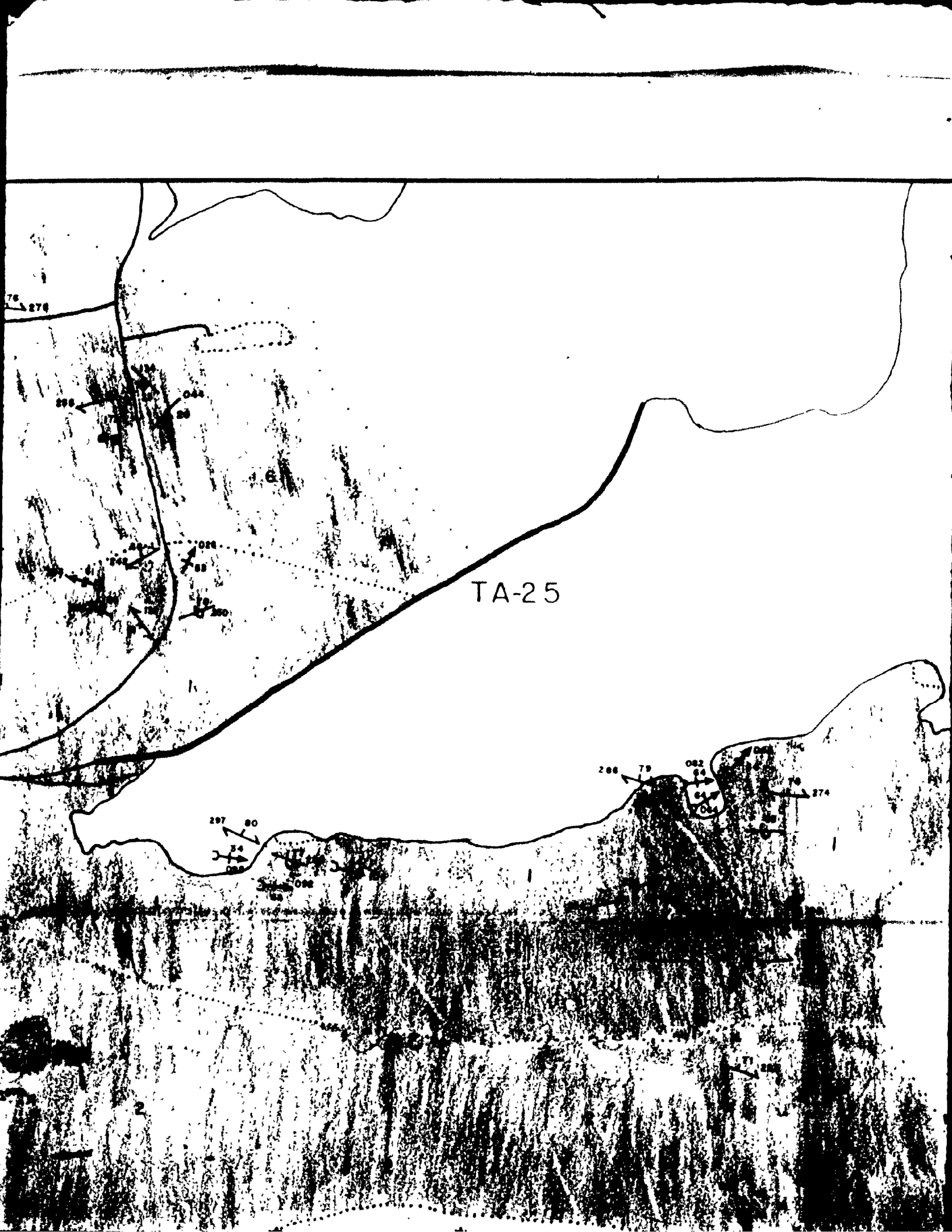
53° 42' -



76° 05'

1





TA-25

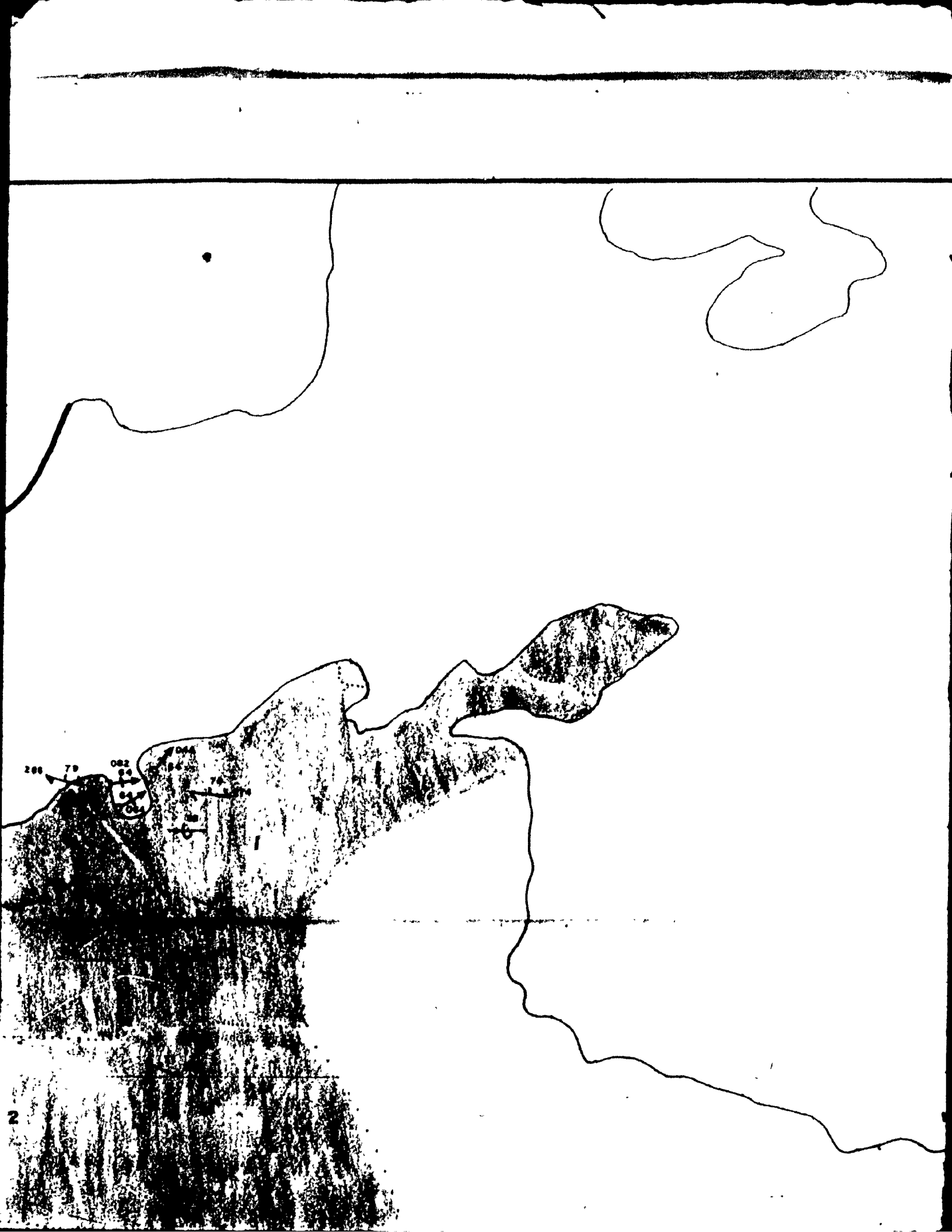
76 276

298
044
88
024
88
200

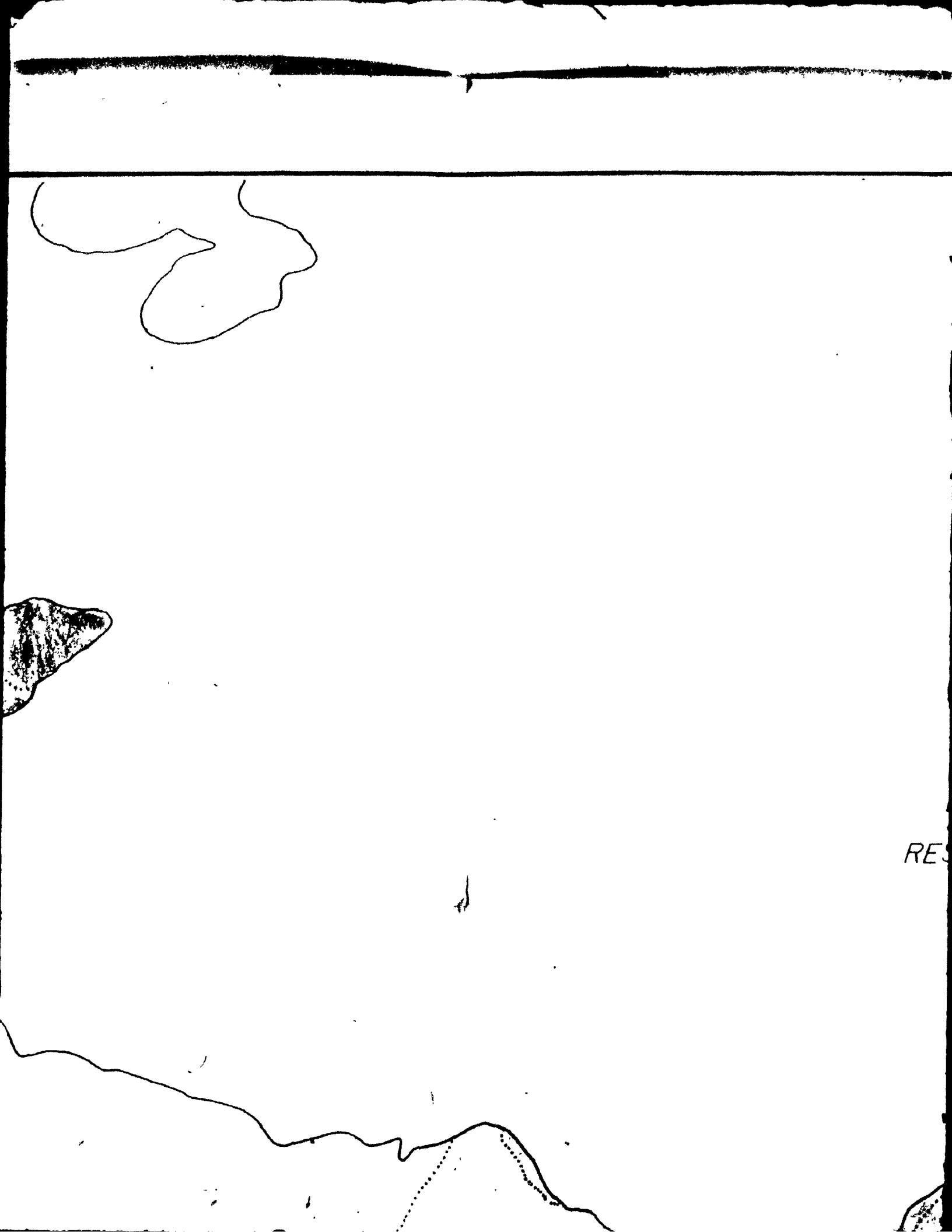
288 79
082
84
04
76 274

297 80
84
082

288



200 79 082 24
D64
74
20



RES

7657'

- 53 42

LG-3
RESERVOIR

76° 57'

LEG E



- 53° 42'



Unconsolidated Sediments

PROTEROZOIC



Gabbro, diabase



Sakami Formation, sandstone, conglomerate

ARCHEAN



Late syntectonic, Middle Tonalite pluton



Late syntectonic, Northern Porphyry



Syntectonic Northern Tonalite, well foliated



Southern Composite pluton, well foliated



Second-Cycle Volcanics, grey argillite

LEGEND

olidated Sediments

PROTEROZOIC

diabase

Formation, sandstone, conglomerate

CHEAN

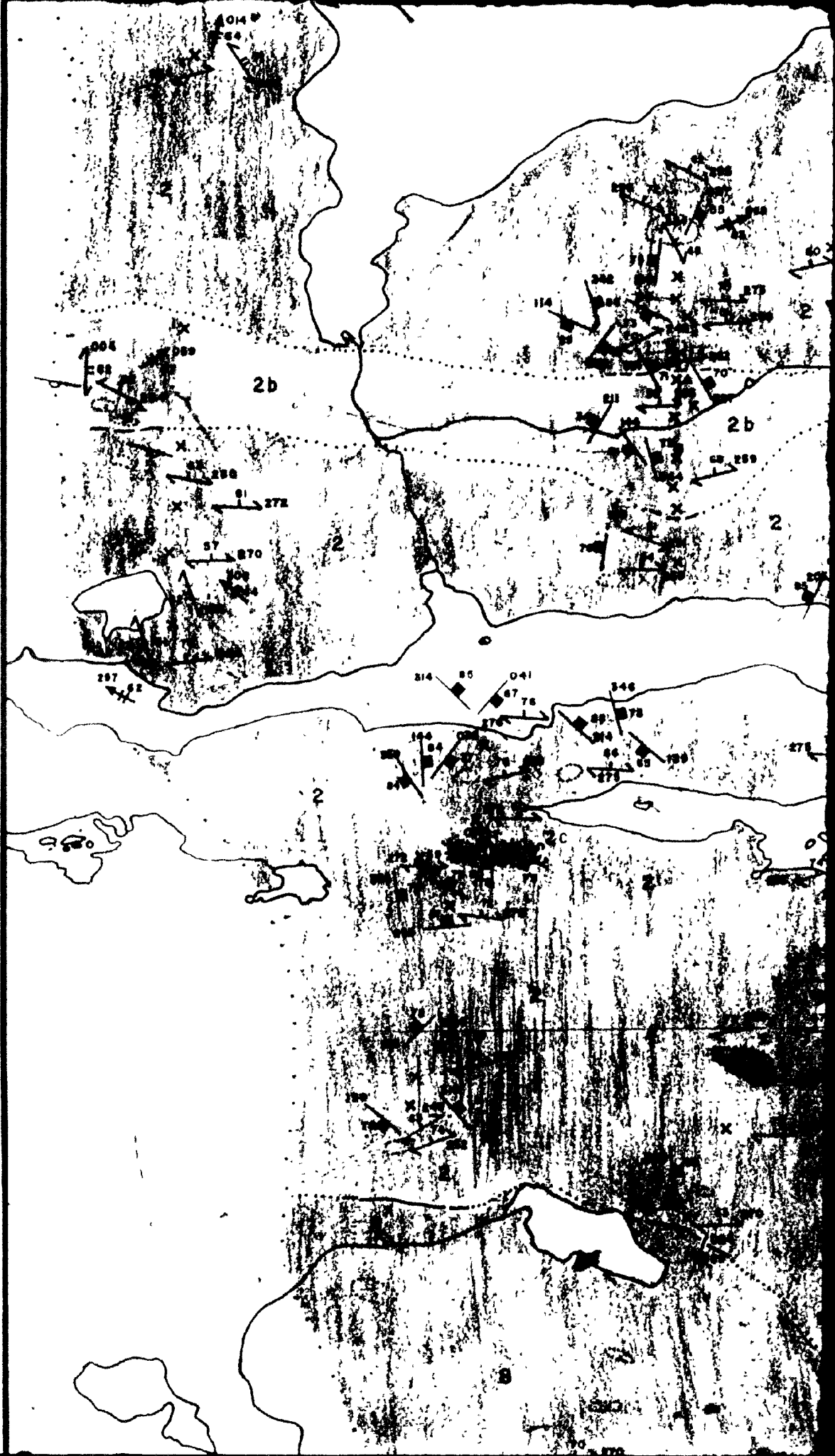
syntectonic, Middle Tonalite pluton, porphyritic in places, weakly foliated

syntectonic, Northern Porphyritic Tonalite-Granodiorite, weakly foliated

ctonic Northern Tonalite, well foliated, porphyritic in places

ern Composite pluton, a, well foliated coarse grained tonalite, b, fine grained tonalite

nd-Cycle Volcanics, grey argillite, massive basaltic andesite, andesite, intermediate volcanoclastics









2

2

2

2b

2b

2b

2

3

3

278
294
270

270

76

71 289

71 281 X

274 69 X
281 78 X

78

78 290

277

292

BYO



71 281 AX

274 282 2b

2

3

3

3

3

TA26A

270

3

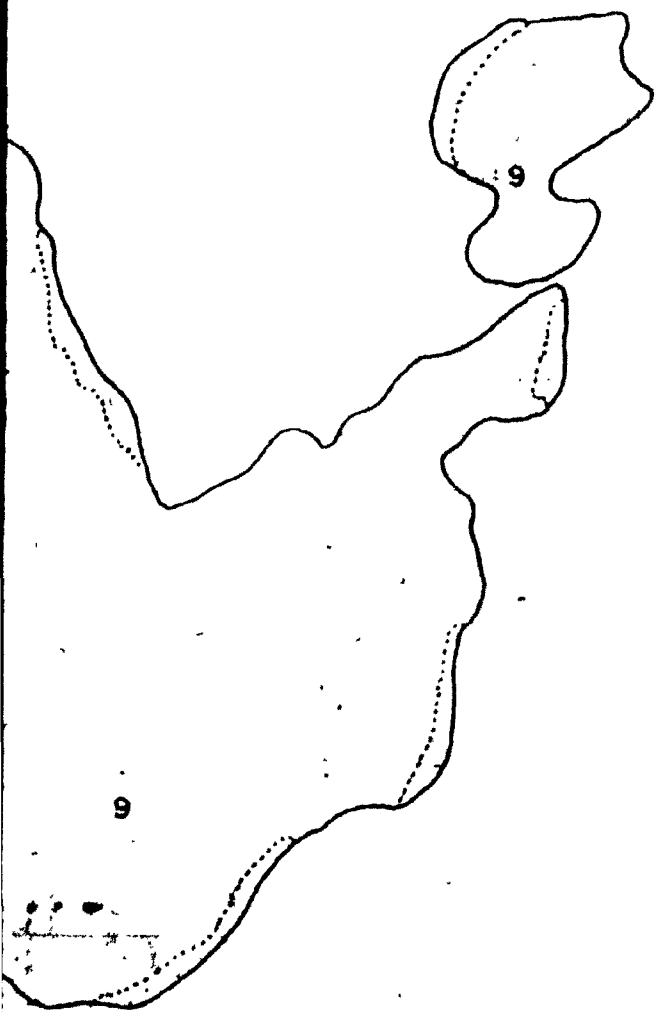
282 283 284 285 286 287 288 289 290 291 292 293 294 295 296 297 298 299 300 301 302 303 304 305 306 307 308 309 310 311 312 313 314 315 316 317 318 319 320 321 322 323 324 325 326 327 328 329 330 331 332 333 334 335 336 337 338 339 340 341 342 343 344 345 346 347 348 349 350 351 352 353 354 355 356 357 358 359 360 361 362 363 364 365 366 367 368 369 370 371 372 373 374 375 376 377 378 379 380 381 382 383 384 385 386 387 388 389 390 391 392 393 394 395 396 397 398 399 400

282 283 284 285 286 287 288 289 290 291 292 293 294 295 296 297 298 299 300 301 302 303 304 305 306 307 308 309 310 311 312 313 314 315 316 317 318 319 320 321 322 323 324 325 326 327 328 329 330 331 332 333 334 335 336 337 338 339 340 341 342 343 344 345 346 347 348 349 350 351 352 353 354 355 356 357 358 359 360 361 362 363 364 365 366 367 368 369 370 371 372 373 374 375 376 377 378 379 380 381 382 383 384 385 386 387 388 389 390 391 392 393 394 395 396 397 398 399 400



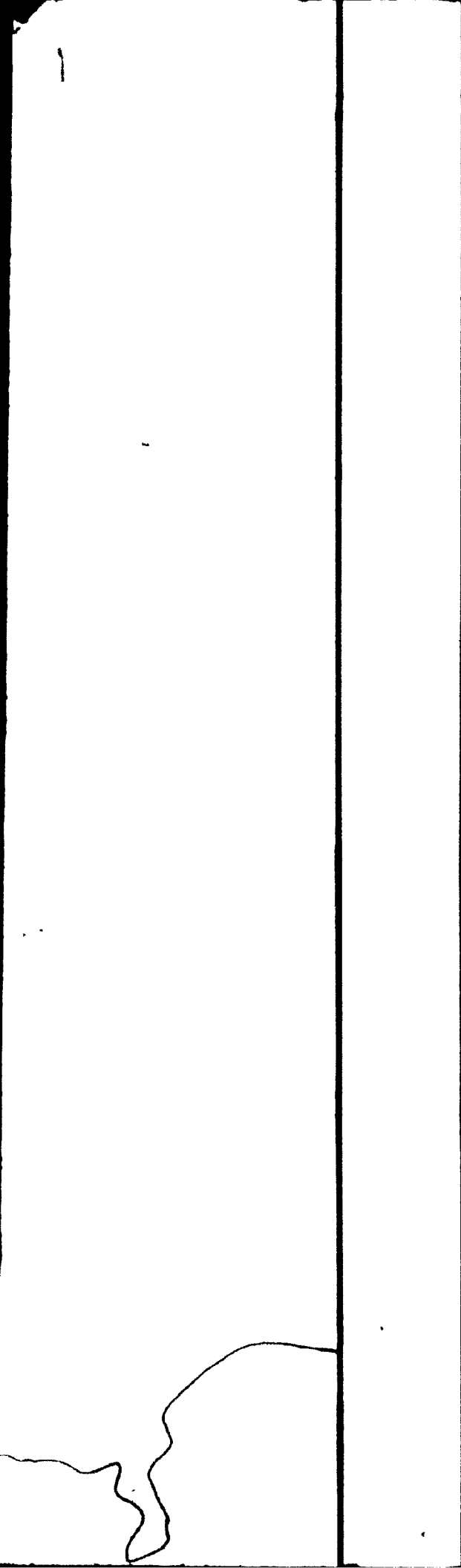
CHAIN LAKES SYNCLINE

RESERVOIR



SYNCLINE





Late syntectonic, Northern Porphyritic



Syntectonic Northern Tonalite, well foliated



Southern Composite pluton, a. well foliated



Second-Cycle Volcanics, grey argillite



Metasediments, immature subarkose, grey



Banded iron formation, oxidized



First-Cycle Volcanics, massive and p



Banded iron formation (oxide f



Light colored basalt (basaltic



Plagioclase-phyric basalt, glass



Basaltic sill



Lower Volcanoclastics and Metasediments
sills



Amphibolite (hornblende schist)

ectonic, Northern Porphyritic Tonalite-Granodiorite, weakly foliated

c Northern Tonalite, well foliated, porphyritic in places

Composite pluton, a, well foliated coarse grained tonalite, b, fine grained tonalite

cycle Volcanics, grey argillite, massive basaltic andesite, andesite, intermediate volcanoclastics

ments, immature subarkose, greywacke, siltstone, polymict ortho- and paraconglomerate, slate

Banded iron formation, oxide facies

e Volcanics, massive and pillowed basalt, gabbro sills, minor volcanoclastics

Banded iron formation (oxide facies)

Light colored basalt (basaltic andesite)

Plagioclase-phyric basalt, glomeroporphyritic gabbro (■) and pillow basalt (▲)

Gabbro sill

anoclastics and Metasediments, mafic volcanoclastics, siltstones, graywacke, conglomerate, gabbro

Amphibolite (hornblende schist)

SYMBOLS

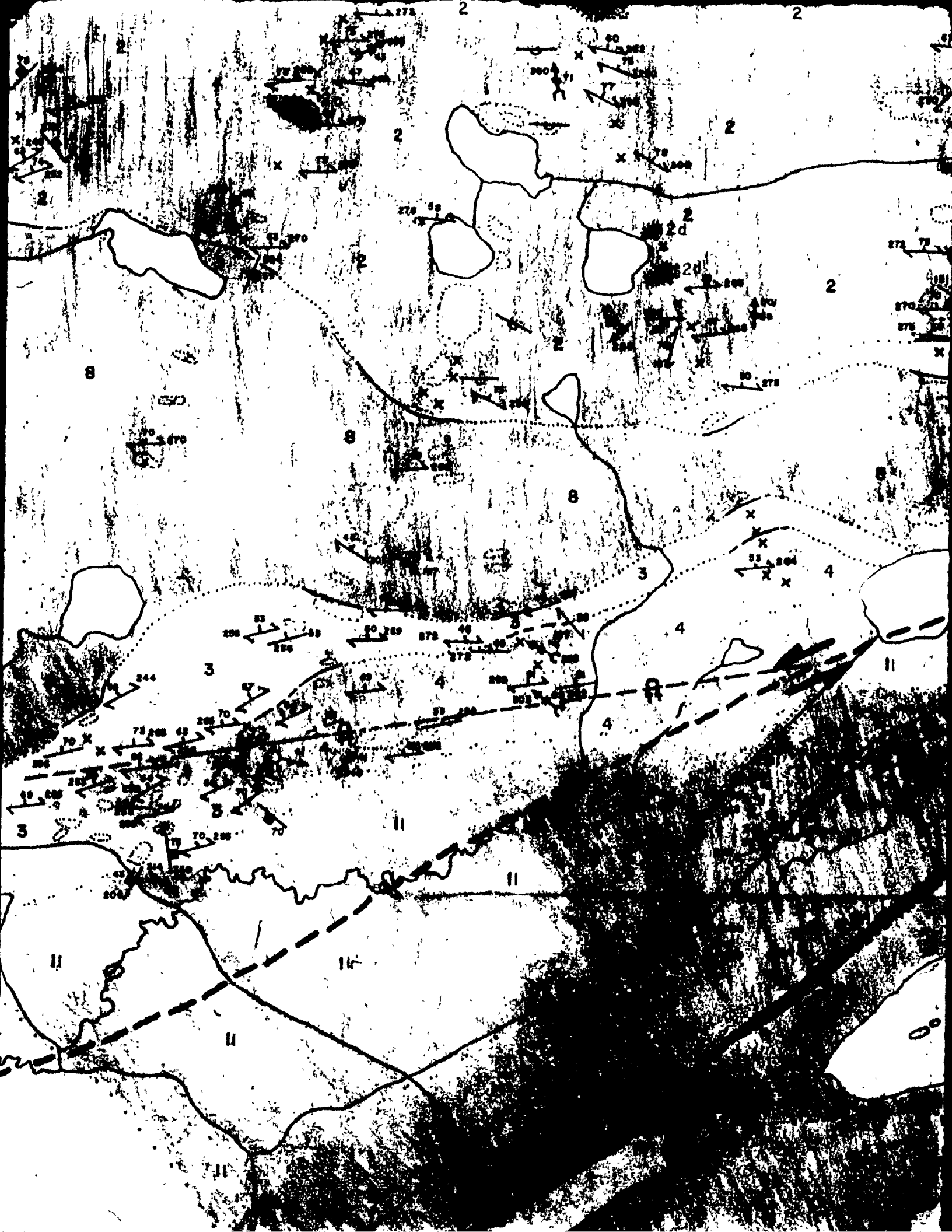
Drift covered area

X

Rock outcrop, area of outcrop

53° 40' -















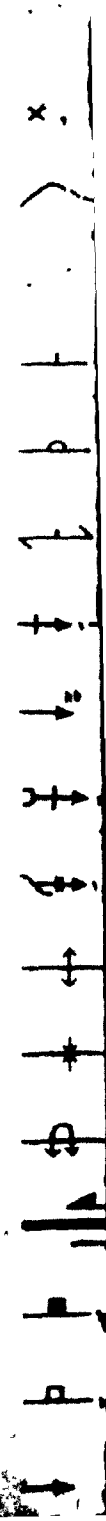
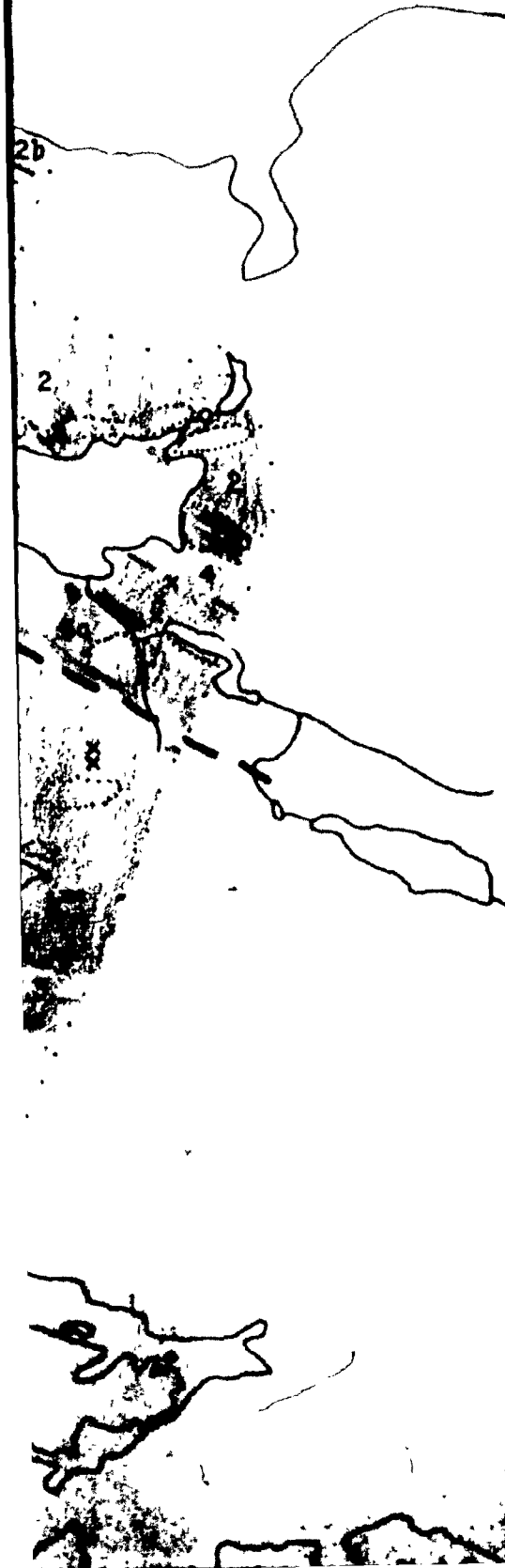
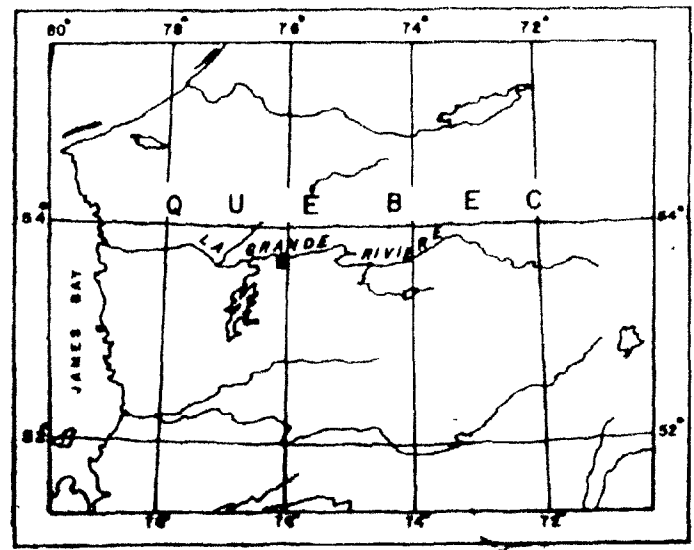
ES SYNCLINE


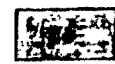
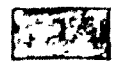



-  Plagioclase-phyrlic bas
-  Gabbro sill
-  Lower Volcanoclastics and Metasills
-  Amphibolite (hornblende)

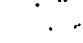




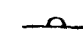
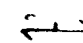
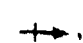

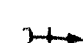








G E O L O G Y
O F T H E
L G - 3 A R E A

- 53 40

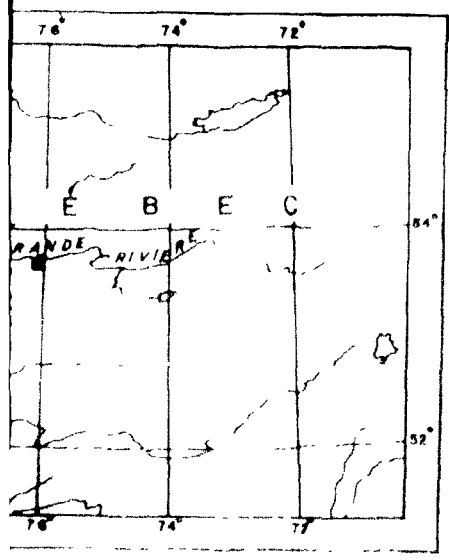


-  Plagioclase-phyrlic basalt, glomeroperphyritic gabbro (m) and pillow basalt (Δ)
-  Gabbro sill
-  Lower Volcanoclastics and Metasediments, mafic volcanoclastics, siltstones, graywacke, conglomerate, gabbro sills
-  Amphibolite (hornblende schist)

SYMBOLS

-  Drift covered area
-  Rock outcrop, area of outcrop
-  Geological contact, defined, approximate, assumed
-  Limit of geological mapping
-  Bedding S_0 , with facing, overturned
-  Pillow facing
-  Schistosity S_1 , fracture cleavage S_2 , fracture cleavage S_3
-  Lineations, L_1, L_2
-  Mineral lineation, hornblende
-  Minor fold, F_1, F_2
-  Kink fold F , dextral, sinistral (when viewed down plunge)
-  Anticline defined, approximate, antiform
-  Syncline defined, approximate, synform
-  Overturned anticline, syncline defined, approximate
-  Sinistral strike slip fault, defined, approximate, assumed
-  Joint, quartz vein
-  Shear zone, with dextral slip
-  Strike-slip

GEOLOGY OF THE 3 AREA






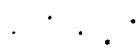



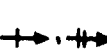
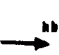
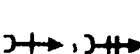





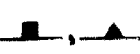
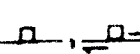

Plagioclase-phyric basalt, glomeroperphyritic gabbro (■) and pillow basalt (▲)

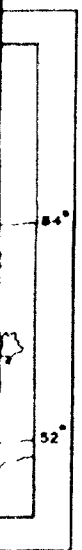
Gabbro sill

conglomerates and Metasediments, mafic volcanoclastics, siltstones, graywacke, conglomerate, gabbro

Amphibolite (hornblende schist)

SYMBOLS

-  Drift covered area
-  Rock outcrop, area of outcrop
-  Geological contact, defined, approximate, assumed
-  Limit of geological mapping
-  Bedding S_0 , with facing, overturned
-  Pillow facing
-  Schistosity S_1 , fracture cleavage S_2 , fracture cleavage S_3
-  Lineations, L_1 , L_2
-  Mineral lineation, hornblende
-  Minor fold, F_1 , F_2
-  Kink fold F , dextral, sinistral (when viewed down plunge)
-  Anticline defined, approximate, antiform
-  Syncline defined, approximate, synform
-  Overturned anticline, syncline defined, approximate
-  Sinistral strike slip fault, defined, approximate, assumed
-  Joint, quartz vein
-  Shear zone, with dextral slip
-  Strike-slip

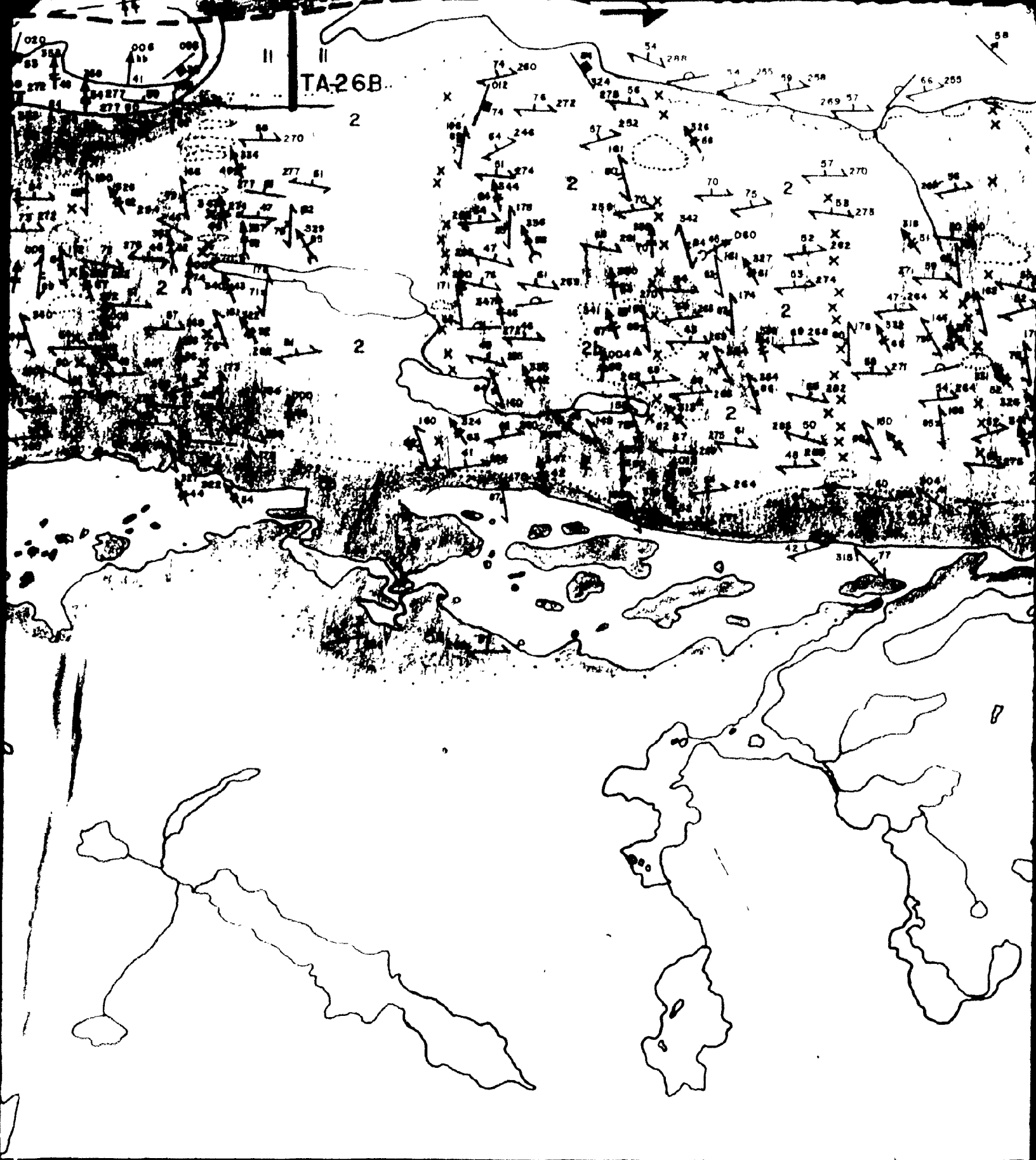




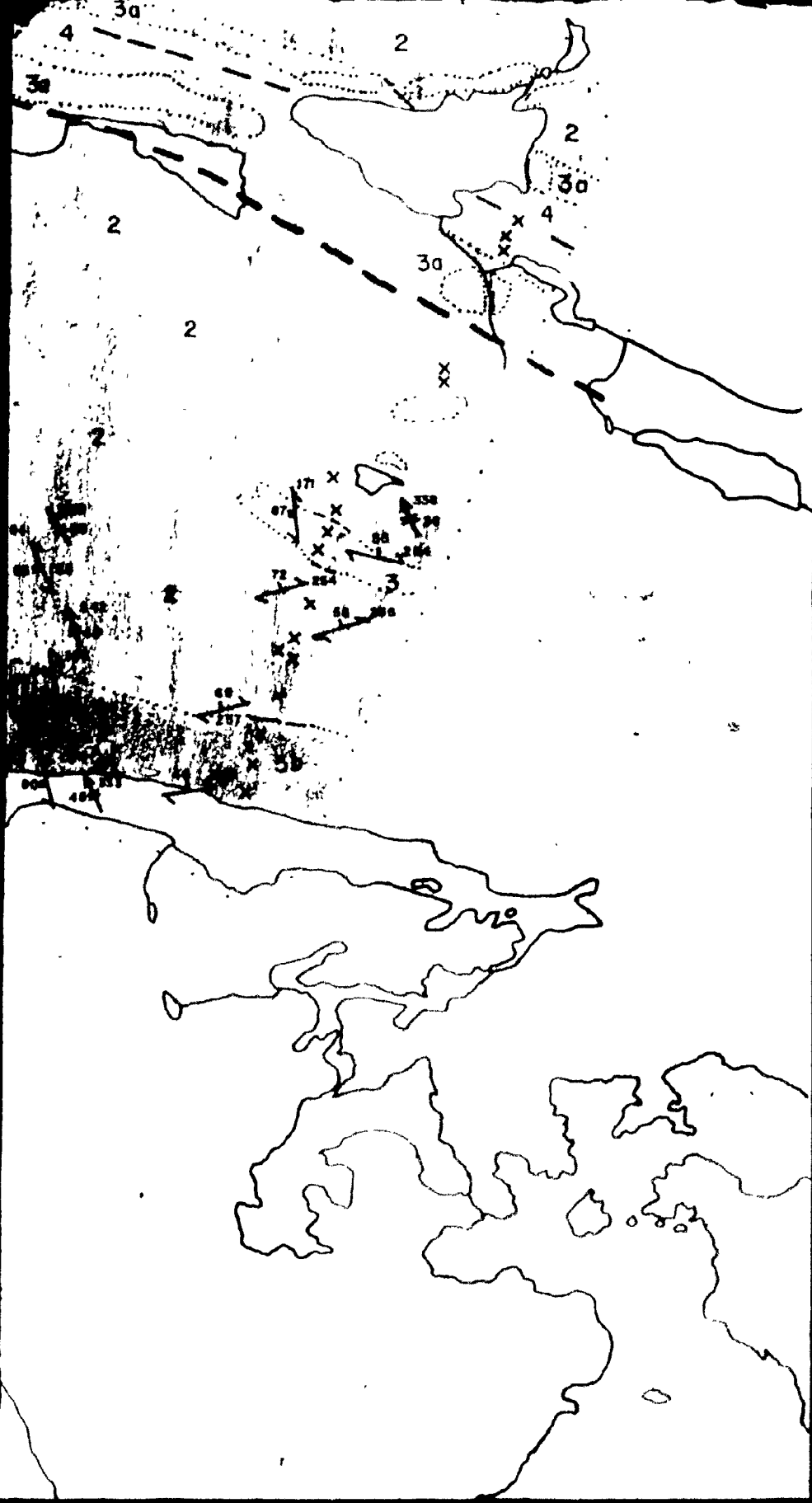
76 05

||

TA-26B

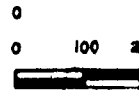
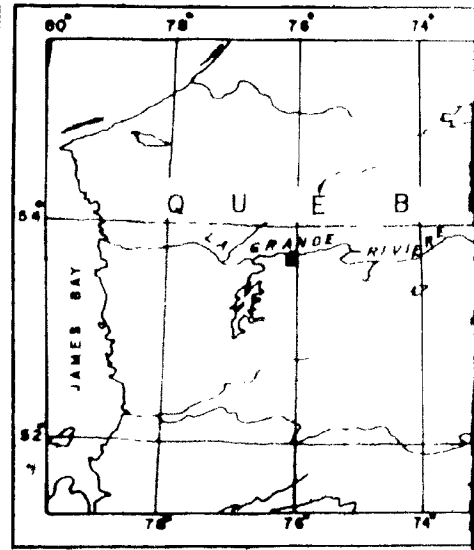






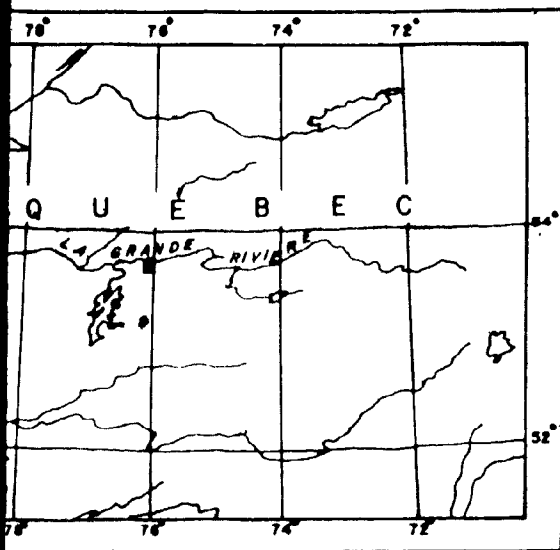
- 53° 40'




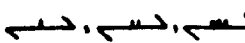
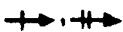

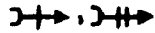

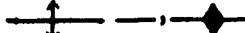



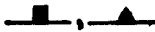


OF THE
LG-3 AREA

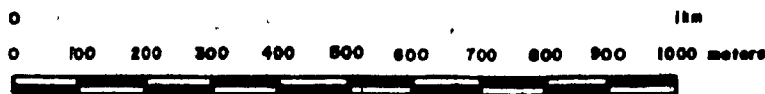


76° 57'

OF THE LG-3 AREA



-  Limit of geological mapping
-  Bedding S_0 , with facing, overturned
-  Pillow facing
-  Schistosity S_1 , fracture cleavage S_2 , fracture cleavage S_3
-  Lineations, L_1, L_2
-  Mineral lineation, hornblende
-  Minor fold, F_1, F_2
-  Kink fold F , dextral, sinistral (when viewed down plunge)
-  Anticline defined, approximate, antiform
-  Syncline defined, approximate, synform
-  Overturned anticline, syncline defined, approximate
-  Sinistral strike slip fault, defined, approximate, assumed
-  Joint, quartz vein
-  Shear zone, with dextral slip
-  Slickenside



Scale 1:10,000

THOMAS SKULSKI

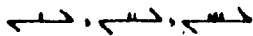
Limit of geological mapping



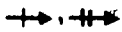
Bedding S_0 , with facing, overturned



Pillow facing



Schistosity S_1 , fracture cleavage S_2 , fracture cleavage S_3



Lineations, L_1, L_2



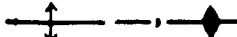
Mineral lineation, hornblende



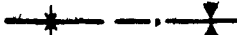
Minor fold, F_1, F_2



Kink fold F , dextral, sinistral (when viewed down plunge)



Anticline defined, approximate, antiform



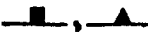
Syncline defined, approximate, synform



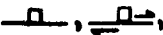
Overturned anticline, syncline defined, approximate



Sinistral strike slip fault, defined, approximate, assumed



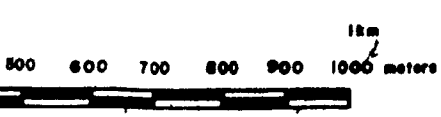
Joint, quartz vein



Shear zone, with dextral slip



Slickenside



1:10,000

THOMAS SKULSKI, 1983